

A 2D Dosimeter based on Glass for Gamma Irradiation

A thesis submitted for the degree of Doctor of Philosophy

By

Ruzalina Baharin

Centre for Sensors and Instrumentation

School of Engineering and Design

Brunel University

May 2016

To my husband and children, you are my inspiration

To my mum and mother-in-law, you are my love

To my big family, you are my motivation

ABSTRACT

The aim of this thesis was to develop a 2D dosimeter based on glass. Porous VYCOR[®] 7930 silicate glass doped with fluorescent quantum dots (QDs), CdSe/ZnS was investigated. Initial studies were made of the radiation resistance of a soda-lime glass microscope slide. The PENELOPE Monte Carlo was used to understand the deposition of radiation in the materials under consideration. In this work, the study of the radiation resistance behaviour was made in term of changes to the optical absorbance. The microscope slide was irradiated with ⁶⁰Co gamma rays and damage at optical absorption bands of 400 – 440 nm and 600 – 620 nm was observed. The long-term annealing of this glass in the dark was measured over a period of 175 days. The effect of changing the dose rate was measured. New measurements of the radiation tolerance of Corning VYCOR[®] 7930 nano-porous glass showed low radiation damage at any region of the visible spectrum at doses up to 900 Gy. It is thus a stable substrate for hosting a material with significant change in properties with radiation. In an optical experiment, VYCOR[®] 7930 with a doping of fluorescent CdSe/ZnS core-shell quantum dots (QDs) which are easily damaged by radiation doses of order 10 Gy demonstrates the possibility as a readout dosimeter by measuring the visible fluorescence. The QDs fluorescence was stable under near UV excitation for a period of at least 6 hours.

DECLARATION

This is to declare that:

- I am responsible for the work submitted in this thesis.
- This work has been written by me.
- All verbatim extracts have been distinguished and the sources specifically acknowledged.
- This work has not been submitted within a degree programme at this or any other institutions.

Ruzalina Baharin

ACKNOWLEDGEMENT

First of all, I would like to express my gratitude to my supervisor, Professor Peter R. Hobson, for his time, guidance and never ending supports during the entire of my research work. Also thank you to my co-supervisor, Dr. David R. Smith, for his motivation and encouragement in completing this dissertation.

I am thankful to Dr Dawn Leslie, for her help and time as a proof reader. Her kindness is always remembered. I sincerely thanks to Christopher Selby for his help during the experiments and also to all Centre for Sensors and Instrumentation staffs for their technical help.

Also to Mrs SitiAiasah Hashim for helping as a second proof reader; Dr. Jafri Zulkepli Hew for his kindness on thesis arrangement; Dr. Zulkafli Ghazali for his support and encouragement that makes me pursue this study and all my good friends for their endless help.

I gratefully acknowledge the Malaysian government, Ministry of Science, Technology and Innovation (MOSTI) and Malaysian Nuclear Agency for their financial support and granting the study leave.

My love and appreciation also goes to my husband, Mohd Khubaib Mohd Abid for his support and encouragement throughout my PhD years. To my mum and mother-in-law, Rafiah Bidin and Faridah Yaakob, your words your prays are always be remembered. Finally, thank you to my children, Khaireen Sumayyah, Abu Abbas Al Mursi, Nurul Soffiya, Ahmad Umar Al Farouq and Muhammad Ubai, for their loves and becoming my inspiration to finish this work.

TABLE OF CONTENTS

ABSTRACT	i
DECLARATION	ii
ACKNOWLEDGEMENT.....	iii
TABLE OF CONTENTS	iv
List of Figures.....	viii
List of Tables	xii
Chapter 1 Introduction	1
1.1 Quality control in radiation facilities.....	2
1.2 Dosimetry system and its material	4
1.3 Monte Carlo Coding	6
1.4 Contribution to knowledge	6
1.5 Research goals.....	7
1.6 Overview of content of thesis	7
Chapter 2 Background	9
2.1 Radiation dosimetry and its application.....	10
2.1.1 Types of dosimeters	11
2.1.2 Radiation measurement.....	13
2.1.3 Dosimetry characteristics	15
2.2 Glass as dosimeter	16
2.2.1 Atomic structure of silicon	18
2.2.2 Generation of X-ray fluorescence.....	22
2.2.3 Photon-interactions	25
2.2.4 The mass attenuation coefficient, μ/ρ	27
2.2.5 Radiation damage in high radiation tolerance glass	28
2.3 Quantum dots in dosimetry	30
2.3.1 Quantum confinement effects.....	31
2.3.2 Synthesis of quantum dots.....	32

2.3.3	Types of quantum dots.....	33
2.3.4	Optical properties in quantum dots.....	33
2.4	Modelling the radiation damage by PENELOPE.....	35
Chapter 3	Monte Carlo and PENELOPE.....	37
3.1	Monte Carlo Modelling.....	38
3.2	Simulation assumptions and considerations.....	39
3.2.1	Molecular Structure.....	40
3.2.2	Radiation Energy.....	41
3.2.3	Beam Particle Forces.....	41
3.3	Particle Interactions.....	41
3.3.1	Photoelectric absorption.....	43
3.3.2	Rayleigh scattering.....	43
3.3.3	Compton scattering.....	43
3.3.4	Pair production.....	44
3.3.5	Electron and positron interactions.....	44
3.4	PENELOPE and CASINO.....	45
Chapter 4	PENELOPE Simulations.....	49
4.1	The simulation.....	50
4.2	pencyl program.....	52
4.2.1	Example of pencyl program.....	53
4.2.2	Results and discussion.....	57
4.3	Simulation parameters.....	63
4.3.1	Simulation on different parameters.....	64
4.3.2	General results.....	69
4.3.3	Different EABS cut-off energy.....	69
4.3.4	Different WCC.....	71
4.4	Energy deposition in every layer.....	72
4.5	Simulation using the quartz.....	73
4.6	With and without build-up material.....	75
4.7	Imaging of radiation in 2D resolution.....	77
4.7.1	Results and discussion.....	80

Figure 4.25 The distribution of deposited charge at top of the graph and distribution of dose at bottom of the graph, throughout the depth of sample. Area 1 is not assigned as there are no distributions of dose and charge throughout the area.	82
4.7.2 Summary	83
Chapter 5 Radiation Effects on Microscope Slide	84
5.1 Study on glass	85
5.2 Gamma-ray irradiation	87
5.2.1 Dose verification	87
5.3 Optical absorbance measurement by spectrophotometer.....	88
5.4 Methodology: Microscope slide.....	94
5.4.1 Irradiation A1	94
5.4.2 Irradiation A2	94
5.4.3 Optical absorbance with spectrophotometer	95
5.5 Results and analysis for microscope slide	96
5.5.1 Reproducibility.....	96
5.5.2 Induced absorbance at different dose.....	98
5.5.3 Induced absorbance for high and low Co-60 dose rate	100
5.5.4 Fading effect.....	102
5.5.5 Summary	105
Chapter 6 Radiation Effects on VYCOR [®] 7930 and Optical System Development.....	107
6.1 Dosimetry and optical system	107
6.2 Methodology: VYCOR [®] 7930	108
6.2.1 Irradiation B1	108
6.2.2 Irradiation B2	109
6.3 Results and analysis for VYCOR [®] 7930	110
6.3.1 Reproducibility.....	111
6.3.2 Radiation induced absorbance.....	112
6.3.3 Build-up material effect	117
6.4 Optical system experiment.....	119
6.4.1 Uniformity of illumination measurement.....	119
6.4.2 Experimental arrangement and methodology of optical system.....	123
6.4.3 Fluorescence images from the quantum dots doped VYCOR [®] 7930	124

6.4.4 Result and data analysis	125
6.5 Summary works on Vycor	127
Chapter 7 Summary and Conclusion.....	128
Bibliography	131
Appendix A	140
Appendix B	154

List of Figures

Figure 2.1 The atomic structure of silicon, Si-14.	18
Figure 2.2 Phenomena of (a) photon emission and (b) photon absorption in general atomic structure.....	20
Figure 2.3 Energy level diagram of silicon showing transitions of an electron from a high shell to a lower shell resulting of the emission of a characteristic X-ray or X-ray fluorescence.	23
Figure 2.4 The fluorescence yield of K, L and M shell versus atomic number, Z . The K-shell plot shows the increasing number of emitted X-rays started from Be-4 and start to slow down after La-57(www.kayelaby.npl.co.uk).....	25
Figure 2.5 The mass attenuation coefficient for Si-14. [http://www.nist.gov/pml/data/xraycoef/index.cfm].....	28
Figure 2.6 The creation of Frenkel pair (interstitial atom and the vacancy).....	29
Figure 2.7 The energy level in band gap increasing with the decreasing size of quantum dots size (courtesy from www.sigmaldrich.com).	32
Figure 2.8 Emission spectra of core-shell CdSe/ZnS quantum dots from Lumidot. (Courtesy http://www.sigmaldrich.com/materials-science/nanomaterials/lumidots.html).....	35
Figure 3.1 Photon interactions with matter. Reproduced from http://www.oecd-neo.org/science/pubs/2009/nea6416-penelope.pdf (page 54).	42
Figure 3.2 Electrons and positrons interactions with matter. Reproduced from http://www.oecd-neo.org/science/pubs/2009/nea6416-penelope.pdf (page 103).	45
Figure 3.3 The backscattered electrons in CdS-Silica-CdS and Silica only samples by CASINO (top) and PENELOPE (bottom). The irradiation was considered by 1 MeV of accelerating voltage. Graphs are reproduced from Baharin <i>et al.</i> (2010).	46
Figure 4.1 The geometry of NaI photon detector from the input file of cyld.in. The incident photon beam moves upwards along the z-axis (assuming $z = 0$) and hits the detector surface.	53
Figure 4.2 The input file, cyld.in used in the simulation example for pencyl program taken from PENELOPE package.....	55
Figure 4.3 The 2D view of sample structures in cyld.in using gviewc.exe viewer. Mat 1 (in purple), Mat 2 (orange) and Mat 3 (blue) represent NaI, Al ₂ O ₃ and Al, respectively.	57
Figure 4.4 Simulated depth-dose distribution in the NaI scintillation detector when an 1.25 MeV photon beam is incident upon it.	58
Figure 4.5 The backscattered fluence distributions of (i) photons and (ii) electrons, when the NaI scintillation detector has an 1.25 MeV photon beam incident upon it.	58
Figure 4.6 Illustration of gamma particles when entering the 10 cm of silicon dioxide with 1 MeV of energy. Yellow line representing photon, red line is electron trajectories and white line is backscattered energy.	60

Figure 4.7 Trajectories of gamma particles when entering the 10 cm of silicon (low atomic number) and lead (high atomic number) with 1 MeV of energy illustrated at top and bottom pictures, respectively.....	62
Figure 4.8 Sample arrangement of QD doped Vycor. Material 1 and 3 is CdSe/ZnS (QDs) with 0.001 cm thickness and 0.31 cm of Vycor as a Material 2. Source is located at z-axis of -10 cm. ..	64
Figure 4.9 The input file (QDVycorQD-40keV.in) for QDs doped Vycor with simulation time of 7200 seconds. 40 keV of photons bombarded onto Vycor with 0.001 cm of QDs on top and bottom.	65
Figure 4.10 Part of the material file for CdSe/ZnS that is needed in the input file (Figure 4.9). The columns labelled F_i , U_i (eV), W_i (eV), KZ and KS are the oscillator strength, excitation energy, resonance energy of bound-shell oscillator, atomic number of K shells and number of oscillators, respectively.	67
Figure 4.11 Part of the material file for Vycor. The columns labelled F_i , U_i (eV), W_i (eV), KZ and KS are the oscillator strength, excitation energy, resonance energy of bound-shell oscillator, atomic number of K shells and number of oscillators, respectively.	68
Figure 4.12 The distribution of charge density particles (left graph) and depth dose materials (right graph) from PENELOPE simulation output files. (Simulation: 40 keV of incident photons bombarded into a sandwich of QDs and Vycor).....	69
Figure 4.13 Distribution of charge density particles and dose over the depth of materials with three different values of EABS cut-off energies on top and bottom graph, respectively. (Simulation: 40 keV of incident photons incident upon a sandwich of QDs and Vycor).	70
Figure 4.14 Backscattered electrons of three different cut-off energy of material absorption in a similar environment. (Simulation: 40 keV of incident photons bombarded into a sandwich of QDs and Vycor).....	71
Figure 4.15 Backscattered electrons distribution with three different values of WCC; 0.1, 1 and 10 keV. There is no significant effect with the changes of WCC values. (Simulation: 40 keV of incident photons incident upon a sandwich of QDs and Vycor).....	72
Figure 4.16 Deposited energy distribution at the top of every layer; QD upper, Vycor and QD bottom. (Simulation: 40 keV of incident photons bombarded into a sandwich of QDs and Vycor). Data were normalised to a thickness of every material.	73
Figure 4.17 Distribution of backscattered electrons from two simulations of 40 keV of photons. The quartz helps stabilizing the data and minimizing the error.....	74
Figure 4.18 The distribution of depth dose at 40 keV on semi-log scale with thousands display unit. The dashed line is representing a piece of 0.1 cm of quartz taped on both side of Vycor and given lighter color as to show the difference of two lines.....	75
Figure 4.19 Distributions of charge density particle and dose over the Vycor depth when using build-up material and without it. (Simulation: 1 MeV of photons incident upon Vycor).	76
Figure 4.20 The distributions of backscattered and transmitted electrons of 1 MeV of photons over Vycor with build-up material and without it. The material increases the backscattered electrons without affecting the transmitted electrons distribution.	76
Figure 4.21 Sample arrangement of lead disc (10 cm × 0.01 cm with 1 cm diameter hole) covering the Vycor (10 cm × 0.31 cm) with sandwich of CdSe/ZnS (10 cm × 0.001 cm).	78
Figure 4.22 Input file.....	79

Figure 4.23 Illustration results of 1 MeV of photons bombarded toward sample (Vycor with sandwich of CdSe/ZnS) covered by lead barrier. Source is located at 10 cm from the sample. At low bottom of the picture are the thicknesses of every element in sample.	80
Figure 4.24 The 2D plot distribution of dose distribution inside the sample of Vycor with sandwich of CdSe/ZnS. The sample covered by a disc of lead with a 1 cm diameter hole in the centre. This is not to scale plot.	81
Figure 4.25 The distribution of deposited charge at top of the graph and distribution of dose at bottom of the graph, throughout the depth of sample. Area 1 is not assigned as there are no distributions of dose and charge throughout the area.....	82
Figure 5.1 Optical absorbance of microscope slide, after 1hour of irradiation at top figure. Darker dot is for sample facing towards detector and lighter dot for sample facing away detector. In the bottom figure, it is very consistent with less than ± 0.002 difference of optical absorbance data between both sides.	92
Figure 5.2 Optical absorbance of VYCOR [®] 7930, after 1hour of irradiation at top figure. Darker dot is for sample facing towards detector and lighter dot for sample facing away detector. In the bottom figure, there is small difference of optical absorbance data between both sides but less than 0.005 OD.	93
Figure 5.3 The optical absorbance spectra (top graph) and radiation induced absorption spectra (bottom graph) with normalisation to a thickness of 1mm of microscope slide after gamma irradiation at 300 Gy and 900 Gy.	99
Figure 5.4 Mean and standard deviation of sample at 250 – 280 nm, 300 – 340 nm, 350 – 500 nm and 600 – 620 nm of wavelength.	100
Figure 5.5 Radiation induced absorbance spectra after 1 hr gamma irradiation of microscope slide at high and low activity of Co-60 at the top graph. Bottom graph shows the ratio of high and low activity of Co-60.	101
Figure 5.6 Annealing behaviour for microscope slide up to 175 days on observation. The microscope slide was irradiated to 300 Gy at 0.20 Gy/min.....	102
Figure 5.7 The average data of radiation induced absorption at the region of 350 - 450 nm of wavelength with normalization to a thickness of 1 mm of microscope slide. Top graph shows 175 days observation on fading behaviour, while the bottom graph is for the same sample expanded to show the first 10 days after irradiation. Microscope slide was irradiated at 300 Gy at 0.20 Gy/min.	103
Figure 6.1 Topography of VYCOR [®] 7930 by SEM at 20 μ m for the left picture and at 20 nm for the right picture. They show at the edge and surface VYCOR [®] 7930 on the left and right pictures, respectively.....	111
Figure 6.2 The optical absorbance of unirradiated Vycor A and Vycor B with the normalization to the 3.1 mm sample thickness.	112
Figure 6.3 Optical absorbance and radiation induced absorption of Vycor A at top and bottom graphs, respectively. Normalization was made to the 3.1 mm sample thickness.	113
Figure 6.4 Optical absorbance and radiation induced absorption of Vycor B at top and bottom graphs, respectively. Normalization was made to a 3.1 mm of sample thickness.	114

Figure 6.5 Radiation induced absorbance (normalised to a thickness of 1 mm and 3.1 mm for microscope slide and Vycor, respectively) by gamma in microscope slide, Vycor A and Vycor B, at the same scale.	115
Figure 6.6 Mean variation and standard deviation of the samples, Vycor A and Vycor B at the top and bottom graphs, respectively.	116
Figure 6.7 Radiation induced absorbance of Vycor C (top graph) and Vycor D (bottom graph) at 300 Gy with and without the build-up material, aluminium (Al). Data were normalised to a 3.1 mm of a sample's thickness.	118
Figure 6.8 The layout of uniformity measurement	120
Figure 6.9 The layout of optical system experiment set-up in the dark room.	123
Figure 6.10 Excitation spectrum of the green quantum dots collected from Horiba Scientific (FluoroLog Spectrofluorometer). It shows the excitation spectrum when measuring fluorescence (1 nm bandwidth) at the peak emission wavelength of 530 nm.....	124
Figure 6.11 Image of the fluorescent QDs in VYCOR [®] 7930 during the light illuminating. Surface markings arise from the cutting process used to produce the glass slab. The blue light comes from the LED and the green light from the QD.	125
Figure 6.12 Ratio of green fluorescence to blue illumination light with the average frames at three point in the bottom graph.	126

List of Tables

Table 1.1 Dosimetry systems that are commonly used in quality control at radiation processing facilities.....	4
Table 2.1 Quantum numbers of a silicon atom.....	22
Table 5.1 Composition of VYCOR [®] 7930 brand porous glass (Corning Incorporated, New York).	85
Table 5.2 Approximate composition of microscope slide. These compositions vary slightly due to the application.....	86
Table 5.3 Dose rate data collected from Farmer 2670 dosimeter during dose validation of high rate activity of Co-60 source.	88
Table 5.4 The spectrophotometer program settings.....	91
Table 5.5 A summary of gamma irradiation experiments and optical absorbance measurement for microscope slide samples.	96
Table 5.6 Reproducibility of gamma-irradiated microscope slide referring to the optical absorbance within the wavelength range of 400 to 440 nm.	97
Table 6.1 Summary of gamma-ray irradiation experiment and optical absorbance measurement for VYCOR [®] 7930.	110
Table 6.2 Mean and standard deviation based on sample with the respect of build-up material and without build-up material.	119
Table 6.3 Data on uniformity of illumination of UV LED. Values considered were marked as Middle and taken from a group of uniform data.....	122
Table 6.4 Data on fluorescence QDs in VYCOR [®] 7930 with the respect of time of picture taken.	126

Chapter 1

Introduction

Quality assurance of irradiated products for the medical and consumer industries is extremely important. The assurance comes in the form of conformance of the dose absorbed by the irradiated products, which is carried out using a dosimetry system. This is what the industries depend on [Narayan *et al.*, 2008; Ferrar, 1999], before the products go into the end-user. Most dosimetry systems have their own advantages and disadvantages depending on the dosimetry application, the radiation source type and the source energy. The high demand for precision dosimetry systems has justified continuous research into many aspects of their development.

A precise dosimetry system is needed in order to provide the required quality assurance of irradiated products. Any dosimetry system must align with the regulation on irradiation facilities and its components like ISO 11137, EN552, and ISO 13485. These guidelines or standards were established to support quality control system in industry [Kuntz, 2004] for example in food irradiation, sterilization, pharmaceutical and polymer treatment. These guidelines have been approved and used as a standard in sterilization plants worldwide.

The necessity to provide accurate dosimetry exists in radiation processing facilities, in order to closely monitor the dose received by irradiated materials. The work presented in this thesis investigates and evaluates the potential of new materials for use in a dosimetry

system. It includes the evaluation of glass as a radiation tolerant material that could stand alone as a dosimeter like soda-lime glass [Farah *et al.*, 2007; Rodrigues Jr. and Caldas, 2002] and coloured glass [Teixeira *et al.*, 2007] or could be a radiation tolerant substrate for quantum dots. The dynamic characteristics of radiation damage in glass suggested the work on microscope slides as one type of soda-lime glass and VYCOR[®] 7930 which has more pure silica.

1.1 Quality control in radiation facilities

In general, dosimetry systems are becoming important tools in radiation processing industries such as sterilization, curing and preservation. This involves irradiators like electron beam accelerators, X-ray machines and Co-60 irradiators. Prior to these applications, medicine has used radiation technology for radiotherapy since the discovery of X-rays by Röntgen back in 1895 [Bartlett, 2008; Jennings, 2007]. Products will be bombarded with ionizing radiation sources of photons at certain doses depending on the application. This is where quality control is compulsory. It involves the validation and verification of industrial plants and irradiated products [Kovacs and Miller, 2004; Kuntz, 2004; McLaughlin and Desrosiers, 1995].

There are three main parts in quality control for radiation processing in the technology industry, as stated below:

- Irradiation facility qualification: this involves the installation qualification (IQ) and operational qualification (OQ) of plants. These procedures are crucial to characterize the plants' parameters during the installation of sources (IQ) or

irradiator, after any changes that applied directly to the sources or irradiators, and also at regular intervals (OQ).

- Process validation: known as performance qualification (PQ) or product dose-mapping in order to get the minimum or maximum dose that can be tolerated by products. This is a mandatory requirement for a new product before going through the irradiation process.
- Routine process control: this is routinely carried out to ensure the irradiation process is controlled within specified limits. Normally this involves using a dosimeter to check that the dose received by a product is certified and within the range of specified limits.

In every part, dosimetry is essential to provide the data to confirm that the irradiation process is accurate and following the quality control procedures. As a service provider, elements IQ and OQ are significant in a dosimetry system, while customers rely on routine process control results. Table 1.1 shows some of the dosimetry systems that are commonly used by referring to the different parts of quality control.

Table 1.1 Dosimetry systems that are commonly used in quality control at radiation processing facilities.

	Dosimetry system	Dosimeter
Irradiation facility qualification	• Physical	• Calorimeter
	• Chemical	• Ceric cerous
Process validation	• Physical	• Radiochromic film
	• Chemical	• Cellulose triacetate (CTA)
Routine process control	• Physical	• Radiochromic film
		• Ionization chamber
	• Chemical	• Cellulose triacetate (CTA)
		• Ceric cerous

1.2 Dosimetry system and its material

Irradiated products require a good dosimetry system with precise dosimetry to ensure the dose delivered is within the specified confidence limits. It is also important to consider the stability factor, structural robustness and measurement sensitivity of any potential dosimeter material. These qualities can be assessed for any dosimetry application. Chapter 2 will consider and explain the variety of dosimetry systems currently used in industry.

Recent studies show the good capability of commercial glass as a dosimeter [Khan and Ali, 1995] and its ability to work well following Co-60 irradiation [Narayan *et al.*, 2008; Mejri *et al.*, 2008; Rodrigues and Caldas, 2002; Zheng *et al.*, 1997] and in electron beam plant applications [Caldas and de Souza, 1991]. Glass is recyclable, rigid, inert and not expensive. However, the main problem presented by commercial glass is the initial strong

fading in the initial radiation damage at one to two days after irradiation [Rodrigues and Caldas, 2002; Khan and Ali, 1995] but researchers have overcome the problem by measuring the glass optical density at regular time intervals after irradiation [Narayan *et al.*, 2008; Farah *et al.*, 2007].

Glass itself has many varieties according to the composition. Silica is the fundamental and biggest component in glass. By addition of additives and impurities, the application of glass changes dramatically. For instance, silica with addition of barium or lanthanum oxide will increase the refractive index of glass, making it better for optical applications. Usman and others did a comparison of the high radiation tolerance types of glass; Pyrex, Quartz and Vycor for developing of new gamma measurement device based on photoconductivity. Pyrex is high impurity material, Quartz with high percent of silica (high purity material) and Vycor between them with 96% of silica [Usman *et al.*, 2005]. Quartz and Vycor show better characteristics as dosimeter material compared to Pyrex. Quartz itself is suitable to be used in high dose rate conditions but in a point of detector construction, Vycor is found to be more promising for gamma radiation measurement.

VYCOR[®] 7930 has a porous structure that is suitable for doping processes. It becomes an interesting matrix for hosting a special material like quantum dots. This advantage is appropriate for the development of a high radiation resistant material with good dosimetric characteristics. Quantum dots that lately hit the optical and electrical world with their unique properties are discussed in Chapter 2 where they were doped in a porous matrix of VYCOR[®] 7930.

1.3 Monte Carlo Coding

In terms of validation and verification, Monte Carlo techniques are highly recommended for comparing to other studies. This method is a numerical solving technique that provides simulations of random variables. A lot of Monte Carlo codes are available and widely used for dosimetry applications such as MCNP, EGSnrc, GATE, CASINO and PTRAN [Drouin *et al.*, 2007; Visvikis *et al.*, 2006]. There are also available in the market, commercial programs such as PK-MASTER™ and PK-TRAINER™ for training purposes [Saylor and Jordan, 2000; Saylor *et al.*, 2002; Connaghan *et al.*, 2004]. In this work, PENELOPE simulation developed by a group from Barcelona Universitat, Spain is used [Sempau *et al.*, 2003; Sempau and Andreo, 2006].

The PENELOPE simulation code is available from the NEA data bank. It is user friendly and not too complicated for an intermediate user with moderate knowledge of radiation physics. Chapter 3 and 4 is deal with this matter.

1.4 Contribution to knowledge

VYCOR® 7930 is a silicate glass with a nanoporous structure that provides the different optical properties depending on the application. It is shown that VYCOR® 7930 is a good hosting material with high radiation tolerance. Consequently, VYCOR® 7930 with doping of quantum dots is enhancing the optical absorbance dosimetry system. According to the literature, there are an extensive number of research projects focusing on combining commercial glass with quantum dots, but currently there are no conclusions made about the resulting dosimetry characteristics. Research specifically on VYCOR® 7930 with quantum dots doping has not yet been approached by other researchers.

By application in an optical system with real-time configuration, the work in this thesis is novel research or at least an innovation on currently available systems. There is also a value-adding quality to the quantum dot and VYCOR[®] 7930 combination, which is a new achievement for both materials.

1.5 Research goals

By referring to works related to the development of 2D dosimetry systems for gamma irradiation, there are two main goals:

1. To investigate and evaluate the effectiveness of materials used in radiation processing industries with respect to glass as a radiation tolerant material.
2. To explore the potential of a new system of real-time two-dimensional dosimetry based on fluorescent quantum dots dispersed in VYCOR[®] 7930.

1.6 Overview of content of thesis

In general, this thesis consists of seven chapters.

Following the introduction and literature review, Chapter 2 explores the background of dosimetry systems in the radiation industry and their importance. There are also descriptions of two particular types of glass: VYCOR[®]7930 and microscope slides. Attention is also given to recent interests in the nano-scale world, e.g. quantum dots (QDs), with this work concentrating on commercially available fluorescent CdSe/ZnS core-shell materials.

A description of the PENELOPE simulation and Monte Carlo coding is given in Chapter 3, whilst Chapter 4 details the PENELOPE simulation programme for a potential dosimeter system.

Spectrophotometry measurements of a silicate glass, used to investigate radiation damage are detailed in Chapter 5 with respect to the dosimetry characteristics; reproducibility, fading effect, lower dose detection, and response of material to the dose.

Chapter 6 details the work on VYCOR[®] 7930 with the development of an optically read-out dosimeter employing VYCOR[®] 7930 and QDs.

Chapter 7, the concluding chapter of this thesis summarises the potential uses of VYCOR[®] 7930 with QDs doping in dosimetry applications as well as making recommendations for further work.

Chapter 2

Background

In the numerous examples of wide and varied industries which employ radiation for various applications (e.g. medicine, agriculture, nuclear power), there is the obligation to closely monitor radiation doses involved. This is important to ensure that the dose delivered is within specified confidence limits. Accurate measurement of dose is important to ensure that the radiation is sufficient to cause the desired effect and indeed that it is not higher than is safe. For example: in radiotherapy applications for breast cancer treatment, a lower dose than required will not kill certain cancer cells but administering a higher dose than is safe will harm the patient and even potentially kill them. In the wire and cable industry, which needs a high dose of electron beam irradiation [Zyball, 2004], a dosimeter such as a cellulose triacetate (CTA) film is used to ensure that the dose delivered is sufficiently received by the wire and cable. At an appropriate dose the polymer will crosslink to provide the desired electrical and mechanical properties.

Therefore, accurate and precise dosimeters are important in a range of applications. In addition, there are other elements that need to be specified to confirm the dosimetric characteristics of a material. It will be discussed in Section 2.1 by narrowing the subject to applications where gamma radiation is being employed.

Section 2.2 describes the characteristics of silicate glass, along with silicon atoms in terms of chemical and physical structures and interactions with photons. The next section

explores the interests in quantum dots applied in optical and electrical fields. As part of the research conducted for this thesis, modelling of the radiation damage was done by Monte Carlo simulation package PENELOPE and is discussed in Section 2.4.

2.1 Radiation dosimetry and its application

A dosimetry system is comprised of a dosimeter and its reader. It was developed to help measure the effects from ionizing radiation like fluorescence and colour changes of film, started from the exploration of radiological unit measurements which was brought to the development of dosimetry systems [Jennings, 2007]. With the discovery of X-rays in 1895, every person in that field struggled to design an instrument to accurately measure the quantity of radiation. In the early years, ‘dose’ was the measured and calculated quantity of radiation considered during the development of radiotherapy practices. Then, the term was also applied for exposure and absorbed dose followed by KERMA (an acronym for Kinetic Energy Released per unit MAss).

Belot, Guilleminot, Villard, were among the early champions in dosimetry [Bartlett, 2008]. They produced methods or instruments to quantitatively measure the radiation. Villard (1908) wrote about a unit of ionization effects in air which was first suggested by Belot (1906). William (1914) then defined the Villard unit in intensity multiplied by time (in seconds). Following the International Congress of Radiology in 1928 and 1935, they agreed with the quantity of X-ray or gamma-ray as a roentgen [Bartlett, 2008].

During the 1920s, research on luminescence dosimetry increased until the 1960s. It was helped by the expanding of interest in solid state dosimetry research, such as polycarbonates for the assessment of radon exposure [Taheri *et al.*, 2006], lithium fluoride

(LiF), widely used as a crystal in X-ray spectrometry [Somma *et al.*, 2010], ionizing radiation detectors [Obryk *et al.*, 2008] and poly allyl diglycol carbonate (CR-39) in UV radiation [El Ghazaly and Al-Thomali, 2013]. Solid state dosimetry research is still active now with the extension of other applications like the measurements of X-ray and gamma radiation by RADOS personal dosimeters with MTS-N (LiF:Mg,Ti) and MCP-N (LiF:Mg,Cu,P) thermoluminescent detectors [Obryk *et al.*, 2010]; for space applications by using TLD from LiF phosphors [Bilski, 2006]; and poly allyl diglycol carbonate (PADC) that has been used in neutron dosimetry for tracking the density of neutron fluence [El-Badry *et al.*, 2007].

These varied research projects are playing an important part in the development of dosimetry systems. Every work contributes to the improvement and innovation of the currently available systems, enhancing their capability in many applications especially in the radiation processing industry, medical treatment, food preservation, nuclear power plants and security devices. Dosimetry systems also help in the monitoring process for personnel working in radiation environments where radiation safety and protection systems are essential.

2.1.1 Types of dosimeters

Generally, radiation dosimeters are categorized into different types depending on the dosimetric system they use. There are ionization chamber dosimeters, film dosimeters, luminescence dosimeters, semiconductor dosimeters and dosimeters designed for specific dosimetry applications [Izewska and Rajan, 2005]. Each type of dosimeter has strengths and weaknesses but the common issues for dosimeters are data storage limits and how the data is going to be readout.

Ionization chambers are gas filled radiation detectors and are widely used in radiotherapy, the nuclear industry and in smoke detectors. They measure the charge produced when a gas is ionized by the incident radiation and provide an output that is proportional to radiation dose. They give an instantaneous reading. One of the popular designs is from Farmer and manufactured by Baldwin [Izewska and Rajan, 2005].

Film dosimeters such as radiographic and radiochromic film, provide a light transmission reading when connected to a densitometer. Radiographic film is used in qualitative and quantitative measurements in radiotherapy and also in radiation protection and radiology. It has radiation sensitive emulsion that ionizes when exposed to radiation and forms a latent image in the film. A densitometer is used to measure the light transmission in terms of optical density (OD). The other film dosimeter is a radiochromic film that contains a special dye (e.g. GAFCHROMIC® EBT2). This dye will polymerize when exposed to radiation. By using a densitometer, the polymer will absorb light and the change in the transmission of light determined.

In luminescence dosimetry, the luminescence phenomenon occurs when energy is released by the material following absorption of radiation). There are fluorescence and phosphorescence processes. They release the energy in the form of ultraviolet, visible and near infrared light. Some materials can accelerate the process with heat or light, known as thermoluminescence or optically stimulated luminescence (OSL), respectively.

Silicon diode dosimeters and metal-oxide semiconductor field effect transistor (MOSFET) dosimeters are widely used for *in vivo* dosimetry. They offer a high sensitivity instrument and are small in size. Charge is generated in the dosimeter when electron-hole

pairs are created during irradiation. The charge is then read out by measuring the changing potentials in the device.

Some dosimetry systems are developed with special materials for specific applications like the widely used Alanine-EPR dosimeter that acts as a reference detector and total body irradiation (TBI) protocol in radiotherapy [Schaecken *et al.*, 2010], plastic scintillators for radiotherapy, diamond dosimeters [Hernandez-Ortiz *et al.*, 2012], gel dosimetry systems that include Fricke gels and polymer gels [De Deene, 2002] and optical waveguide dosimeters for food irradiation.

2.1.2 Radiation measurement

In radiation dosimetry, an understanding of the radiation specifications is needed to measure the radiation and its effects. It involves a method to quantify energy from ionizing radiation that was deposited in a medium either directly or indirectly. Standard quantities that are used to describe radiation doses are particle and energy fluence, KERMA, CEMA (converted energy per unit mass), absorbed dose and stopping power [Seuntjens *et al.*, 2005].

Particle fluence and energy fluence are used to explain monoenergetic ionizing radiation beams like photon beams and charged particle beams. The particle fluence, Φ is described as a number of particles, dN on a sphere of cross-sectional area dA ,

$$\Phi = \frac{dN}{dA} \quad (\text{Equation 2.1})$$

The energy fluence, Ψ is described as a radiant energy, dE on a sphere of cross-sectional area dA ,

$$\Psi = \frac{dE}{dA} \quad (\text{Equation 2.2})$$

or,

$$\Psi = \frac{dN}{dA} E \quad (\text{Equation 2.3})$$

and the unit is J/m^2 .

KERMA, K , is a non stochastic quantity to describe the indirect ionizing radiation like photons and neutrons. It measures an energy transferred from premier particles to the charged particles in the medium as described below,

$$K = \frac{d\bar{E}_{tr}}{dm} E \quad (\text{Equation 2.4})$$

The unit for K is J/kg , best known as the gray (Gy) where $1 \text{ J/kg} = 1 \text{ Gy}$.

CEMA is measuring energy of directly ionizing radiation like electrons and photons, which is described by,

$$C = \frac{dE_c}{dm} \quad (\text{Equation 2.5})$$

Where C is the energy lost by charged particles in a material and its unit is J/kg or gray (Gy).

Absorbed dose is the energy transferred to the matter from the ionizing radiation. It sums the energy that entering the material and deducting the energy loss including in the form of radiative losses (bremsstrahlung). It is described as,

$$D = \frac{d\bar{\epsilon}}{dm} \quad (\text{Equation 2.6})$$

The unit is J/kg or gray (Gy).

Stopping power is the average energy loss of charged particles when they travel passing through the matter. Normally, it is calculated from the theory and widely used in radiation measurement. The ESTAR, PSTAR and ASTAR programs provide the stopping power and range tables for the use of calculations in radiation measurement [Berger *et al.*, 2005].

2.1.3 Dosimetry characteristics

In the radiation processing industry, quality, or in industry terms, quality assurance (QA), of end-products depends on how good the dosimetry system is. Radiation dosimeters especially in the medical field must comply with several dosimetric properties, such as accuracy and precision, dose rate dependence, energy dependence, directional dependence, spatial resolution, physical size, linearity, readout convenient, convenience of use and thermal fading. These terms are defined as follows:

- Accuracy and precision: they relate to the uncertainty of the dose measurement. When the dose measurement is accurate this means it is near to the true value. On the other hand, precision relates to the smallest change in dose that can be determined.
- Readout convenience: dosimeters with direct readout like ionization chambers are more convenient than passive dosimeters like TLDs or films and can be used for real-time dose measurement.

- **Spatial resolution:** the smallest volume that can be measured independently of the overall irradiated volume. **Convenience of use:** some dosimeters are rugged and easy to handle. Ionization chambers for example, are reusable, have a long life span and are easy to use. In comparison, TLDs needs more attention during handling and processing.
- **Thermal fading:** this effect cannot be ignored. Therefore, measurements for all dosimeters are required to be taken after certain specified time.

These characteristics are normally referred to as the dosimetry system (M/Q), which is, dosimeter reading M and dosimetric quantity Q. The proportional relationship is for an ideal environment; however, a correction is needed for most dose reading data to maintain the linearity.

With the specific properties of dosimetry systems now defined, the discussion in this thesis will now consider different materials that can be used to construct a dosimeter. In many cases, the need for dosimeters with inert and robust materials is really important. The demand is also for cost effectiveness, efficient and user friendly dosimeters. Hence the first work carried out for this thesis was to investigate the dosimetry properties of glass which is easy to get, inexpensive and rugged.

2.2 Glass as dosimeter

Glass has been a material studied in radiation physics research since the 1950s. With desirable characteristics such as radiation resistance, physical robustness and ease of availability, these features brought researchers to study the capability of glass as a dose indicator or dosimeter material for both low and high dose measurements. Some glasses are

very radiation resistant like pure silica (quartz) and special Schott and Corning glasses containing cerium, and some, such as those containing lead but no cerium, have low radiation tolerance [Delaye *et al.*, 2011; Hong *et al.*, 2008; Narayan *et al.*, 2008; Obata *et al.*, 2006; Zheng *et al.*, 1997].

Recent research shows the capability of glass to be utilized as a dosimeter. Commercial glass, silica glass and VYCOR[®] are amongst the types of glasses that catch the attention of researchers. These are highlighted as having particularly favourable characteristics, such as being inexpensive, rigid, recyclable and inert, which affect the overall costs involved and ease of manufacture.

Narayan [*et al.*, 2008] stated that glass is optically sensitive to gamma radiation. It potentially offers a material for methods or equipment in dosimetry systems which require robust apparatus. Glass demonstrated good dosimetric characteristics with lower detection limit, provides optical absorption data and also can be used as a thermoluminescence material. Even in different colour, glass shows the characteristics of dosimetry [Teixeira *et al.*, 2007].

Soda-lime glass is made from 70%-74% of quartzite sand (silicon dioxide, SiO₂) by weight, with the remainder being other substances to simplify the processing, mainly limestone (calcium carbonate, CaCO₃) and soda ash (sodium carbonate, Na₂CO₃): for example, the melting point of silica is extremely high (1,700°C), there is a need for a fluxing agent, such as soda ash; traces of magnesia (magnesium oxide, MgO), alumina (aluminium oxide, Al₂O₃) and other such compounds, in order to refine the glass depending on application and to improve glass colour or as a colouring agent. By using copper as a

colouring agent for an instance, the glass can become blue, and even green if a higher percentage of copper oxide is used.

There are varieties of glass with different chemical compositions and hence physical qualities. They are mainly borosilicate glass, fibre glass, commercial glass and lead glass. In some special applications like in pharmaceuticals, optics and optoelectronic materials, laboratory equipment, there are special glass used which include glass ceramics, optical glass and aluminosilicate glass.

2.2.1 Atomic structure of silicon

Other than oxygen the major component of glass is silicon. Silicon has an atomic structure that changes when exposed to radiation, the incident energy being received by the electrons. Figure 2.1 shows the atomic structure of silicon.

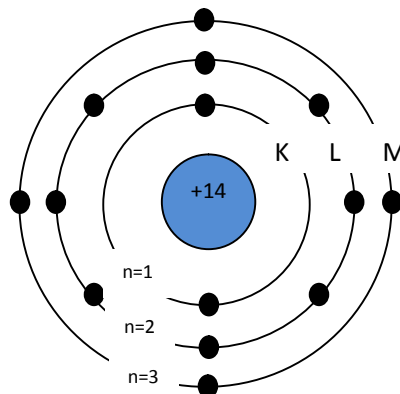


Figure 2.1 The atomic structure of silicon, Si-14.

In order to appreciate the concept of ‘quantum numbers’ of silicon, n , that relate to X-ray fluorescence, understanding of the Bohr Model is crucial. Introduced in 1913 by Niels Bohr, the Bohr Model was an improvement of Thompson (1904) and Rutherford (1911) in

the understanding of the atom. Even though it is still under debate, the Bohr Model is acceptable and relevant to quantum mechanics. The main points in the Bohr Model are,

- The nucleus (neutrons and protons) is at the centre of the atom and is orbited by electrons.
- Each orbit or energy shell or energy level has certain energy. The nearest orbit to the nucleus has the lowest energy and this increases with the orbit number.
- Electrons can jump into higher or lower orbits by absorbing or emitting radiation, respectively. This situation is supported by Planck's law as illustrated in Figure 2.2.

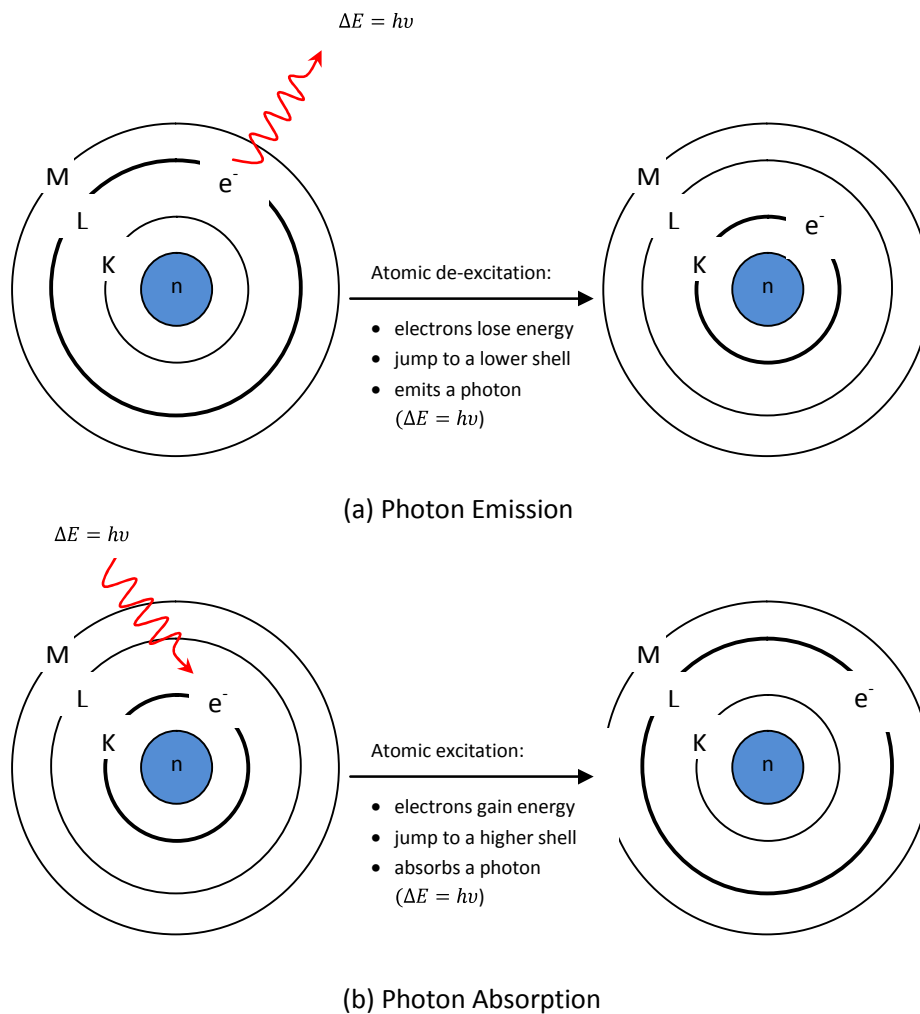


Figure 2.2 Phenomena of (a) photon emission and (b) photon absorption in general atomic structure

The Bohr Model and Planck's Law are the important parts in the basic knowledge of quantum mechanics [Svidzinsky *et al.*, 2005]. Lots more research came from popular scientists including Albert Einstein, Louis de Broglie, Heisenberg, and Schrödinger. They produced philosophy and analysis in quantum physics subject. These chronological researches provide pros and cons at satisfactory level in physics field. Among them, the Copenhagen Interpretation is the most popular explanation and extensively accepted by

scientists around the world [Tegmark, 1998]. The Copenhagen Interpretation provides the explanation and justification for quantum mechanics on mathematical formulations and experimental results that could not be covered by classical physics theory.

When linked to this work, the wave function which is one of the basic principles in the Copenhagen Interpretation, is the best for quantizing the energy levels in an atom. The wave function can explain an electron in an atom with four quantum numbers; principle quantum number (n), orbital quantum number (l), magnetic quantum number (m) and spin projection quantum number (s), as described below:

- Principle quantum number (n): shell number of an atom or an orbit in Bohr's model with $n = 1, 2 \dots$
- Orbital quantum number (l): subshell number with $l = 0, 1, 2, \dots, n - 1$ or also known as s orbital for $l = 0$, p orbital for $l = 1$, d orbital for $l = 2$ and f orbital for $l = 3$.
- Magnetic quantum number (m): subshell's shape orientation with $-l \leq m \leq l$. For instance, p orbital ($l = 1$) which has three dumb-bell shaped orbitals. Meaning, m for an electron in p orbital is -1, 0 and 1.
- Spin projection quantum number (s): intrinsic angular momentum of an electron which tells the position of electron either in 'spin up' or 'spin down'.

Consequently, by understanding this concept, the quantum numbers of silicon can be obtained and are shown in Table 2.1. In addition, the shorthand notation of the silicon atom

is $1s^2 2s^2 2p^6 3s^2 3p^2$. This explains the formation of X-ray fluorescence in silicon that will be discussed in the next section.

Table 2.1 Quantum numbers of a silicon atom.

Shell number, n	Orbit in Bohr's model	Subshell number, l	Orbital	Magnetic quantum number, m	Electrons in subshell	Shorthand notation		
1	K	0	S	0	2	$1s^2$		
2	L	0	S	0	2	$2s^2$		
			P	-1			6	$2p^6$
				0				
1								
3	M	0	S	0	2	$3s^2$		
			P	-1			2	$3p^2$
				0				
1								

2.2.2 Generation of X-ray fluorescence

The emission of energy happens when an electron jumps to a lower shell to recombine with a vacant state. The energy released is equal to the difference between the ionization energy of the two shells and is emitted as a characteristic X-ray by a process called X-ray fluorescence.

As discussed in section 2.2.1, the K shell is the shell nearest to the nucleus and has the highest ionization energy. Depending on the element the K shell is followed by L, M, N shells and so on. Each shell has its own characteristic ionization energy and these are different for every element. In silicon, the ionization energy for the K shell is 1.84 keV, the L shell is 0.11 keV and the M shell is 0.01 keV. On the other hand, the ionization energy

for the K shell in silicon is different from the ionization energy for the K shell in cadmium which is 26.72 keV.

To produce characteristic X-rays in silicon, there are a few transitions that can happen as stated below:

- K : electron transits from n=2 to n=1 level (L-to-K transition)
- K : electron transits from n=3 to n=1 level (M-to-K transition)
- L : electron transits from n=3 to n=2 level (M-to-L transition)

Figure 2.3 shows the energy levels of possible electron transitions in silicon that produce characteristic X-ray emission.

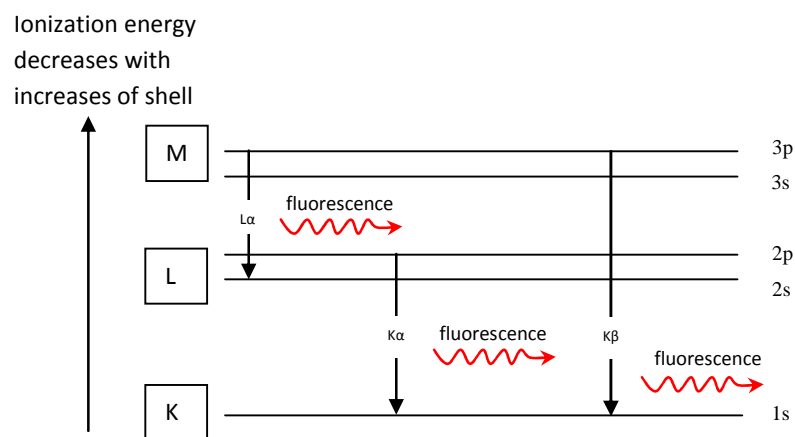


Figure 2.3 Energy level diagram of silicon showing transitions of an electron from a high shell to a lower shell resulting of the emission of a characteristic X-ray or X-ray fluorescence.

These three transitions show the generation of characteristic X-rays. The probability of this happening actually depends on the fluorescent yield of the shell. The transition of an

electron to a lower shell to fill a hole can be followed either by the emission of a characteristic X-ray or by the emission of an Auger electron. The emission of an Auger electron is a non-radiative process which happens when the energy transfers to that electron.

The fluorescence yield ω_i is depicted as a number of emitted X-rays in a particular atom when compared to the total number of ionizations as described in Equation 2.7 [Hubbell *et al.*, 1994].

$$\omega_i = \frac{Z^4}{A_i + Z^4} \quad (\text{Equation 2.7})$$

Z is the atomic number of the target atom and A is a constant for K (1×10^6) or L (1×10^8) series. Figure 2.4 shows the fluorescent yield ω_i of characteristic X-rays (K, L and M series). For silicon, Si-14, the fluorescence yield from the K-shell is 5% meaning that, the probability for transition of an electron (to fill a vacancy in the K-shell) that will result in the emission of an X-ray is 5%.

There are also lists of characteristic X-ray line energies in K-series, L-series and M-series for atomic numbers (4 to 90) that can be downloaded from (www.kayelaby.npl.co.uk). The edge energy or ‘critical excitation’ energy is the lowest energy in a particular shell that can create a vacancy (by ejecting an electron). Like silicon, Si-14, the energy of an excitation photon that can ionize K electrons must be at least 1.84 keV. On the other hand, the characteristic X-ray line energy presents the difference value in binding energies of the shell, which is between the ‘initial’ and ‘final’ vacancies. The ‘initial’ vacancy is created

from the emission of an X-ray or by the excitation of electron. The ‘final’ vacancy is then generated when an electron from that shell jumps to fill the ‘initial’ vacancy.

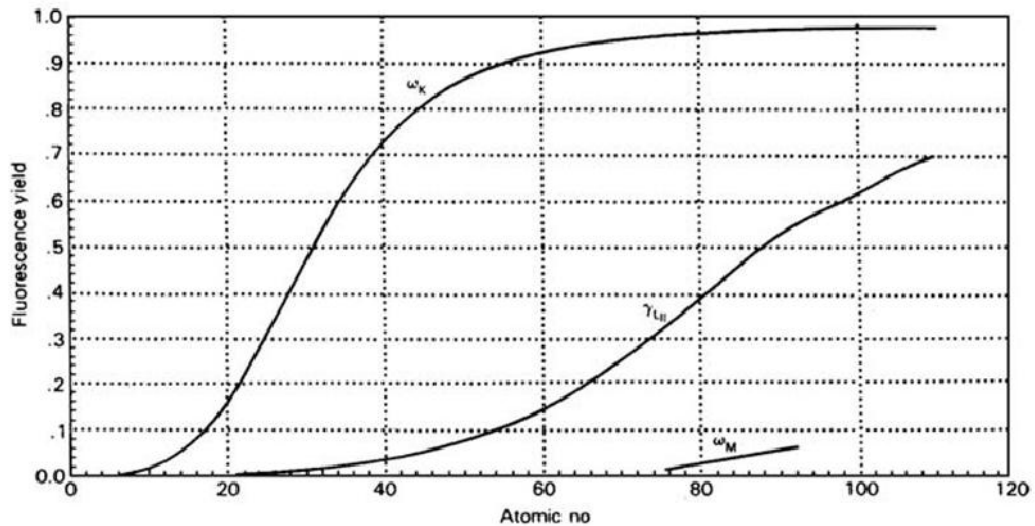


Figure 2.4 The fluorescence yield of K, L and M shell versus atomic number, Z . The K-shell plot shows the increasing number of emitted X-rays started from Be-4 and start to slow down after La-57 (www.kavelaby.npl.co.uk).

2.2.3 Photon-interactions

From the creation of a characteristic X-ray itself, an interaction has happened between an incident particle and the matter. The nature of the interaction of incident particles with matter depends on the energy of the particles as well as if they are charged or non-charged particles. Primarily, heavy charged particles (e.g. alphas, protons) with high velocities will transfer only small amount of energy (in a single collision) whenever they interact with electrons. This means that they travel in almost a straight path without deflection. As they move, they interact with many electrons and lose energy continuously primarily by ionisation. This reaction can leave an atom in an excited state.

Non-charged particles, specifically photons in this context, when they interact with the particles of the matter will undergo an attenuation process (with some of the photons). This process is related to absorption or scattering of their energy by different mechanisms, namely the photoelectric effect, Compton scattering and pair production. The factors that affect the number of photons transmitted depend on the photon energy and the materials' properties (atomic number Z , density, thickness):

- Photoelectric effect: occurs when an incident photon of energy E is absorbed and ejects electrons from the outer shell of the atom. Then, the ionized atom emits a characteristic X-ray and becomes stable. Important at low energy $E < 200$ keV.
- Compton (incoherent) scattering: occurs when the incident photon of energy E is deflected with angle θ when interacting with an atomic electron. The incident photon absorbs the energy and emits a lower energy (Compton) photon with energy E' . Important at intermediate energies 200 keV $< E < 1.5$ MeV.
- Pair production: occurs when the incident photon of energy E is converted into an electron-positron pair. Pair production only occurs above the threshold energy of 1.02 MeV. This is the dominant process for high energy photons ($E \gg 1$ MeV).

All the above interactions are dependent on mass attenuation coefficient values in order to measure the absorption or scattering energy. This is defined in the next section.

2.2.4 The mass attenuation coefficient, μ/ρ

Consider a narrow beam of monoenergetic photons with intensity I_0 , moving into matter with density ρ and thickness x . Subsequently, the photon intensity becomes I , and can be described by the exponential attenuation law where μ is a linear attenuation coefficient:

$$\frac{I}{I_0} = \exp\left[-\left(\frac{\mu}{\rho}\right)x\right] \quad (\text{Equation 2.8})$$

In common configuration, the mass attenuation coefficient is more convenient with normalization of μ with density ρ . The unit is cm^2/g .

Figure 2.5 shows the mass attenuation coefficients of silicon (cm^2/g) over the energy of photon (MeV). In general, three regions can be picked up from the graph which correlates with the processes involved during photon interactions with matter as discussed above:

- At an energy less than 0.1 MeV. This region is dominated by photoelectric absorption. There is a sharp discontinuity at nearly 0.002 MeV which is known as an absorption edge.
- The energy between 0.1 MeV to 1 MeV. This is where the Compton scattering dominates.
- At energy greater than 1 MeV. This is where pair production dominates.

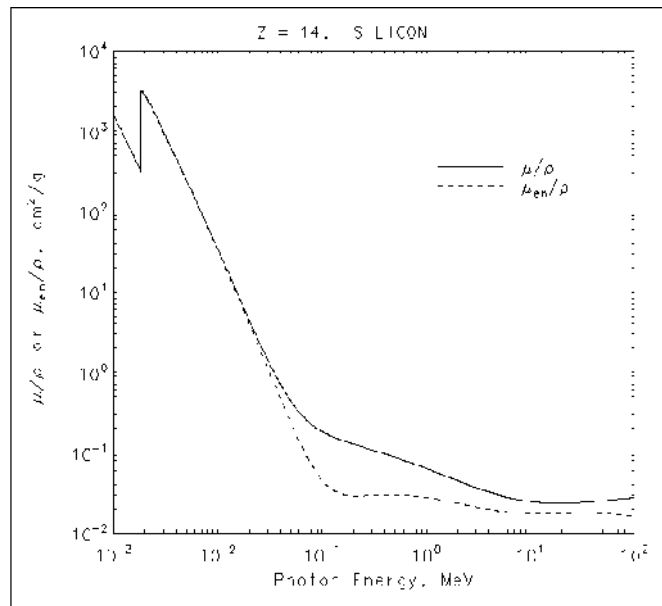


Figure 2.5 The mass attenuation coefficient for Si-14.
[\[http://www.nist.gov/pml/data/xraycoef/index.cfm\]](http://www.nist.gov/pml/data/xraycoef/index.cfm)

The edge energy and mass attenuation coefficients in every element are an individual characteristic. By looking at the values, one will know the elements contained in materials. This principle is important in the development of X-ray radiography research.

2.2.5 Radiation damage in high radiation tolerance glass

Radiation damage is best described as an event of energy transfer from incident particles of a radiation source to the material atoms. Initially, the incident particles with energy E_i strike the material atom. At this point, there are two variables involved; one is the type of radiation source, such as fast neutrons, gamma-ray, UV-ray, etc., and second is the energy of the particles involved. Subsequently, the energy E_i is transferred to the first atom it encounters which is called a primary knock-on atom (PKA).

The consequence of this event is that the atom is displaced from its lattice site and becomes an interstitial atom; this effect is important for radiation comprising heavy particles such as protons alphas and neutrons. The vacant site that was left by the atom together with the interstitial atom creates a point defect and is known as a Frenkel pair (as pictured in Figure 2.6). A group of Frenkel pairs is then created as a result of radiation damage in a crystal lattice as illustrated in the equation below in terms of the quantification of radiation damages.

$$R = N \int_{E_{min}}^{E_{max}} \int_{T_{min}}^{T_{max}} \phi(E_i) \sigma(E_i, T) \nu(T) dT dE_i \quad (\text{Equation 2.9})$$

Where R is the number of atom displacements per unit volume per unit time and N is the material atom density. $\phi(E_i)$ is the energy dependant flux, $\sigma(E_i, T)$ and $\nu(T)$ are the collision cross section between the incident particles with material atom, and the number of atom displacements, respectively. Since Frenkel defects occur within the same material there is no change of density, therefore the volume and mass remained the same.

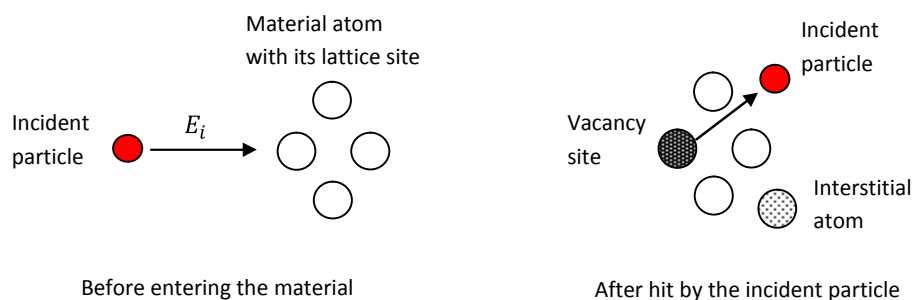


Figure 2.6 The creation of Frenkel pair (interstitial atom and the vacancy).

Frenkel pairs or Frenkel defects are one type of crystal point defect that is important in understanding silicon properties either physical or mechanical. There is also an external influence called extrinsic point defects. It is labelled as a substitutional impurity when a non-silicon atom like oxygen, dopants or carbon fills a lattice site. If they fill a non-lattice site, it becomes an interstitial impurity. These defects introduce new effects to silicon for further applications in electronic and optical fields.

2.3 Quantum dots in dosimetry

Quantum dots are a new material in dosimetry research [Stodilka *et al.*, 2009; Hong *et al.*, 2008; Miyoshi *et al.*, 2003; Liu *et al.*, 2000; Huston *et al.*, 1996]. They are in a special group of materials named semiconductors from periodic groups of II-VI, III-IV or IV-VI materials. Their size is very small, 2-10 nm (10-50 atoms) in diameter but they display unique optical and electrical properties. The smaller the quantum dots in diameter, the more energy they can produce in emitted light. They can also be found in different common shapes like pyramids, cylinders and spheres.

Quantum dots are nanocrystals typically composed from thousand of atoms and confine all electrons in three dimensions. Under optical excitation, photons are emitted as light at a longer wavelength.. The wavelength of these fluorescent photons, typically in the visible region of the spectrum, can be controlled or tuned by changing the size of the quantum dots. This ability gives industry a number of promising products and a wide range of other potential applications. They can also interact with ionizing radiation which reduces the fluorescent efficiency. Quantum dots thus show promise for potential applications in dosimetry systems.

The current commercial uses of quantum dots are in four main areas namely displays, lighting, solar and biological. In display technology, they are incorporated into organic light emitting diodes (OLEDs) which offer significant advantages to the industry. For lighting, quantum dot based LEDs deliver high quality white light that lasts longer than traditional lamps or bulbs. Quantum dots also help to provide low cost solar cells that are in demand as a cleaner energy source and also provide good resistance as coating materials in biomedical fields.

2.3.1 Quantum confinement effects

Quantum dots fluoresce when the excited electrons jump into holes at the ground state. Due to quantum confinement, the size of quantum dots is responsible for determining the fluorescence energy as shown in Figure 2.7. The energy of emitted photons is inversely proportional to the size of the quantum dot. As the energy in the band gap increases, the quantum dot size decreases and more energy is required in order to excite the electrons. At the same time, the quantum dots fluoresce by changing from red colour at lower energy to blue colour at higher energy.

Electrons in quantum dots are treated according to Pauli's exclusion principle, when the quantum dot size is smaller than the Bohr radius of the exciton, which is the average distance between electrons in the conduction band and holes in the valence band. Pauli's exclusion principle is saying that no two electrons can stay in one state or can have the same energy quantum states.

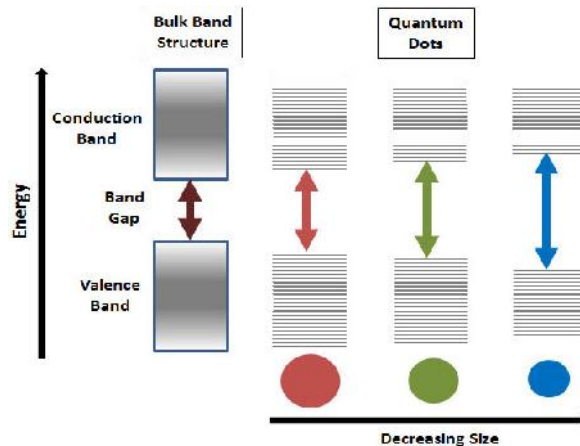


Figure 2.7 The energy level in band gap increasing with the decreasing size of quantum dots size (courtesy from www.sigmaldrich.com).

Instead of quantum dots which are in 3D quantum confinement, there are other quantum confinements available. Quantum wires and quantum wells confine the electrons or holes in 2D and 1D, respectively.

2.3.2 Synthesis of quantum dots

Quantum dots are produced in a number of ways, mainly self-assembly techniques, colloidal synthesis and 'high temperature dual-injection' used in bulk manufacturing of quantum dots. Quantum dots need an environmentally stable matrix and rigid like glass or a PVA solution as a host. The possible production methods are as follows:

- Self-assembled technique: the fabrication of two different quantum dots by lithographic process. The process is expensive and normally used for experimental studies.
- Colloidal synthesis: the synthesis of quantum dots semiconductor by dissolving the precursor compound in solution. At a certain super saturation level, the quantum

dots start to grow. The production can be made on a large scale and with non-toxic precursors.

- Bulk manufacturing: the production of quantum dots by ‘high temperature dual injection’ for hundreds of kilograms to tonnes. It includes colloidal synthesis with the additional process of molecular cluster synthesis, which is time consuming.

2.3.3 Types of quantum dots

Quantum dots can be classified in a few types depending on their structure and composition. Some of them are available commercially:

- Core-type quantum dots: single component material with uniform compositions like PbS quantum dots and CdTe quantum dots.
- Core-shell quantum dots: have an outer shell made from a different semiconductor around the core semiconductor material. It provides an increased fluorescent yield because it reduces the influence of the surface trap states which lead to non-radiative de-excitation [Reiss *et al.*, 2009]. One example is CdSe/ZnS (quantum dots of CdSe in the core and ZnS in the shell). Sigma Aldrich uses this type for their product Lumidot™.
- Alloyed quantum dots: when two different semiconductors are alloyed together and provide composition-tunable properties without changing the size. An example is cadmium selenium telluride.

2.3.4 Optical properties in quantum dots

Quantum dots show excellent characteristics to be applied in various fields especially in imaging applications. They have strong photoluminescent emission, which is the key

advantage as imaging agents [Immucci *et al.*, 2011]. Even though the quantum dots come from the same material, they can emit different light colour with the different sizes. Initial research has shown that quantum dots will damage when subject to ionizing radiation [Stodilka *et al.*, 2009].

In the work presented in this thesis, commercial core-shell CdSe/ZnS quantum dots from Sigma Aldrich (Lumidot™) were used with fluorescence spectra as shown in Figure 2.8. They are available in various sizes and kept stabilized with hexadecylamine ligands and dispersed in toluene. The ligands keep the stable interactions with quantum dots and also make quantum dots water soluble. The particle sizes used in this work were 2.5 nm (blue, $\lambda_m = 480$ nm), 3.3 nm (green, $\lambda_m = 530$ nm) and 6.3 nm (red, $\lambda_m = 640$ nm).

CdSe/ZnS quantum dots are among the radiation sensitive colloidal. They have shown high radiation-induced characteristics in research using them [Pugh-Thomas *et al.*, 2011; Liu *et al.*, 2010; Withers *et al.*, 2008]. In optical applications, quantum dots demonstrate the ability to provide the photoluminescence image during radiation exposure [Immucci *et al.*, 2011; Stodilka *et al.*, 2009].

Immucci and group [Immucci *et al.*, 2011] used the potential of fluorescent characteristics of CdSe/ZnS quantum dots in dosimetry applications. They imaged the photoluminescence of CdSe/ZnS quantum dots following one-hour of pulsed-laser illumination. Previously, they irradiated CdSe/ZnS quantum dots with a Cobalt-60 source at 0.1, 1.0, 10 and 100 Gy and measured the spectra using a fluorescence spectrophotometer. This work suggested the possibility of real-time dosimetry during the exposure to ionising radiation.

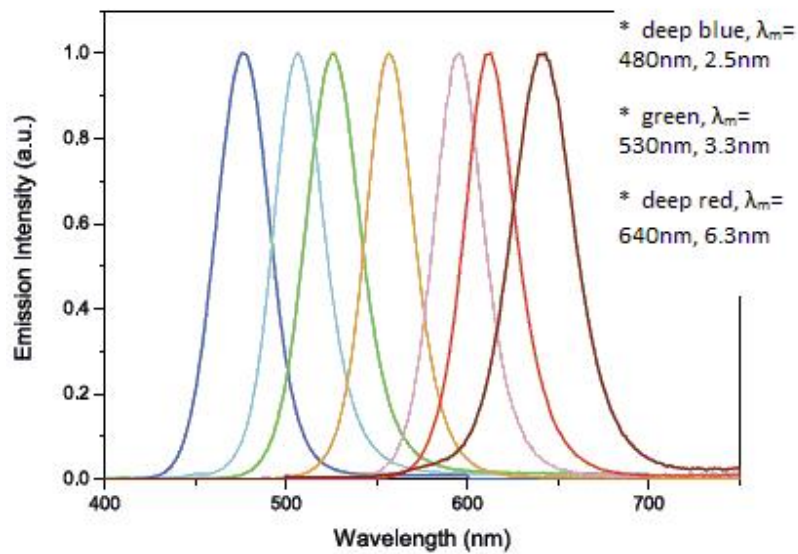


Figure 2.8 Emission spectra of core-shell CdSe/ZnS quantum dots from Lumidot. (Courtesy <http://www.sigmaldrich.com/materials-science/nanomaterials/lumidots.html>).

2.4 Modelling the radiation damage by PENELOPE

PENELOPE is a Monte Carlo code that simulates the interactions of 50 eV to 1 GeV electrons, photons and positrons in any material in complex geometries of various compositions [Francesc *et al.*, 2009]. This program is free and open software developed by a group of researchers from Universitat de Barcelona using ANSI/ISO standard FORTRAN 77 and run on FORTRAN compiler.

This simulation package was used in this thesis to facilitate the understanding of radiation energy deposition. It was related to the material damage that occurs when particles strike it with a few types of interactions, namely, elastic, inelastic and radiative collisions. In PENELOPE, the transport algorithm is controlled by a set of parameters; the

absorption energies, (EABS), an interaction distance parameter (DSMAX), lower and upper bound of cut-off angle between hard and soft elastic events (C1 and C2), and cut-off energies for inelastic collisions and bremsstrahlung emissions (WCC and WCR). These parameters are self tuned by the user.

PENELOPE has a wide range of energy and extensive geometry modelling methodology and is straightforward to use, particularly for simple geometries. The simulation is started with a main steering program that can be chosen from the package. There are `penslab`, `pencyl` and `penmain`. These codes are ready to use and users only provide simple elements depending on the application. Some applications are not applicable with these codes, so users can modify or extend the program. This is why PENELOPE was used for the work presented in this thesis. Chapters 3 and 4 will detail the work in regards to the radiation damage modelled by PENELOPE.

Chapter 3

Monte Carlo and PENELOPE

In this chapter the use of Monte Carlo codes and PENELOPE simulations are explained and discussed. It includes the investigation of the trajectories of both electrons and photons throughout the depth of a sample following irradiation as well as the effects of irradiation on individual atoms in the sample and on their scattering properties. The stability and uniformity of Monte Carlo make it the best simulation code for this application. PENELOPE is a user-friendly programme with easy language and non-complex applications, which provides the rationale for its selection. Moreover, the ability to simulate the behaviour of the sample prior to the experimental work provides invaluable insights.

Section 3.1 gives a brief overview of Monte Carlo simulation and its involvement in dosimetry. Section 3.2 explains the assumptions and basic considerations in detailing the simulation, such as the media composition, which is assumed to be homogenous, and the beam forces between particles, which are assumed to be zero. These are the fundamental approximations and modelling simplifications implemented in the presented Monte Carlo simulation. They are useful in order to ensure that a simulation runs without any interference from other factors and parameters. Section 3.3 discusses the interaction of different particles with matter, particularly photons, electrons and positrons. Section 3.4 addresses the comparison made by Baharin *et al.* (2010) between PENELOPE and CASINO simulations.

3.1 Monte Carlo Modelling

The most favourable and accurate simulation code in radiation transport is Monte Carlo code. It can describe physical processes in different media, across a range of energies and geometries. Monte Carlo simulations provide a set of particle trajectories over a period of time [Salvat and Fernández-Varea, 2009; Singh *et al.*, 2008; Napchan, 1992] and track the free movement of particles that end with an interaction event. The interactions of incident particles with target atoms generate number of effects by use of random numbers in the form of probabilistic functions. The generation of a particle track will continue until the energy loss or the secondary particles (backscattered electrons and bremsstrahlung) produced are diminished or the particle direction changes. This track or particle history is produced in a Monte Carlo simulation by using an 'interaction model' [Salvat and Fernández-Varea, 2009].

Commonly, a set of differential cross-section (DCS) of interaction mechanisms are used and provide the probability distribution functions (PDF) of random variables. These random variables characterise the track of a particle based on the type of interaction that has happened, the free path between the interaction events, the particle's energy loss and angular deflection [Salvat *et al.*, 2008; Kuhr and Fitting, 1999].

There are varieties of Monte Carlo codes for the simulation of electron and photon transport available worldwide such as GEANT4, GATE, EGSnrc, MCNPX, CASINO, PENELOPE and many more [Faddegon *et al.*, 2009; Guimarães *et al.*, 2008; Drouin *et al.*, 2007; Chiavassa *et al.*, 2005; Pfeiffer and Pia, 2002]. All types are dependent on work objectives and applications. Like in medical physics, especially radiotherapy and

brachytherapy, GEANT4 is as it was specifically developed to simulate high energy particle passing through matter for applications such as dosimetry [Guimarães *et al.*, 2008; Ivanchenko, 2003; Pia, 2003].

There are also groups that develop commercial Monte Carlo simulations for the purpose of modelling, education and training. The Radiation Process Simulation and Modelling User Group (RPSMUG) provides training in Monte Carlo simulation for non-expert personnel in mathematical modelling [Connaghan *et al.*, 2004; Saylor *et al.*, 2002; Saylor and Jordan, 2000].

The specific modelling code used for work presented in this thesis is the PENELOPE simulation code developed by scholars from Universitat of Barcelona. This code is available for users who are registered with Nuclear Energy Agency (NEA) and simulating the transport of electrons, positrons and photons in any material geometry [Salvat and Fernández-Varea, 2009; Chica *et al.*, 2008].

In this work, PENELOPE was chosen because of its stability, effectiveness on results and ease of use [Faddegon *et al.*, 2009; Vilches *et al.*, 2007]. This choice is also due to good accuracy in the description of electron transport at low energies and the detailed simulation of photon processes such as X-ray fluorescence. There is a published comparison between PENELOPE and CASINO [Baharin *et al.*, 2010] which will be discussed briefly in Section 3.4.

3.2 Simulation assumptions and considerations

In Monte Carlo, there are some assumptions and steps which are made in order to ease the simulation. Firstly, the media involved in the simulation are homogeneous with specific

composition and density, given by its stoichiometric formula (atomic number Z_i , number of atoms per molecule n_i). The molecules or atoms are assumed to be distributed randomly in the medium with uniform density. Secondly, molecules are individual in character and there is no accumulation among them. They are treated like different atoms and not linked to one another. Then, there are no forces between the beam particles. The particles are assumed to be moving in straight paths and are independent of each other [Salvat and Fernández-Varea, 2009].

Every interaction mechanism is characterised by a set of differential cross-sections (DCS). DCSs are the essential element in a Monte Carlo simulation. Each interaction and mechanism relies on related DCSs. The DCSs quantify various parameters in the probability distribution functions that are associated with the interactions such as energy transfer, angular deflection, the generation of secondary particles etc. [Salvat and Fernández-Varea, 2009; Salvat *et al.*, 2008].

To derive the DCSs, there are a few variables that need to be described. In the following sections there are considerations of the molecular structure of a sample or material that will interact with the incident particles, the energy of the incident particles and also the forces among the beam particles.

3.2.1 Molecular Structure

At lower than 10 keV of radiation energy, molecular structure is important to consider as it gives a small impact. The user must know the density and sample composition or stoichiometric index of the mixture. The effects of heavy or light atoms are different.

3.2.2 Radiation Energy

There is a significant difference when looking into the radiation energy. For any energy below 1 MeV, the interactions are producing the effects that are caused by molecular binding and aggregations. These situations are attracting experts to do more research on surface irradiation. This energy region is appropriate for surface treatment, microdosimetry and electron surface spectroscopy [Bartlett, 2008; Kovacs and Miller, 2004; McLaughlin and Desrosiers, 1995]. Higher energy, 1 to 5 MeV, is used by industrial experts in order to sterilize end-products before going to market. A lot of research being done has stated that this is the best energy range for most of the applications in medical products, tubing and cable products for high energy electrical power and polymer modification products [Doran, 2009; Kovacs and Miller, 2004; Kuntz, 2004].

3.2.3 Beam Particle Forces

Particles involved in the simulation are assumed to be spreading independently. There are no forces between or among them as presumed in elementary transport theory. Therefore the particles are moving in straight trajectories without considering other path characteristics. However this picture is only relevant with high energy radiation. In low energy, the distances between atoms and also the forces between atoms are comparable with the energy wavelength.

3.3 Particle Interactions

Monte Carlo simulation contains the transport history of particles and their interactions with matter in PDF form. As stated above, a set of DCS will provide the interaction mechanism with certain assumptions and considerations.

In the radiation transport simulation, there are number of particles that interact in the matter (molecules or atoms) with associated effects; e.g. photons, electrons, positrons, neutrons etc. are treated differently due to the energy of the radiation, particles type and number of atoms or molecules in the target matter. To look into details, further discussion is given below on photon interactions with matter. There is also a brief discussion of electron and positron interactions.

The main interaction processes of photons with atoms are photoelectric absorption, Rayleigh (coherent) scattering, Compton (incoherent) scattering and electron-positron pair production, which are shown in Figure 3.1.

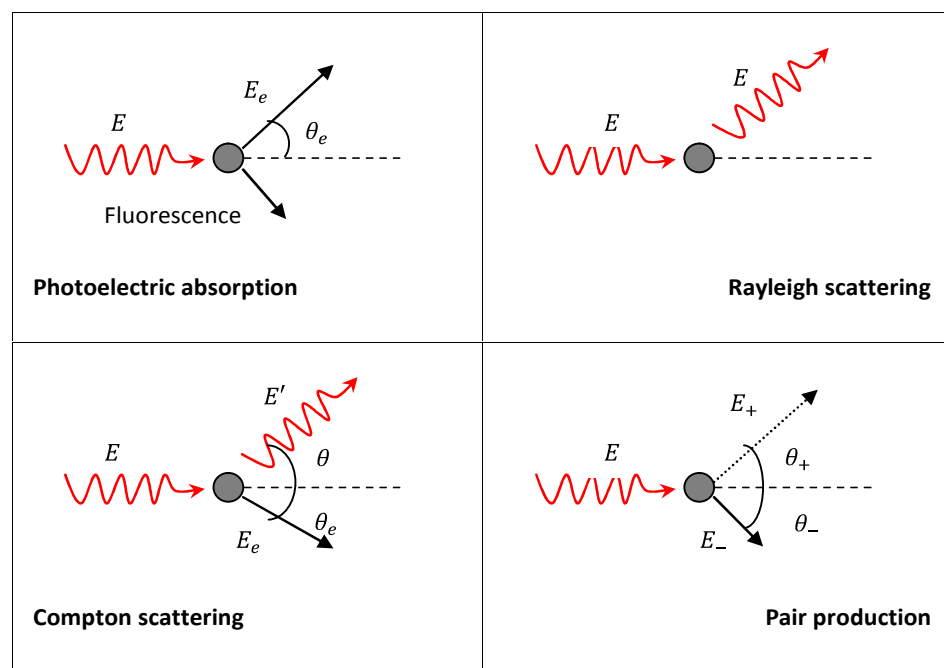


Figure 3.1 Photon interactions with matter. Reproduced from <http://www.oecd-nea.org/science/pubs/2009/nea6416-penelope.pdf> (page 54).

3.3.1 Photoelectric absorption

For low energy photon beams, photoelectric absorption or photoelectric effects is explained as the energy of a photon, E that is absorbed by an atom. This event produces fluorescence resulting from the excitation of the target atom. The simple correlation is given in Equation 3.1:

$$E_g = E - U_i \quad (\text{Equation 3.1})$$

Where, E is the incident photon energy, E_g is the photon energy that leaves the parent atom, and $-U_i$ is the binding energy of each individual shell.

3.3.2 Rayleigh scattering

In Rayleigh scattering, photon energy is scattered with no excitation effect on the target atom. The energy of incident photons and scattered photons are the same:

$$\text{incident photons, } E = \text{scattered photons, } E \quad (\text{Equation 3.2})$$

3.3.3 Compton scattering

In Compton scattering, the incident photon energy E is absorbed and a lower energy of scattered photons, E' is produced together with the energy difference between them. This energy difference, E_g , is transferred to the atomic electron:

$$E_g = E - E' \quad (\text{Equation 3.3})$$

3.3.4 Pair production

At threshold energy of 1.022 MeV, the interaction of photons with a nuclei produces an electron and positron pair. These high energy photons, E converted into mass, m by using the Einstein's equation, where c is the speed of light:

$$E = mc^2 \quad \text{(Equation 3.4)}$$

While the rest mass of an electron is 9.11×10^{-31} kg (0.511 MeV) and the same goes to positron, the energy of the incident photon must be higher than the total energy of the electron and positron in order to generate them. On the other hand, the nucleus is absorbing the momentum generated from the conversion process.

3.3.5 Electron and positron interactions

The basic interactions of electrons and positrons with matter are elastic and inelastic scattering, bremsstrahlung emission and positron annihilation as illustrated in Figure 3.2.

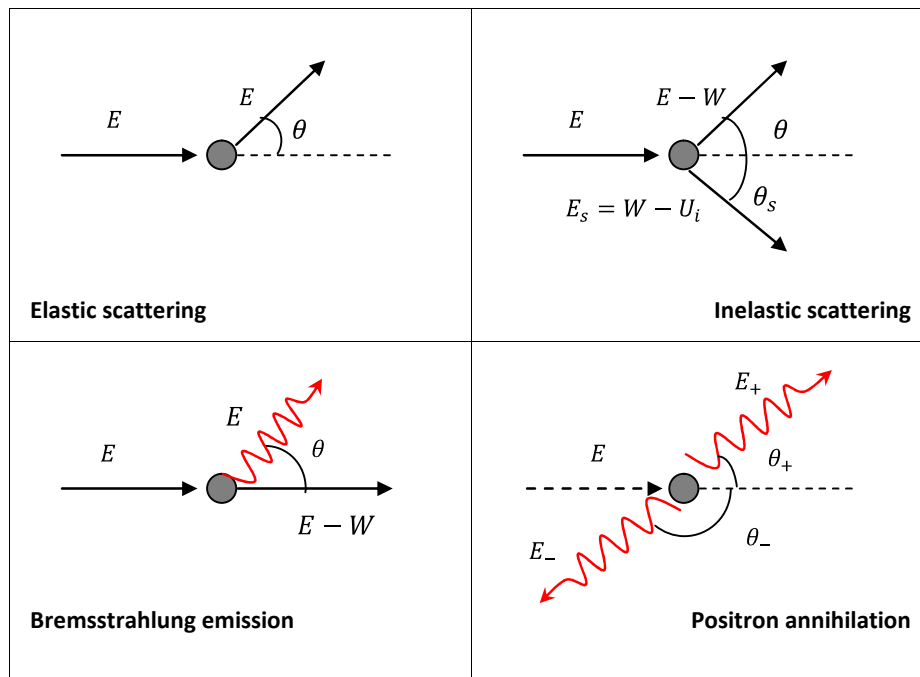


Figure 3.2 Electrons and positrons interactions with matter. Reproduced from <http://www.oecd-nea.org/science/pubs/2009/nea6416-penelope.pdf> (page 103).

3.4 PENELOPE and CASINO

In Baharin *et al.* (2010), a comparison between PENELOPE and CASINO simulation codes was done to get the reliable simulation that is need to be used in this related work. The simulation was done at 1 MeV of accelerating electrons onto a silica (SiO_2) slab of 0.1 cm thickness, which is known in this work as Silica only. The exposure was considered at the sample surface and directed towards the sample. The second sample was silica with doping of quantum dots of CdS. 1000 nm of CdS was deposited on each face of silica, making the sample look like a sandwich of CdS between silica slabs. CdS was considered

to be uniformly distributed throughout sample's surface and is referred to as CdS-Silica-CdS sample.

Figure 3.3 shows the distribution of backscattered electrons throughout the depth of samples (CdS-Silica-CdS and Silica only) by CASINO. The CdS-Silica-CdS curve was multiplied by a factor of 5 for clarity.

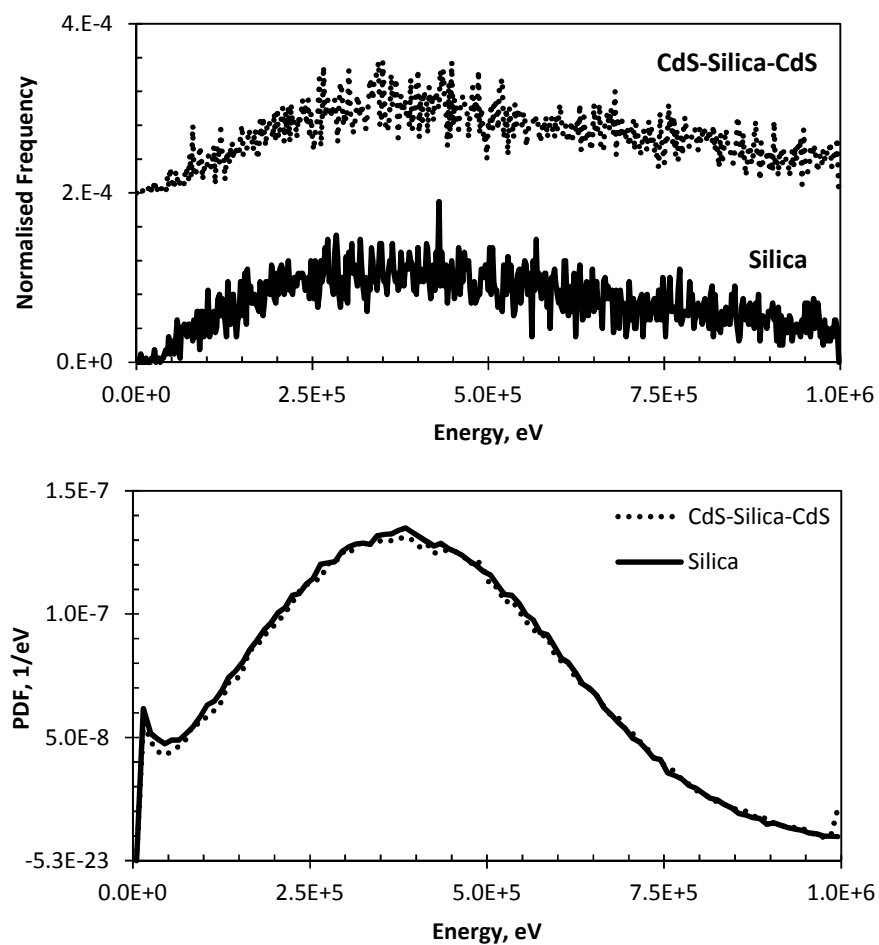


Figure 3.3 The backscattered electrons in CdS-Silica-CdS and Silica only samples by CASINO (top) and PENELOPE (bottom). The irradiation was considered by 1 MeV of accelerating voltage. Graphs are reproduced from Baharin *et al.* (2010).

The above graphs clearly show the different features of the two simulation packages. As represented in the top graph, CASINO used class I simulation which is pure condensed simulation. In this simulation, each individual particle interaction is simulated. Both curves show very high fluctuations in the data, therefore giving limitations on the statistics analysis. Using PENELOPE, the bottom graph, shows a more complex profile with respect to the electrons energy. The profile is correct when considering the bremsstrahlung photons as well as electrons.

On the other hand, PENELOPE used class II simulation or mixed simulation that deals with 'hard' and 'soft' interactions. The interactions are differentiated between 'hard' and 'soft' by looking at the energy transfer and deflection of particles. For energy transfer larger than cut-off values, it called hard interactions and soft interactions for low energy transfer. The same is done with angular deflections, where values larger or smaller than a specific cut-off value will go under hard and soft interactions, respectively.

From both type, class II simulation is quickest compared to class I. This is the advantage of time saving in computer time consumed during the simulation. Moreover, between class I and class II simulations, class II is better with a higher accuracy that comes from the exact DCSs and robustness resulting from the simulation parameters and simple tracking algorithm. On top of this, more work using PENELOPE was done. Chapter 4 shows the details.

Quoting from Baharin *et al.* (2010), "In CASINO, the electrons trajectory is moving from the entry point through the material until their energy is absorbed or they are backscattered out of the material. CASINO is however limited to planar layer structures

and does not simulate bremsstrahlung emission of photons explicitly. Mathematical models are applied to calculate the probability of the scattered electrons, the scattering angle, distance between scattering events and the energy rate loss. The more sophisticated Monte Carlo code PENELOPE enables the simulation of electrons, positrons, and photons in any material, in complex geometries, over the energy range of a few hundred eV to 1 GeV. The cross-sections acquired from both numerical databases and analytical models were used in scattering models for the different types of interaction mechanisms.”

Chapter 4

PENELOPE Simulations

This chapter describes the work done using PENELOPE simulations (2008 version) in order to study the trajectories of electrons and photons in irradiated matter. There are a number of interactions which may arise depending on a number of variables, including the type and initial energy of the primary particle, and the density of the target matter. In PENELOPE, photons, electrons or positrons in the energy range 50 eV – 1 GeV are considered. There are four basic interactions when photons hit matter; photoelectric absorption, Rayleigh scattering, Compton scattering and pair production, whilst electrons and positrons may interact via elastic scattering, inelastic scattering, bremsstrahlung emission and positron annihilation. These interactions produce important effects that need to be understood fully prior to conducting simulations.

In order to ensure understanding and appreciation for elements of the PENELOPE programme, simulations were done by referring to an example simulation provided in the PENELOPE manual (this is fully discussed in Section 4.2). Each line represents particular tasks required to achieve the simulation's aim i.e. to provide a better picture of what is happening in the matter when it is hit by irradiated particles. As such, simulation parameters need to be considered carefully (See section 4.3 on the simulation of QD doped Vycor).

Section 4.4 details simulations for different thicknesses of materials with energy deposition detectors. To best represent the experimental setup, simulations were also run for quartz (see Section 4.5). As suggested in the gamma radiation work (see Section 4.6), aluminium was used as a build-up material in front of the sample to examine the effect on particle trajectories in irradiated matter. Section 4.6 shows the difference with and without aluminium. The final part of this work described in Section 4.7 demonstrates the gamma radiation 2D imaging resolution of Vycor with a doping of QDs.

4.1 The simulation

PENELOPE is a Monte Carlo code that simulates 50 eV to 1 GeV electrons, photons and positrons in any material in complex geometries of various compositions [Francesc *et al.*, 2009]. This program is free and open software developed by a group of researchers from Universitat de Barcelona using ANSI/ISO standard FORTRAN 77 and run on FORTRAN compiler. The simulations presented in this work were run on a main program (`pencyl` or `penmain`) that only needs physical information of the material and appropriate program parameter values from the user and as such, does not necessarily require the user to be well versed in the complicated scattering and radiation transport mechanisms.

Initially, PENELOPE needs to read the physical information of each material that will be used in the simulation. The input material data file is created from the support program `MATERIAL` that gets the data from a database. There are a few questions about the material that need to be answered step by step, either by self key-in from the keyboard or by referring to `pdcompos.p08` a file that can be found in the simulation package. In this case, the user needs to know the number of atoms or the stoichiometric index of the

material. Once done, the input material data file (*material.mat*) is created and saved in the work folder. It is advisable to put all files in one work folder for the program to run.

Subsequently, the simulation will take place in either `pencyl` (electron-photon transport in cylindrical structure) or `penmain` (for general quadric structure). These are the two main PENELOPE programs, provided with the standard distribution, that work separately depending on user selection but the work structure is identical. They read an input (*.in*) file that has the same format and produce a set of fixed output files. The output files consist of generic information on simulated showers, deposited energies, distribution energy of backscattered electron and etc. Those files will automatically save, overwriting the older output file in the same directory, if applicable. Therefore, it should be borne in mind that all data needs to be saved in a different directory before every run in order to prevent the loss of older data.

In the `pencyl` program, the study of radiation transport can be based on a real system such as a radiation detector, scintillation chamber or dosimetry system. It simulates electrons and photons in any structure defined by the user and can be done in a single layer or a multilayered geometry. Within Section 4.3, the details of the `pencyl` program are discussed with reference to the package example.

Meanwhile, `penmain` is developed such that a user may run PENELOPE without having to write the main program. It also works together with the `PENGEOM` package which provides the material system geometry. In this program, the input data file controls the whole function.

Because of the sample arrangement and thesis scope, all simulations shown in this work were done using the `pencyl` program.

4.2 `pencyl` program

To perform the simulation in a certain amount of time, `pencyl` reads a simple input (*.in*) file that defines the functional data i.e. the material geometry, particle source, material data (*.mat*), simulation parameters, local maximum step lengths, absorption energies, interaction forcing, counter array dimensions, tallied ranges, energy-deposition detectors, absorbed dose, charge distributions and job properties. Furthermore, the *.mat* file has to be put together in the same work folder with *.in* file and `pencyl` application before the simulation can run. With the command prompt, the simulation starts and ends depending on time allocated. As a result, the output file is generated, which contains generic information about the simulation environment, for instance, number of transmitted, backscattered and absorbed primary particles, also a possible number of secondary particles (transmitted, backscattered and absorbed) generated, simulation speed, etc. Moreover, details of continuous distributions like depth-dose distribution, energy distribution of transmitted particles and depth distribution of deposited charge are produced in histogram profile and can be viewed using the GNU PLOT application (<http://www.gnuplot.info>). These distributions are useful in understanding the transportation and deposition energy of emerging particles.

4.2.1 Example of pencyl program

In order to explain how it works, this section discusses the worked example from the PENELOPE 2008 package [Francesc *et al.*, 2008]. This uses the `pencyl` program with the sample structure shown in Figure 4.1 and input file, `cyld.in` in Figure 4.2.

The sample structure used in this simulation consists of three layers of different thicknesses. The primary particles of photon beam with an initial energy of 1.25 MeV (E_0) are emitted from the source and move upward along the z -axis to hit the sample. In this program, the source and the sample structure are assumed to be symmetrical about the z -axis. The sample is a 7.62 cm \times 7.62 cm NaI scintillation detector (NaI is a Material 1 and named as a Mat 1 in this description) which is encased in aluminium (Al = Mat 3). The NaI depth is 9.72 cm and Al thickness is 0.08 cm. Half of the inner surface is covered by 0.16 cm thickness of Al_2O_3 (Mat 2).

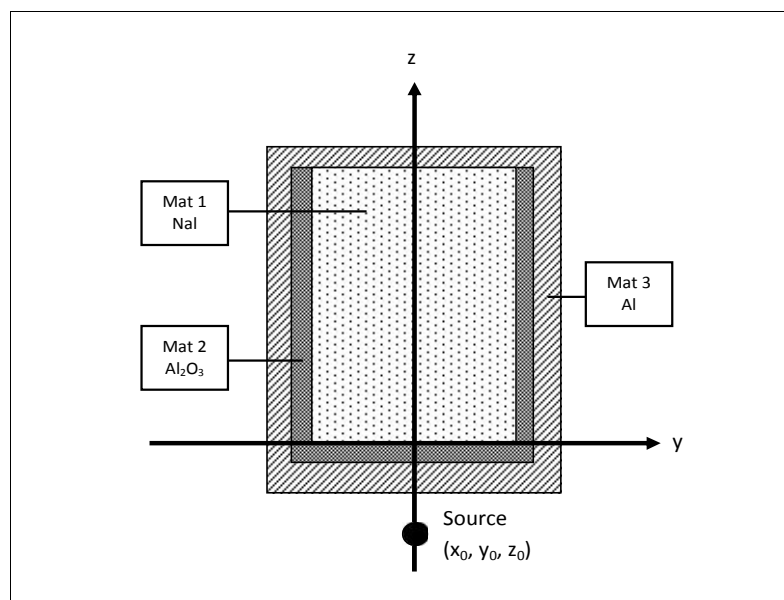


Figure 4.1 The geometry of NaI photon detector from the input file of `cyld.in`. The incident photon beam moves upwards along the z -axis (assuming $y = 0$) and hits the detector surface.

The following descriptions pertain to the input file shown in Figure 4.2. TITLE represents the work that needs to be simulated and can contain up to 65 characters. The geometry definition list may only contain the keywords of GSTART, LAYER-, CENTRE, CYCLIND and GEND--. These are followed in sequence. Each of the keywords is 6 characters in length, a dash (-) being used to replace characters as necessary. LAYER gives the lower and upper values of the z-axis plane (ZLOW ZHIGH) and the last column gives the LAYER number. CENTRE represents the sample coordinate (x,y) at z=0 and CYCLIND, the coordinates of the material in that particular layer and radius (inner and outer) of the specific layer.

The next block is a source definition. The first line (SKPAR) identifies the primary particle used in the simulation, where 1, 2 or 3 represent electrons, photons and positrons, respectively and the initial energy (in eV) is stated in the line SENERG. SPOSIT gives the source coordinates (x,y,z) and SCONE gives the beam angles (in degree) of the source.

Subsequently, the material input data and simulation parameters are defined. MFNAME is a material file name also defined in the MATERIAL program. Following this, is a set of material simulation parameters that contains absorption energies (EABS), elastic scattering parameters, C1 (M) and C2 (M), and cut-off energy losses for inelastic collisions, WCC (M) and for bremsstrahlung emission, WCR (M). The EABS were set to 100 keV, 1 keV and 100 keV so as to keep at a lower limit of the energy interval. It was recommended by the PENELOPE developer to start with the value of 50 eV. The elastic scattering parameters were set at $C1 = C2 = 0.1$. These values are limited to the interval [0,0.2] and have a very weak influence on the results.

```

TITLE  NaI detector with Al cover and AL203 reflecting foil
.
GSTART >>>>>>> Beginning of the geometry definition list.
LAYER      -0.24  -0.16  1
CENTRE     0.00   0.00
CYLIND     3      0.00  4.05
LAYER      -0.16   0.00  2
CYLIND     2      0.00  3.97
CYLIND     3      3.97  4.05
LAYER      0.00   7.72  3
CYLIND     1      0.00  3.81
CYLIND     2      3.81  3.97
CYLIND     3      3.97  4.05
LAYER      7.72   9.72  4
CYLIND     3      0.00  4.05
GENE      <<<<<<<< End of the geometry definition list.
.
>>>>>>> Source definition.
SKPAR      2                      [Primary particles: 1=electron, 2=photon, 3=positron]
SENERG     1.25e6                  [Initial energy (monoenergetic sources only)]
SPOSIT     0 0 -10.0               [Coordinates of the source centre]
SCONE      0 0 0                   [Conical beam; angles in deg]
.
>>>>>>> Material data and simulation parameters.
MFNAME     NaI.mat                 [Material file, up to 20 chars]
MSIMPA     1.0e5 1000 1.0e5 0.1 0.1 1.0e4 1000 [EABS(1:3),C1,C2,WCC,WCR]
MFNAME     Al203.mat              [Material file, up to 20 chars]
MSIMPA     1.0e5 1000 1.0e5 0.1 0.1 1.0e4 1000 [EABS(1:3),C1,C2,WCC,WCR]
MFNAME     Al.mat                 [Material file, up to 20 chars]
MSIMPA     1.0e5 1000 1.0e5 0.1 0.1 1.0e4 1000 [EABS(1:3),C1,C2,WCC,WCR]
.
>>>>>>> Energy-deposition detectors (up to 25).
ENDETC     0 1.3e6 130             [Energy window and number of bins]
EDBODY     3 1                    KL, KC [Active body; one line for each body]
.
>>>>>>> Dose and charge distributions.
DOSE2D     3 1 50 50              [Tally 2D dose and charge dists. in body KL,KC]
.
>>>>>>> Job properties.
RESUME     dump.dmp               [Resume from this dump file, 20 chars]
DUMPTO     dump.dmp              [Generate this dump file, 20 chars]
DUMPP      60                     [Dumping period, in sec]
NSIMSH     1.0e9                  [Desired number of simulated showers]
TIME       1.0e9                  [Allotted simulation time, in sec]
.
END                                               [Ends the reading of input data]

```

Figure 4.2 The input file, cyld.in used in the simulation example for pencyl program taken from PENELOPE package.

The cut-off energies, which are important to establish the simulation accuracy and speed, were set to be less than the EABS i.e. $WCC = 10$ keV and $WCR = 1$ keV. The next section details trial runs which were used to determine initial parameter settings for EABS, WCC and C1.

In the energy-deposition detectors part of the input file (see Figure 4.2), there is just one detector located with the certain number of bins and one active body at layer 3, first cylinder. Since there is just one detector, only one program (DOSE2D) is required to tally the 2D view, depth-radius, absorbed dose and charge distribution in NaI scintillator (cylinder 1 of layer 3 when referring to the input file). As a point to note, the user can put up to five different bodies with a DOSE2D in each body.

At the end of the program, there is a job of resuming and dumping the data generated. The simulation will resume at the point that it previously stopped and create a dump file at the interval time provided. It should be noted that the input file has to be the same as the previous one; otherwise the simulation will stop immediately. Throughout the program, one dot (.) is located in every definition or parameter block, in order to avoid blank lines in the input file.

PENELOPE also provides a geometric viewer, **gviewc.exe**, which gives a 2D view across the sample structures (see Figure 4.3).

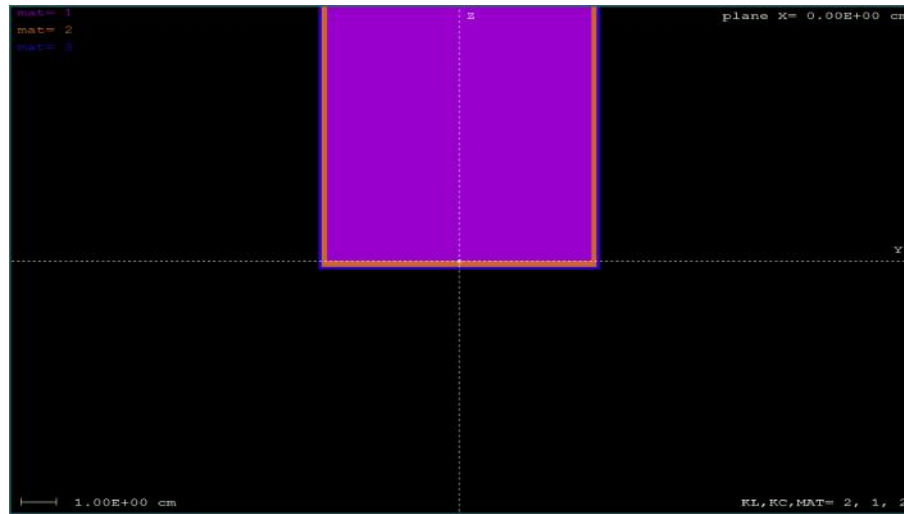


Figure 4.3 The 2D view of sample structures in cyl.d.in using gviewc.exe viewer. Mat 1 (in purple), Mat 2 (orange) and Mat 3 (blue) represent NaI, Al₂O₃ and Al, respectively.

4.2.2 Results and discussion

In pencyl, a number of distributions of simulations in materials were produced giving detailed information on particle transport and energy depositions, i.e. the depth-dose distribution, depth-distribution of deposited charge, backscattered and transmitted energy of electron, photon and positron, also the 2D dose distribution. Figures 4.4 and 4.5 give two examples of graphs generated.

Figure 4.4 shows the distribution of dose over the depth of NaI detector. Here, three events can be seen at 0 cm, 7.72 cm and at the end of graph (~9.80 cm). When the photon hits the aluminium case and inner surface, the dose curve exhibits a high surface dose and then builds up to a maximum at the entrance of NaI scintillator (Mat 1), which is at 0 cm. Subsequently, the dose drops off rapidly. This pattern occurred inside the scintillator and due to the absorption of photons by the NaI crystal would in practise be detected by

scintillation. At 7.72 cm (the exit of the scintillator), the dose makes a very small increase when the particles hit the Al case and then it drops again.

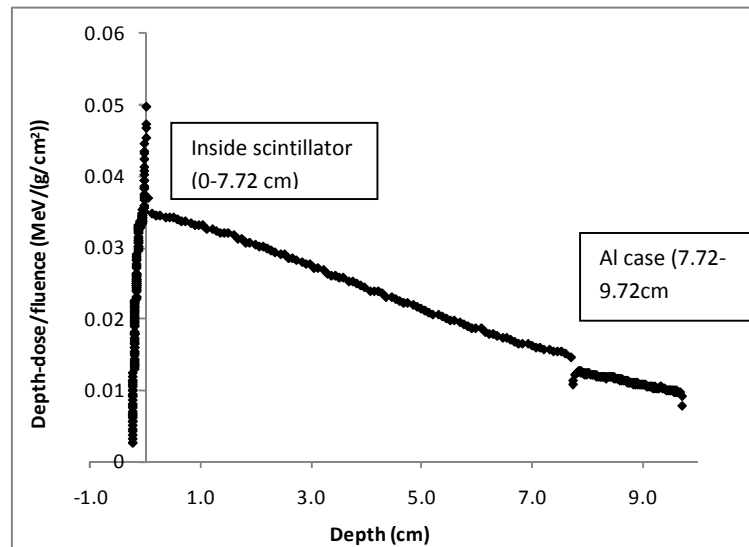


Figure 4.4 Simulated depth-dose distribution in the NaI scintillation detector when an 1.25 MeV photon beam is incident upon it.

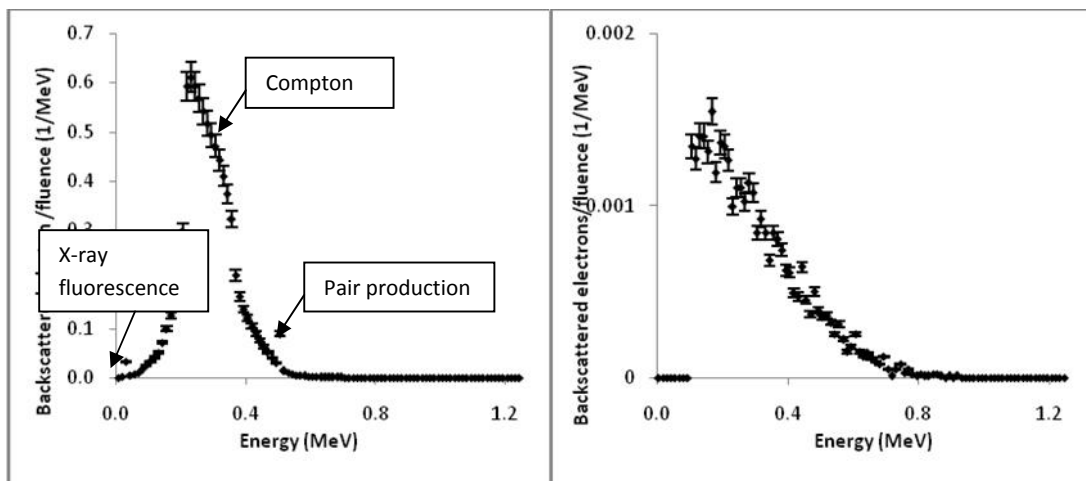


Figure 4.5 The backscattered fluence distributions of (i) photons and (ii) electrons, when the NaI scintillation detector has an 1.25 MeV photon beam incident upon it.

As illustrated in Figure 4.5 above, the distributions of backscattered photons and electrons are significantly different. The probability of backscattered photons being produced is much higher than electrons, which explains why a NaI scintillator is suitable for detecting the gamma rays. In addition, the distribution of backscattered photons shows the interaction of gamma rays with NaI crystals at three points; ~ 0.03 MeV, ~ 0.23 MeV and ~ 0.511 MeV. At low energy, X-ray fluorescence was observed when iodine (K-edge = 33.2 keV) was excited; where, at the middle energy clearly indicates the Compton scattering effect which, half the energy received by photons and the other half transferred to the scattering electrons). This drop off of energy results from the inelastic scattering which is the nature of Compton scattering. Then at 0.511 MeV, we see the effect of pair production, where one particle escapes detection.

4.2.3 Radiation damage by Compton scattering

As stated in Chapter 2, in general gamma-rays can create radiation damage in glass by the Compton scattering of electrons. It is started when an incident photon with energy E strikes the atomic electrons of particular matter (dominant in photon energy E between 200 keV to 1.5 MeV). The incident photon is then split into a low energy Compton scattered electron with angle θ , the rest of the energy being deposited in the matter. This is the point when the energy scattered is detected and the energy deposition can be quantified by a detector.

Figure 4.6 shows the trajectories of gamma particles when bombarding into 10 cm thickness of silica with 1 MeV of photon energy. The illustration was generated by the *shower* application from the simulation package.

The whole figure is a 2D material with given thickness of the material, starting from 0 cm on the left to 10 cm on the right end. The thickness and sample position are stated in the bottom right of the picture. The bottom left of the picture gives the material information. The upper left and right are legends used in the picture and energy in eV, respectively. The green line on the left side represents a source of photons with 1 MeV of energy. It is assumed there is no gap between the source and the material. It was arranged that way in order to only describe the distribution of particles inside the matter without dealing with air or other surrounding elements.

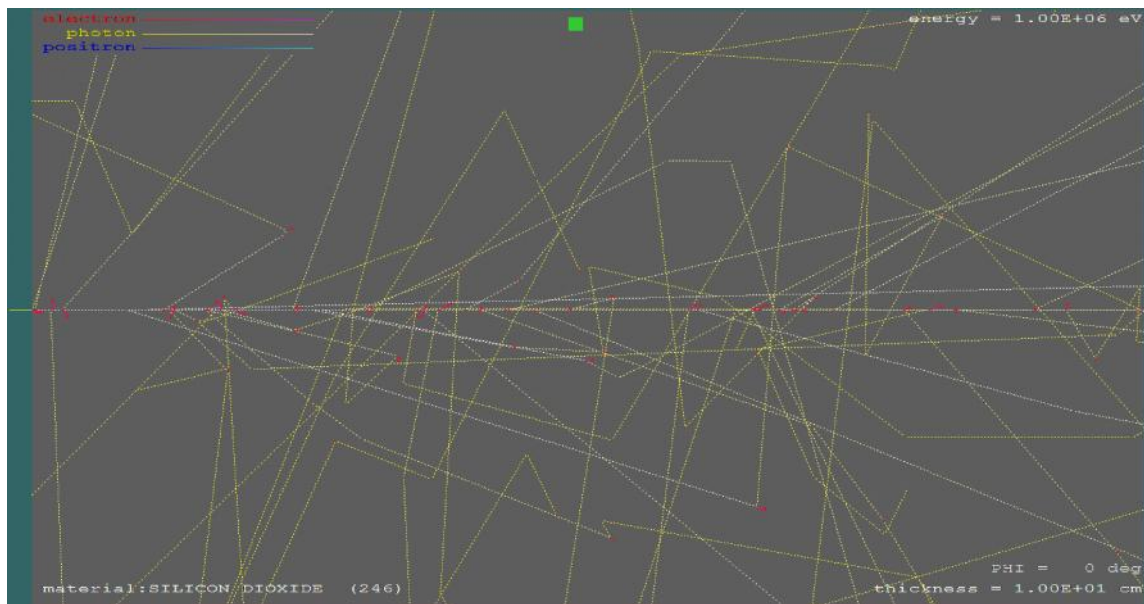


Figure 4.6 Illustration of gamma particles when entering the 10 cm of silicon dioxide with 1 MeV of energy. Yellow line representing photon, red line is electron trajectories and white line is backscattered energy.

The figure shows the particles moving randomly inside the material, deflected at certain angles. Photons and electrons are moving in a straight line in almost the same direction. However, electrons will jump out from the line at certain points because of the

collision with the materials electrons. The interactions can be Compton scattering, photoelectric effect and pair production.

Referring to the fundamental law of gamma-ray attenuation below,

$$I(x) = I_0 e^{-\mu x} \quad (\text{Equation 4.1})$$

where, I_0 is the intensity of incident gamma-ray when entering an absorber with thickness x and the emerging intensity is I . The linear attenuation coefficient μ shows the dependence of the energy of gamma-ray, atomic number of absorber and also density.

Clearly shown in Figure 4.7, the penetration of photons was stopped in a much shorter distance by lead when compared to silicon. At the same incident gamma energy and element thickness, the element's atomic number is a deciding factor contributing to the penetration depth of photons. An element with high atomic number has the possibility to stop higher energy photons. While low atomic number allows the photons to penetrate further.

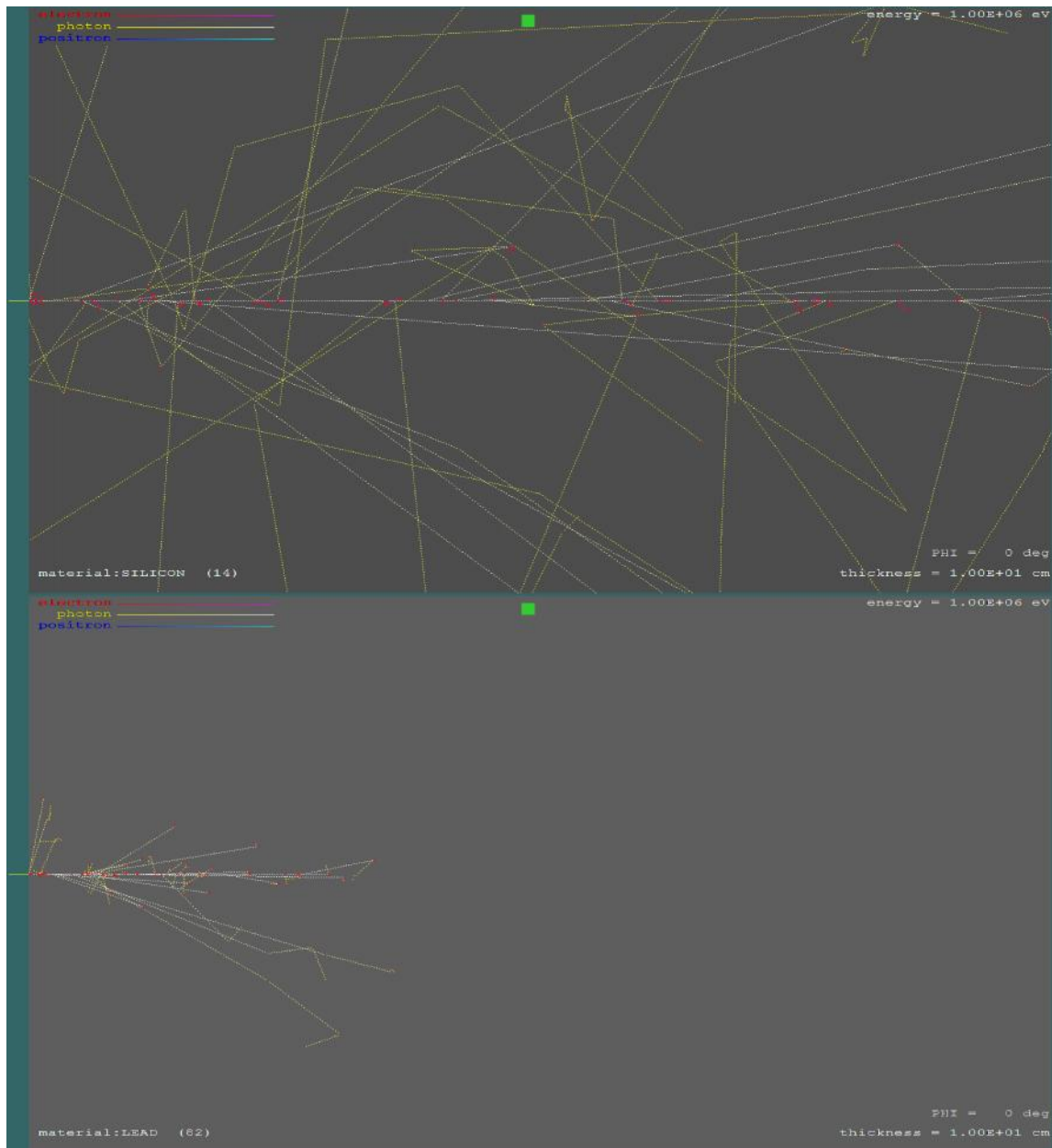


Figure 4.7 Trajectories of gamma particles when entering the 10 cm of silicon (low atomic number) and lead (high atomic number) with 1 MeV of energy illustrated at top and bottom pictures, respectively.

After all, simulation parameters are the most important values need to be considered. They drive the simulation according to the combination parameters regulated by user and this will be explained in the next section.

4.3 Simulation parameters

The PENELOPE algorithm for particle transport is determined by simulation parameters, which are the absorption energies (EABS), the distance DSMAX, lower and upper bound of cut-off angle between hard and soft elastic events C1 and C2, and cut-off energies for inelastic collisions and bremsstrahlung emissions, WCC and WCR, respectively. They can be tuned by the user in order to change the simulation time and get the range of energies needed. In fact the correct combination of simulation parameters, especially C1, C2, WCC and WCR, will explain precisely what happens during particle transport in each material. In this particular work, only five of these are considered: EABS, C1, C2, WCC and WCR:

- EABS – determined by the experiment characteristics or by required space resolution. Normally it depends on the simulation requirement or by 1% from energy of primary particles. In order to study the effect of this parameter, it is significant to start at lower energy (50 keV) with the increasing values.
- C1, C2 – set the lower and upper bound of the average energy loss of projectile particles, respectively. They put limitations on the cut-off angle of electrons between two hard events. PENELOPE limits the values at the interval [0,0.2].
- WCC, WCR – set the limitations in particles interactions between soft and hard events. WCC is important in low energy and WCR at high energy. Increasing the values will speed up the simulation.

All these simulation parameters are critical parameters due to the nature of electron, positron and photon transports algorithm of PENELOPE in material and sample arrangement.

4.3.1 Simulation on different parameters

To investigate the importance of these simulation parameters, simulations were done on a model sample of QDs in Vycor as shown in a schematic diagram in Figure 4.8. In this model, CdSe/ZnS quantum dots (QDs) are considered to be uniformly distributed within a layer of 0.001 cm thickness on the top and bottom of the Vycor glass (thickness 0.31 cm).

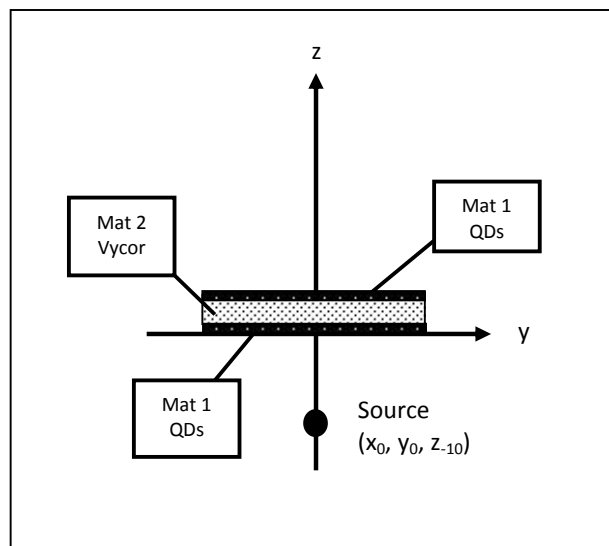


Figure 4.8 Sample arrangement of QD doped Vycor. Material 1 and 3 is CdSe/ZnS (QDs) with 0.001 cm thickness and 0.31 cm of Vycor as a Material 2. Source is located at z-axis of -10 cm.

```

TITLE 40keV of photon on sandwich of QDs and 0.31cm of Vycor
.
GSTART >>>>>>> Beginning of the geometry definition list.
LAYER          0.00 +0.001  1
CENTRE         0.00  0.00
CYLIND  1      0.00  1.00
LAYER          +0.001 +0.311  2
CENTRE         0.00  0.00
CYLIND  2      0.00  1.00
LAYER          +0.311 +3.12  3
CENTRE         0.00  0.00
CYLIND  1      0.00  1.00
GEND  <<<<<<<< End of the geometry definition list.
.
>>>>>>> Source definition.
SKPAR  2          [Primary particles: 1=electron, 2=photon, 3=positron]
SENERG 40000      [Initial energy (monoenergetic sources only)]
SPOSIT  0 0 -10.0 [Coordinates of the source centre]
SCONE   0 0 180   [Conical beam; angles in deg]
.
>>>>>>> Material data and simulation parameters.
MFNAME  CdSe_ZnS.mat [Material file, up to 20 chars]
MSIMPA  1.0e3 1.0e3 1.0e3 0.1 0.1 1e3 1e3 [EABS(1:3),C1,C2,WCC,WCR]
MFNAME  Vycor.mat   [Material file, up to 20 chars]
MSIMPA  1.0e3 1.0e3 1.0e3 0.1 0.1 1e3 1e3 [EABS(1:3),C1,C2,WCC,WCR]
.
>>>>>>> Counter array dimensions and pdf ranges.
NBTL    0 0.15 150 [Track-length interval and no. of TL-bins]
.
>>>>>>> Energy-deposition detectors (up to 25).
ENDETC  0.0 1000.e3 180 [Energy window and number of bins]
EDSPC   spc-enddet-01.dat [Output spectrum file name, 20 chars]
EDBODY  1 1 [Active body; one line for each body]
ENDETC  0.0 1000.e3 180 [Energy window and number of bins]
EDSPC   spc-enddet-02.dat [Output spectrum file name, 20 chars]
EDBODY  2 1 [Active body; one line for each body]
ENDETC  0.0 1000.e3 180 [Energy window and number of bins]
EDSPC   spc-enddet-03.dat [Output spectrum file name, 20 chars]
EDBODY  3 1 [Active body; one line for each body]
.
>>>>>>> Dose and charge distributions.
DOSE2D  1 1 100 100 [Tally 2D dose and charge dists. in body KL,KC]
DOSE2D  2 1 100 100 [Tally 2D dose and charge dists. in body KL,KC]
DOSE2D  3 1 100 100 [Tally 2D dose and charge dists. in body KL,KC]
.
>>>>>>> Job properties.
RESUME  dump.dmp [Resume from this dump file, 20 chars]
DUMPTO  dump.dmp [Generate this dump file, 20 chars]
DUMPP   60 [Dumping period, in sec]
NSIMSH  2.0e9 [Desired number of simulated showers]
TIME    7200 [Allotted simulation time, in sec]
.
END [Ends the reading of input data]

```

Figure 4.9 The input file (QDVycorQD-40keV.in) for QDs doped Vycor with simulation time of 7200 seconds. 40 keV of photons bombarded onto Vycor with 0.001 cm of QDs on top and bottom.

The main program `pency1` is used to simulate electron and photon transport in several layers of material structures. This input file (Figure 4.9) consists of the material geometry definition as in Figure 4.8, the source energy and initial photon energy (40 keV, chosen to be approximately equal to X-ray energy), the material data file, coordinates of energy-deposition detectors (3 detectors) and the simulation time (2 hours).

This simulation requires two material files; *CdSe_ZnS.mat* and *Vycor.mat*, which are partly shown in Figure 4.10 and Figure 4.11, respectively. The complete file contains detailed transitions for each shell in every single atom, including stopping power for electrons and positrons, Rayleigh scattering, Compton and pair-production cross sections, photoelectric cross sections, positron ionisation cross sections, electron ionisation cross sections, electron and positron elastic cross sections, bremsstrahlung angular distribution, electron scaled bremsstrahlung x-section. This depends on the chemical composition of the material with stoichiometric index of the elements, mass density and mean excitation energy. The full version can be found in Appendix A.

```

PENELOPE (v. 2008) Material data file .....
Material: CdSe/ZnS
Mass density = 5.5700000E+00 g/cm**3
Number of elements in the molecule = 4
  Element: Cd (Z=48), atoms/molecule = 2.85259319E-01
  Element: Se (Z=34), atoms/molecule = 4.06104357E-01
  Element: Zn (Z=30), atoms/molecule = 4.90380792E-01
  Element: S (Z=16), atoms/molecule = 1.00000000E+00

Molecular density = 2.61517870E+22 1/cm**3

*** Electron/positron inelastic scattering.
Plasma energy = 4.58154598E+01 eV
Mean excitation energy = 3.07283105E+02 eV
Number of oscillators = 29

-----
      Fi          Ui (eV)          Wi (eV)          KZ   KS
-----
  1  7.17569765E+00  0.00000000E+00  1.60857021E+01   0  30
  2  7.75640111E+00  1.22114128E+01  2.86414836E+01   0   8
  3  2.81220871E+00  2.01855592E+01  4.63236619E+01   0   5
  4  8.71488423E+00  7.36087034E+01  1.64533138E+02   0   6
  5  1.55128022E+00  1.30334589E+02  2.94571405E+02   0   5
  6  1.62441743E+00  1.66000000E+02  3.77457779E+02  34   7
  7  4.00000000E+00  1.68000000E+02  3.82078965E+02  16   4
  8  2.00000000E+00  1.70000000E+02  3.86562362E+02  16   3
  9  8.12208713E-01  1.73000000E+02  3.93345581E+02  34   6
 10  2.00000000E+00  2.32000000E+02  5.27504629E+02  16   2
 11  8.12208713E-01  2.34000000E+02  5.32024466E+02  34   5
 12  1.71155591E+00  4.08000000E+02  9.27622585E+02  48   9
 13  1.14103727E+00  4.15000000E+02  9.43529656E+02  48   8
 14  1.14103727E+00  6.21000000E+02  1.41187210E+03  48   7
 15  5.70518637E-01  6.55000000E+02  1.48916702E+03  48   6
 16  5.70518637E-01  7.75000000E+02  1.76198996E+03  48   5
 17  1.96152317E+00  1.02400000E+03  2.32810527E+03  30   4
 18  9.80761584E-01  1.04700000E+03  2.38039129E+03  30   3
 19  9.80761584E-01  1.19800000E+03  2.72369376E+03  30   2
 20  1.62441743E+00  1.43900000E+03  3.27161623E+03  34   4
 21  8.12208713E-01  1.47900000E+03  3.36255438E+03  34   3
 22  8.12208713E-01  1.65600000E+03  3.76496895E+03  34   2
 23  2.00000000E+00  2.47600000E+03  5.62926556E+03  16   1
 24  1.14103727E+00  3.54200000E+03  8.05284641E+03  48   4
 25  5.70518637E-01  3.73200000E+03  8.48481630E+03  48   3
 26  5.70518637E-01  4.02200000E+03  9.14414006E+03  48   2
 27  9.80761584E-01  9.66300000E+03  2.19691249E+04  30   1
 28  8.12208713E-01  1.26620000E+04  2.87874424E+04  34   1
 29  5.70518637E-01  2.67150000E+04  6.07373650E+04  48   1

*** Compton scattering (Impulse Approximation).
Number of shells = 21

```

Figure 4.10 Part of the material file for CdSe/ZnS that is needed in the input file (Figure 4.9). The columns labelled F_i , U_i (eV), W_i (eV), KZ and KS are the oscillator strength, excitation energy, resonance energy of bound-shell oscillator, atomic number of K shells and number of oscillators, respectively.

```

PENELOPE (v. 2008) Material data file .....
Material: Vycor
Mass density = 1.5000000E+00 g/cm**3
Number of elements in the molecule = 4
  Element: Si (Z=14), atoms/molecule = 1.0000000E+00
  Element: B (Z= 5), atoms/molecule = 2.0000000E+00
  Element: Na (Z=11), atoms/molecule = 2.0000000E+00
  Element: O (Z= 8), atoms/molecule = 6.0000000E+00

Molecular density = 4.71260330E+21 1/cm**3

*** Electron/positron inelastic scattering.
Plasma energy = 2.47144892E+01 eV
Mean excitation energy = 1.12702110E+02 eV
Number of oscillators = 11

-----
      Fi          Ui (eV)          Wi (eV)          KZ   KS
-----
  1  1.0000000E+01  0.0000000E+00  8.06097755E+00   0  30
  2  2.6000000E+01  1.36076923E+01  3.51871875E+01   0   3
  3  2.4000000E+01  3.1240000E+01  7.91460274E+01   0   2
  4  4.0000000E+00  6.6000000E+01  1.67339693E+02  11   2
  5  2.0000000E+00  1.0400000E+02  2.63621625E+02  14   3
  6  4.0000000E+00  1.0400000E+02  2.63638057E+02  14   4
  7  2.0000000E+00  1.5400000E+02  3.90349555E+02  14   2
  8  4.0000000E+00  1.9200000E+02  4.86673542E+02   5  30
  9  1.2000000E+01  5.3800000E+02  1.36366900E+03   8   1
 10  4.0000000E+00  1.0750000E+03  2.72476839E+03  11   1
 11  2.0000000E+00  1.8440000E+03  4.67392376E+03  14   1

*** Compton scattering (Impulse Approximation).
Number of shells = 10

```

Figure 4.11 Part of the material file for Vycor. The columns labelled F_i , U_i (eV), W_i (eV), KZ and KS are the oscillator strength, excitation energy, resonance energy of bound-shell oscillator, atomic number of K shells and number of oscillators, respectively.

For Vycor, the elements involved are silicon (Si), oxygen (O), boron (B) and sodium (Na), with mass density of 1.5 g/cm^3 . The number of atoms of each element is 1, 2, 2 and 6 for Si, B, Na and O, respectively. In CdSe/ZnS, there are cadmium (Cd), selenium (Se), zinc (Zn) and sulphur (S) with an estimation of 25% of each element to the stoichiometric index. The mass density is 5.57 g/cm^3 .

To study the effects of cut-off energy on the results, different values of EABS (absorption energy) and WCC (cut-off energy losses for inelastic collisions) were examined. Since, owing to the low energy used in this simulation, there is no effect on C1, C2 (cut-off angle) and WCR (cut-off energy for Bremsstrahlung emission), these were kept constant.

4.3.2 General results

As the energy is low, the interactions generated between particles and materials are expected to be low. Figure 4.12 shows the distributions generated from the default parameter settings, which are 1 keV for EABS, 0.1 for C1 and C2; and 1 keV for WCC and WCR. Changes were made for EABS and WCC. C1, C2 and WCR were kept the same as they only become important at higher energies.

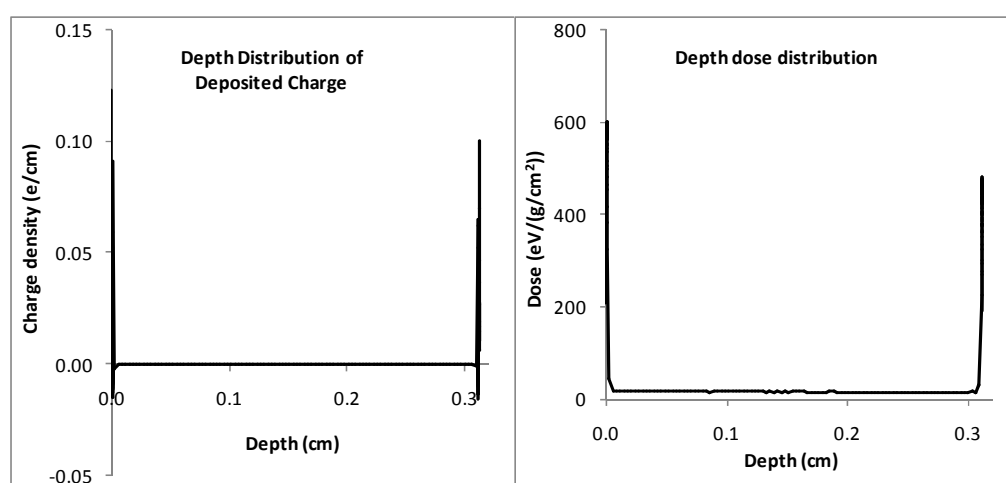


Figure 4.12 The distribution of charge density particles (left graph) and depth dose materials (right graph) from PENELOPE simulation output files. (Simulation: 40 keV of incident photons bombarded into a sandwich of QDs and Vycor).

4.3.3 Different EABS cut-off energy

Three different values of EABS were used: 0.1, 1 and 10 keV. Figure 4.13 details the fluctuation activities seen in the QD layers (0.0 to 0.001 cm and 0.311 to 0.312 cm). Overall, there is small or no charge deposited and depth dose distribution inside the Vycor as the QD works as radiation absorber. Hence the cut-off energy is likely to be no different over the depth of material.

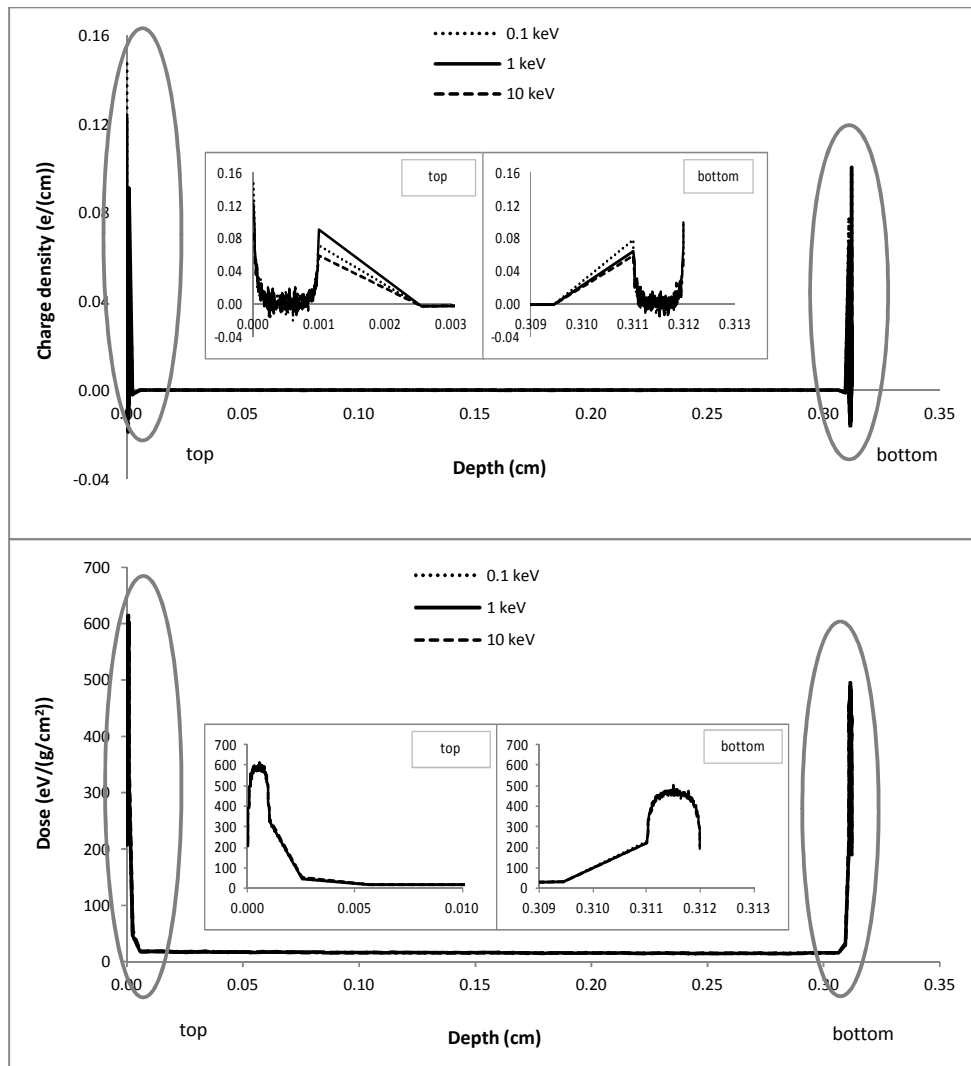


Figure 4.13 Distribution of charge density particles and dose over the depth of materials with three different values of EABS cut-off energies on top and bottom graph, respectively. (Simulation: 40 keV of incident photons incident upon a sandwich of QDs and Vycor).

Figure 4.14 shows the difference in the backscattered electrons. The 1 keV solid line appears as a good selection of cut-off energy for simulation at low energy. In fact, it is definitely true by using 1% from primary particles energy. The 0.1 keV dotted lines also

could be an option but it will slow down the simulation job. Obviously for the 10 keV dashed line there will be more points neglected even though the simulation time is faster.

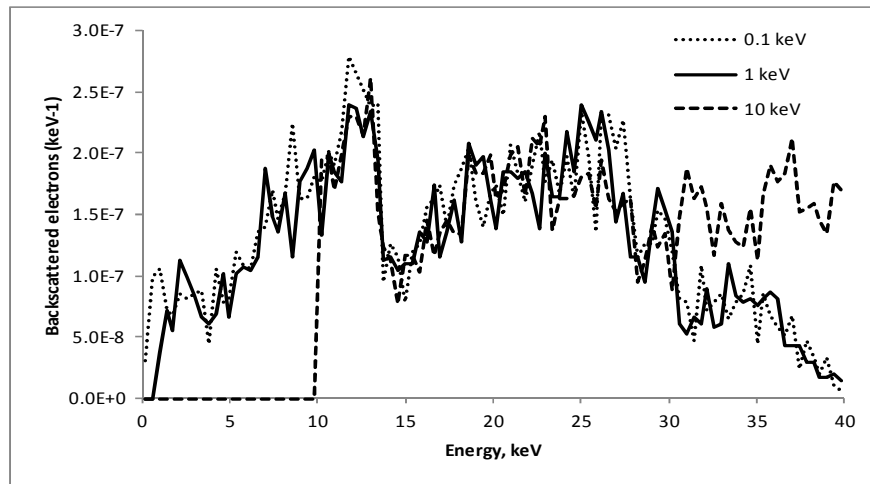


Figure 4.14 Backscattered electrons of three different cut-off energy of material absorption in a similar environment. (Simulation: 40 keV of incident photons bombarded into a sandwich of QDs and Vycor).

4.3.4 Different WCC

As well as the default settings of WCC and WCR (1 keV), two other values were examined i.e. 0.1 and 10 keV. With these three different values, there is an effect on the distribution backscattered electrons is seen, as shown in Figure 4.15. There is a consistent excess in the region of cut-off 30 to 40 keV.

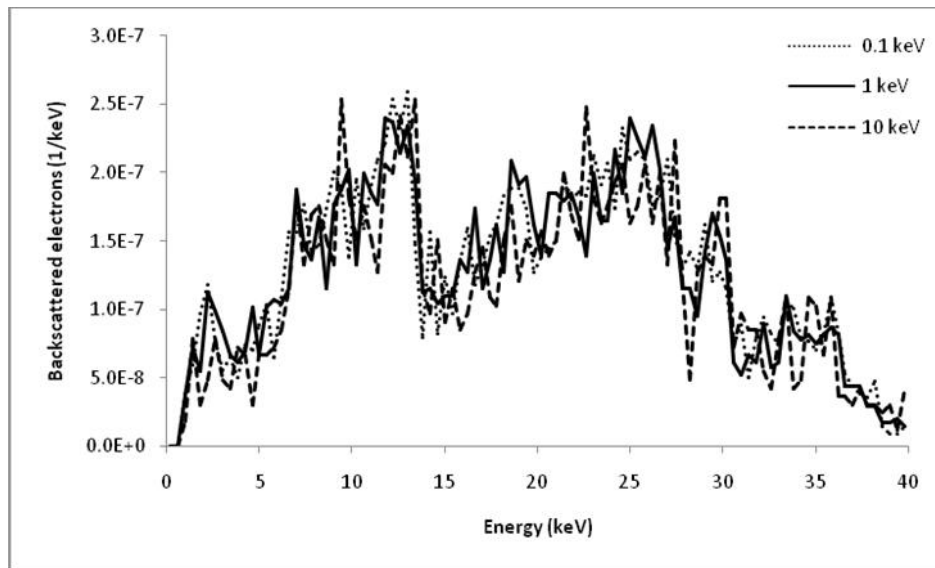


Figure 4.15 Backscattered electrons distribution with three different values of WCC; 0.1, 1 and 10 keV. There is no significant effect with the changes of WCC values. (Simulation: 40 keV of incident photons incident upon a sandwich of QDs and Vycor).

4.4 Energy deposition in every layer

There is an advantage for the user to check the energy deposited in every layer of material by using PENELOPE simulation. Up to 25 detectors may be used, meaning 25 slices or layers can be made in order to find out the value of deposited energy in each layer inside material or among the different materials. The user is required to define the layers in the geometry definition list in the input file. Each layer must have different spectrum files starting with *spc-enddet-01.dat*, followed by *spc-enddet-02.dat* and continued up to numbers of detectors required. These are included in the energy-deposition detectors block of the input file.

This simulation is carried out using the same input file from Section 4.2 (*QDVycorQD-40keV.in*). Three detectors were put on the upper layer of QD, the Vycor and bottom layer

of QD as specified in the '>>>>>>>> Energy-deposition detectors (up to 25).' section in the input file. When photons penetrate the materials, the plot of energy deposited in each layer is as shown in Figure 4.16. As expected, the Vycor had a very small amount or negligible amount of energy deposited in it, most of the deposited energy being found in the two QD-doped layers. Each QD layer shows the same energy profile with the top layer absorbing slightly more energy than the bottom layer.

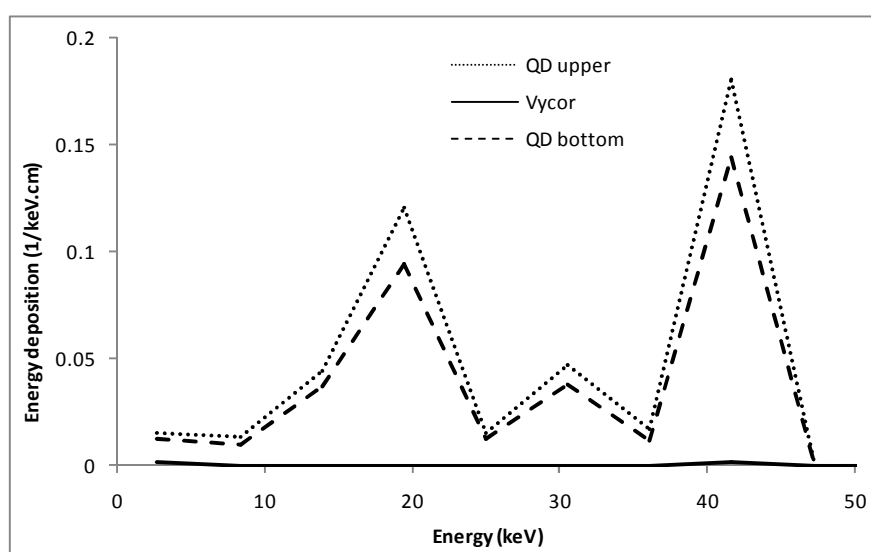


Figure 4.16 Deposited energy distribution at the top of every layer; QD upper, Vycor and QD bottom. (Simulation: 40 keV of incident photons bombarded into a sandwich of QDs and Vycor). Data were normalised to a thickness of every material.

4.5 Simulation using the quartz

To facilitate describing the energy and dose distribution work done in Chapter 6, a sample was defined as QD doped Vycor that was sealed together with quartz. It is made from Spectrosil 2000 with the dimension of 50 mm × 25 mm × 1 mm and was used to protect the quantum dots from oxygen and water vapour. Simulations were done in order to see the difference between the material with and without quartz. Comparisons were made on

depth-dose and backscattered electron distributions. These are the main characteristics in PENELOPE and happened to be the most significant factors among other outputs.

Figures 4.17 and 4.18 show the distributions from the two simulations. In Figure 4.17, the distributions are clearly different and show that quartz could be quoted as helping data to stabilize and minimizing the error. Uncertainties used in this data are at 5% error.

For dose distributions throughout the depth of material, a similar pattern is seen inside the sample in Figure 4.18 and shows no different between two simulations. In both cases, the dashed line was having a 0.1 cm of quartz taped on both side of Vycor. As a highly radiation tolerant material, quartz was used to protect QD surface from atmospheric oxygen and water vapour as these will degrade the QD.

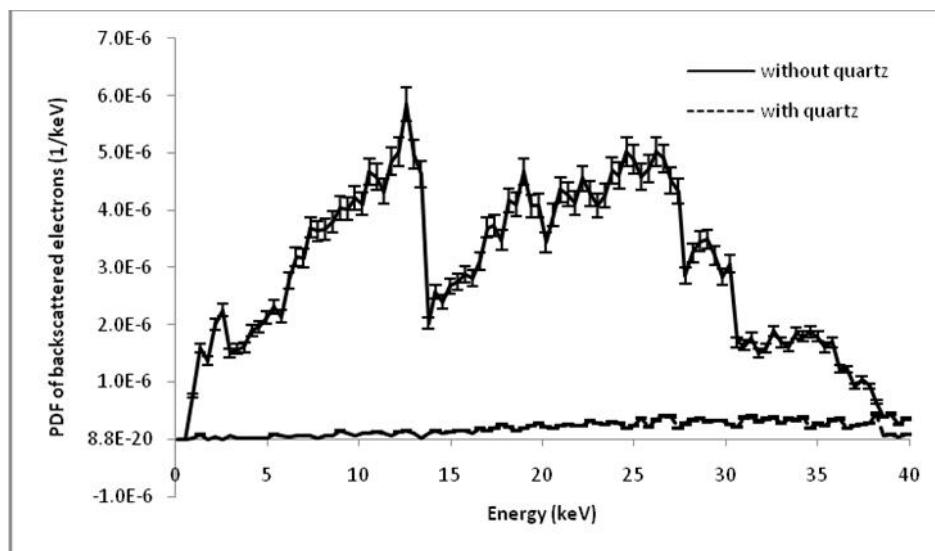


Figure 4.17 Distribution of backscattered electrons from two simulations of 40 keV of photons. The quartz helps stabilizing the data and minimizing the error.

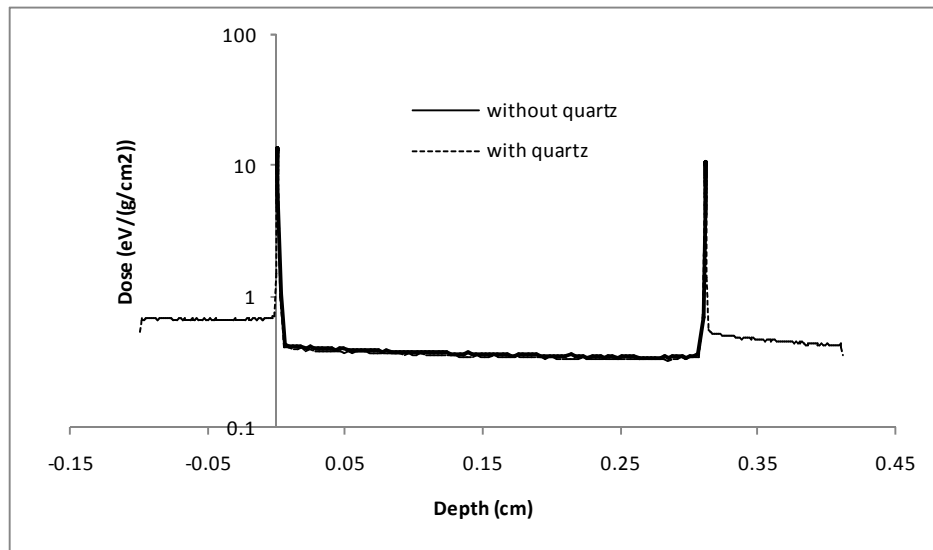


Figure 4.18 The distribution of depth dose at 40 keV on semi-log scale with thousands display unit. The dashed line is representing a piece of 0.1 cm of quartz taped on both side of Vycor and given lighter color as to show the difference of two lines.

4.6 With and without build-up material

In the radiation processing industry, build-up material is used with the purpose of enhancing the radiation onto the material. In addition, it gives uniformity to the deposited charge and dose distributions throughout the material depth (refer to Figure 4.19).

Therefore, simulations were done on Vycor with build-up material made from aluminium with a thickness of 0.16 cm and compared with the Vycor simulations without it. The point source is 1 MeV of monochromatic photons incident upon the sample.

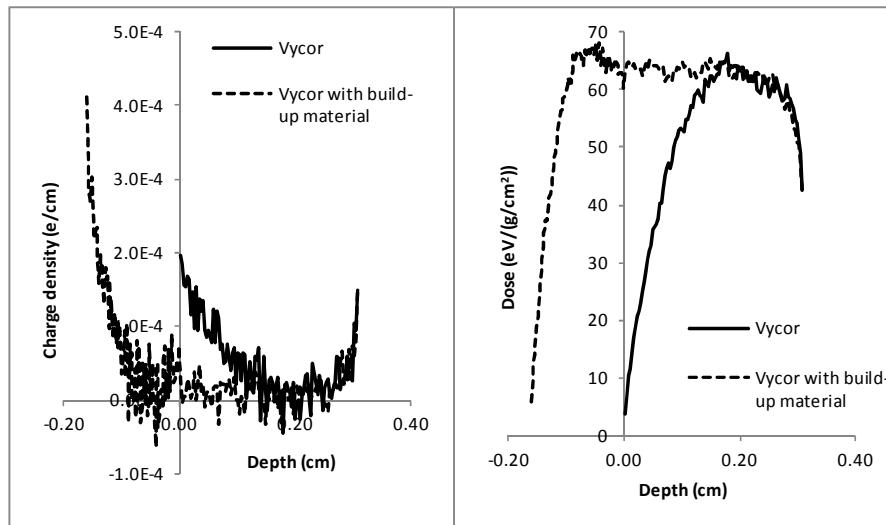


Figure 4.19 Distributions of charge density particle and dose over the Vycor depth when using build-up material and without it. (Simulation: 1 MeV of photons incident upon Vycor).

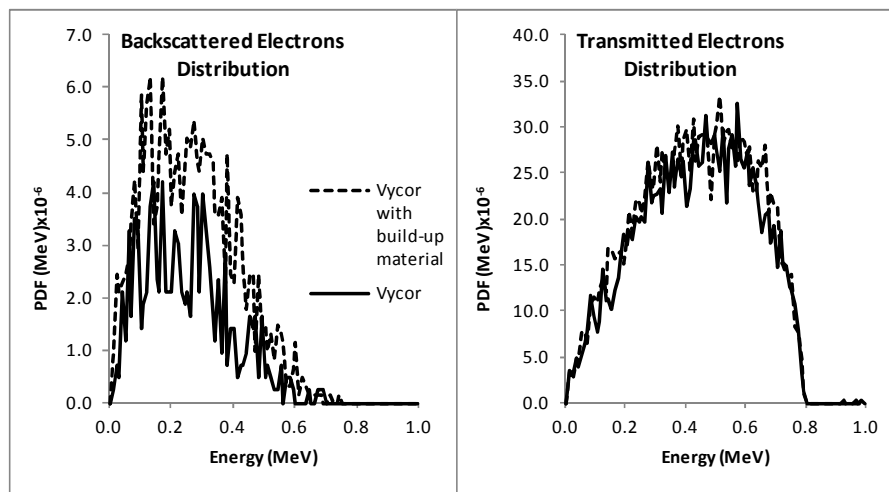


Figure 4.20 The distributions of backscattered and transmitted electrons of 1 MeV of photons over Vycor with build-up material and without it. The material increases the backscattered electrons without affecting the transmitted electrons distribution.

In the distribution of backscattered electrons shown in Figure 4.20 above, a normal pattern is seen. The backscattered electrons (BSE) start to develop at 0.1 MeV (as per absorption energies given at 100 keV) and come to an end at nearly 0.8 MeV. As energy increases, the number of BSE stops increasing after reaching 0.2 MeV. When comparing the BSE with transmitted electrons, there is a significant distribution difference between them. When energy reaches about 0.1 MeV, electrons start to differentiate into backscattered electrons and transmitted electrons. Backscattered electrons are generated when elastic collisions happen between electrons and sample atoms. As the kinetic energy does not apparently change, the trajectory of electrons deviates strongly depending on atomic number, Z of the sample, and then they escape the sample surface as backscattered electrons.

4.7 Imaging of radiation in 2D resolution

PENELOPE offers 2D imaging results from a simulation. It provides a description of the dose and charge distributions throughout the depth and radius of a target. In one dimensional graph, the consideration is taken place at one side with respect to the thickness of sample. In order to get some indication of the possibility of imaging resolution PENELOPE was used to, simulate 1 MeV photons incident upon Vycor sandwiched between layers of CdSe/ZnS. A disc of lead, of thickness 0.01 cm, with a 1 cm diameter hole in the middle was used to cover the sample to provide an irradiated region with two very different absorption and fluorescence properties.

Figure 4.21 and 4.22 show the schematic diagram of sample arrangement and input file, respectively, for this simulation.

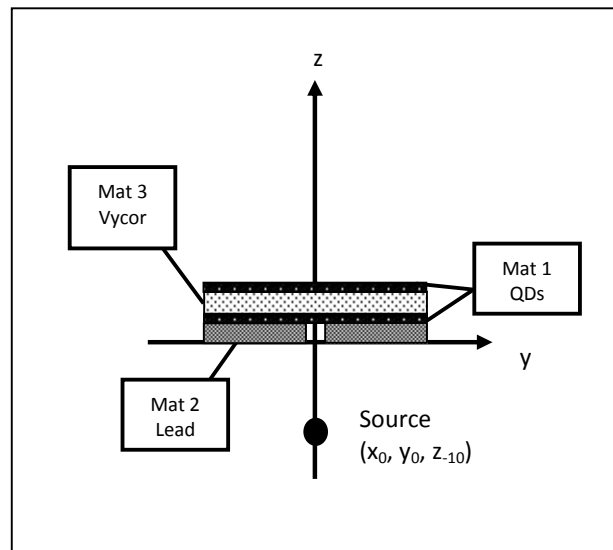


Figure 4.21 Sample arrangement of lead disc (10 cm × 0.01 cm with 1 cm diameter hole) covering the Vycor (10 cm × 0.31 cm) with sandwich of CdSe/ZnS (10 cm × 0.001 cm).

In this simulation, three detectors of energy deposition were located at the surface of the lead (Layer 2 (2 1)); CdSe/ZnS (Layer 3 (3 1)) and Vycor (Layer 4 (4 1)). The simulation was run for 2 hours. CdSe/ZnS was assumed to be uniformly distributed on the Vycor surface on both sides.

TITLE 1000keV of photon on 0.309cm sandwich of CdSe/ZnS-doped vycor with Lead barrier

GSTART >>>>>>> Beginning of the geometry definition list.

```

LAYER          0.00  +0.01  1
CENTRE         0.00  0.00
CYLIND    2    0.50  5.00
LAYER          0.01  +0.011  2
CENTRE         0.00  0.00
CYLIND    1    0.00  5.00
LAYER         +0.011  +0.32  3
CENTRE         0.00  0.00
CYLIND    3    0.00  5.00
LAYER         +0.320  +0.321  4

```

```

CENTRE          0.00    0.00
CYLIND          1      0.00    5.00
GEND  <<<<<<<< End of the geometry definition list.
.
>>>>>>> Source definition.
SKPAR           2                [Primary particles: 1=electron, 2=photon, 3=positron]
SENERG         1000000           [Initial energy (monoenergetic sources only)]
SPOSIT          0  0  -10.0       [Coordinates of the source centre]
SCONE           0  0  180         [Conical beam; angles in deg]
.
>>>>>>> Material data and simulation parameters.
MFNAME          CdSe_ZnS.mat      [Material file, up to 20 chars]
MSIMPA          1.0e4 1.0e4 1.0e4 0.1 0.1 1000 1000 [EABS(1:3),C1,C2,WCC,WCR]
MFNAME          Lead.mat         [Material file, up to 20 chars]
MSIMPA          1.0e4 1.0e4 1.0e4 0.1 0.1 1000 1000 [EABS(1:3),C1,C2,WCC,WCR]
MFNAME          Vycor.mat        [Material file, up to 20 chars]
MSIMPA          1.0e4 1.0e4 1.0e4 0.1 0.1 1000 1000 [EABS(1:3),C1,C2,WCC,WCR]
.
>>>>>>> Counter array dimensions and pdf ranges.
NBTL            0    0.15150      [Energy window and number of bins]
.
>>>>>>> Energy-deposition detectors (up to 25).
ENDETC          0.0 1.0e6 180     [Energy window and number of bins]
EDSPC           spc-enddet-01.dat [Output spectrum file name, 20 chars]
EDBODY          2  1                KL, KC [Active body; one line for each body]
ENDETC          0.0 1.0e6 180     [Energy window and number of bins]
EDSPC           spc-enddet-02.dat [Output spectrum file name, 20 chars]
EDBODY          3  1                KL, KC [Active body; one line for each body]
ENDETC          0.0 1.0e6 180     [Energy window and number of bins]
EDSPC           spc-enddet-03.dat [Output spectrum file name, 20 chars]
EDBODY          4  1                KL, KC [Active body; one line for each body]
.
>>>>>>> Dose and charge distributions.
DOSE2D          1  1  100 100     [Tally 2D dose and charge dists. in body KL,KC]
DOSE2D          1  2  100 100     [Tally 2D dose and charge dists. in body KL,KC]
DOSE2D          2  1  100 100     [Tally 2D dose and charge dists. in body KL,KC]
DOSE2D          3  1  100 100     [Tally 2D dose and charge dists. in body KL,KC]
.
>>>>>>> Job properties.
DUMPTO          dump.dmp         [Generate this dump file, 20 chars]
DUMPP           60                [Dumping period, in sec]
NSIMSH          2.0e9            [Desired number of simulated showers]
TIME            7200             [Allotted simulation time, in sec]
.
END                [Ends the reading of input data]

```

Figure 4.22 Input file.

4.7.1 Results and discussion

Results and discussion in this section have been arranged as in Figures 4.21 and 4.22, by referring to the particular areas of lead, CdSe/ZnS and Vycor together with the graphs generated. The discussion considers the dose distribution throughout the sample and the deposited charge over the designated area.

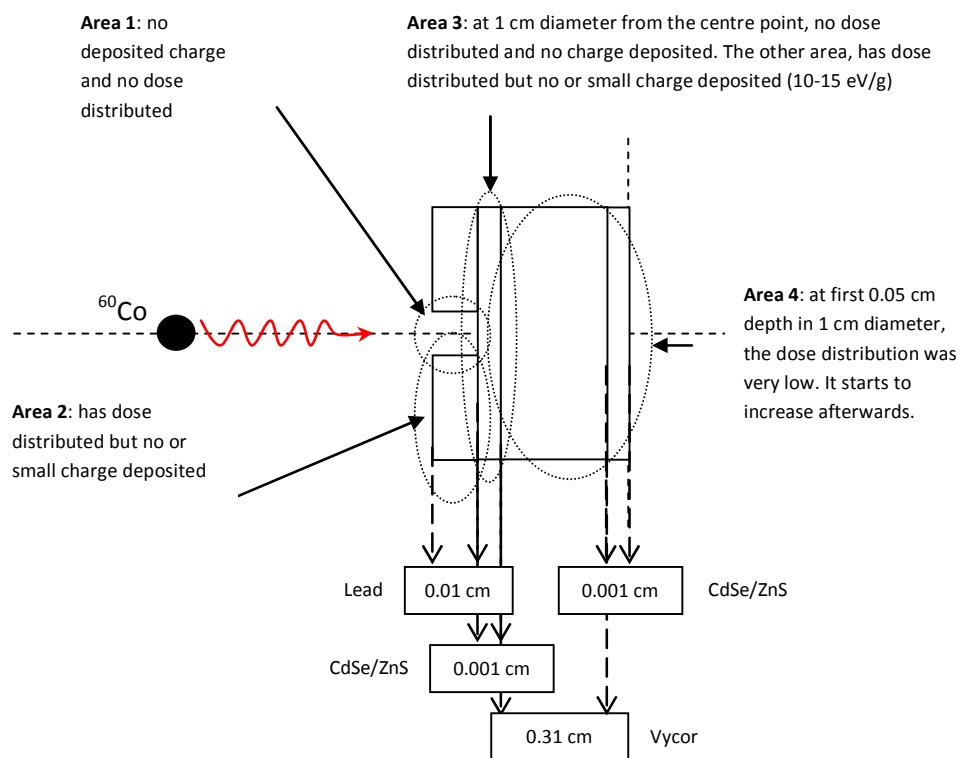


Figure 4.23 Illustration results of 1 MeV of photons bombarded toward sample (Vycor with sandwich of CdSe/ZnS) covered by lead barrier. Source is located at 10 cm from the sample. At low bottom of the picture are the thicknesses of every element in sample.

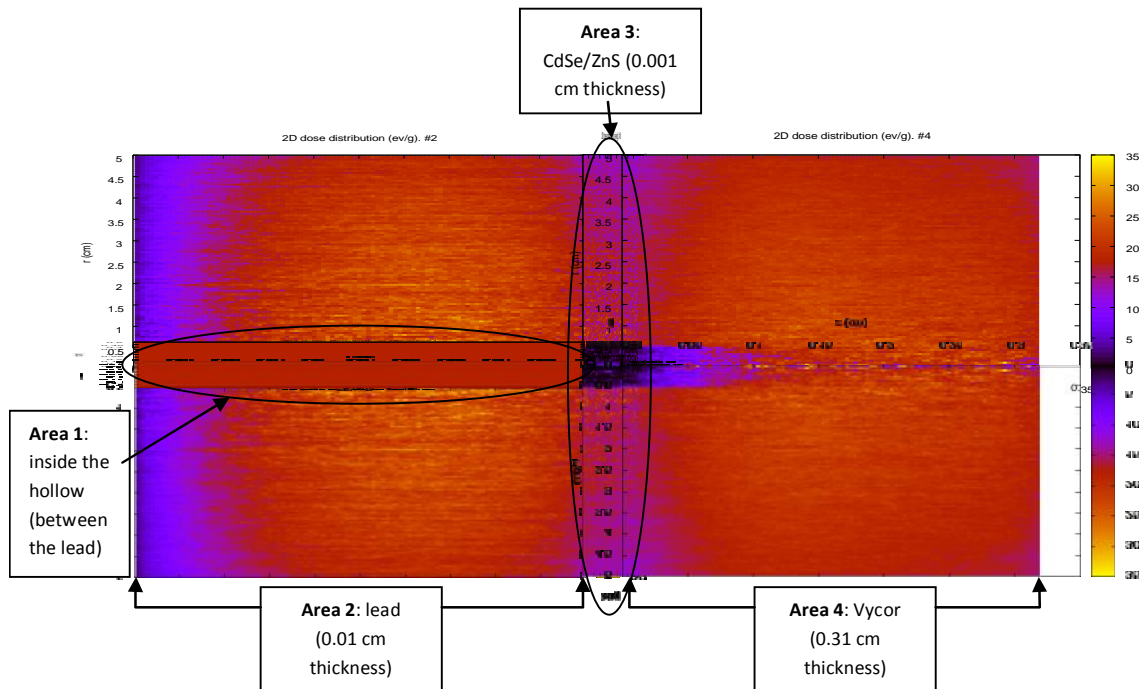


Figure 4.24 The 2D plot distribution of dose distribution inside the sample of Vycor with sandwich of CdSe/ZnS. The sample covered by a disc of lead with a 1 cm diameter hole in the centre. This is not to scale plot.

Along with Figures 4.21 and 4.22, the descriptions of each area were tackled by also referring to one dimensional profile in Figure 4.24:

- Area 1: 1 cm diameter hole in the centre of lead. It is shown that no dose or charge is deposited along this area (at the diameter of 1.0 cm) after gamma-ray bombardment of the sample.
- Area 2: Lead with 0.01 cm of thickness. The dose distribution was very small at the first of 0.002 cm of thickness and increases afterwards at the average of 15 to 20 eV/g. At the surface attached to CdSe/ZnS, the dose distribution was decreased. In contrast, the charge deposited was very small at 0 to 0.001 e/cm³.

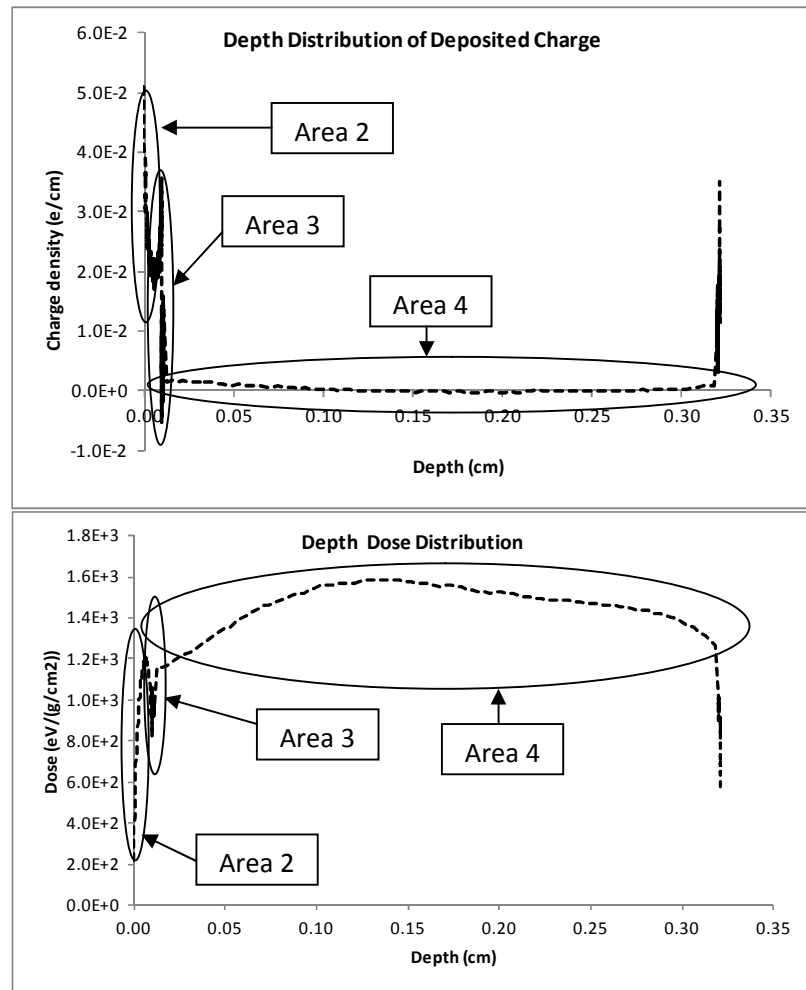


Figure 4.25 The distribution of deposited charge at top of the graph and distribution of dose at bottom of the graph, throughout the depth of sample. Area 1 is not assigned as there are no distributions of dose and charge throughout the area.

- Area 3: CdSe/ZnS with 0.001 cm of thickness. The average of 10 to 15 eV/g of dose distributed along the depth of CdSe/ZnS except at 1.0 cm diameter from the center point. This area did not receive any dose. Subsequently, the charge deposited was also low inside the CdSe/ZnS.

- Area 4: Vycor with 0.31 cm of thickness. After the first 0.05 cm at the beginning of Vycor depth in 1.0 cm of diameter, the dose distribution was very low. It starts to increase afterwards. On the other hand, charge deposited was low inside the Vycor.

4.7.2 Summary

At 1 MeV, photons interact with lead and have Compton interactions. The photons lose their energy and may be scattered around by the lead. Lead followed by QDs most likely stabilized the dose throughout the Vycor depth as seen in Figure 4.25. There is very little charge accumulating in the Vycor that can be seen in Figure 4.25 (top). Lead is helping in reducing the charges and the QDs are uniformly transferring the charge at such energies. This area (Area 3) also has very small thickness at 0.001 cm.

These are the critical findings from the image of the 2D resolution. Many discussions could be made from that with the combination of one dimensional profile graph.

To summarize, the PENELOPE simulations carried out demonstrate the potential of Vycor sandwiched between layers of QDs to image a radiation field in 2D. The software providing important data points in every layer assigned during the simulation process.

Chapter 5

Radiation Effects on Microscope Slide

This chapter and Chapter 6 detail the experimental work done on a sodium silicate microscope slide and a porous silicate glass VYCOR[®] 7930 respectively to assess their potential use in dosimetry applications in the radiation industries. The work presented includes irradiation work with a Co-60 source and optical absorbance measurements taken with a dual-beam spectrophotometer. All the work detailed was carried out by me using a Co-60 source for radiation, a Hitachi U-4100 spectrophotometer from Hitachi for optical absorbance measurements and a scanning electron microscope (SEM) for imaging.

There are three phases of work concerning these glasses; first is a study of the radiation resistance behaviour of a microscope slide in term of changes to its optical absorbance; the second phase is the study of the radiation resistance behaviour of VYCOR[®] 7930 which has apparently not been investigated previously; and thirdly, the development of an optical system for fluorescence of VYCOR[®] 7930 doped with CdSe/ZnS quantum dots, (QDs).

In terms of section organization in Chapter 5, Section 5.1 discusses the components in the glass; microscope slide and VYCOR[®] 7930. Section 5.2 describes the basic experimental work in gamma irradiation and dose verification by a Farmer 2670 ionisation chamber. Section 5.3 explains the basics of optical absorbance measurements with spectrophotometer methodology. Subsequently, Section 5.4 discusses the methodology and

experimental work employed for the microscope slide followed by conclusions on the effects of gamma radiation in term of optical absorbance in Section 5.5.

5.1 Study on glass

Samples used in this work were silicate glass microscope slide and the porous silicate glass VYCOR[®] 7930. The microscope slide is a standard slide used under a microscope. It is commercially available in the market and normally made from 70% to 74% of silica. Physically transparent, a microscope slide has poor resistance to heat, high thermal expansion and is generally good in transmitting light (depending on the exact type of glass and the light colour). On the other hand; VYCOR[®] 7930 was invented and is manufactured by Corning Incorporated, USA with 96% of silica (SiO₂), 3% of borosilicate (B₂O₃) and 1% of other elements. Compared to a microscope slide, the manufacturing process of VYCOR[®] 7930 is similar to that used in the formation of porous glass which is the etching process of borate phase from sodium-borosilicate glass. It is made for certain applications that involve thermal shock and high temperature activity, or require nanoporous inert materials, especially in science and engineering fields. Tables 5.1 and 5.2 show the approximate compositions of VYCOR[®] 7930 and a standard microscope slide, respectively.

Table 5.1 Composition of VYCOR[®] 7930 brand porous glass (Corning Incorporated, New York).

Elements	Percentage (%)
Silicon dioxide (SiO ₂)	96
Borosilicate (B ₂ O ₃)	3
Sodium oxide (Na ₂ O)	0.4
R ₂ O ₃ +RO ₂ (mostly Al ₂ O ₃ and ZrO ₂)	0.6

Table 5.2 Approximate composition of microscope slide. These compositions vary slightly due to the application.

Elements	Percentage (%)
Silicon dioxide (SiO ₂)	72.2
Sodium oxide (Na ₂ O)	14.3
Potassium oxide (K ₂ O)	1.2
Calcium oxide (CaO)	6.4
Magnesium oxide (MgO)	4.3
Aluminium oxide (Al ₂ O ₃)	1.2
Ferric oxide (Fe ₂ O ₃)	0.03
Sulfur trioxide (SO ₃)	0.3

Since the 1990's, research has been carried out on commercial plate windows for application in high-dose dosimeters for ionizing radiation [Narayan *et al.*, 2008; Farah *et al.*, 2007; Caldas and Teixeira, 2002; Rodrigues Jr. and Caldas, 2002; Zheng *et al.*, 1997; Khan and Ali, 1995]. These studies have demonstrated that commercial plate window glass is a moderately radiation tolerant glass. Due to this, the microscope slide has been chosen for this study as it has approximately similar composition to commercially available plate window glass. Both of these glasses are transparent.

The main ingredients, SiO₂ (silica) in a microscope slide and VYCOR[®] 7930, are dependent on the intended functions of glass. Silica has very strong covalent bonds Si-O-Si which is hard in structure and has a high melting point. This structure makes silica insoluble in water and organic solvents. The addition of other ingredients in the form of different elements (Na, K, Ca, Mg, Al, Fe and B) is required to adjust the physical and chemical properties of the glass depending on the final application.

5.2 Gamma-ray irradiation

Brunel University has two Co-60 irradiation sources. One is a low activity of gamma-rays at 2.4 Ci as of June 2009 and another source with higher activity at 437.6 Ci as of August 2010. All irradiation results presented were made with the sample placed at 10 cm from the source. In every irradiation, samples were handled with great care especially on the surface in order to avoid any contact with fingerprints and also surface scratches. The intensity of light transmitted from the samples will degrade with only small surface scratches [Price, 1994]. Samples were held at the edge and were kept in a special case made from plastic which was wrapped with dark cloth during the transition from laboratory room to irradiation bunker and vice versa. This helped to reduce any possibility of optical annealing of radiation damage due to artificial light sources or direct sunlight.

5.2.1 Dose verification

To validate the dose, the Co-60 source activity was monitored using a Farmer 2670. The Farmer 2670 is a dosimeter that accurately measures radiation with an air ionisation chamber. It is not influenced by the changing of temperature and time. This was done to measure the delivered dose rate to the material was accurately. The correction which needed to be applied was less than 1% when compared to the activity of gamma source versus time provided by Brunel University, calculated since the source was purchased. Table 5.3 below states the dose rate of the Co-60 source collected from the Farmer 2670 dosimeter. All data were collected in 30s time duration. Data sets 1, 2 and 5 were collected without 0.16 cm thickness of aluminium (Al) present; data sets 3 and 4 were with Al located in front of the ionisation chamber. The same Farmer 2670 dosimeter was used to calibrate the low activity of Co-60 source.

Table 5.3 Dose rate data collected from Farmer 2670 dosimeter during dose validation of high rate activity of Co-60 source.

Background (Gy/min)		Source exposed (Gy/min)				
Door open	Door close	Data 1	Data 2	Data 3 (with Al)	Data 4 (with Al)	Data 5
0.003	0.002	0.072	0.072	0.071	0.071	0.070

Background readings were taken at two situations. The first measurement was taken when the door to the facility was intentionally open, and the door was closed during the second measurement. The average measurement of both situations, 0.002 Gy/min is relatively low when compared to the gamma dose rate measurements when the source was exposed. The gamma dose rate during the source exposed is at almost 30 times higher than the background reading by the ratio comparison. When deducted the background reading, the actual dose rate was achieved.

The mean data based on the samples during the source exposure was 0.071 Gy/min and 0.071 Gy/min with the aluminium present. The dose rate ratio was 1.005.

5.3 Optical absorbance measurement by spectrophotometer

In the laboratory, optical absorbance is measured by a spectrophotometer. Practically, the spectrophotometer measures the intensity of light received by the detector at different wavelengths. The light is produced by the light source and passes through the sample after wavelength selection by a monochromator. The general structure of a spectrophotometer

consists of four parts; the light source, monochromator, sample holder and light detector. A Hitachi U-4100 spectrophotometer was used in this work and is a UV/Visible/NIR dual-beam spectrophotometer, which utilizes both ultraviolet and visible light sources:

- Light source: some examples are ultraviolet and visible light. Ultraviolet light is derived from a deuterium lamp in the 190 – 380 nm range of wavelength. Visible light is supplied by tungsten-lamp or tungsten-halogen bulb across a range of 380 – 2600nm of wavelength. The actual changeover wavelength in the UV can be selected by the user.
- Monochromator: responsible for providing single wavelength radiation selected from the available range of wavelengths. It consists of an entrance slit, a collimator, a dispersing system, a focusing lens and an exit slit.
- Sample holder: the place where sample is located during the measurement. The holder position must be at a precise and reproducible location with respect to the lightbeam.
- Detector and measuring system: The U4100 uses a photomultipliers (down to about 850 nm) and a PbS detector (for the infrared). The photodetector is the last part of the spectrophotometer, providing a signal that is proportional to the sample absorption as a function of wavelength and sent to a computer for display and data analysis.

The measurement includes the amount of absorbed light that genuinely arises from the light passing through the sample, light loss from reflections that arise from the change in refractive index between air and the sample and light loss from bulk scattering. Considering the bulk scattering effect, the measurement has to be taken as near as possible

to the detector. This will reduce the scatter effect coming from the sample before reaching the detector.

To facilitate the elimination of other contributions, absorption data is subtracted from the absorption data of an un-irradiated sample and the data obtained is then consider the radiation induced absorption only. With these data, one can evaluate the suitability of any transparent material as a dosimeter or dose indicator.

Generally, optical absorbance is defined as the amount of light absorbed into the sample when it passes through the sample at specific wavelengths as shown below in the correlation of absorbance at certain wavelengths, A_λ with light intensity:

$$A_\lambda = \log_{10}\left(\frac{I_0}{I}\right) \quad (\text{Equation 5.2})$$

In transmittance measurements, the correlation between absorbance and transmittance is given by,

$$\text{Transmittance (in percentage)} = 10^{-\text{Absorbance}} \times 100\% \quad (\text{Equation 5.3})$$

The spectrophotometer program setting was set as in Table 5.4 and identical in all measurement runs. Each measurement started with the baseline reading that needs to be recorded without the sample in the spectrophotometer. This procedure needs to be performed each time a new measurement needs to be done. The baseline is important in order to remove background noise coming from environmental elements like carbon

dioxide and impurities in the air and drift in the light sources or the photodetectors. Then, the sample was put into the sample holder located very near to the detector. During measurements, data were sent to a desktop PC and stored in ASCII format. Afterwards data were imported manually into software packages for analysis.

Table 5.4 The spectrophotometer program settings.

Wavelength	Start at 800 nm End at 200 nm Changeover at 319 nm
Scan speed	240 nm/min
Slit width	1.00 nm

In order to standardize the sample reading mechanism using spectrophotometer at all experiment work, the optical absorbance of both sample surfaces were measured. The sample surfaces were labelled as F1 (with labelling) and F2 in order to get the optical absorbance differences between them. Figures 5.1 and 5.2 illustrate no significant difference in optical absorbance for both sides of samples of microscope slide and VYCOR[®] 7930, respectively. The consideration was made in the wavelength range of 350 – 750 nm as shown in the bottom graph of both Figure 5.1 and 5.2. There might be a small difference but it is negligible. Other common experimental errors like fingerprints on the samples and dust and grease contamination from the surroundings may be responsible for the slight differences in data readings. The handling precautions taken with the samples before and during experiments helped to minimise these errors. Subsequently, for all work, it was ensured that the surface labelled (F1) faced towards detector.

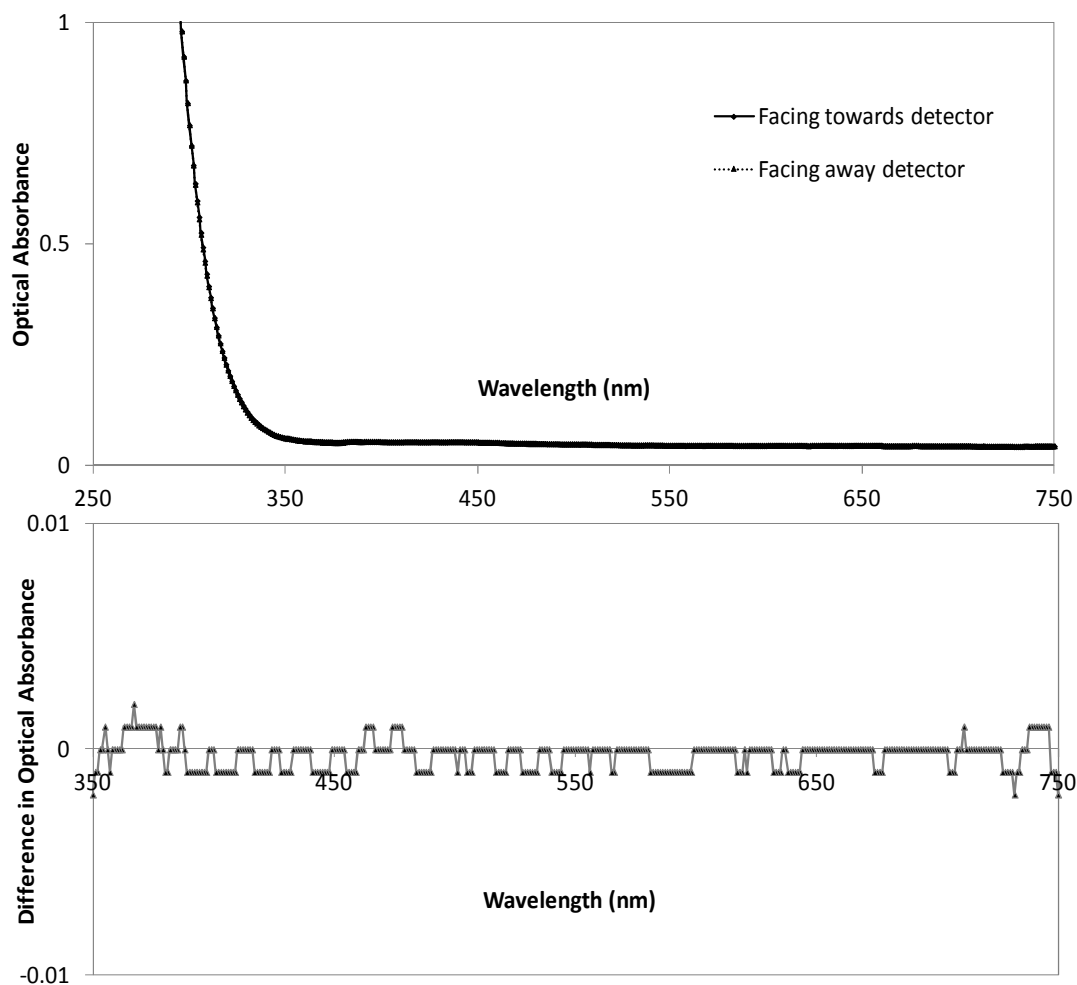


Figure 5.1 Optical absorbance of microscope slide, after 1 hour of irradiation at top figure. Darker dot is for sample facing towards detector and lighter dot for sample facing away detector. In the bottom figure, it is very consistent with less than ± 0.002 difference of optical absorbance data between both sides.

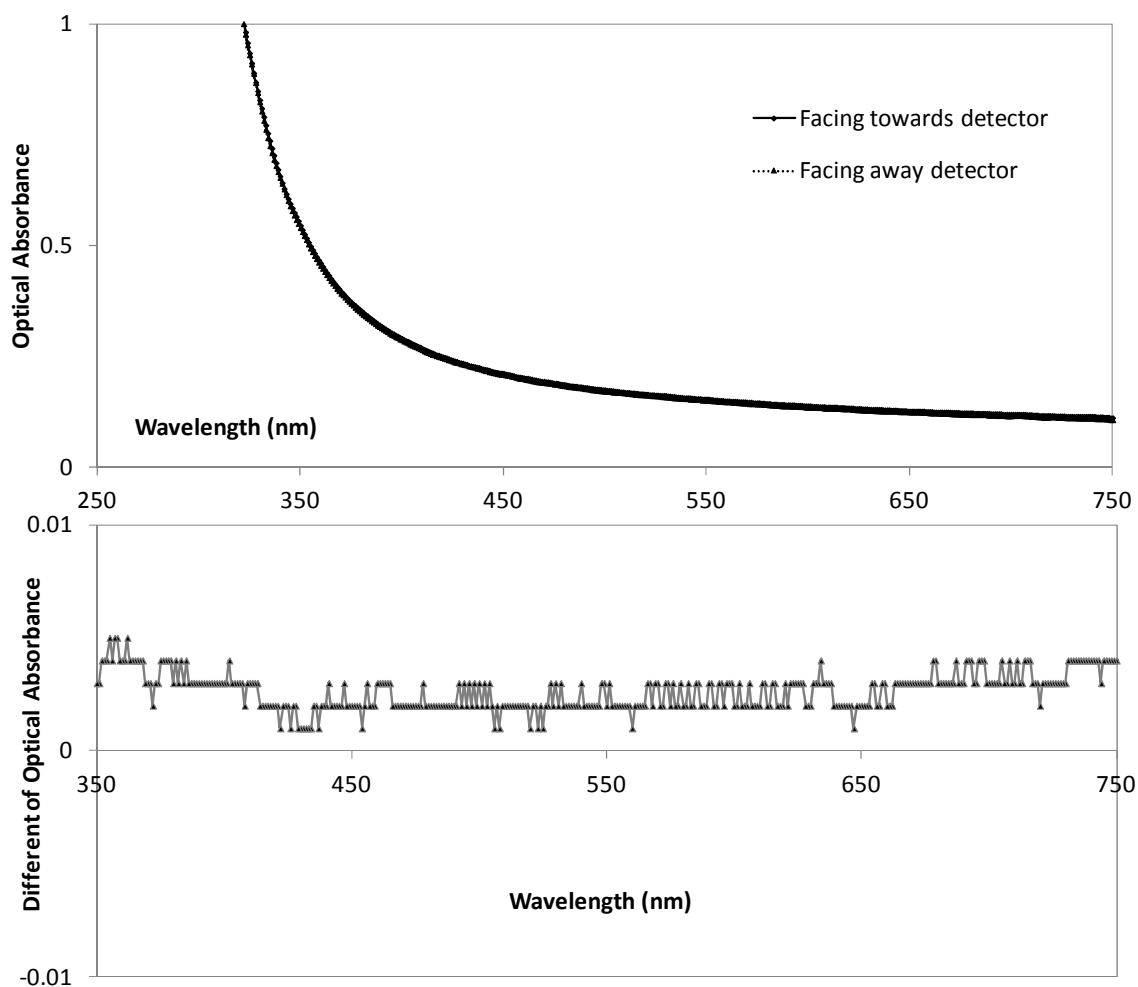


Figure 5.2 Optical absorbance of VYCOR[®] 7930, after 1 hour of irradiation at top figure. Darker dot is for sample facing towards detector and lighter dot for sample facing away detector. In the bottom figure, there is small difference of optical absorbance data between both sides but less than 0.005 OD.

5.4 Methodology: Microscope slide

In this section, experimental work was divided to the optical absorbance measurement (before and after the gamma irradiation) and gamma irradiation. Sample 1 was irradiated at 300 Gy (named as Irradiation A1) and Sample 2 was irradiated twice with 300 Gy at first irradiation followed by 600 Gy. This irradiation named as Irradiation 2. During the irradiation process, a Farmer 2670 dosimeter was used to check the dose rate.

5.4.1 Irradiation A1

For Irradiation A1, one sample of microscope slide with dimension of 2.5cm × 7.5cm × 0.1cm thick was used and labelled as Sample 1 at the left-end of the sample. The sample was placed at 10 cm from the Co-60 source. The labelled surface was treated as front slide. In this work, irradiations were done at the same dose, 300 Gy by different activities of Co-60 (at dose rate of 0.200 Gy/min and 9.13 Gy/min of low and high activities of gamma-ray, respectively. These dose rates were obtained by referring to the source activity on Dec, 2009). Both irradiations were made in order to get the influence factor from different activity of gamma-ray at same dose.

5.4.2 Irradiation A2

In Irradiation A2, one microscope slide was used, labelled as Sample 2. It was irradiated two times at different doses by an approximately 437.6 Ci as per August 2010 of Co-60. The first irradiation took 40 minutes to get 300 Gy; the second irradiation took 80 minutes to get 600 Gy. The second irradiation took place eight days after the first (the sample was stored in the dark at 20°C) which increased the total irradiation to 900 Gy.

Prior to all irradiation activities, every sample was cleaned with highly purified ethyl alcohol to remove any dirt and grease contamination, and then dried with absorbent paper. The samples were next wrapped with tissue paper and stored in a dark storage area at room temperature. Irradiation and optical absorbance measurement activities were done in a dark or dimly lit area, so that the effect of light on the samples was minimized.

5.4.3 Optical absorbance with spectrophotometer

The optical absorbance of the samples was measured using a spectrophotometer prior to irradiation. This served as a reference in order to determine the induced absorbance of the irradiated samples. After one hour of irradiation, the optical absorbance of the samples was measured again. For consistency, all measurements were done at one hour after irradiation [Teixeira *et al.*, 2007; Farah *et al.*, 2007]. The measurement was taken at the starting wavelength 800 nm, down to 200 nm. The samples were kept in an air-conditioned dark storage area at room temperature, 20°C. The optical absorbance measurement of Sample 1 from Irradiation A1 was also taken at subsequent times over a period of 175 days in order to investigate the fading effect of glass due to the gamma irradiation.

Table 5.5 shows the summary of gamma irradiation experiments and optical absorbance measurement on microscope slide samples.

Table 5.5 A summary of gamma irradiation experiments and optical absorbance measurement for microscope slide samples.

Irradiation (Samples)	Dose (Gy)	Dose rate of gamma-ray (Gy/min)		Optical Absorbance Measurement (OD)	
A1 (Sample 1)	300	0.20 at 10cm of low activity	9.13 at 10cm of high activity	<ul style="list-style-type: none"> • Before irradiation 	<ul style="list-style-type: none"> • 1hr after irradiation • 1 to 175 days after irradiation
A2 (Sample 2)	First at 300 Second at 600	0.75 at 10 cm of high activity		<ul style="list-style-type: none"> • Before irradiation 	<ul style="list-style-type: none"> • 1hr after irradiation

5.5 Results and analysis for microscope slide

By measuring the optical absorbance of a microscope slide before and after the irradiation, the radiation induced absorbance, fading effect and the reproducibility of the data can be discussed. The effect of the activity of Co-60 source at the same dose applied to the sample is also considered. After irradiation, the colour of the microscope slide is changed from clear glass to a yellowish tint.

5.5.1 Reproducibility

Reproducibility is important in order to maintain the constancy of every single dosimeter [Narayan *et al.*, 2008; Caldas and Teixeira, 2002]. It indicates good manufacturing processes and how stable the material is. Microscope slide glass and commercial window

glass [Narayan *et al.*, 2008; Farah *et al.*, 2007; Rodrigues Jr. and Caldas, 2002; Zheng *et al.*, 1997; Khan and Ali, 1995] have demonstrated reliable reproducibility. Both of them are mainly made from silica in a range of 72% – 76%. Previous studies have shown the value of silica as a main component in radiation tolerance glass.

The induced optical absorbance at 300 Gy for Sample 1 and 2 was measured in order to study the reproducibility effect in dosimetric techniques. The particular wavelength range of interest is from 400 to 440 nm, which is the absorption band area for most samples of this type of glass [Narayan *et al.*, 2008; Caldas and Teixeira, 2002; Zheng *et al.*, 1997].

Table 5.6 Reproducibility of gamma-irradiated microscope slide referring to the optical absorbance within the wavelength range of 400 to 440 nm.

	Sample 1	Sample 2
Mean of the samples	0.0699	0.0657
†	0.0000469	0.0000736

Table 5.6 shows the results by looking at the standard deviation of the optical absorbance in the range of 400 to 440 nm of wavelength. The variation (σ) between samples indicates that both samples have similarity and has well reproducible between samples. The samples need to be dust free with no scratches on the surface in order to lessen the variation of optical absorbance data.

5.5.2 Induced absorbance at different dose

The top graph in Figure 5.3 shows the optical absorbance spectra of a gamma-irradiated microscope slide as a function of wavelength from 250 to 750 nm at 300 Gy and 900 Gy, for different accumulated dose. At the bottom graph shows the radiation induced absorption spectra for the same sample.

All graphs were normalized to the sample's thickness, 1 mm. There were two optical absorption bands found, in the range of 350 – 450 nm and in the range of 600 - 620 nm, which were identical for all doses. These absorption bands were caused by the colour centres created by the radiation. Both doses present similar pattern of absorption bands but different intensity.

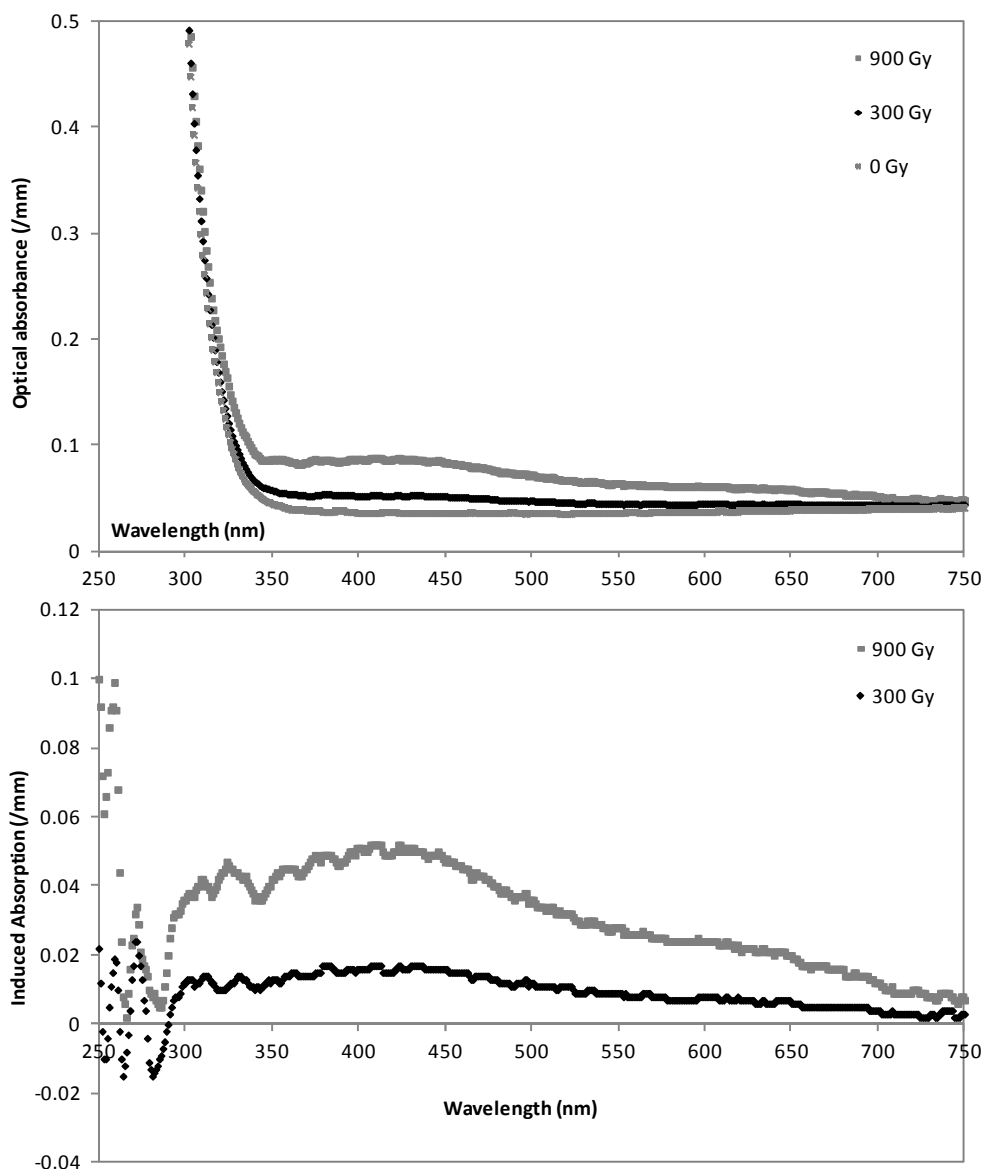


Figure 5.3 The optical absorbance spectra (top graph) and radiation induced absorption spectra (bottom graph) with normalisation to a thickness of 1mm of microscope slide after gamma irradiation at 300 Gy and 900 Gy.

Differences between doses and 0 Gy were applied at the region of 600 – 620 nm, 350 – 500 nm, and 300 – 340 nm. Figure 5.4 illustrates the data. The fluctuations at the region of 250 – 300 nm are due to noise from the spectrophotometer during the measurement since the intrinsic absorption of the glass is so high that virtually no light is transmitted through it

to the photodetector. Relatively, the radiation damage at the area of 350 – 500 nm is twice to the area of 600 – 620 nm when respect to the mean value. On the other hand, sigma represents almost three times variation in 350 – 500 nm regions when compared to 600 – 620 nm regions.

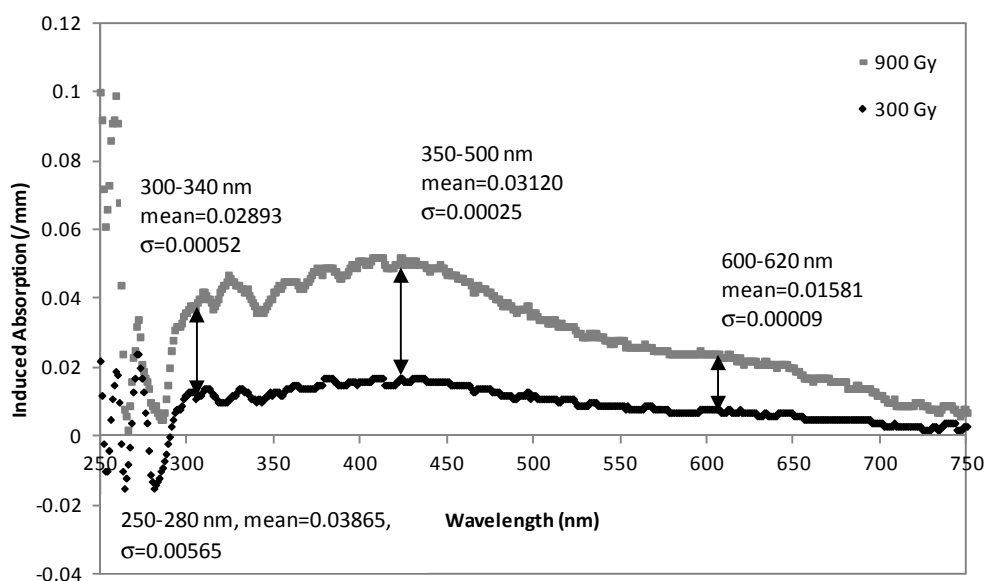


Figure 5.4 Mean and standard deviation of sample at 250 – 280 nm, 300 – 340 nm, 350 – 500 nm and 600 – 620 nm of wavelength.

5.5.3 Induced absorbance for high and low Co-60 dose rate

The top graph in Figure 5.5 shows the radiation induced absorbance spectra of a microscope slide after a dose of 300 Gy. Every measurement was taken after 1 hr following irradiation by either the high or low activity Co-60 source. The high activity rate is expected to have higher induced absorbance than the low rate due to the effects of annealing at room temperature. Even though the same dose (300 Gy) was imposed, the

radiation induced is likely to be dependent on the dose rate. The optical absorption bands found around 420 nm and 600 nm correlate with the same features seen in Figure 5.3.

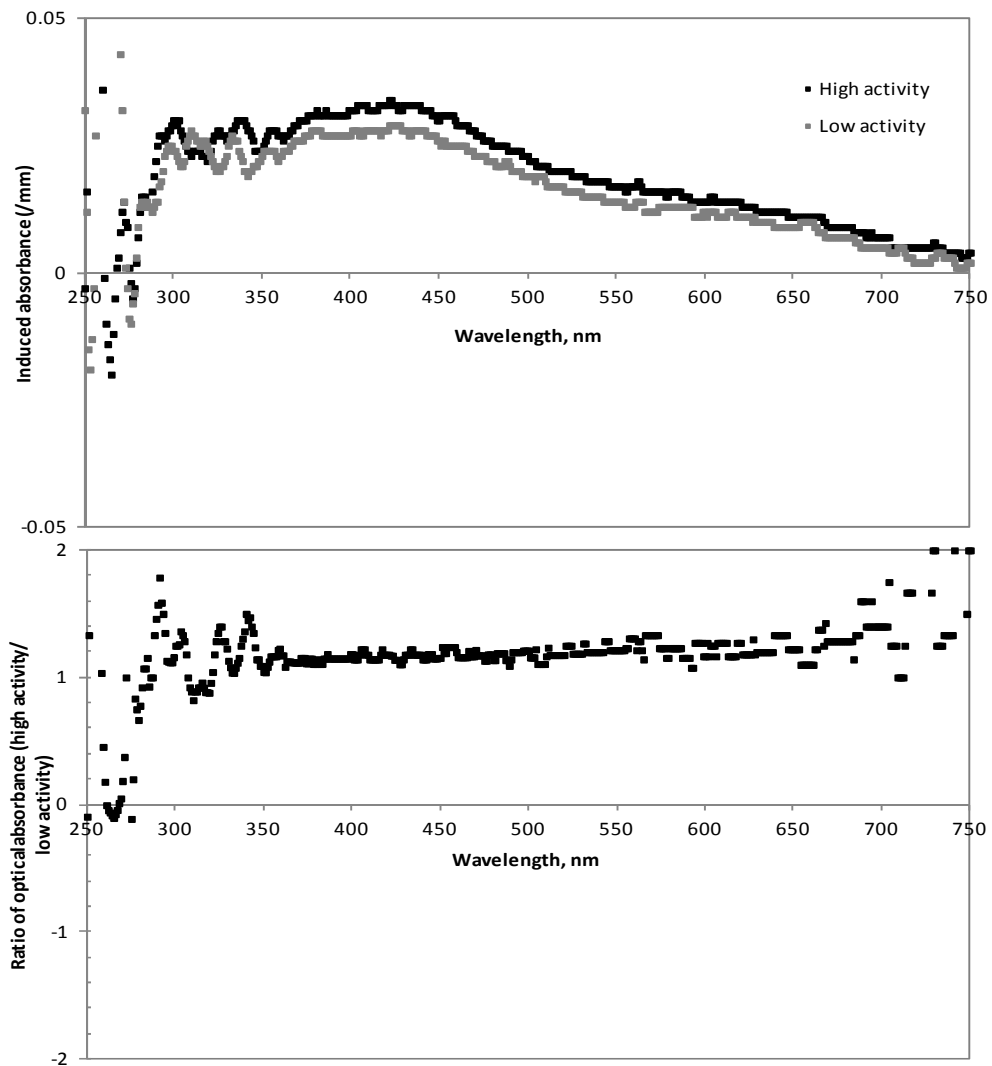


Figure 5.5 Radiation induced absorbance spectra after 1 hr gamma irradiation of microscope slide at high and low activity of Co-60 at the top graph. Bottom graph shows the ratio of high and low activity of Co-60.

The ratio of high activity to low activity of Co-60 source is shown at the Figure 5.5 (bottom graph). At the region of 350 to 700 nm, the ratio of induced absorbance is 1.2 to each other at the average of 20%. At the region of 270 to 350 nm, the relative is at 15% different. At

far end in the ultraviolet region, 260 nm and below, the fluctuation is high and no indication can be made with regard to the relative study between both activities.

5.5.4 Fading effect

The fading effect is an important characteristic for a dosimeter. Most glasses show quick initial fading following irradiation which is a disadvantage for any potential application as a dosimeter. To overcome this problem, the evaluation of glass must be completed within the first 2 hours [Farah *et al.*, 2007]. Narayan *et al.* also suggested that the environment and procedures followed during the dosimetric application need to be identical at all times [Narayan *et al.*, 2008]. Fading happens due to the annealing process and it was measured in the microscope slide up to 175 days after the gamma irradiation as shown in Figure 5.6.

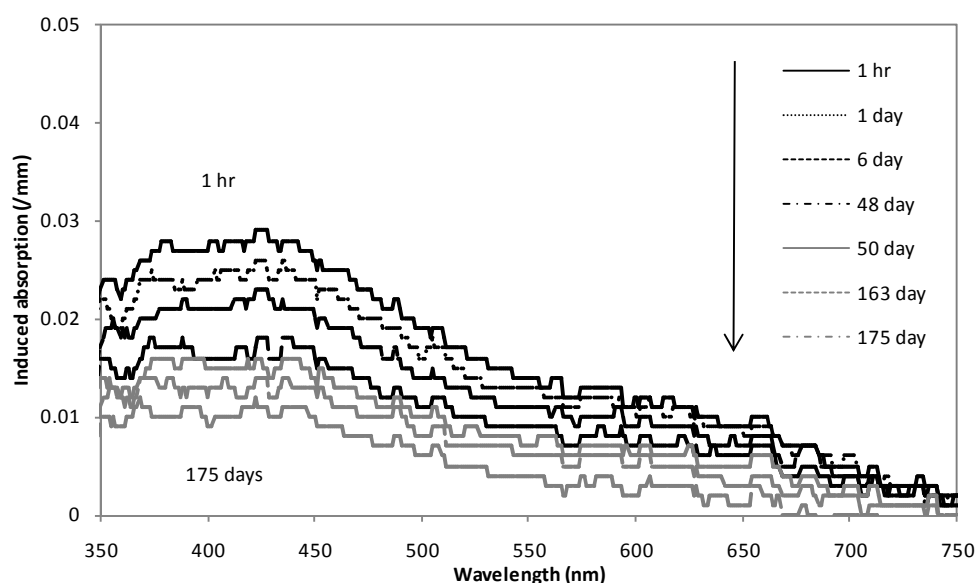


Figure 5.6 Annealing behaviour for microscope slide up to 175 days on observation. The microscope slide was irradiated to 300 Gy at 0.20 Gy/min.

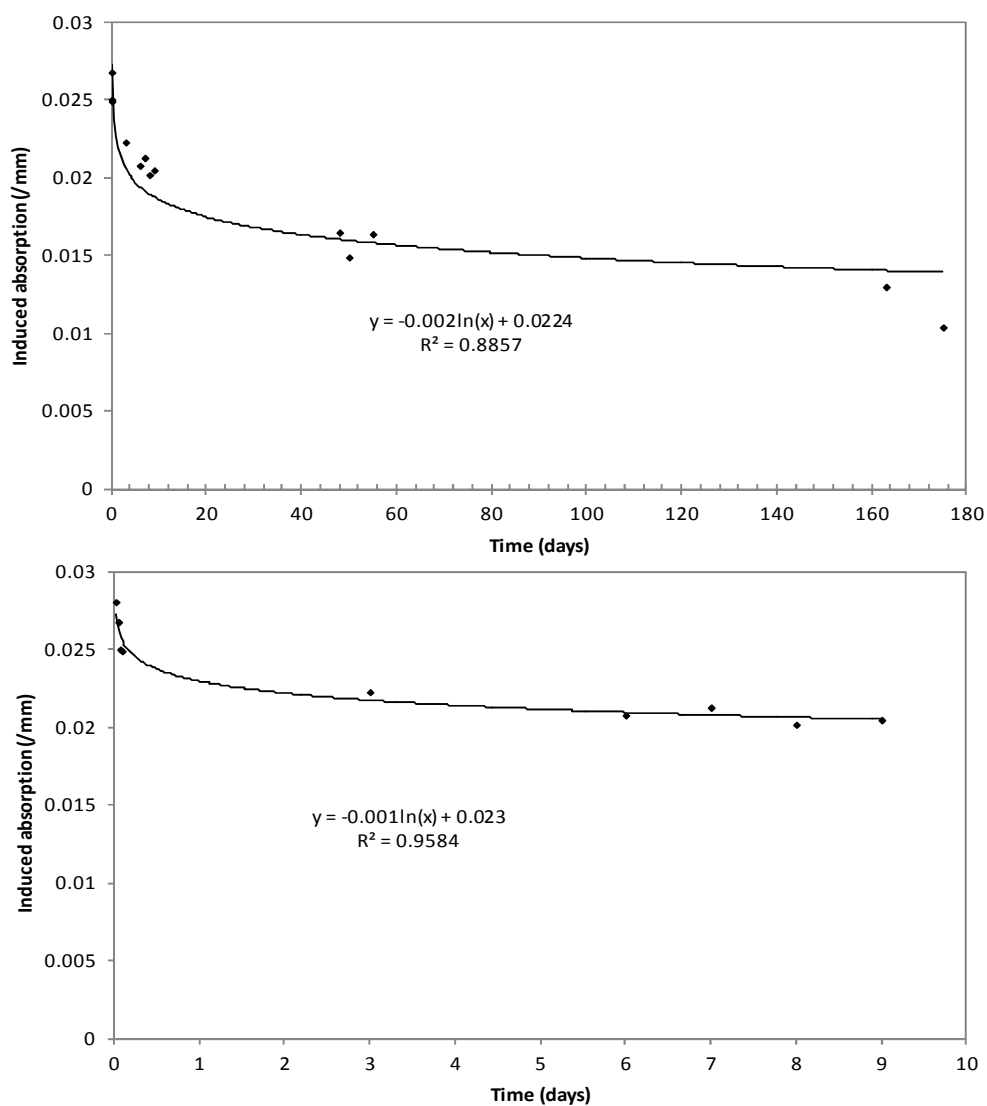


Figure 5.7 The average data of radiation induced absorption at the region of 350 - 450 nm of wavelength with normalization to a thickness of 1 mm of microscope slide. Top graph shows 175 days observation on fading behaviour, while the bottom graph is for the same sample expanded to show the first 10 days after irradiation. Microscope slide was irradiated at 300 Gy at 0.20 Gy/min.

Subsequently, Figure 5.7 shows the fading behaviour over 175 days following irradiation in the wavelength region 350 – 450 nm. The microscope slide was stored in the dark at room temperature, 20°C, between measurements. There is a fast fading effect at short-term stage

(within 2 days) and long-term slow fading up to 175 days. At long-term stage, the data can be fitted by first-order decay kinetics,

$$A = A_0 e^{-Bt} \quad (\text{Equation 5.4})$$

where, A is the induced absorption and B is the constant of first order reaction rate and Equation 5.4 becomes,

$$\ln A = -Bt + \ln A_0 \quad (\text{Equation 5.5})$$

From the graph at the top of Figure 5.7as,

$$y = -0.002 \ln x + 0.0224 \quad (\text{Equation 5.6})$$

While short-term fading was said to be due to a combination of first-order decay kinetics with the second-order decay kinetics, which is shown in Equation 5.7 below [Farah *et al.*, 2007; Sheng *et al.*, 2002],

$$A = A_0 e^{-Bt} + \frac{C}{(1 + Cdx)} \quad (\text{Equation 5.7})$$

However, from the bottom graph in Figure 5.9, this data can still be fitted by first-order decay kinetics,

$$y = -0.001 \ln x + 0.023 \quad (\text{Equation 5.8})$$

5.5.5 Summary

The optical absorbance of a microscope slide changes following gamma irradiation due to radiation damage. The interaction creates free electrons and holes, with electrons trapped in glass structural defects like at interstitial or vacancy sites. These events form the colour centres that are capable of absorbing light in the visible region of the spectrum. In order to relate the visible light absorption to gamma irradiation dose, measurements were made by spectrophotometer showing radiation induced absorbance at particular wavelengths.

Various different dosimetric techniques (lower dose detection, dose response to gamma radiation, reproducibility and fading behaviour) in a microscope slide were observed by looking at the resulting changes in optical absorbance, in line with the possibility study of this material for dosimetry usage. The results obtained in this work are in agreement with the other scholars that used commercial plate window glass in their works [Narayan *et al.*, 2008; Farah *et al.*, 2007; Caldas and Teixeira, 2002; Rodrigues Jr. and Caldas, 2002; Zheng *et al.*, 1997; Khan and Ali, 1995].

As a summary, standard commercial microscope slide glass is responsive to the low dose of gamma radiation (300 Gy and 600 Gy). Even at low doses, a standard microscope slide has the ability to detect the radiation. To overcome the fading behaviour which is a disadvantage of microscope slide glass, the optical absorption measurement has to be performed within an interval time of 1 hour.

Radiation damage of a microscope slide was analysed by the observation of optical absorption bands at the region of 300 – 340 nm, 350 – 500 nm and 600 – 620 nm

wavelength. The results clearly show that radiation damage effects in the glass cause changes to the absorption in this region.

Chapter 6

Radiation Effects on VYCOR[®] 7930 and Optical System Development

This chapter describes the second and third phases of the overall experimental work carried out for this thesis. As stated in Chapter 5, work with a microscope slide gave rise to the thought of evaluating another type of glass, VYCOR[®] 7930 and investigating its use with fluorescent radiation sensitive quantum dots. The work was to see how well the glass will tolerate radiation compared with the specific material of VYCOR[®] 7930, investigating the capability of VYCOR[®] 7930 as a dosimeter. As part of the study, nanocrystals, known as quantum dots, QDs (in this work we used Lumidot[™] which are CdSe/ZnS core-shell and commercially available from Sigma-Aldrich) were utilized by doping into the porous VYCOR[®] 7930.

6.1 Dosimetry and optical system

As explained in Chapter 2, dosimetry can be conducted by a variety of systems depending on the application. The dose measurement in radiotherapy is critical as it involves a patient as a direct subject to irradiate. The radiation level measurement in hazardous areas like nuclear power plants requires more sensitive dosimeters. These applications generally involve an optical system. Optical systems that can be implemented in dosimetry systems are varied and constructed with many types of materials. It involves luminescence,

photoluminescence and thermoluminescence effects [Narayan *et al.*, 2008] of materials like fibre-optic-coupled [Huston *et al.*, 2004] and doped silica glass [Justus *et al.*, 1997] like that developed by the Naval Research Laboratory, Washington; CdS doped glass by Miyoshi and group [Miyoshi *et al.*, 2008; Miyoshi *et al.*, 2006; Miyoshi *et al.*, 2004; Miyoshi *et al.*, 2003; Miyoshi *et al.*, 1997; Miyoshi *et al.*, 1995] and CdSe quantum dot-doped glass [Dekanozishvili *et al.*, 2009; Santhi and Trojanek, 2004].

Many researchers, with support from industry, have started to employ the advantages of glass in dosimetry applications as discussed in Chapter 5. A group from Washington have developed a number of research projects on optical based dosimeters since the early 90's [Justus *et al.*, 1997; Justus *et al.*, 1995] and patented the findings of optical glass composite studies with the United States Patent Office [Huston and Justus, 1998]. Further steps were taken by Hobson and colleagues to study radiation damage in a variety of different glasses, followed by the current work to determine a good hosting glass for recently developed nano materials, called quantum dots, for dosimetry [Leslie *et al.*, 2012; Hobson *et al.*, 2012; Baharin *et al.*, 2010].

6.2 Methodology: VYCOR[®] 7930

For the VYCOR[®] 7930 glass, the same methodology in Section 5.4.2 was implemented and is here referred as Irradiation B1. In a second irradiation, referred to here as B2, one plate of aluminium was used as a build-up material during irradiation.

6.2.1 Irradiation B1

In this work, two samples of VYCOR[®] 7930 were used, labelled as Vycor A and Vycor B. The glass samples were heated slowly in a vacuum oven to 140 °C and then cooled under

vacuum back to room temperature. This procedure is recommended by the manufacturer to remove as much absorbed water vapour as possible prior to use. The first irradiation was done at 300 Gy and second irradiation at 600 Gy after eight days of first irradiation. Therefore the total cumulative dose was 900 Gy. The optical absorbance was measured before and after irradiation. Table 6.1 shows the irradiation time for each sample.

6.2.2 Irradiation B2

Instead of exposing only samples to Co-60 source, aluminium of 0.16 cm thickness was also used in this work as a build-up material. Aluminium was put in front of the samples of VYCOR[®] 7930, labelled as Vycor C and Vycor D. The samples were irradiated with 300 Gy of Co-60 at a dose rate of 0.315 Gy/min. After one hour of irradiation, an optical absorbance reading was taken by spectrophotometer. Caution was taken during sample handling to avoid surface contamination of dust, grease and fingerprints. The laboratory room where the spectrophotometer was located was kept in dim light to avoid any background effect on the samples. The room temperature was at 20°C.

Table 6.1 Summary of gamma-ray irradiation experiment and optical absorbance measurement for VYCOR[®] 7930.

Irradiation (Samples)	Dose (Gy)	Dose rate of gamma-ray (Gy/min)	Optical Absorbance Measurement (OD)	
			• Before irradiation	• 1hr after irradiation
B1 (Vycor A and Vycor B)	First at 300 Second at 600	0.75 Gy/min at 10 cm of high activity	• Before irradiation	• 1hr after irradiation
B2 (Vycor C and Vycor D)	300	0.315 Gy/min at 10 cm of high activity with build-up material (aluminium)	• Before irradiation	• 1hr after irradiation

6.3 Results and analysis for VYCOR[®] 7930

Even though microscope slide glass and VYCOR[®] 7930 are made from silica as the basic component, VYCOR[®] 7930 is expected to react differently to radiation due to the very high percentage of silica, which is about 96%. Structurally, VYCOR[®] 7930 has a nano-porous structure which provides the novelty of this work when it is used together with quantum dots.

Figure 6.1 shows the topography of a VYCOR[®] 7930 surface using an SEM at two different magnifications. The figure shows the porous structure of VYCOR[®] 7930 surface at low and high magnifications.. It provides a large surface area for material absorption when comparing to the volume of VYCOR[®] 7930 [Brown *et al.*, 1997]. The porous structure results in an inert material with applications involving surface interactions and nano size materials.

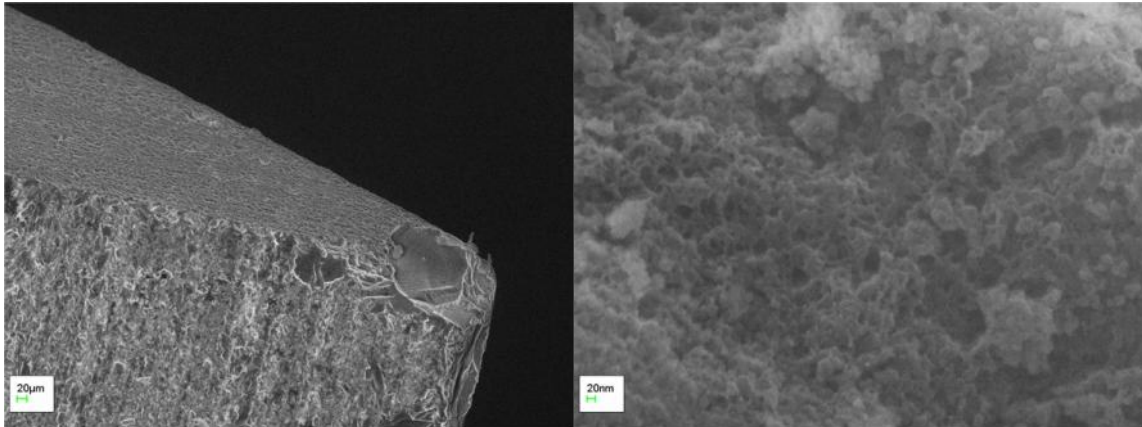


Figure 6.1 Topography of VYCOR® 7930 by SEM at 20 μm for the left picture and at 20 nm for the right picture. They show at the edge and surface VYCOR® 7930 on the left and right pictures, respectively.

6.3.1 Reproducibility

Reproducibility was considered by using two samples of VYCOR® 7930; Vycor A and Vycor B. An identical experimental method was used with both samples. Figure 6.2 shows the optical absorbance for both unirradiated Vycor A and Vycor B. The curve is identical for both samples. However, the supplier could not confirm if the VYCOR® 7930 supplied for this work was from a single batch or from the same piece (before being cut into the small pieces which were supplied to Brunel). Due to this fact, the VYCOR® 7930 samples were treated independently.

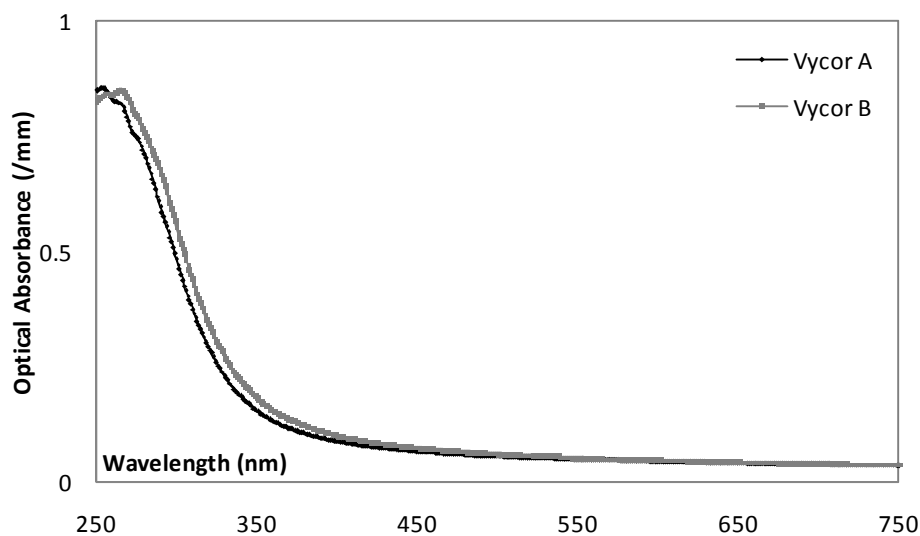


Figure 6.2 The optical absorbance of unirradiated Vycor A and Vycor B with the normalization to the 3.1 mm sample thickness.

6.3.2 Radiation induced absorbance

The radiation induced absorbance was deduced from the difference in the optical absorbance of the non-irradiated material and that of the irradiated material. It measures the ability of a material to absorb radiation from the different values of energy level (non-irradiated and irradiated measurement). In this case it provides the radiation indicator characteristics of the material. Figures 6.3 and 6.4 show the optical absorbance and the radiation induced absorption (normalized to the sample's thickness, 3.1 mm) of Vycor A and Vycor B. The first irradiation was carried at 300 Gy, and then second irradiation of 600 was carried out eight days after that. Therefore, the accumulated dose, 900 Gy data were obtained by taking the difference between the after and before 600 Gy measurements and adding the difference to the 300 Gy data.

The radiation induced absorption spectra for both samples show a very small amount of damage has taken place. There is a small increase in absorbance at the region of 600 – 620 nm in both samples. However, basically VYCOR[®] 7930 shows that the damage is negligible at the region of 450 nm and below. Beyond the mid ultra-violet region the data is dominated by instrument noise due to the very strong intrinsic absorption of the glass.

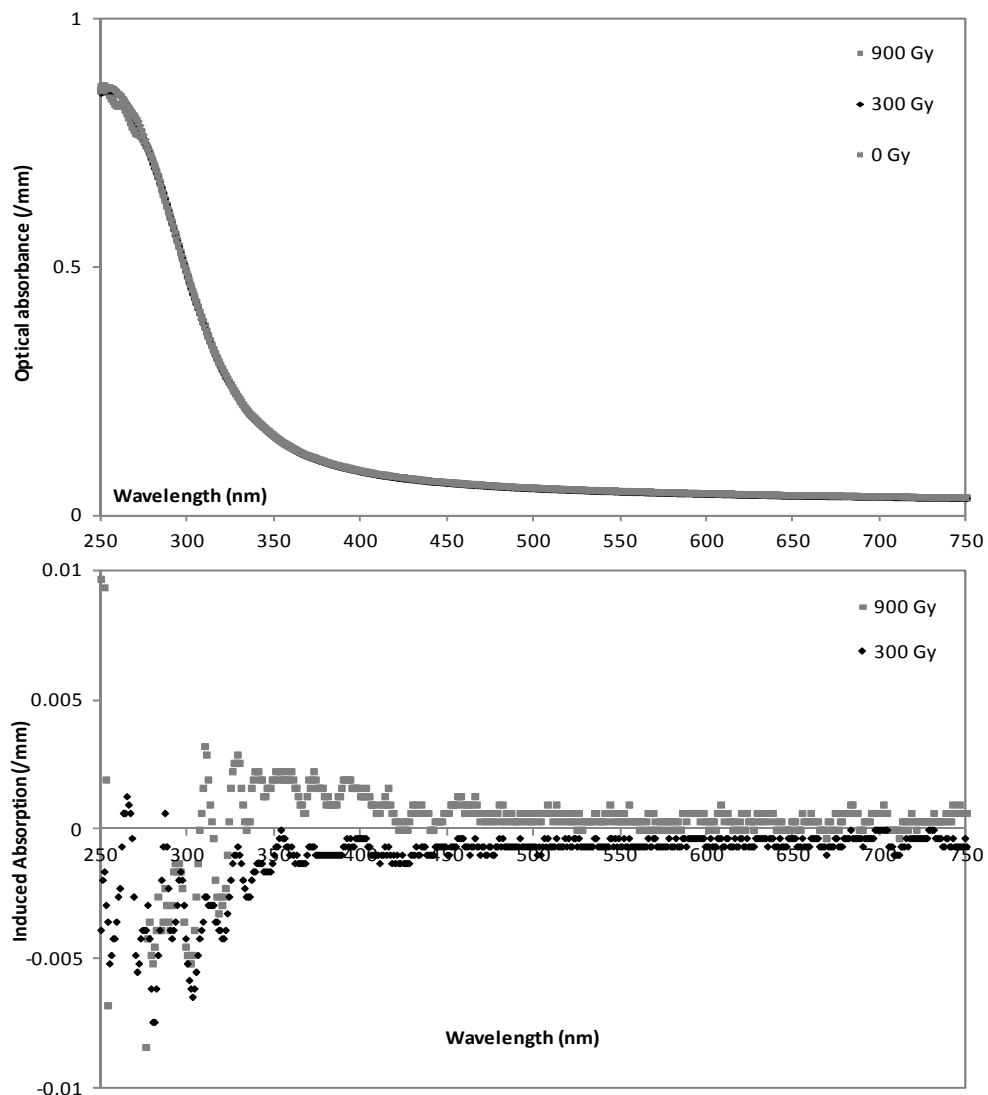


Figure 6.3 Optical absorbance and radiation induced absorption of Vycor A at top and bottom graphs, respectively. Normalization was made to the 3.1 mm sample thickness.

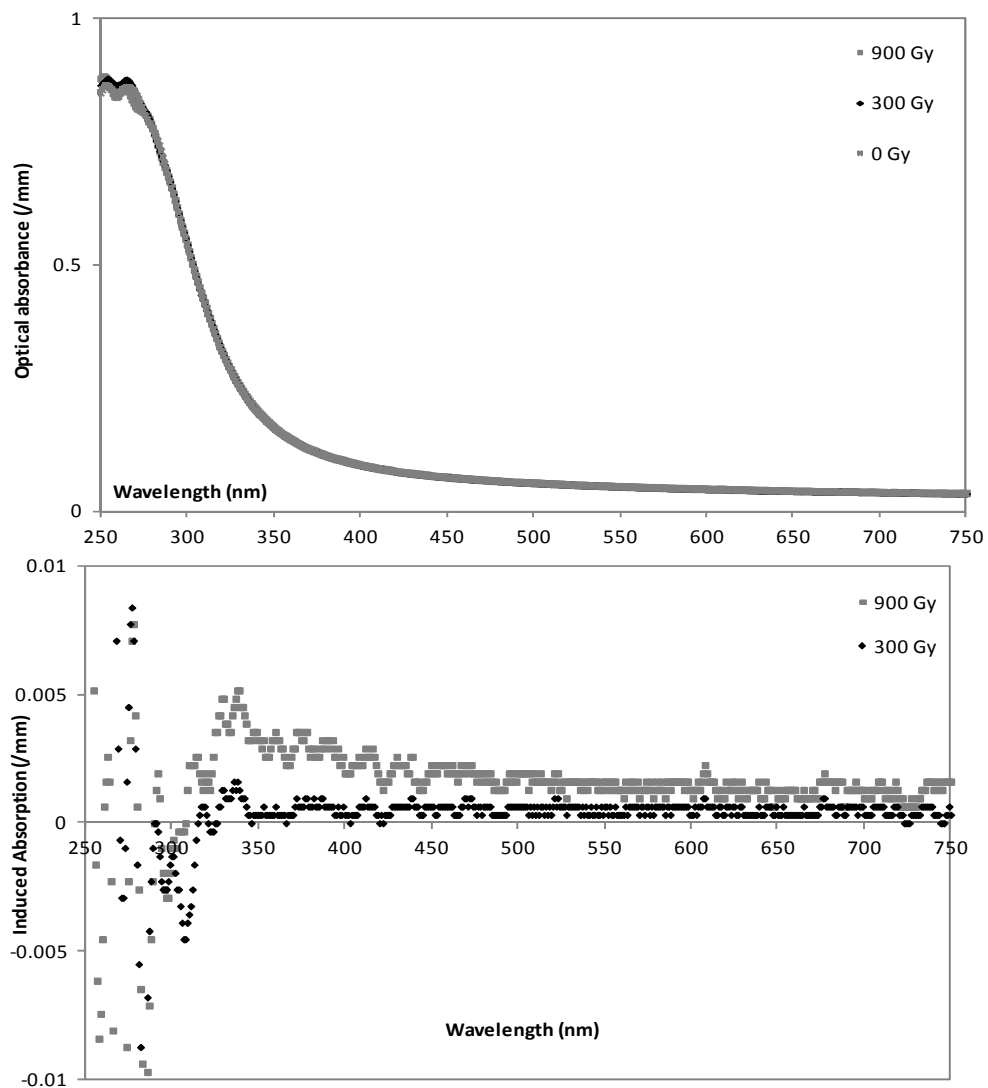


Figure 6.4 Optical absorbance and radiation induced absorption of Vycor B at top and bottom graphs, respectively. Normalization was made to a 3.1 mm of sample thickness.

On the other hand, Figure 6.5 below shows the differences in radiation induced absorbance of a microscope slide, Vycor A and Vycor B at the same scale. The microscope slide demonstrates more than 20 times the damage when compared to VYCOR[®] 7930 samples after a dose of 900 Gy.

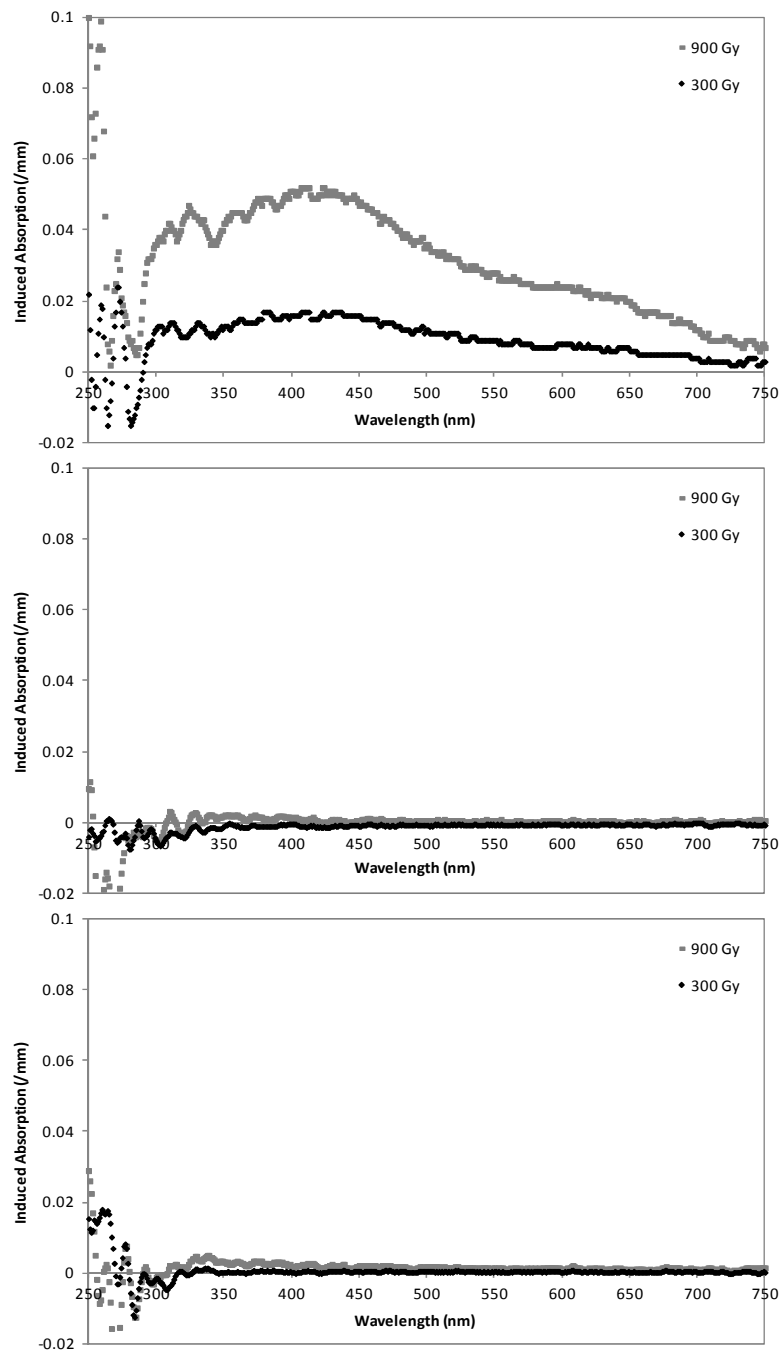


Figure 6.5 Radiation induced absorbance (normalised to a thickness of 1 mm and 3.1 mm for microscope slide and Vycor, respectively) by gamma in microscope slide, Vycor A and Vycor B, at the same scale.

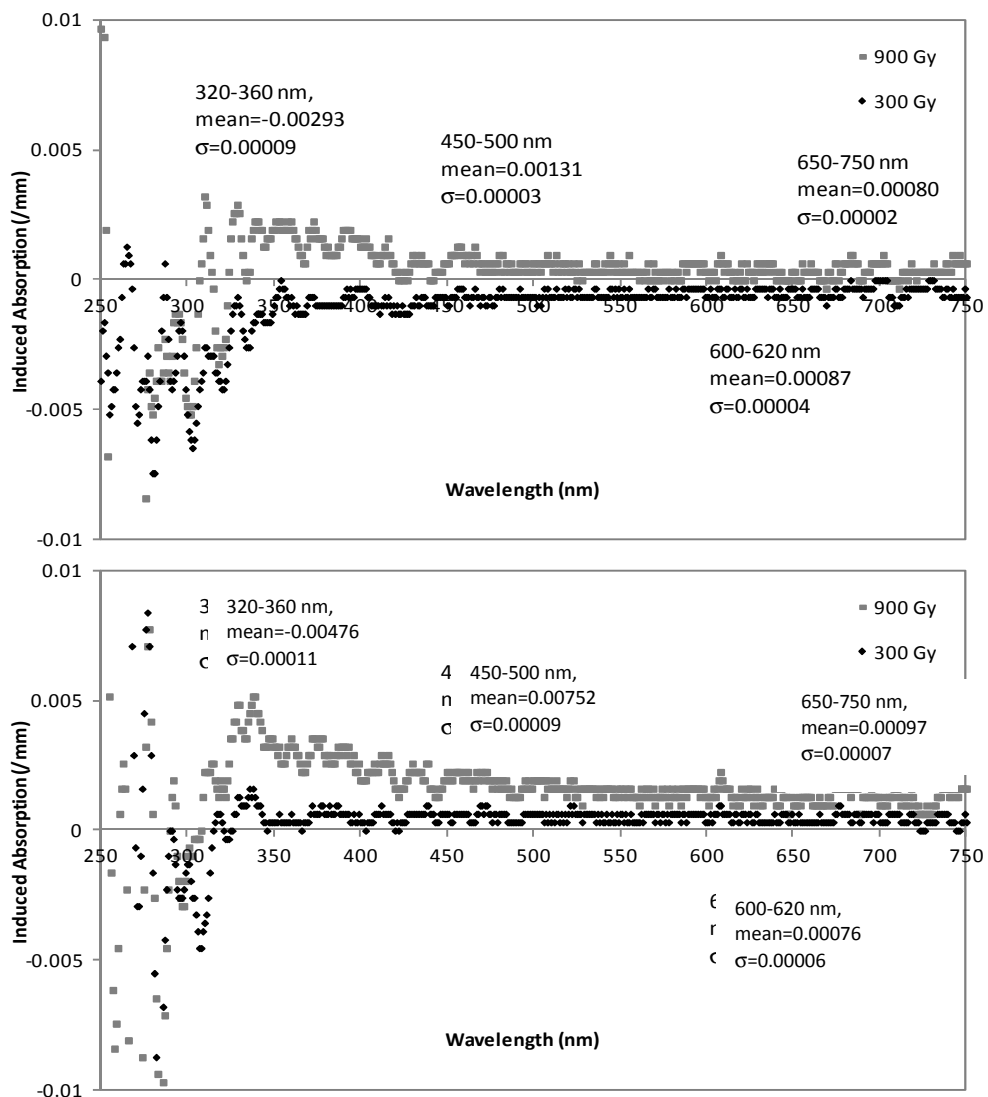


Figure 6.6 Mean variation and standard deviation of the samples, Vycor A and Vycor B at the top and bottom graphs, respectively.

The difference between two spectra of radiation induced absorbance at the region of 650 – 750 nm, 600 – 620 nm, 450 – 500 nm and 320 – 360 nm were analysed and illustrated in Figure 6.6. The mean and standard deviation were determined based on the sample and clearly showed identical values in both of them. In the red region, after 650 nm, as the variation is small, there is no evidence of any induced absorbance happened.

At the blue region, 400 – 450 nm, the mean values is about two times variation relatively with 600 – 620 nm regions. In the ultraviolet region, the variation in mean and sigma are high and it is due to the noise during the measurement.

In the Vycor A spectra, the line for 300 Gy is clearly seen to be just below 0 at all wavelengths. This is probably due to a positioning error during the experiment.

6.3.3 Build-up material effect

Build-up material is an important tool in solid state dosimetry like in non-destructive analysis. It is used to reduce uncertainties by improving the uniformity of the radiation beam when it hits the sample. Radiation has to go through the build-up material prior to reaching the sample. Moreover, the charge and dose is uniformly distributed throughout the sample thickness.

Figure 6.7 indicates the behaviour of radiation induced absorbance in Vycor C and Vycor D when aluminium build-up material is included during the irradiation compared with the spectra obtained without using aluminium. Both samples react differently. The best explanation that can be made is that the difference is due to the prepositioning error that occurred during the gamma irradiation with the aluminium present. Table 6.2 depicts the mean and standard deviation in Vycor C and Vycor D.

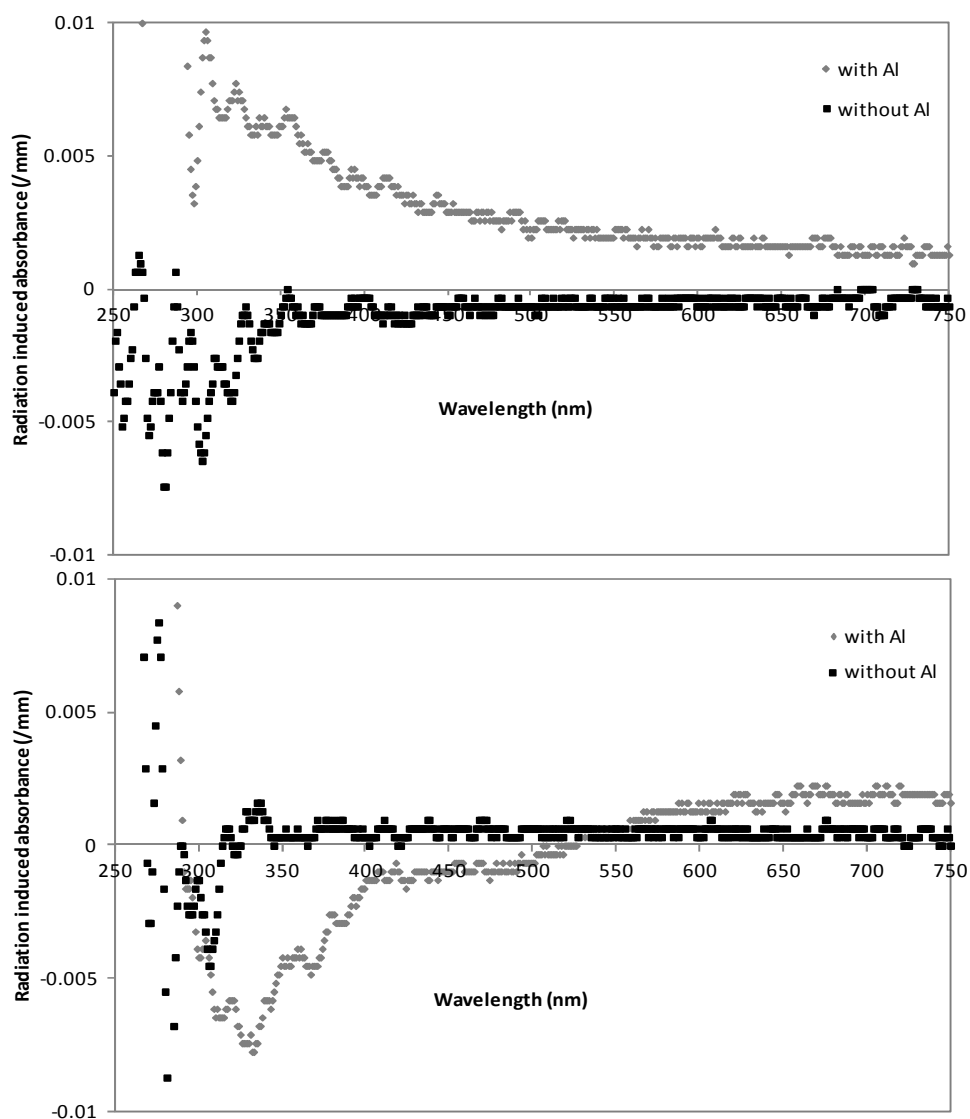


Figure 6.7 Radiation induced absorbance of Vycor C (top graph) and Vycor D (bottom graph) at 300 Gy with and without the build-up material, aluminium (Al). Data were normalised to a 3.1 mm of a sample's thickness.

At the area of 550 – 750 nm of wavelength, the variation (sigma, σ) between Vycor C and D is big as expected from the different patterns that occurred from both samples.

Below 550 nm, the variation is smaller.

Table 6.2 Mean and standard deviation based on sample with the respect of build-up material and without build-up material.

	Vycor C	Vycor D
550 – 750 nm	Mean: 0.00727 †: 0.00042	Mean: 0.00048 †: 0.00001
250 – 549 nm	Mean: 0.00214 †: 0.00034	Mean: 0.00105 †: 0.00024

6.4 Optical system experiment

In this work, sample involved was a piece of 50 mm × 25 mm × 3 mm VYCOR[®] with a doping of 300 μL of CdSe/ZnS (QDs) with toluene. The QDs used were commercial core-shell CdSe/ZnS from Sigma Aldrich (Lumidot[™]) with particle sizes of 2.5 nm (blue, $\lambda_m = 480$ nm), 3.3 nm (green, $\lambda_m = 530$ nm) and 6.3 nm (red, $\lambda_m = 640$ nm). They were stabilized with hexadecylamine ligands. The fluorescence spectra of the QDs are as shown in Figure 2.8 in Chapter 2. The optical system was set up in a dark room in one of the laboratories at Brunel University. A Nikon camera was used to picture any possible fluorescence effect from the sample.

Prior to that, the illumination field for excitation was checked and uniformity across the beam was taken by measurement of the absolute intensity (W per cm²) of fluorescence dye.

6.4.1 Uniformity of illumination measurement

This measurement was carried out to get parallel beam of light with reasonable uniformity of illumination of fluorescence dye inside the sample cuvette. It included two experiments;

Experiment A and Experiment B, as described below. The layout set-up in this work was as shown in Figure 6.8.

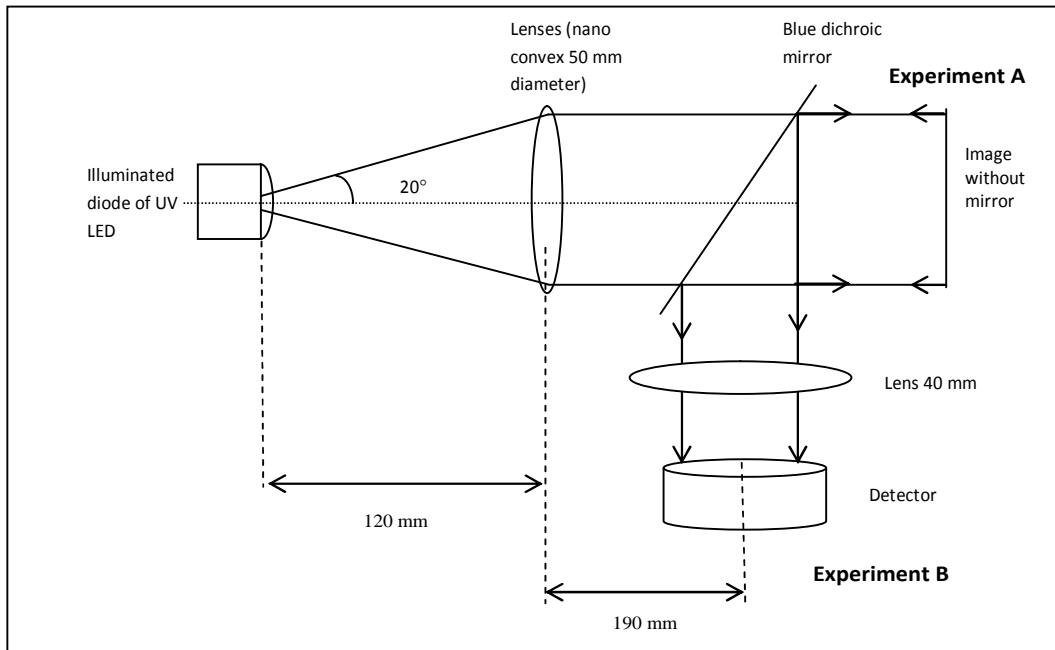


Figure 6.8 The layout of uniformity measurement

Experiment A

The first set-up was done without a mirror with a violet LED for 20° viewing angle and 50 mm diameter plano-convex lenses with a 10 V DC power supply and power meter, Newport model 2935-C, for uniformity check up. The image distance and lens diameter was at the same length, 50 mm, throughout the experiment.

The point source of light was enlarged in diameter by a lens to form a collimated beam to illuminate a reasonable area of the Vycor. At this point, the illumination field for excitation was checked.

Experiment B

Subsequently, the second set-up was done using a blue dichroic mirror located after the lens. The illumination uniformity of the light coming back from a Coumarin-540 dye in a 10×10 cuvette was measured. It was measured by using a detector which connected to the power meter, Newport model 2935-C. Readings were taken at points across the image in overall flux (μW) as shown in Table 6.3.

Uniformity of illumination (d) was measured from Ramane *et al.* [2012],

$$d = \frac{\text{Average of illumination, } E_{\text{ave}}}{\text{Maximum of illumination, } E_{\text{max}}} \quad \text{Equation 6.1}$$

Measurement was taken at which the values of absolute intensity, W , is start to uniform or stabile until it began to drop back. These values are labelled as Middle as shown in Table 6.3.

- Data A: data taken from 15 mm until 27 mm. Therefore, $E_{\text{ave}}=159.52/13$ and

$$E_{\text{max}}=12.37. \text{ Subsequently, } d = \frac{159.52/13}{12.37} = 0.992$$

- Data B: data taken from 20 mm until 25 mm. Therefore, $E_{\text{ave}}=71.66/6$ and

$$E_{\text{max}}=11.97. \text{ Subsequently, } d = \frac{71.66/6}{11.97} = 0.998$$

From both Data A and Data B, the uniformity of illumination, d is almost 1.

Table 6.3 Data on uniformity of illumination of UV LED. Values considered were marked as Middle and taken from a group of uniform data.

LED to lenses, f	Detector (vertical), mm	Detector (horizontal), mm	W, μ W	Remarks
120 mm	9.5 mm (Data A)	0	1.77	} Middle
		5	2.01	
		10	6.97	
		15	12.09	
		16	12.31	
		17	12.35	
		18	12.35	
		19	12.37	
		20	12.37	
		21	12.37	
		22	12.35	
		23	12.32	
		24	12.28	
		25	12.22	
	26	12.12		
	27	12.02		
	28	11.89		
	11.5 mm (Data B)	0	1.64	} middle
		1	1.64	
		2	1.66	
		3	1.69	
		4	1.77	
		5	1.95	
		6	2.52	
		7	3.23	
		8	4.30	
		9	5.42	
		10	6.61	
11		7.97		
12		9.16		
13		10.28		
14	11.05			
15	11.53			
16	11.75			
17	11.81			
18	11.85			
19	11.86			
20	11.92			
21	11.94			
22	11.97			
23	11.97			
24	11.97			
25	11.92			
26	11.89			
27	11.7			
28	11.65			

6.4.2 Experimental arrangement and methodology of optical system

In this work, an illumination system was used with the experimental arrangement as shown in Figure 6.9. It consisted of a 400 nm violet LED, a bandpass filter centred on 400 nm (± 10 nm), a collimating lens and a 45° dichroic mirror (450 nm cut-off). The LED received 10 mA current from the power meter and constantly illuminated the sample for a few hours. In every one hour, images of fluorescence (Figure 6.9) emitting from the sample were taken by using the static camera. All pictures have the same lens aperture and exposure time (4 s), and the camera position is constant from frame to frame.

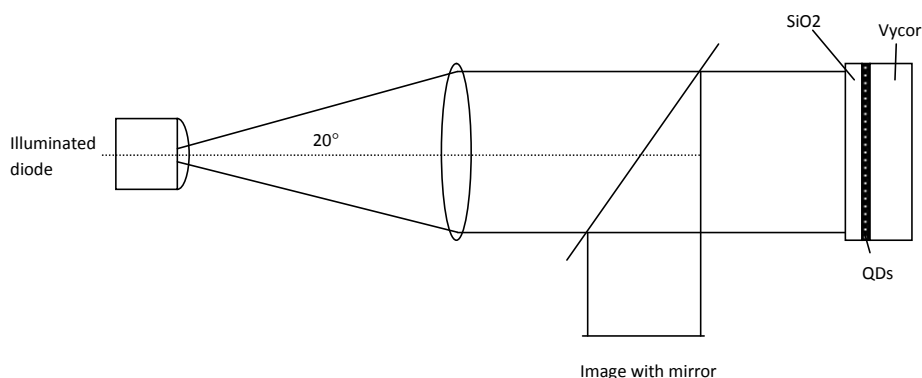


Figure 6.9 The layout of optical system experiment set-up in the dark room.

The sample used was a prototype 2D imaging dosimeter comprising green light emitting quantum dots absorbed into VYCOR[®] 7930. The QD solution was prepared by using 3 mL of toluene and 300 μ L of CdSe/ZnS and dispensed into a VYCOR[®] 7930. The doping process was done carefully to avoid spillage of the CdSe/ZnS QDs. Toluene was utilized to dilute the CdSe/ZnS. Then the surface was covered with a Suprasil 2000 cover

slip (1 mm thick) and the edges sealed with Kapton tape. The fluorescence spectrophotometer used to collect data was from Horiba Scientific (FluoroLog Spectrofluorometer). The excitation spectrum of the green QDs measured at the emission peak at 530 nm, is shown in Figure 6.10. The spurious peak at 530 nm is due to elastically scattered light, after 540 nm there is no fluorescence occurs (zero excitation intensity from 540 nm to 600 nm).

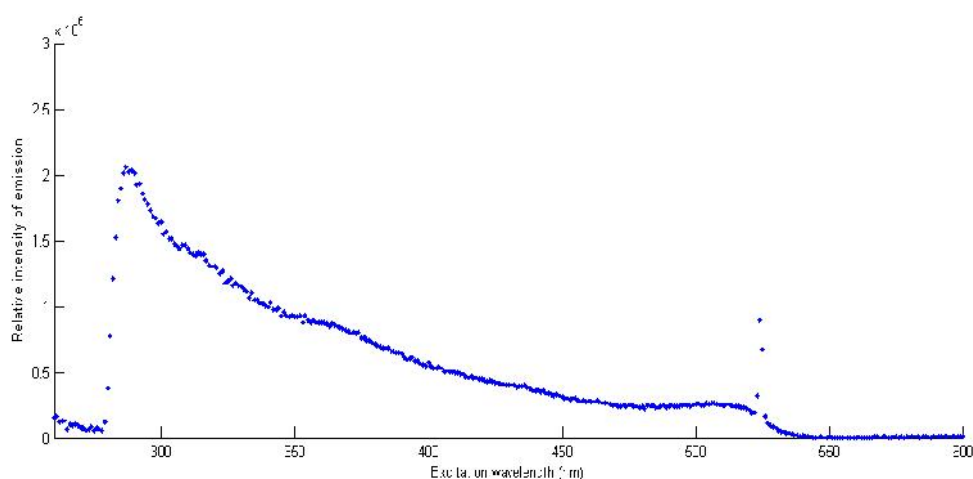


Figure 6.10 Excitation spectrum of the green quantum dots collected from Horiba Scientific (FluoroLog Spectrofluorometer). It shows the excitation spectrum when measuring fluorescence (1 nm bandwidth) at the peak emission wavelength of 530 nm.

6.4.3 Fluorescence images from the quantum dots doped VYCOR[®] 7930

Figure 6.11 shows the fluorescing QDs after 1 hour of continuous light illumination from the 400 nm LED.

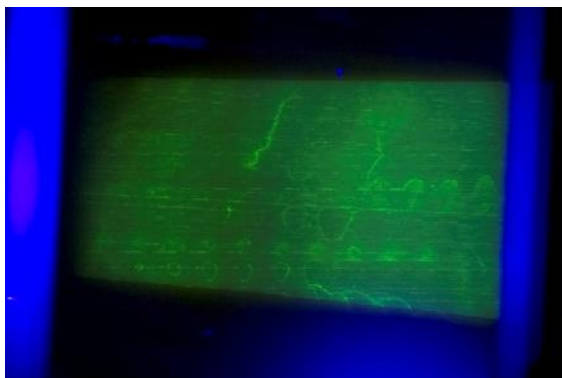


Figure 6.11 Image of the fluorescent QDs in VYCOR[®] 7930 during the light illuminating. Surface markings arise from the cutting process used to produce the glass slab. The blue light comes from the LED and the green light from the QD.

Even though the fluorescence is not clearly shown in the picture, there was a reduction in the glow from the image in every hour. It shows that the QDs do fluoresce when illuminated by the light. The QDs received energy from the light and fluorescence as a result of that activity. These observations suggest that QDs have the potential to be an indicator of radiation.

6.4.4 Result and data analysis

Table 6.4 and Figure 6.12 (top) show the ratio of green fluorescence from the QDs to the blue colour of the illumination light in order to check the influence of LED power in a change of fluorescence. Data in Table 6.4 for the green QDs in VYCOR[®] 7930 were established from the 5×5 spreadsheet pixel average. The black level (dark count) is < 5 when compared to the overall data so can be ignored. It was found that the fluorescence of QDs is not influenced by the LED power. Subsequently, Figure 6.12 (bottom) shows the constant fluorescence of QDs over a period of eight hours under constant illumination light.

Table 6.4 Data on fluorescence QDs in VYCOR® 7930 with the respect of time of picture taken.

Time of day	QD (green)	Illumination (blue)	Ratio = green/blue	Average of green/blue
Time 1 (09:45)	11615	17175	0.67627	} 0.67941
Time 2 (09:45)	11946	17502	0.68255	
Time 3 (12:13)	12136	17656	0.68736	} 0.68943
Time 4 (12:13)	12156	17579	0.69151	
Time 5 (17:53)	12023	17589	0.68355	} 0.67746
Time 6 (17:53)	12002	17759	0.67583	
Time 7 (17:53)	11966	17780	0.67300	

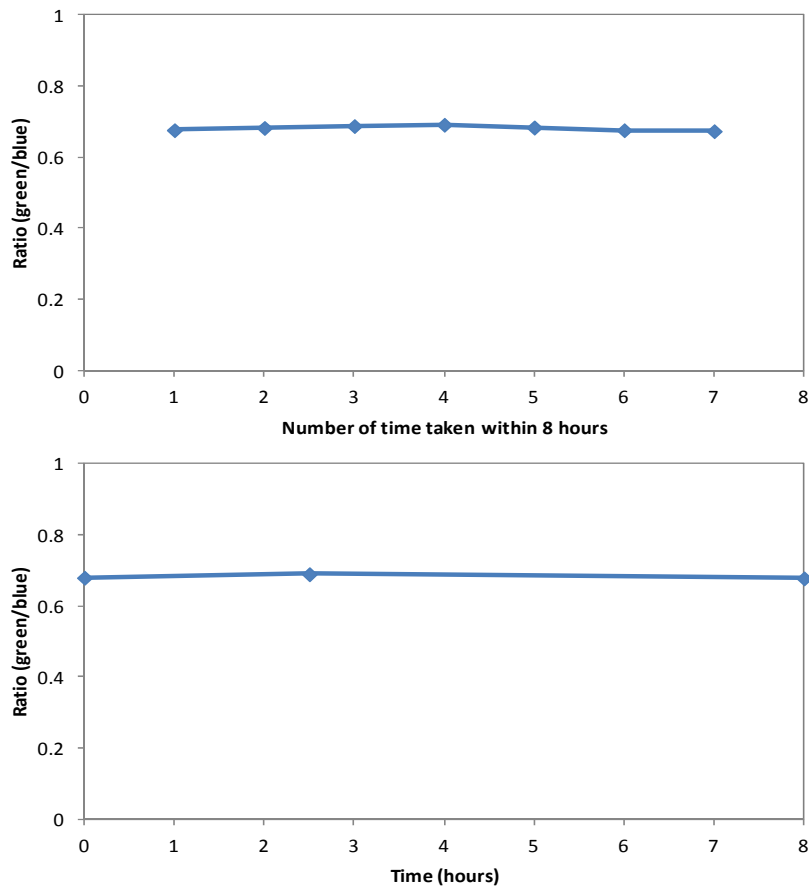


Figure 6.12 Ratio of green fluorescence to blue illumination light with the average frames at three point in the bottom graph.

6.5 Summary works on Vycor

Generally, VYCOR[®] 7930 is made to provide thermal shock protection and as a high temperature resistance material hence the glass being structurally porous. Corning Incorporated manufactures this glass type mostly for cooking appliances which require materials with high temperature resistance. There is a group exploring radiation dosimetry with an optical system and their report on their preliminary research states that VYCOR[®] 7930 worked well for radiation dosimetry when applying zinc sulphide (ZnS) nanocrystallites [Justus *et al.*, 1995]. However, Klaumunzer suggests that Vycor is not good for application in track generating ion dosimetry [Klaumunzer, 2000].

The work done in this thesis has shown that VYCOR[®] 7930 is a radiation tolerant material. The damage is low even with accumulated doses. The work with VYCOR[®] 7930 with QD doping has shown that all the damage is done to the QDs and not to the VYCOR[®] 7930. VYCOR[®] 7930 has proven to be a stable material to host and support the QDs.

In the optical system experiment, VYCOR[®] 7930 has demonstrated its potential as a readout dosimeter. The fluorescence was stable for up to 6 hours after irradiation and degrades after two days. VYCOR[®] 7930 with QD doping works as a dosimeter by measuring the fluorescence before, after and during the irradiation and has the potential to be developed into a 2D real-time dosimetry system. The important remark that can be made is the potential of VYCOR[®] 7930 with QDs doping for dosimetry applications. VYCOR[®] 7930 works well as a host for QDs and QDs provide the ability to fluoresce.

Chapter 7

Summary and Conclusion

Any type of radiation dosimetry is depends on the material used as a dosimeter. Dosimeter's material has to be inert, tough, sensitive to dose and good in reproducibility. These characteristics are parts of the dosimetric techniques that have to be considered in developing a dosimeter. This thesis was determined to provide findings from VYCOR[®] 7930 with doping of QDs with an optical readout to enable real-time 2D dosimetry. The electron/photon Monte Carlo code PENELOPE was used to enable realistic modelling of the dosimeter.

In this thesis, works were concentrated on the response of glass towards ⁶⁰Co gamma radiation. Radiation damage was monitored by optical absorbance measurement with the respect of the wavelength in the near-UV to near-IR region. A soda-lime, microscope slide was evaluated in order to agree with commercial plate window glass as their silica component is identical at about 70% to 74%. It was shown that the microscope slide demonstrates the radiation damage at absorption bands region of 400 nm to 440 nm and 600 nm to 620 nm of the wavelength. It was due to the formation of colour centres during the irradiation process. The presence of impurities was reported to influence that particular effect.

Evaluation of the nano-porous VYCOR[®] 7930 was carried out. It shows that VYCOR[®] 7930 has low radiation damage at any region at doses up to 900 Gy. Thus VYCOR[®] 7930 is shown to be a stable substrate for hosting a material with significant change in properties with radiation. In an optical experiment, VYCOR[®] 7930 with doping of fluorescent CdSe/ZnS core-shell quantum dots (QDs) demonstrates the possibility as a readout dosimeter by measuring the fluorescence. The QDs fluorescence was stable for a period of at least 6 hours.

To summarize, VYCOR[®] 7930 with QDs doping shows good potential in dosimetry application, which is VYCOR[®] 7930 works as a host and QDs provide the ability to fluoresce. Fluorescent QDs of different emission wavelengths can be simultaneously excited by a single near-UV light source (e.g. violet LED). This provides the potential for some energy discrimination if a different size QDs, thus different emission colour, is absorbed into opposite faces of the VYCOR[®] 7930 slab since low energy electrons (or photons) will cause preferential damage to the layer nearest to the source. High energy radiation provides a more uniform deposition of energy and damages both sets of QD more uniformly. Looking at the colour as well as the intensity change could thus provide some further information.

Future work

As VYCOR[®] 7930 with doping of quantum dots shows a promising material as a dosimeter, further work in real-time experiment is really worthwhile to continue. This work will relate to the potential dosimetry for 2D and real-time dosimetry. The pilot experiment

is expected to be done in gamma irradiation bunker with the optical system demonstrated in this thesis.

Bibliography

Alouani-Bibi F, Lazurik VT, Rogov YV and Tabata T. (2000). Approximation of charge-deposition density in thin slabs irradiated by electrons. *Radiation Physics and Chemistry*. 59, 239-248.

Baharin R, Hobson PR, Leslie DE and Smith DR. (2012). Effect of gamma radiation on potential ionising detectors and dosimeters based on quantum dots. *Proceedings of the IEEE Nano 2012 Conference*. Birmingham.

Baharin R, Hobson PR and Smith DR. (2010). Simulation of MeV electron energy deposition in CdS quantum dots absorbed in silicate glass for radiation dosimetry. *Journal of Physics: Conference Series*. 245 012007.

Bartlett DT. (2008). 100 years of solid state dosimetry and radiation protection dosimetry. *Radiation Measurements*. 43, 133-138.

Berger MJ, Coursey JS, Zucker MA and Chang J. (2005). ESTAR, PSTAR and ASTAR: Stopping power and range tables for electrons, protons and helium ions. (version 1.2.3). [Online] Available: <http://physics.nist.gov/Star>. National Institute of Standards and Technology, Gaithersburg, MD.

Beezhold W, Beutler DE, Garth JC and Griffin PJ. (2003). A review of the 40-year history of the NSREC's dosimetry and facilities session (1963-2003). *IEEE Transactions on Nuclear Science*. 50 (3), 635.

Brown DW, Sokol PE, Clarke AP, Alam MA and Nuttall WJ. (1997). The structure of solid CO₂ in porous Vycor glass. *Journal Physics of Condensation Matter*. 9, 7317-7325.

Caldas LVE and Teixeira MI. (2002). Commercial glass for high doses using different dosimetric techniques. *Radiation Protection Dosimetry*. 101 (1-4), 149-152.

Capoen B, Gacoin T, Nèdèlec JM, Turrell S and Bouazaoui M. (2001). Spectroscopic investigations of CdS nanoparticles in sol-gel derived polymeric thin films and bulk silica matrices. *Journal of Materials Science*. 36, 2565-2570.

- Chahboun A, Rolo AG, Filonovich SA and Gomes MJM. (2006). Factors influencing the passivation of CdS quantum dots embedded in silica glass. *Solar Energy Materials & Solar Cells*. 90, 1413-1419.
- Chernov V, Rogalev B and Barboza-Flores M. (2005). Dose rate effect on the yield of radiation induced response with thermal fading. *Radiation Measurements*. 39, 329-335.
- Chiavassa S, Lemosquet A, Aubineau-Lanière I, de Carlan L, Clairand I, Ferrer L, Bardiès M, Franck D and Zankl M. (2005). Dosimetric comparison of Monte Carlo codes (EGS4, MCNP, MCNPX) considering external and internal exposures of the zupal phantom to electron and photon sources. *Radiation Protection Dosimetry*. 116 (1-4), 631-635.
- Chica U, Anguiano M and Lallena AM. (2008). Benchmark of PENELOPE for low and medium energy X-rays. *Physica Medica*. xx, 1-7.
- Connaghan JP, Saylor MC, Calvert GW, Yeadon SC, Pyne CH, Mellor P and Patil DS. (2004). Mathematical modelling of industrial radiation processes application and end-user training. *Radiation Physics and Chemistry*. 71, 333-336.
- Corning (2001). VYCOR[®] brand porous glass 7930. *Corning Incorporated* [Online]. Available at <http://www.corning.com/docs/specialtymaterials/pisheets/Vycor%207930.pdf> (Accessed: 31 May 2009).
- CR Nave (2013). Quantum Physics. *HyperPhysics* [Online]. Available at <http://hyperphysics.phy-astr.gsu.edu/hbase/hph.html> (Accessed: 28 February 2013).
- De Deene Y. 2002. Gel dosimetry for the dose verification of intensity modulated radiotherapy treatments. *Z Medical Physics*. 12 (2)77-88.
- Dekanozishvili G, Driaev D, Kalabegishvili T and Kvatchadze V. (2009). Thermoluminescence and absorption spectra of CdSe quantum dot-doped glass irradiated by X-rays. *Journal of Luminescence*. 129, 1154-1157.
- Delaye J-M, Peugeot S, Bureau G and Calas G. (2011). Molecular dynamics simulation of radiation damage in glasses. *Journal of Non-Crystalline Solids*. [Online] doi:10.1016/j.jncrysol.2011.02.026.
- Doran SJ. (2009). The history and principles of chemical dosimetry for 3-D radiation fields: Gels, polymers and plastics. *Applied Radiation and Isotopes*. 67, 393-398.
- Drouin D, Couture AR, Joly D, Tastet X, Aimez V and Gauvin R. (2007). CASINO V2.42 - A fast and easy-to-use modelling tool for scanning electron microscopy and microanalysis users. *Scanning*. 29, 92-101.
- El-Badry BA, Zaki MF, Hegazy TM and Morsy AA. 2007. Neutron response study using poly allyl diglycol carbonate. *Pramana*. 69 (4) 669-674.

- El Ghazaly M and Al-Thomali TA. 2013. Characterization of photoluminescence spectra from poly allyl diglycol carbonate (CR-39) upon excitation with the ultraviolet radiation of various wavelengths. *Radiation effects and defects in solids*. 168 (4) 316-321.
- Faddegon BA, Kawrakow I, Kubyshev Y, Perl J, Sempau J and Urban L. (2009). Accuracy of EGSnrc, Geant4 and PENELOPE Monte Carlo systems for simulation of electron scatter in external beam radiotherapy. *Physics Medical Biology*. 54 (20) 6151-6163.
- Farah K, Kovacs A, Mejri A and Ouada HB. (2007). Effect of post-irradiation thermal treatments on the stability of gamma-irradiated glass dosimeter. *Radiation Physics and Chemistry*. 76, 1523-1526.
- Feng Q, Dong L, Huang J, Li Q, Fan Y, Xiong J and Xiong C. (2010). Flexible monodisperse quantum dots with efficient luminescence. *Angewandte Chemie International Edition*. 49, 9943-9946.
- Guimarães CC, Moralles M and Okuno E. (2008). Performance of GEANT4 in dosimetry: Calculations of X-spectra and kerma-to-dose equivalent conversion coefficients. *Radiation Measurements*. 43, 1525-1531.
- Hammer NI, Emrick T and Barnes MD. (2007). Quantum dots coordinated with conjugated organic ligands: new nanomaterials with novel photophysics. *Nanoscale Resources Letter*. 2, 282-290.
- Hashim S, Al-Ahbab S, Bradley DA, Webb M, Jeynes C, Ramli AT and Wagiran H. (2009). The thermoluminescence response of doped SiO₂ optical fibres subjected to photon and electron irradiations. *Applied Radiation and Isotopes*. 67, 423-427.
- Hernandez-Ortiz M, Bernal R, Cruz-Vazquez C, Morales J and Castano VM. 2012. High dosage thermoluminescence diamond dosimeters. *Journal of Superhard Materials*. 34 (4) 234-238.
- Hobson PR, Leslie DE and Simth DR. (2011). Effect of gamma radiation on potential ionising radiation detectors and dosimeters based on quantum dots. *Nuclear Science Symposium and Medical Imaging Conference Record 2011*. 3015-1017.
- Hollas JM. (1996). *Modern Spectroscopy*. 4th edition. New York.
- Hong SI, Lee YN, Cho SY, Whiteside WS and Park HJ. (2008). The spectroscopic analysis of γ -irradiated glass by colorimetry, ESR and XPS. *Radiation Measurements*. 43, 1365-1371.
- Hosono H, Kajihara K, Suzuki T, Ikuta Y, Skuja L and Hirano M. (2002). Vacuum ultraviolet optical absorption band of non-bridging oxygen hole centers in SiO₂ glass. *Solid State Communications*. 122, 117-120.
- Hsu B-C, Chang ST, Chen T-C, Kuo P-S, Chen PS, Pei Z and Liu CW. (2003). A high efficient 820 nm MOS Ge quantum dot photodetector. *IEEE Electron Device Letters*. 24 (5), 318-320.

- Huston AL, Justus BL and Johnson TL. (1996). Fiber-optic-coupled, laser heated thermoluminescence dosimeter for remote radiation sensing. *Applied Physics Letters*. 68 (24), 3377-3379.
- Huston AL and Justus BL. (1998). Optically transparent, optically stimuable glass composites for radiation dosimetry. *United States Patent Documents*. Patent number 5,811,822.
- Immucci AN, Chamson-Reig A, Yu K, Wilkinson D, Li C, Stodlika RZ and Carson JLL. (2011). Method for imaging quantum dots during exposure to gamma radiation. *Proceedings SPIE* 7925, 792504. [Online] [doi:10.1117/12.875379](https://doi.org/10.1117/12.875379).
- Ivanchenko VN. (2003). GEANT4 toolkit for simulation of HEP experiments. *Nuclear Instruments and Methods in Physics Research A*. 502, 666-668.
- Izewska J and Rajan G. (2005). Radiation dosimeters. In: Podgorsak EB (technical editor). *Radiation Oncology Physics: A Handbook for Teachers and Students*. Austria: IAEA Vienna. 71-99.
- Jasieniak J, Pacifico J, Signorini R, Chiasera A, Ferrari M, Martucci A and Mulvaney P. (2007). Luminescence and amplified stimulated emission in Cdse-ZnS-nanocrystal-doped TiO₂ and ZrO₂ waveguides. *Advanced Functional Materials*. 17, 1654-1662.
- Jennings WA. (2007). Evolution over the past century of quantities and units in radiation dosimetry. *Journal of Radiological Protection*. 27, 5-16. [Online] [doi:10.1088/0952-4746/27/1/R01](https://doi.org/10.1088/0952-4746/27/1/R01).
- Joy DC. (1995). A database on electron-solid interactions. *Scanning*. 17, 270-275.
- Justus BL and Huston AL. (1995). Ultraviolet dosimetry using thermoluminescence of semiconductor-doped Vycor glass. *Applied Physics Letters*. 67 (9), 1179-1181.
- Justus BL, Falkenstein P, Huston AL, Plazas MC, Ning Holly and Miller RW. (2004). Gated fiber-optic-coupled detector for in vivo real-time radiation dosimetry. *Applied Optics*. 43 (8), 1663-1668.
- Justus BL, Rychnovsky S, Miller MA, Pawlovich KJ and Huston AL (1997). Optically stimulated luminescence radiation dosimetry using doped silica glass. *Radiation Protection Dosimetry*. 74 (3), 151-154.
- Kaye & Laby Online (2008). Absorption of photons. *Tables of Physical & Chemical Constants* [Online]. Available at www.kayelaby.npl.co.uk (Accessed: 20 February 2013).
- Khan HM and Ali SW. (1995). Environmental effects on dosimetric properties of commercially available window glass sheets. *Radiation Physics and Chemistry*. 46 (4-6), 1203-1206.
- Klaumünzer S. (2000). Radiation compaction of porous Vycor glass. *Nuclear Instruments and Method in Physics Research B*. 166-167, 459-464.
- Kovacs A and Miller A (2004). Present status and expected progress in radiation processing dosimetry. In: IAEA. *Emerging Applications of Radiation Processing, 28-30 April 2003, Vienna, Austria: IAEA Vienna*. 85-93.

- Kuhr J-Ch and Fitting H-J. (1999). Monte Carlo simulation of electron emission from solids. *Journal of Electron Spectroscopy and Related Phenomena*. 105, 257-273.
- Kuntz F. (2004). Quality assurance in radiation processing, dosimetry and control methods for radiation processing. In: IAEA. *Emerging Applications of Radiation Processing, Vienna, Austria: IAEA Vienna*.
- Liu GQ, Liao YB and Tao XY. (2010). Characteristic of spontaneous emission from CdSe/ZnS core-shell quantum dots near the surface of self-assembled three-dimensional photonic crystals. *Journal of Modern Optics*. iFirst, 1-5.
- Liu HC, Gao M, McCaffrey J, Wasilewski ZR and Fafard S. (2000). Quantum dot infrared photodetectors. *Applied Physics Letters*. 78 (1), 79-81.
- Lu SG, Mak YJ, Wong KH, Zhang LY and Yao X. (2003). Nonlinear optical properties in CdS /silica nanocomposites. *Microelectronic Engineering*. 66, 171-179.
- Maly P and Miyoshi T. (2000). Effect of photodarkening on photoluminescence dynamics in CdS-doped glass. *Journal of Luminescence*. 90, 129-134.
- McLaughlin W and Desrosiers MF. (1995). Dosimetry systems for radiation processing. *Radiation Physics and Chemistry*. 46 (4-6), 1163-1174.
- Mejri A, Farah K, Eleuch H and Ouada HB. (2008). Application of commercial glass in gamma radiation processing. *Radiation Measurements*. 43, 1372-1376.
- Miyoshi T, Furukawa H, Nitta K, Okuni H and Matsuo N. (1997). Effects of light and X-ray irradiation on CdS-doped glass. *Solid State Communications*. 104 (8), 451-454.
- Miyoshi T, Kawamura T, Kobayashi T, Shinohara T, Takeshita T, Takahashi Y, Tamechika M, Tokuda N, Fukumoto T and Kaneda T. (2004). Thermoluminescence of X-ray-irradiated CdS-doped glass. *Japanese Journal of Applied Physics*. 43 (4A), 1427-1428.
- Miyoshi T, Makidera Y, Kawamura T, Matsuo N and Kaneda T. (2003). Thermoluminescence in semiconductor-doped glasses. *Journal of Luminescence*. 102-103, 614-617.
- Miyoshi T, Matsuki H and Matsuo N. (1995). Influence of microcrystallite size on photodarkening effects in CdS-doped glasses. *Japanese Journal of Applied Physics*. 34 (4A), 1837-1838.
- Miyoshi T, Migita K, Tamechika M, Toduka M, Fukumoto T and Kaneda T. (2006). CdS-doped glass as dosimetric material with electron spins resonance. *Japanese Journal of Applied Physics*. 45 (9A), 7105-7107.
- Miyoshi T, Ushigusa K, Migita K, Tamechika M, Tokuda N and Kaneda T. (2008). Thermoluminescence and induced absorption in X-ray-irradiated CdS-doped glasses. *Journal of Material Sciences*. 43, 203-206.
- Napchan E. (1992). Monte Carlo simulation of electron trajectories. *European Microscopy and Analysis*. 21-23.

- Narayan P, Vaijapurkar SG, Senwar KR, Kumar D and Bhatnagar PK. (2008). Application of commercial glasses for high gamma dose measurement using optical densitometric technique. *Radiation Measurements*. 43, 1237-1241.
- Obata S, Yoshida T, Tanabe T, Allen C, Okada M and Xu Q. (2006). Effects of secondary electrons emitted from surroundings on defect formation in silica glass under γ -ray irradiation. *Nuclear Instruments and Methods in Physics Research B*. 250, 169-173.
- Obyrk B, Bilski B, Glaser M, Fuerstner M, Budzanowski M and Olko P. 2010. The response of TL lithium fluoride detectors to 24 GeV/c protons for doses ranging up to 1 MGy. *Radiation Measurements*. 45 (3-6) 643-645.
- Obyrk B, Cywicka-Jakiel T, Budzanowski M, Bilski P, Hranitzky C, Olko P and Stadtmann H. (2008). Measurements and Monte Carlo simulations of the response of the RADOS personal dosimeters with MTS-N (LiF:Mg,Ti) and MCP-N (LiF:Mg,Cu,P) thermoluminescent detectors to X- and gamma-rays. *Radiation Measurements*. 43, 616-620.
- Panettieri V, Duch MA, Jornet N, Ginjaume M, Carrasco P, Badal A, Ortego X and Ribas M. (2007). Monte Carlo simulation of MOSFET detectors for high-energy photon beams using the PENELOPE code. *Physics Med Biology*. 52, 303-316.
- Pfeiffer A and Pia MG. (2002). Tools for simulation and analysis. Proceedings of ICHEP 2002. Amsterdam. 888-890.
- Pia MG. (2003). The GEANT4 toolkit: Simulation capabilities and application results. *Nuclear Physics B*. 125, 60-68.
- Price TJ. (1994). Development of dense scintillating radiation hard fluoride glasses for the electromagnetic calorimeter of the proposed Compact Muon Solenoid. *PhD Thesis*. Brunel University.
- Pugh-Thomas D, Walsh BM and Gupta MC. (2011). CdSe(ZnS) nanocomposite luminescent high temperature sensor. *Nanotechnology*. 22, 185503. [Online] [doi:10.1088/0957-4484/22/18/185503](https://doi.org/10.1088/0957-4484/22/18/185503).
- Reynaert N, van der Marck SC, Schaart DR, van der Zee W, van Vliet-Vroegindewij C, Tomsej M, Jansen J, Heijmen B, Coghe M and De Wagter C. (2007). Monte Carlo treatment planning for photon and electron beams. *Radiation Physics and Chemistry*. 76, 643-686.
- Rodrigues Jr. AdA and Caldas LVE. (2002). Commercial plate window glass tested as a routine dosimeter at a gamma irradiation facility. *Radiation Physics and Chemistry*. 63, 765-767.
- Rysiakiewicz-Pasek E, Zalewska M and Polanska J. (2008). Optical properties of CdS-doped porous glasses. *Optical Materials*. 30, 777-779.
- Ryzhii V. (1996). The theory of quantum-dot infrared phototransistors. *Semiconductor Science Technology*. 11, 759-765.

- Salvatore Coffa (2005). Light from silicon. *IEEE Spectrum* [Online]. Available at <http://m.spectrum.ieee.org/semiconductors/processors/light-from-silicon/> (Accessed: 28 January 2013).
- Salvat F and Fernández-Varea JM. (2009). Overview of physical interaction models for photon and electron transport used in Monte Carlo codes. *Metrologia*. 46 (1), S112-S138.
- Salvat F, Fernandez-Varea JM and Sempau J. (2008). PENELOPE-2008: A code system for Monte Carlo simulation of electron and photon transport. OECD-NEA Data Bank. Available at <http://www.oecd-nea.org/science/pubs/2009/nea6416-penelope.pdf> (Accessed: 28 January 2013).
- Salvat F, Fernandez-Varea JM, Sempau J and Llovet X. (2006). Monte Carlo simulation of bremsstrahlung emission by electrons. *Radiation Physics and Chemistry*. 75, 1201-1219.
- Santhi S and Trojanek F. (2005). Investigation of nonlinear properties of CdS-doped glasses. *Physica E*. 27, 38-44.
- Saylor MC and Jordan TM. (2000). Application of mathematical modelling technologies to industrial radiation processing. *Radiation Physics and Chemistry*. 57, 697-700.
- Saylor MC, Connaghan JP, Yeadon SC, Herring CM and Jordan TM. (2002). Design and application of process control charting methodologies to gamma irradiation practices. *Radiation Physics and Chemistry*. 65, 621-626.
- Schaeken B, Lelie S, Meijnders P, Van den Weyngaert D, Janssens H and Verellen D. 2010. Alanine/EPR dosimetry applied to the verification of a total body irradiation protocol and treatment planning dose calculation using a humanoid phantom. *Medical Physics*. 37(12) 6292-6299.
- Seltzer SM and Hubbell JH (2011). Table of X-ray mass attenuation coefficients and mass energy-absorption coefficients from 1 keV to 20 MeV for elements Z=1 to 92 and 48 additional substances of dosimetric interest [Online]. Available at <http://www.nist.gov/pml/data/xraycoef/index.cfm> (Accessed: 28 February 2013).
- Sempau J and Andreo P. (2006). Configuration of the electron transport algorithm of PENELOPE to simulate ion chambers. *Physics Medicine Biology*. 51, 3533-3548.
- Sempau J, Fernandez-Varea JM, Acosta E and Salvat F. (2003). Experimental benchmarks of the Monte Carlo code PENELOPE. *Nuclear Instruments and Methods in Physics Research B*. 207, 107-123.
- Seuntjens JP, Strydom W and Shortt KR. (2005). Dosimetric principles, quantities and units. In: Podgorsak EB (technical editor). *Radiation Oncology Physics: A Handbook for Teachers and Students*. Austria: IAEA Vienna. 45-70.
- Sharma SC, Murphree J and Chajraborty T. (2008). Photoluminescence spectra of thin films containing CdSe/ZnS quantum dots irradiated by 532-nm laser radiation and gamma-rays. *Journal of Luminescence*. 128, 1771-1776.

- Sheng J, Kadono K and Yazawa T. 2002. Fading behaviour of X-ray induced color centers in soda-lime silicate glass. *Applied Radiation and Isotopes*. 57, 813-817.
- Sigma-Aldrich (2011) Lumidots: Quantum Dot Nanocrystals. Available at: <http://www.sigmaaldrich.com/materials-science/nanomaterials/lumidots.html> (Accessed: 28 February 2013).
- Singh M, Singh G, Singh B and Sandhu BS. (2008). Experimental observation of energy dependence of saturation thickness of multiply scattered gamma photos. *Radiation Physics and Chemistry*. 77, 991-995.
- Somma F, Aloe P, d'Acapito F, Montereali RM, Polosan S, Secu M and Vincenti MA. 2010. Optical and X-ray absorption spectroscopy in lead doped lithium fluoride crystals. *IOP Conference Series: Materials Science and Engineering*. 15 012035 doi:10.1088/1757-899X/15/1/012035.
- Sonawane RS, Apte SK, Naik SD, Raskar DB and Kale BB. (2008). Preparation and optical study of CdS nanocrystals embedded phosphate glass. *Material Research Bulletin*. 43, 618-624.
- Sorensen L, Strouse GF and Stiegman AE. (2006). Fabrication of stable low-density silica aerogels containing luminescent ZnS capped CdSe quantum dots. *Advanced Materials*. 18, 1965-1967.
- Stodilka RZ, Carson JLL, Yu K, Zaman MB, Li C and Wilkinson D. (2009). Optical degradation of CdSe/ZnS quantum dots upon gamma-ray irradiation. *Journal of Physical Chemistry C*. **113** (6), 2580-2585.
- Svidzinsky AA, Scully MO and Herschbach DR. (2005). *Bohr's 1913 molecular model revisited*. Available: <http://www.pnas.org/cgi/doi/10.1073/pnas.0505778102>. Last accessed 10th October 2012.
- Taheri M, Jafarizadeh M, Baradaran S and Zainali G. 2006. Development of a high efficiency personal/environmental radon dosimeter using polycarbonate detectors. *Journal of Radiation Protection*. 26(4). 389-395.
- Teixeira MI, Ferraz GM and Caldas LVE. (2007). Thermal treatments to minimize fading effects of colored glass radiation detectors. *Nuclear Instruments and Methods in Physics Research B*. 263, 67-71.
- Usman S, Shoaib L and Anno JN. (2005). Gamma-ray induced photoconductivity in Pyrex, Quartz and Vycor. *IEEE Transactions on Nuclear Science*. **52** (6), 3054-3058.
- Vilches M, Garcia-Pareja S, Guerrero R, Anguiano M and Lallena AM. (2007). Monte Carlo simulation of the electron transport through thin slabs: A comparative study of PENELOPE, GEANT3, GEANT4, EGSnrc and MCNPX. *Nuclear Instruments and Methods in Physics Research B*. 254, 219-230.
- Withers NJ, Sankar K, Akins BA, Memon TA, Gu T, Gu J, Smolyakov GA, Greenberg MR, Boyle TJ and Osinski M. (2008). Rapid degradation of CdSe/ZnS colloidal quantum dots exposed to gamma irradiation. *Applied Physics Letters*. 93, 173101.

Zheng Z, Jiansheng C, Jiating Z, Honggui D, Yongfu Z, Shangze H and Jie F. (1997). Study on the possibility of reading two kinds of data from one glass detector. *Radiation Physics and Chemistry*. 50 (3), 303-305.

Zyball A (2004). Radiation processing of polymers. In: IAEA. *Emerging Applications of Radiation Processing, 28-30 April 2003, Vienna, Austria: IAEA Vienna*. 117-125.

Appendix A

In PENELOPE, material data file (.mat) is developed prior to execute the simulation. It is providing the detailed transitions in material depending on material's chemical composition key-in by user or selected from *pdcompos.p08* as in Appendix B. Figure A.1 until A.5 below show part of material data (.mat) for NaI, Al₂O₃, Al, Vycor and CdSe/ZnS, respectively, since the original data will take up more than 600 pages.

```
PENELOPE (v. 2008) Material data file .....
Material: SODIUM IODIDE (253)
Mass density = 3.66700000E+00 g/cm**3
Number of elements in the molecule = 2
  Element: Na (Z=11), atoms/molecule = 1.00000000E+00
  Element: I (Z=53), atoms/molecule = 1.00000000E+00

Molecular density = 1.47329327E+22 1/cm**3

*** Electron/positron inelastic scattering.
Plasma energy = 3.60571885E+01 eV
Mean excitation energy = 4.52000000E+02 eV
Number of oscillators = 16
```

	Fi	Ui (ev)	wi (ev)	KZ	KS
1	1.00000000E+00	5.13900000E+00	1.02548913E+01	11	5
2	5.00000000E+00	1.04500000E+01	2.03471431E+01	53	30
3	2.00000000E+00	2.06100000E+01	3.87390725E+01	53	30
4	6.00000000E+00	3.40000000E+01	6.36831750E+01	11	3
5	1.20000000E+01	5.83333333E+01	1.08763910E+02	0	2
6	8.00000000E+00	1.49000000E+02	2.73890779E+02	53	30
7	6.00000000E+00	6.26000000E+02	1.16601337E+03	53	9
8	4.00000000E+00	6.38000000E+02	1.18835234E+03	53	8
9	4.00000000E+00	8.81000000E+02	1.64095433E+03	53	7
10	2.00000000E+00	9.37000000E+02	1.74525038E+03	53	6
11	2.00000000E+00	1.07500000E+03	2.00228618E+03	11	1
12	2.00000000E+00	1.07800000E+03	2.00787392E+03	53	5
13	4.00000000E+00	4.56300000E+03	8.49898084E+03	53	4
14	2.00000000E+00	4.85800000E+03	9.04844187E+03	53	3
15	2.00000000E+00	5.19500000E+03	9.67613309E+03	53	2
16	2.00000000E+00	3.31760000E+04	6.17931369E+04	53	1

```
*** Compton scattering (Impulse Approximation).
Number of shells = 13
```

	Fi	Ui (ev)	Ji(0)	KZ	KS
1	6.00000000E+00	9.56483333E+00	8.66166667E-01	0	30
2	2.00000000E+01	4.72610000E+01	2.71900000E-01	0	30
3	8.00000000E+00	1.49000000E+02	2.12250000E-01	53	30
4	6.00000000E+00	6.26000000E+02	5.21000000E-02	53	9
5	4.00000000E+00	6.38000000E+02	5.15000000E-02	53	8
6	4.00000000E+00	8.81000000E+02	7.74000000E-02	53	7
7	2.00000000E+00	9.37000000E+02	7.48000000E-02	53	6
8	2.00000000E+00	1.07500000E+03	8.15000000E-02	11	1
9	2.00000000E+00	1.07800000E+03	1.26000000E-01	53	5
10	4.00000000E+00	4.56300000E+03	2.85000000E-02	53	4
11	2.00000000E+00	4.85800000E+03	2.72000000E-02	53	3
12	2.00000000E+00	5.19500000E+03	5.47000000E-02	53	2
13	2.00000000E+00	3.31760000E+04	1.53000000E-02	53	1

```
*** RELAX: Z = 11, no. of shells = 5, no. of transitions = 14
```

i	Shell	f	Ui (ev)
1	1s1/2 K	2	1.07500000E+03
2	2s1/2 L1	2	6.60000000E+01
3	2p1/2 L2	2	3.40000000E+01

4 2p3/2 L3 4 3.4000000E+01
 5 3s1/2 M1 1 5.1390000E+00

S0	S1	S2	Probability	Energy (eV)
K	L2		6.68996000E-03	1.04098000E+03
K	L3		1.32959000E-02	1.04098000E+03
K	L1	L1	8.70552000E-02	9.35040000E+02
K	L1	L2	8.90021000E-02	9.63100000E+02
K	L1	L3	1.75052000E-01	9.63300000E+02
K	L1	M1	5.73825000E-03	9.94370000E+02
K	L2	L2	1.46296000E-02	9.91160000E+02
K	L2	L3	3.82369000E-01	9.91360000E+02
K	L2	M1	2.69932000E-03	1.02243000E+03
K	L3	L3	2.18165000E-01	9.91560000E+02
K	L3	M1	5.30407000E-03	1.02263000E+03
L1	X		1.16019000E-04	6.44800000E+01
L1	L2	X	3.34898000E-01	2.80600000E+01
L1	L3	X	6.64986000E-01	2.82600000E+01

*** RELAX: z = 53, no. of shells = 17, no. of transitions = 525

i	Shell	f	Ui (eV)
1	1s1/2 K	2	3.31760000E+04
2	2s1/2 L1	2	5.19500000E+03
3	2p1/2 L2	2	4.85800000E+03
4	2p3/2 L3	4	4.56300000E+03
5	3s1/2 M1	2	1.07800000E+03
6	3p1/2 M2	2	9.37000000E+02
7	3p3/2 M3	4	8.81000000E+02
8	3d3/2 M4	4	6.38000000E+02
9	3d5/2 M5	6	6.26000000E+02
10	4s1/2 N1	2	1.93000000E+02
11	4p1/2 N2	2	1.41000000E+02
12	4p3/2 N3	4	1.31000000E+02
13	4d3/2 N4	4	5.80000000E+01
14	4d5/2 N5	6	5.60000000E+01
17	5s1/2 O1	2	2.06100000E+01
18	5p1/2 O2	2	1.04500000E+01
19	5p3/2 O3	3	1.04500000E+01

S0	S1	S2	Probability	Energy (eV)
K	L2		2.54309000E-01	2.83175000E+04
K	L3		4.72118000E-01	2.86123000E+04
K	M2		4.39088000E-02	3.22397000E+04
K	M3		8.51517000E-02	3.22950000E+04
K	M4		4.12249000E-04	3.25388000E+04
K	M5		5.65058000E-04	3.25501000E+04
K	N2		9.15607000E-03	3.30417000E+04
K	N3		1.79119000E-02	3.30417000E+04
K	N4		7.32237000E-05	3.31182000E+04
K	N5		1.00070000E-04	3.31200000E+04
K	O2		7.32127000E-04	3.31532000E+04
K	O3		1.37130000E-03	3.31544000E+04
K	L1	L1	8.91673000E-03	2.28402000E+04
K	L1	L2	1.06418000E-02	2.31446000E+04
K	L1	L3	1.30507000E-02	2.34476000E+04
K	L1	M1	3.17941000E-03	2.69467000E+04
K	L1	M2	2.02890000E-03	2.70749000E+04
K	L1	M3	2.51372000E-03	2.71323000E+04
K	L1	M4	1.68000000E-04	2.73606000E+04
K	L1	M5	1.83814000E-04	2.73728000E+04
K	L1	N1	6.84137000E-04	2.78111000E+04
K	L1	N2	4.10625000E-04	2.78566000E+04
K	L1	N3	5.05507000E-04	2.78679000E+04
K	L1	N4	3.01428000E-05	2.79421000E+04
K	L1	N5	3.28600000E-05	2.79438000E+04
K	L2	L2	1.33390000E-03	2.34490000E+04
K	L2	L3	2.82368000E-02	2.37520000E+04
K	L2	M1	1.57310000E-03	2.72511000E+04
K	L2	M2	4.55341000E-04	2.73793000E+04
K	L2	M3	4.53287000E-03	2.74367000E+04
K	L2	M4	2.03331000E-04	2.76650000E+04
K	L2	M5	6.81651000E-04	2.76772000E+04
K	L2	N1	3.25647000E-04	2.81155000E+04
K	L2	N2	9.04264000E-05	2.81610000E+04
K	L2	N3	8.81532000E-04	2.81723000E+04
K	L2	N4	3.60726000E-05	2.82465000E+04
K	L2	N5	1.20073000E-04	2.82482000E+04

K	L3	L3	1.41721000E-02	2.40550000E+04
K	L3	M1	1.89061000E-03	2.75541000E+04
K	L3	M2	4.42382000E-03	2.76823000E+04
K	L3	M3	4.67357000E-03	2.77397000E+04
K	L3	M4	8.13596000E-04	2.79680000E+04
K	L3	M5	7.49837000E-04	2.79802000E+04
K	L3	N1	3.89866000E-04	2.84185000E+04
K	L3	N2	8.64481000E-04	2.84640000E+04
K	L3	N3	9.14422000E-04	2.84753000E+04
K	L3	N4	1.44039000E-04	2.85495000E+04
K	L3	N5	1.32428000E-04	2.85512000E+04
K	M1	M1	2.79178000E-04	3.10532000E+04
K	M1	M2	3.02645000E-04	3.11814000E+04
K	M1	M3	3.67138000E-04	3.12388000E+04
K	M1	M4	2.32233000E-05	3.14671000E+04
K	M1	M5	2.44589000E-05	3.14793000E+04
K	M1	N1	1.19826000E-04	3.19176000E+04
K	M1	N2	6.12717000E-05	3.19631000E+04
K	M1	N3	7.38715000E-05	3.19744000E+04
K	M1	N4	4.20010000E-06	3.20486000E+04
K	M1	N5	4.44713000E-06	3.20503000E+04
K	M2	M2	3.73070000E-05	3.13096000E+04
K	M2	M3	7.22172000E-04	3.13670000E+04
K	M2	M4	2.49538000E-05	3.15953000E+04
K	M2	M5	8.32602000E-05	3.16075000E+04
K	M2	N1	6.27548000E-05	3.20458000E+04
K	M2	N2	1.48233000E-05	3.20913000E+04
K	M2	N3	1.40835000E-04	3.21026000E+04
K	M2	N4	4.44717000E-06	3.21768000E+04
K	M2	N5	1.48233000E-05	3.21785000E+04
K	M3	M3	3.86652000E-04	3.14244000E+04
K	M3	M4	1.05990000E-04	3.16527000E+04
K	M3	M5	9.53676000E-05	3.16649000E+04
K	M3	N1	7.58480000E-05	3.21031000E+04
K	M3	N2	1.41567000E-04	3.21487000E+04
K	M3	N3	1.51453000E-04	3.21600000E+04
K	M3	N4	1.87766000E-05	3.22341000E+04
K	M3	N5	1.67993000E-05	3.22359000E+04
K	M4	M5	1.21717000E-05	3.18932000E+04
K	M4	N1	4.44716000E-06	3.23315000E+04
K	M4	N2	4.44716000E-06	3.23770000E+04
K	M4	N3	1.87255000E-05	3.23883000E+04
K	M4	N5	2.10657000E-06	3.24643000E+04
K	M5	M5	2.86227000E-06	3.19054000E+04
K	M5	N1	4.77035000E-06	3.23436000E+04
K	M5	N2	1.50265000E-05	3.23892000E+04
K	M5	N3	1.71738000E-05	3.24005000E+04
K	M5	N4	2.14665000E-06	3.24746000E+04
K	M5	N5	9.54089000E-07	3.24764000E+04
K	N1	N1	1.24217000E-05	3.27819000E+04
K	N1	N2	1.24217000E-05	3.28274000E+04
K	N1	N3	1.48109000E-05	3.28388000E+04
K	N1	N4	7.16603000E-07	3.29129000E+04
K	N1	N5	9.55497000E-07	3.29147000E+04
K	N2	N2	1.37022000E-06	3.28729000E+04
K	N2	N3	2.55791000E-05	3.28843000E+04
K	N2	N4	6.85131000E-07	3.29584000E+04
K	N2	N5	2.51218000E-06	3.29602000E+04
K	N3	N3	1.38134000E-05	3.28956000E+04
K	N3	N4	3.22323000E-06	3.29698000E+04
K	N3	N5	2.99304000E-06	3.29715000E+04
K	N4	N5	4.94134000E-07	3.30457000E+04
L1	L2		1.99879000E-05	3.04400000E+02
L1	L3		3.45078000E-04	6.07400000E+02
L1	M2		1.31549000E-02	4.25753000E+03
L1	M3		2.08889000E-02	4.31349000E+03
L1	M4		1.88269000E-04	4.55643000E+03
L1	M5		2.81209000E-04	4.56906000E+03
...				
...				
...				

Figure A.1 Part of material data of NaI (file: *NaI.in*).

PENELOPE (v. 2008) Material data file
 Material: ALUMINUM OXIDE (106)
 Mass density = 3.9700000E+00 g/cm**3
 Number of elements in the molecule = 2
 Element: O (Z= 8), atoms/molecule = 3.0000000E+00
 Element: Al (Z=13), atoms/molecule = 2.0000000E+00

Molecular density = 2.34480848E+22 1/cm**3

*** Electron/positron inelastic scattering.
 Plasma energy = 4.02064714E+01 eV
 Mean excitation energy = 1.45200000E+02 eV
 Number of oscillators = 8

	Fi	Ui (eV)	Wi (eV)	KZ	KS
1	6.0000000E+00	9.0750000E+00	2.37039206E+01	13	5
2	1.2000000E+01	1.3620000E+01	3.51275760E+01	8	3
3	6.0000000E+00	2.8480000E+01	7.04218597E+01	8	2
4	4.0000000E+00	7.7000000E+01	1.88126532E+02	13	3
5	8.0000000E+00	7.7000000E+01	1.88355537E+02	13	4
6	4.0000000E+00	1.2100000E+02	2.95413064E+02	13	2
7	6.0000000E+00	5.3800000E+02	1.31288976E+03	8	1
8	4.0000000E+00	1.5640000E+03	3.81652161E+03	13	1

*** Compton scattering (Impulse Approximation).
 Number of shells = 7

	Fi	Ui (eV)	Ji(0)	KZ	KS
1	1.8000000E+01	1.2105000E+01	6.1100000E-01	0	30
2	6.0000000E+00	2.8480000E+01	5.7900000E-01	8	2
3	8.0000000E+00	7.7000000E+01	1.6800000E-01	13	4
4	4.0000000E+00	7.7000000E+01	1.6800000E-01	13	3
5	4.0000000E+00	1.2100000E+02	3.0500000E-01	13	2
6	6.0000000E+00	5.3800000E+02	1.1300000E-01	8	1
7	4.0000000E+00	1.5640000E+03	6.8600000E-02	13	1

*** RELAX: Z = 8, no. of shells = 4, no. of transitions = 8

i	Shell	f	Ui (eV)
1	1s1/2 K	2	5.3800000E+02
2	2s1/2 L1	2	2.8480000E+01
3	2p1/2 L2	2	1.3620000E+01
4	2p3/2 L3	2	1.3620000E+01

S0	S1	S2	Probability	Energy (eV)
K	L2		1.9076800E-03	5.2309000E+02
K	L3		3.8002700E-03	5.2313000E+02
K	L1	L1	1.7864400E-01	4.7882000E+02
K	L1	L2	1.1622400E-01	4.9386000E+02
K	L1	L3	2.3041800E-01	4.9390000E+02
K	L2	L2	1.1082200E-02	5.0890000E+02
K	L2	L3	2.9111500E-01	5.0894000E+02
K	L3	L3	1.6680900E-01	5.0898000E+02

*** RELAX: Z = 13, no. of shells = 6, no. of transitions = 34

i	Shell	f	Ui (eV)
1	1s1/2 K	2	1.5640000E+03
2	2s1/2 L1	2	1.2100000E+02
3	2p1/2 L2	2	7.7000000E+01
4	2p3/2 L3	4	7.7000000E+01
5	3s1/2 M1	2	9.0750000E+00
6	3p1/2 M2	1	9.0750000E+00

S0	S1	S2	Probability	Energy (eV)
K	L2		1.2369900E-02	1.4863000E+03
K	L3		2.4552800E-02	1.4867100E+03
K	M2		7.5585400E-05	1.5575700E+03
K	M3		1.5003900E-04	1.5575700E+03
K	L1	L1	7.8394400E-02	1.3118000E+03
K	L1	L2	8.3218000E-02	1.3496500E+03
K	L1	L3	1.6272500E-01	1.3501200E+03
K	L1	M1	1.3588400E-02	1.4206900E+03
K	L1	M2	8.9679400E-04	1.4259700E+03
K	L1	M3	1.7648500E-03	1.4259800E+03

```

K L2 L2 1.4292000E-02 1.3875000E+03
K L2 L3 3.66942000E-01 1.38797000E+03
K L2 M1 6.49294000E-03 1.45854000E+03
K L2 M2 3.01318000E-04 1.46382000E+03
K L2 M3 3.65883000E-03 1.46383000E+03
K L3 L3 2.09226000E-01 1.38844000E+03
K L3 M1 1.27063000E-02 1.45901000E+03
K L3 M2 3.65189000E-03 1.46429000E+03
K L3 M3 4.20421000E-03 1.46430000E+03
K M1 M1 5.81139000E-04 1.52958000E+03
K M1 M2 7.17440000E-05 1.53486000E+03
K M1 M3 1.36311000E-04 1.53487000E+03
L1 M2 2.07691000E-06 1.22300000E+02
L1 M3 4.02982000E-06 1.14180000E+02
L1 M1 M2 2.61944000E-03 1.04010000E+02
L1 M1 M3 5.21749000E-03 1.04020000E+02
L1 X 2.49536000E-04 1.19050000E+02
L1 L2 X 3.29551000E-01 3.78500000E+01
L1 L3 X 6.51103000E-01 3.83200000E+01
L1 M1 X 1.12532000E-02 1.08890000E+02
L2 X 1.60533000E-05 8.12000000E+01
L2 M1 X 9.99984000E-01 7.10400000E+01
L3 X 1.50001000E-05 8.07300000E+01
L3 M1 X 9.99985000E-01 7.05700000E+01

*** Electron scaled brems x-section, ZE0 = 1.02956E+01, NDATA = 57
1.00E+03 2.02428E+01 2.04392E+01 2.06260E+01 2.07960E+01 2.09509E+01
2.12243E+01 2.14464E+01 2.16198E+01 2.17487E+01 2.18420E+01
2.19118E+01 2.19622E+01 2.19965E+01 2.20182E+01 2.20337E+01
2.20480E+01 2.20602E+01 2.20672E+01 2.20676E+01 2.20693E+01
2.20793E+01 2.20847E+01 2.20859E+01 2.20812E+01 2.20716E+01
2.20679E+01 2.20648E+01 2.20644E+01 2.20641E+01 2.20641E+01
2.20641E+01 2.20641E+01 1.879E+01
1.50E+03 2.36972E+01 2.39030E+01 2.40955E+01 2.42648E+01 2.44132E+01
2.46594E+01 2.48334E+01 2.49378E+01 2.49800E+01 2.49747E+01
2.49412E+01 2.48846E+01 2.48084E+01 2.47168E+01 2.46196E+01
2.45244E+01 2.44290E+01 2.43267E+01 2.42131E+01 2.40988E+01
2.39974E+01 2.39520E+01 2.39051E+01 2.38658E+01 2.38273E+01
2.38175E+01 2.38092E+01 2.38082E+01 2.38074E+01 2.38073E+01
2.38072E+01 2.38071E+01 2.118E+01
2.00E+03 2.62229E+01 2.64526E+01 2.66609E+01 2.68315E+01 2.69687E+01
2.71669E+01 2.72674E+01 2.72868E+01 2.72376E+01 2.71383E+01
2.70124E+01 2.68647E+01 2.66953E+01 2.65087E+01 2.63181E+01
2.61350E+01 2.59571E+01 2.57759E+01 2.55863E+01 2.54016E+01
2.52329E+01 2.51522E+01 2.50734E+01 2.50129E+01 2.49515E+01
2.49362E+01 2.49242E+01 2.49226E+01 2.49214E+01 2.49213E+01
2.49211E+01 2.49210E+01 2.282E+01
3.00E+03 2.98469E+01 3.01205E+01 3.03544E+01 3.05184E+01 3.06218E+01
3.06994E+01 3.06349E+01 3.04824E+01 3.02616E+01 2.99919E+01
2.96972E+01 2.93853E+01 2.90611E+01 2.87320E+01 2.84040E+01
2.80846E+01 2.77759E+01 2.74796E+01 2.71965E+01 2.69239E+01
2.66643E+01 2.65438E+01 2.64270E+01 2.63365E+01 2.62435E+01
2.62211E+01 2.62031E+01 2.62008E+01 2.61990E+01 2.61988E+01
2.61986E+01 2.61985E+01 2.496E+01
4.00E+03 3.24434E+01 3.27288E+01 3.29619E+01 3.31035E+01 3.31660E+01
3.31267E+01 3.29127E+01 3.26003E+01 3.22173E+01 3.17896E+01
3.13478E+01 3.09004E+01 3.04507E+01 3.00056E+01 2.95709E+01
2.91542E+01 2.87583E+01 2.83836E+01 2.80297E+01 2.76928E+01
2.73770E+01 2.72327E+01 2.70925E+01 2.69828E+01 2.68693E+01
2.68419E+01 2.68200E+01 2.68171E+01 2.68150E+01 2.68147E+01
2.68145E+01 2.68144E+01 2.630E+01
5.00E+03 3.44903E+01 3.47329E+01 3.49236E+01 3.50233E+01 3.50446E+01
3.49205E+01 3.46041E+01 3.41582E+01 3.36199E+01 3.30332E+01
3.24489E+01 3.18778E+01 3.13191E+01 3.07783E+01 3.02619E+01
2.97779E+01 2.93245E+01 2.88912E+01 2.84715E+01 2.80769E+01
2.77232E+01 2.75627E+01 2.74053E+01 2.72809E+01 2.71538E+01
2.71227E+01 2.70980E+01 2.70949E+01 2.70924E+01 2.70921E+01
2.70919E+01 2.70919E+01 2.720E+01
...
...
...

```

Figure A.2 Part of material data of Al₂O₃. (file: *Al2O3.mat*).

PENELOPE (v. 2008) Material data file
 Material: ALUMINUM (13)
 Mass density = 2.69890000E+00 g/cm**3
 Number of elements in the molecule = 1
 Element: Al (Z=13), atoms/molecule = 1.00000000E+00

Molecular density = 6.02370384E+22 1/cm**3

*** Electron/positron inelastic scattering.
 Plasma energy = 3.28594850E+01 eV
 Mean excitation energy = 1.66000000E+02 eV
 Number of oscillators = 5

	Fi	Ui (eV)	Wi (eV)	KZ	KS
1	3.00000000E+00	0.00000000E+00	1.57851860E+01	0	30
2	2.00000000E+00	7.70000000E+01	1.68185797E+02	13	3
3	4.00000000E+00	7.70000000E+01	1.68514704E+02	13	4
4	2.00000000E+00	1.21000000E+02	2.63983937E+02	13	2
5	2.00000000E+00	1.56400000E+03	3.40945998E+03	13	1

*** Compton scattering (Impulse Approximation).
 Number of shells = 5

	Fi	Ui (eV)	Ji(0)	KZ	KS
1	3.00000000E+00	0.00000000E+00	8.42280277E-01	0	30
2	4.00000000E+00	7.70000000E+01	1.68000000E-01	13	4
3	2.00000000E+00	7.70000000E+01	1.68000000E-01	13	3
4	2.00000000E+00	1.21000000E+02	3.05000000E-01	13	2
5	2.00000000E+00	1.56400000E+03	6.86000000E-02	13	1

*** RELAX: Z = 13, no. of shells = 6, no. of transitions = 34

i	Shell	f	Ui (eV)
1	1s1/2 K	2	1.56400000E+03
2	2s1/2 L1	2	1.21000000E+02
3	2p1/2 L2	2	7.70000000E+01
4	2p3/2 L3	4	7.70000000E+01
5	3s1/2 M1	2	9.07500000E+00
6	3p1/2 M2	1	9.07500000E+00

S0	S1	S2	Probability	Energy (eV)
K	L2		1.23699000E-02	1.48630000E+03
K	L3		2.45528000E-02	1.48671000E+03
K	M2		7.55854000E-05	1.55757000E+03
K	M3		1.50039000E-04	1.55757000E+03
K	L1 L1		7.83944000E-02	1.31180000E+03
K	L1 L2		8.32180000E-02	1.34965000E+03
K	L1 L3		1.62725000E-01	1.35012000E+03
K	L1 M1		1.35884000E-02	1.42069000E+03
K	L1 M2		8.96794000E-04	1.42597000E+03
K	L1 M3		1.76485000E-03	1.42598000E+03
K	L2 L2		1.42920000E-02	1.38750000E+03
K	L2 L3		3.66942000E-01	1.38797000E+03
K	L2 M1		6.49294000E-03	1.45854000E+03
K	L2 M2		3.01318000E-04	1.46382000E+03
K	L2 M3		3.65883000E-03	1.46383000E+03
K	L3 L3		2.09226000E-01	1.38844000E+03
K	L3 M1		1.27063000E-02	1.45901000E+03
K	L3 M2		3.65189000E-03	1.46429000E+03
K	L3 M3		4.20421000E-03	1.46430000E+03
K	M1 M1		5.81139000E-04	1.52958000E+03
K	M1 M2		7.17440000E-05	1.53486000E+03
K	M1 M3		1.36311000E-04	1.53487000E+03
L1	M2		2.07691000E-06	1.22300000E+02
L1	M3		4.02982000E-06	1.14180000E+02
L1	M1 M2		2.61944000E-03	1.04010000E+02
L1	M1 M3		5.21749000E-03	1.04020000E+02
L1	X		2.49536000E-04	1.19050000E+02
L1	L2 X		3.29551000E-01	3.78500000E+01
L1	L3 X		6.51103000E-01	3.83200000E+01
L1	M1 X		1.12532000E-02	1.08890000E+02
L2	X		1.60533000E-05	8.12000000E+01
L2	M1 X		9.99984000E-01	7.10400000E+01
L3	X		1.50001000E-05	8.07300000E+01
L3	M1 X		9.99985000E-01	7.05700000E+01

*** Electron scaled brems x-section, ZE0 = 1.30000E+01, NDATA = 57

1.00E+03	3.64421E+00	3.68020E+00	3.71473E+00	3.74672E+00	3.77642E+00	
	3.83024E+00	3.87596E+00	3.91379E+00	3.94450E+00	3.96974E+00	
	3.99179E+00	4.01136E+00	4.02890E+00	4.04514E+00	4.06178E+00	
	4.08005E+00	4.09910E+00	4.11666E+00	4.13073E+00	4.14272E+00	
	4.15403E+00	4.15897E+00	4.16287E+00	4.16496E+00	4.16704E+00	
	4.16745E+00	4.16767E+00	4.16769E+00	4.16772E+00	4.16772E+00	
	4.16774E+00	4.16774E+00				3.453E+00
1.50E+03	4.33180E+00	4.36863E+00	4.40340E+00	4.43453E+00	4.46241E+00	
	4.51038E+00	4.54724E+00	4.57334E+00	4.58994E+00	4.59937E+00	
	4.60477E+00	4.60702E+00	4.60668E+00	4.60442E+00	4.60184E+00	
	4.60016E+00	4.59875E+00	4.59588E+00	4.59029E+00	4.58383E+00	
	4.57884E+00	4.57685E+00	4.57442E+00	4.57151E+00	4.56660E+00	
	4.56528E+00	4.56423E+00	4.56409E+00	4.56398E+00	4.56398E+00	
	4.56396E+00	4.56393E+00				3.944E+00
2.00E+03	4.84343E+00	4.88288E+00	4.91950E+00	4.95109E+00	4.97818E+00	
	5.02165E+00	5.04992E+00	5.06385E+00	5.06533E+00	5.05788E+00	
	5.04605E+00	5.03113E+00	5.01374E+00	4.99478E+00	4.97581E+00	
	4.95815E+00	4.94123E+00	4.92334E+00	4.90332E+00	4.88324E+00	
	4.86585E+00	4.85820E+00	4.85007E+00	4.84256E+00	4.83332E+00	
	4.83096E+00	4.82908E+00	4.82883E+00	4.82862E+00	4.82862E+00	
	4.82859E+00	4.82856E+00				4.296E+00
3.00E+03	5.58241E+00	5.63469E+00	5.68032E+00	5.71425E+00	5.73797E+00	
	5.76341E+00	5.76433E+00	5.74968E+00	5.72277E+00	5.68701E+00	
	5.64670E+00	5.60336E+00	5.55808E+00	5.51210E+00	5.46619E+00	
	5.42139E+00	5.37819E+00	5.33714E+00	5.29850E+00	5.26130E+00	
	5.22529E+00	5.20833E+00	5.19135E+00	5.17747E+00	5.16245E+00	
	5.15875E+00	5.15576E+00	5.15537E+00	5.15508E+00	5.15504E+00	
	5.15500E+00	5.15498E+00				4.776E+00
4.00E+03	6.11567E+00	6.17334E+00	6.22203E+00	6.25494E+00	6.27410E+00	
	6.28318E+00	6.26059E+00	6.21923E+00	6.16415E+00	6.10044E+00	
	6.03417E+00	5.96668E+00	5.89795E+00	5.82904E+00	5.76166E+00	
	5.69779E+00	5.63773E+00	5.58110E+00	5.52749E+00	5.47656E+00	
	5.42817E+00	5.40496E+00	5.38184E+00	5.36347E+00	5.34461E+00	
	5.33996E+00	5.33623E+00	5.33574E+00	5.33538E+00	5.33533E+00	
	5.33529E+00	5.33528E+00				5.088E+00
5.00E+03	6.53119E+00	6.59146E+00	6.64068E+00	6.67055E+00	6.68366E+00	
	6.67472E+00	6.62861E+00	6.56182E+00	6.48087E+00	6.39212E+00	
	6.30296E+00	6.21458E+00	6.12623E+00	6.03873E+00	5.95424E+00	
	5.87520E+00	5.80172E+00	5.73271E+00	5.66727E+00	5.60560E+00	
	5.54772E+00	5.51989E+00	5.49232E+00	5.47065E+00	5.44887E+00	
	5.44350E+00	5.43920E+00	5.43865E+00	5.43824E+00	5.43817E+00	
	5.43813E+00	5.43814E+00				5.307E+00
6.00E+03	6.86867E+00	6.92930E+00	6.97710E+00	7.00243E+00	7.00841E+00	
	6.98046E+00	6.91117E+00	6.82039E+00	6.71580E+00	6.60465E+00	
	6.49520E+00	6.38856E+00	6.28350E+00	6.18054E+00	6.08206E+00	
	5.99049E+00	5.90581E+00	5.82649E+00	5.75128E+00	5.68079E+00	
	5.61527E+00	5.58391E+00	5.55295E+00	5.52879E+00	5.50467E+00	
	5.49871E+00	5.49395E+00	5.49333E+00	5.49288E+00	5.49281E+00	
	5.49278E+00	5.49277E+00				5.466E+00
8.00E+03	7.39673E+00	7.45338E+00	7.49421E+00	7.50739E+00	7.49709E+00	
	7.42963E+00	7.31577E+00	7.18114E+00	7.03507E+00	6.88562E+00	
	6.74169E+00	6.60437E+00	6.47216E+00	6.34500E+00	6.22484E+00	
	6.11346E+00	6.01069E+00	5.91462E+00	5.82378E+00	5.73924E+00	
	5.66182E+00	5.62543E+00	5.58980E+00	5.56212E+00	5.53428E+00	
	5.52743E+00	5.52198E+00	5.52128E+00	5.52075E+00	5.52067E+00	
	5.52062E+00	5.52060E+00				5.676E+00
1.00E+04	7.79853E+00	7.84740E+00	7.87805E+00	7.87694E+00	7.84923E+00	
	7.74258E+00	7.58728E+00	7.41389E+00	7.23261E+00	7.05155E+00	
	6.87947E+00	6.71726E+00	6.56358E+00	6.41783E+00	6.28120E+00	
	6.15439E+00	6.03722E+00	5.92769E+00	5.82441E+00	5.72873E+00	
	5.64213E+00	5.60208E+00	5.56315E+00	5.53301E+00	5.50243E+00	
	5.49492E+00	5.48894E+00	5.48815E+00	5.48757E+00	5.48749E+00	
	5.48744E+00	5.48742E+00				5.800E+00
1.50E+04	8.50742E+00	8.53040E+00	8.53091E+00	8.49244E+00	8.42232E+00	
	8.22598E+00	7.98174E+00	7.72903E+00	7.47872E+00	7.23761E+00	
	7.01295E+00	6.80438E+00	6.61105E+00	6.43066E+00	6.26332E+00	
	6.10776E+00	5.96353E+00	5.82835E+00	5.70092E+00	5.58372E+00	
	5.47944E+00	5.43198E+00	5.38644E+00	5.35171E+00	5.31690E+00	
	5.30838E+00	5.30160E+00	5.30072E+00	5.30006E+00	5.29997E+00	
	5.29990E+00	5.29988E+00				5.939E+00
2.00E+04	9.25427E+00	9.11244E+00	8.96775E+00	8.81867E+00	8.66892E+00	
	8.37891E+00	8.09740E+00	7.82428E+00	7.55956E+00	7.30334E+00	
	7.05582E+00	6.81725E+00	6.59004E+00	6.37379E+00	6.17047E+00	
	5.97957E+00	5.80257E+00	5.64127E+00	5.49697E+00	5.36771E+00	
	5.25627E+00	5.21316E+00	5.18334E+00	5.16365E+00	5.09186E+00	
	5.05711E+00	5.06609E+00	5.07214E+00	5.06942E+00	5.06753E+00	
	5.07090E+00	5.06870E+00				5.967E+00
3.00E+04	9.63372E+00	9.57416E+00	9.48647E+00	9.35054E+00	9.17842E+00	
	8.78366E+00	8.35891E+00	7.95488E+00	7.58045E+00	7.23724E+00	
	6.92468E+00	6.64044E+00	6.37838E+00	6.13266E+00	5.90607E+00	
	5.69769E+00	5.50500E+00	5.32279E+00	5.14843E+00	4.98887E+00	

	4.84790E+00	4.78191E+00	4.71972E+00	4.67528E+00	4.63655E+00	
	4.62715E+00	4.61979E+00	4.61888E+00	4.61818E+00	4.61806E+00	
	4.61801E+00	4.61804E+00				5.943E+00
4.00E+04	1.00576E+01	9.94837E+00	9.81019E+00	9.62276E+00	9.40006E+00	
	8.91357E+00	8.41149E+00	7.94585E+00	7.52282E+00	7.14051E+00	
	6.79468E+00	6.48095E+00	6.19175E+00	5.91931E+00	5.66730E+00	
	5.43618E+00	5.22214E+00	5.01931E+00	4.82454E+00	4.64464E+00	
	4.48331E+00	4.40764E+00	4.33745E+00	4.28881E+00	4.24835E+00	
	4.23882E+00	4.23145E+00	4.23056E+00	4.22985E+00	4.22973E+00	
	4.22969E+00	4.22973E+00				5.879E+00
5.00E+04	1.03665E+01	1.02121E+01	1.00293E+01	9.79829E+00	9.53439E+00	
	8.97625E+00	8.41642E+00	7.90615E+00	7.44855E+00	7.03788E+00	
	6.66782E+00	6.33224E+00	6.02309E+00	5.73137E+00	5.46033E+00	
	5.21159E+00	4.98033E+00	4.76117E+00	4.55089E+00	4.35415E+00	
	4.17454E+00	4.09106E+00	4.01493E+00	3.96335E+00	3.92101E+00	
	3.91143E+00	3.90411E+00	3.90321E+00	3.90252E+00	3.90242E+00	
	3.90237E+00	3.90238E+00				5.814E+00
6.00E+04	1.07748E+01	1.04562E+01	1.01367E+01	9.81704E+00	9.50444E+00	
	8.91944E+00	8.37666E+00	7.87331E+00	7.40668E+00	6.97369E+00	
	6.57317E+00	6.20519E+00	5.86885E+00	5.55814E+00	5.27072E+00	
	5.00602E+00	4.76076E+00	4.53440E+00	4.32411E+00	4.11952E+00	
	3.91450E+00	3.81786E+00	3.73602E+00	3.68640E+00	3.64184E+00	
	3.63280E+00	3.62499E+00	3.62406E+00	3.62341E+00	3.62325E+00	
	3.62338E+00	3.62326E+00				5.749E+00
8.00E+04	1.10986E+01	1.07212E+01	1.03449E+01	9.97233E+00	9.61109E+00	
	8.94161E+00	8.32840E+00	7.76693E+00	7.25289E+00	6.78107E+00	
	6.34947E+00	5.95876E+00	5.60384E+00	5.27727E+00	4.97382E+00	
	4.69238E+00	4.42926E+00	4.18258E+00	3.94937E+00	3.72034E+00	
	3.49136E+00	3.38399E+00	3.29432E+00	3.24099E+00	3.19213E+00	
	3.18175E+00	3.17386E+00	3.17302E+00	3.17232E+00	3.17217E+00	
	3.17220E+00	3.17208E+00				5.649E+00
1.00E+05	1.13189E+01	1.08938E+01	1.04721E+01	1.00580E+01	9.65936E+00	
	8.92564E+00	8.26025E+00	7.65616E+00	7.10753E+00	6.60886E+00	
	6.15656E+00	5.75083E+00	5.38408E+00	5.04742E+00	4.73365E+00	
	4.44068E+00	4.16582E+00	3.90561E+00	3.65696E+00	3.41143E+00	
	3.16597E+00	3.05062E+00	2.95372E+00	2.89511E+00	2.84124E+00	
	2.82987E+00	2.82133E+00	2.82042E+00	2.81966E+00	2.81952E+00	
	2.81947E+00	2.81938E+00				5.569E+00
1.50E+05	1.16708E+01	1.11399E+01	1.06208E+01	1.01240E+01	9.65512E+00	
	8.80669E+00	8.05714E+00	7.39115E+00	6.79610E+00	6.26467E+00	
	5.79072E+00	5.36727E+00	4.98478E+00	4.63206E+00	4.29858E+00	
	3.98007E+00	3.67950E+00	3.39494E+00	3.12546E+00	2.86399E+00	
	2.60666E+00	2.48287E+00	2.36855E+00	2.28940E+00	2.22556E+00	
	2.21192E+00	2.20134E+00	2.20014E+00	2.19913E+00	2.19899E+00	
	2.19890E+00	2.19885E+00				5.431E+00
2.00E+05	1.19362E+01	1.13050E+01	1.06967E+01	1.01301E+01	9.60656E+00	
	8.67437E+00	7.86917E+00	7.16879E+00	6.55377E+00	6.00900E+00	
	5.52492E+00	5.09100E+00	4.69680E+00	4.33230E+00	3.98766E+00	
	3.65852E+00	3.34891E+00	3.05882E+00	2.78439E+00	2.51688E+00	
	2.24996E+00	2.11864E+00	1.99332E+00	1.90292E+00	1.83115E+00	
	1.81539E+00	1.80273E+00	1.80128E+00	1.80009E+00	1.79989E+00	
	1.79982E+00	1.79981E+00				5.355E+00
3.00E+05	1.23304E+01	1.15518E+01	1.08162E+01	1.01561E+01	9.56310E+00	
	8.52288E+00	7.64391E+00	6.89559E+00	6.25557E+00	5.69663E+00	
	5.19873E+00	4.75082E+00	4.34229E+00	3.96413E+00	3.60758E+00	
	3.26825E+00	2.94889E+00	2.65364E+00	2.37640E+00	2.10505E+00	
	1.83159E+00	1.69528E+00	1.56303E+00	1.46418E+00	1.37975E+00	
	1.36026E+00	1.34464E+00	1.34281E+00	1.34129E+00	1.34106E+00	
	1.34095E+00	1.34096E+00				5.336E+00
4.00E+05	1.26507E+01	1.17580E+01	1.09289E+01	1.02101E+01	9.58024E+00	
	8.48283E+00	7.56730E+00	6.78768E+00	6.12403E+00	5.54853E+00	
	5.03688E+00	4.57574E+00	4.15377E+00	3.76265E+00	3.39757E+00	
	3.05533E+00	2.73495E+00	2.43599E+00	2.15463E+00	1.87981E+00	
	1.60546E+00	1.46840E+00	1.33427E+00	1.23137E+00	1.13702E+00	
	1.11500E+00	1.09736E+00	1.09495E+00	1.09327E+00	1.09310E+00	
	1.09285E+00	1.09286E+00				5.416E+00
...						
...						
...						

Figure A.3 Part of material data of Al (file: Al.mat).

PENELOPE (v. 2008) Material data file

Material: Vycor

Mass density = 1.5000000E+00 g/cm**3

Number of elements in the molecule = 4

Element: Si (Z=14), atoms/molecule = 1.0000000E+00

Element: B (Z= 5), atoms/molecule = 2.0000000E+00

Element: Na (Z=11), atoms/molecule = 2.0000000E+00

Element: O (Z= 8), atoms/molecule = 6.0000000E+00

Molecular density = 4.71260330E+21 1/cm**3

*** Electron/positron inelastic scattering.

Plasma energy = 2.47144892E+01 eV

Mean excitation energy = 1.12702110E+02 eV

Number of oscillators = 11

	Fi	Ui (eV)	wi (eV)	KZ	KS
1	1.0000000E+01	0.0000000E+00	8.06097755E+00	0	30
2	2.6000000E+01	1.36076923E+01	3.51871875E+01	0	3
3	2.4000000E+01	3.1240000E+01	7.91460274E+01	0	2
4	4.0000000E+00	6.6000000E+01	1.67339693E+02	11	2
5	2.0000000E+00	1.0400000E+02	2.63621625E+02	14	3
6	4.0000000E+00	1.0400000E+02	2.63638057E+02	14	4
7	2.0000000E+00	1.5400000E+02	3.90349555E+02	14	2
8	4.0000000E+00	1.9200000E+02	4.86673542E+02	5	30
9	1.2000000E+01	5.3800000E+02	1.36366900E+03	8	1
10	4.0000000E+00	1.0750000E+03	2.72476839E+03	11	1
11	2.0000000E+00	1.8440000E+03	4.67392376E+03	14	1

*** Compton scattering (Impulse Approximation).

Number of shells = 10

	Fi	Ui (eV)	Ji(0)	KZ	KS
1	1.0000000E+01	0.0000000E+00	1.64937202E+00	0	30
2	2.6000000E+01	1.36076923E+01	4.03076923E-01	0	30
3	2.8000000E+01	3.62057143E+01	4.00285714E-01	0	30
4	4.0000000E+00	1.0400000E+02	1.49000000E-01	14	4
5	2.0000000E+00	1.0400000E+02	1.49000000E-01	14	3
6	2.0000000E+00	1.5400000E+02	2.75000000E-01	14	2
7	4.0000000E+00	1.9200000E+02	1.86000000E-01	5	30
8	1.2000000E+01	5.3800000E+02	1.13000000E-01	8	1
9	4.0000000E+00	1.0750000E+03	8.15000000E-02	11	1
10	2.0000000E+00	1.8440000E+03	6.35000000E-02	14	1

*** RELAX: Z = 14, no. of shells = 6, no. of transitions = 46

i	Shell	f	Ui (eV)
1	1s1/2 K	2	1.8440000E+03
2	2s1/2 L1	2	1.5400000E+02
3	2p1/2 L2	2	1.0400000E+02
4	2p3/2 L3	4	1.0400000E+02
5	3s1/2 M1	2	1.3460000E+01
6	3p1/2 M2	2	8.1510000E+00

S0	S1	S2	Probability	Energy (eV)
K	L2		1.59791000E-02	1.73939000E+03
K	L3		3.17052000E-02	1.73998000E+03
K	M2		2.72402000E-04	1.83596000E+03
K	M3		5.40444000E-04	1.83596000E+03
K	L1 L1		7.47954000E-02	1.52540000E+03
K	L1 L2		8.01214000E-02	1.56828000E+03
K	L1 L3		1.56131000E-01	1.56897000E+03
K	L1 M1		1.41124000E-02	1.66332000E+03
K	L1 M2		1.95584000E-03	1.67040000E+03
K	L1 M3		3.81585000E-03	1.67043000E+03
K	L2 L2		1.39905000E-02	1.61116000E+03
K	L2 L3		3.56408000E-01	1.61185000E+03
K	L2 M1		6.76231000E-03	1.70620000E+03
K	L2 M2		6.64732000E-04	1.71328000E+03
K	L2 M3		7.97675000E-03	1.71331000E+03
K	L3 L3		2.03104000E-01	1.61254000E+03
K	L3 M1		1.31982000E-02	1.70689000E+03
K	L3 M2		7.96407000E-03	1.71397000E+03
K	L3 M3		9.16547000E-03	1.71400000E+03
K	M1 M1		6.64748000E-04	1.80124000E+03
K	M1 M2		1.66185000E-04	1.80832000E+03
K	M1 M3		3.25975000E-04	1.80835000E+03

K	M2	M2	6.39199000E-06	1.81540000E+03
K	M2	M3	1.08669000E-04	1.81543000E+03
K	M3	M3	6.39185000E-05	1.81546000E+03
L1	M2		5.83271000E-06	1.55240000E+02
L1	M3		1.07340000E-05	1.45030000E+02
L1	M1	M1	1.03158000E-02	1.24290000E+02
L1	M1	M2	5.00684000E-03	1.31370000E+02
L1	M1	M3	9.95440000E-03	1.31400000E+02
L1	M2	M2	3.23120000E-05	1.38450000E+02
L1	M3	M3	6.62381000E-05	1.38510000E+02
L2	M3		1.82830000E-09	1.02150000E+02
L3	M2		8.54246000E-10	1.00630000E+02
L3	M3		8.43116000E-10	1.01460000E+02
L1	X		3.26940000E-04	1.51550000E+02
L1	L2	X	3.28841000E-01	4.28800000E+01
L1	L3	X	6.45440000E-01	4.35700000E+01
L2	X		4.72000000E-05	1.08670000E+02
L2	M1	X	6.57611000E-01	9.50400000E+01
L2	M2	X	3.34881000E-01	1.02120000E+02
L2	M3	X	7.46220000E-03	1.02150000E+02
L3	X		4.42068000E-05	1.07980000E+02
L3	M1	X	6.56668000E-01	9.43500000E+01
L3	M2	X	1.38649000E-01	1.01430000E+02
L3	M3	X	2.04639000E-01	1.01460000E+02

*** RELAX: z = 5, no. of shells = 3, no. of transitions = 0

i	Shell	f	Ui (ev)	
1	1s1/2	K	2	1.92000000E+02
2	2s1/2	L1	2	1.13860000E+01
3	2p1/2	L2	1	1.13860000E+01

*** RELAX: z = 11, no. of shells = 5, no. of transitions = 14

i	Shell	f	Ui (ev)	
1	1s1/2	K	2	1.07500000E+03
2	2s1/2	L1	2	6.60000000E+01
3	2p1/2	L2	2	3.40000000E+01
4	2p3/2	L3	4	3.40000000E+01
5	3s1/2	M1	1	5.13900000E+00

S0	S1	S2	Probability	Energy (ev)
K	L2		6.68996000E-03	1.04098000E+03
K	L3		1.32959000E-02	1.04098000E+03
K	L1	L1	8.70552000E-02	9.35040000E+02
K	L1	L2	8.90021000E-02	9.63100000E+02
K	L1	L3	1.75052000E-01	9.63300000E+02
K	L1	M1	5.73825000E-03	9.94370000E+02
K	L2	L2	1.46296000E-02	9.91160000E+02
K	L2	L3	3.82369000E-01	9.91360000E+02
K	L2	M1	2.69932000E-03	1.02243000E+03
K	L3	L3	2.18165000E-01	9.91560000E+02
K	L3	M1	5.30407000E-03	1.02263000E+03
L1	X		1.16019000E-04	6.44800000E+01
L1	L2	X	3.34898000E-01	2.80600000E+01
L1	L3	X	6.64986000E-01	2.82600000E+01

*** RELAX: z = 8, no. of shells = 4, no. of transitions = 8

i	Shell	f	Ui (ev)	
1	1s1/2	K	2	5.38000000E+02
2	2s1/2	L1	2	2.84800000E+01
3	2p1/2	L2	2	1.36200000E+01
4	2p3/2	L3	2	1.36200000E+01

S0	S1	S2	Probability	Energy (ev)
K	L2		1.90768000E-03	5.23090000E+02
K	L3		3.80027000E-03	5.23130000E+02
K	L1	L1	1.78644000E-01	4.78820000E+02
K	L1	L2	1.16224000E-01	4.93860000E+02
K	L1	L3	2.30418000E-01	4.93900000E+02
K	L2	L2	1.10822000E-02	5.08900000E+02
K	L2	L3	2.91115000E-01	5.08940000E+02
K	L3	L3	1.66809000E-01	5.08980000E+02

*** Electron scaled brems x-section, ZEQU = 8.90352E+00, NDATA = 57

1.00E+03	4.75466E+01	4.80006E+01	4.84297E+01	4.88150E+01	4.91608E+01	
	4.97583E+01	5.02255E+01	5.05716E+01	5.08070E+01	5.09529E+01	
	5.10382E+01	5.10721E+01	5.10625E+01	5.10167E+01	5.09476E+01	
	5.08670E+01	5.07761E+01	5.06777E+01	5.05785E+01	5.04981E+01	
	5.04530E+01	5.04377E+01	5.04147E+01	5.03838E+01	5.03350E+01	
	5.03193E+01	5.03067E+01	5.03051E+01	5.03038E+01	5.03036E+01	
	5.03035E+01	5.03036E+01				4.354E+01
1.50E+03	5.51505E+01	5.56386E+01	5.60909E+01	5.64800E+01	5.68123E+01	
	5.73417E+01	5.76844E+01	5.78540E+01	5.78699E+01	5.77671E+01	
	5.75922E+01	5.73582E+01	5.70740E+01	5.67508E+01	5.64081E+01	
	5.60637E+01	5.57162E+01	5.53601E+01	5.49938E+01	5.46344E+01	
	5.43063E+01	5.41562E+01	5.40051E+01	5.38856E+01	5.37809E+01	
	5.37544E+01	5.37319E+01	5.37291E+01	5.37270E+01	5.37267E+01	
	5.37266E+01	5.37263E+01				4.866E+01
2.00E+03	6.06647E+01	6.12066E+01	6.16919E+01	6.20775E+01	6.23750E+01	
	6.27717E+01	6.29208E+01	6.28732E+01	6.26605E+01	6.23271E+01	
	6.19288E+01	6.14759E+01	6.09677E+01	6.04150E+01	5.98514E+01	
	5.93059E+01	5.87747E+01	5.82405E+01	5.76947E+01	5.71680E+01	
	5.66833E+01	5.64494E+01	5.62246E+01	5.60585E+01	5.59031E+01	
	5.58649E+01	5.58345E+01	5.58307E+01	5.58277E+01	5.58273E+01	
	5.58270E+01	5.58267E+01				5.207E+01
3.00E+03	6.85315E+01	6.91436E+01	6.96578E+01	7.00000E+01	7.01935E+01	
	7.02669E+01	6.99988E+01	6.95252E+01	6.88934E+01	6.81486E+01	
	6.73459E+01	6.65031E+01	6.56318E+01	6.47503E+01	6.38747E+01	
	6.30241E+01	6.22025E+01	6.14111E+01	6.06509E+01	5.99219E+01	
	5.92359E+01	5.89193E+01	5.86173E+01	5.83897E+01	5.81625E+01	
	5.81080E+01	5.80648E+01	5.80592E+01	5.80550E+01	5.80544E+01	
	5.80542E+01	5.80538E+01				5.639E+01
4.00E+03	7.41812E+01	7.47497E+01	7.52034E+01	7.54565E+01	7.55370E+01	
	7.53378E+01	7.47398E+01	7.38935E+01	7.28650E+01	7.17246E+01	
	7.05557E+01	6.93826E+01	6.82167E+01	6.70763E+01	6.59707E+01	
	6.49140E+01	6.39079E+01	6.29449E+01	6.20198E+01	6.11387E+01	
	6.03326E+01	5.99743E+01	5.96289E+01	5.93603E+01	5.90879E+01	
	5.90228E+01	5.89710E+01	5.89642E+01	5.89592E+01	5.89585E+01	
	5.89580E+01	5.89580E+01				5.899E+01
5.00E+03	7.86226E+01	7.90431E+01	7.93573E+01	7.94855E+01	7.94543E+01	
	7.90500E+01	7.82192E+01	7.70605E+01	7.56609E+01	7.41381E+01	
	7.26273E+01	7.11613E+01	6.97444E+01	6.83911E+01	6.71092E+01	
	6.59088E+01	6.47796E+01	6.36874E+01	6.26115E+01	6.15982E+01	
	6.07128E+01	6.03245E+01	5.99459E+01	5.96468E+01	5.93455E+01	
	5.92725E+01	5.92148E+01	5.92076E+01	5.92016E+01	5.92010E+01	
	5.92005E+01	5.92005E+01				
...						
...						
...						
...						
...						

Figure A.4 Part of material data of Vycor (file: *Vycor.mat*).

PENELOPE (v. 2008) Material data file

Material: CdSe/ZnS

Mass density = 5.5700000E+00 g/cm**3

Number of elements in the molecule = 4

Element: Cd (Z=48), atoms/molecule = 2.85259319E-01

Element: Se (Z=34), atoms/molecule = 4.06104357E-01

Element: Zn (Z=30), atoms/molecule = 4.90380792E-01

Element: S (Z=16), atoms/molecule = 1.00000000E+00

Molecular density = 2.61517870E+22 1/cm**3

*** Electron/positron inelastic scattering.

Plasma energy = 4.58154598E+01 eV

Mean excitation energy = 3.07283105E+02 eV

Number of oscillators = 29

	Fi	Ui (ev)	wi (ev)	KZ	KS
1	7.17569765E+00	0.00000000E+00	1.60857021E+01	0	30
2	7.75640111E+00	1.22114128E+01	2.86414836E+01	0	8
3	2.81220871E+00	2.01855592E+01	4.63236619E+01	0	5
4	8.71488423E+00	7.36087034E+01	1.64533138E+02	0	6
5	1.55128022E+00	1.30334589E+02	2.94571405E+02	0	5
6	1.62441743E+00	1.66000000E+02	3.77457779E+02	34	7
7	4.00000000E+00	1.68000000E+02	3.82078965E+02	16	4
8	2.00000000E+00	1.70000000E+02	3.86562362E+02	16	3
9	8.12208713E-01	1.73000000E+02	3.93345581E+02	34	6
10	2.00000000E+00	2.32000000E+02	5.27504629E+02	16	2
11	8.12208713E-01	2.34000000E+02	5.32024466E+02	34	5
12	1.71155591E+00	4.08000000E+02	9.27622585E+02	48	9
13	1.14103727E+00	4.15000000E+02	9.43529656E+02	48	8
14	1.14103727E+00	6.21000000E+02	1.41187210E+03	48	7
15	5.70518637E-01	6.55000000E+02	1.48916702E+03	48	6
16	5.70518637E-01	7.75000000E+02	1.76198996E+03	48	5
17	1.96152317E+00	1.02400000E+03	2.32810527E+03	30	4
18	9.80761584E-01	1.04700000E+03	2.38039129E+03	30	3
19	9.80761584E-01	1.19800000E+03	2.72369376E+03	30	2
20	1.62441743E+00	1.43900000E+03	3.27161623E+03	34	4
21	8.12208713E-01	1.47900000E+03	3.36255438E+03	34	3
22	8.12208713E-01	1.65600000E+03	3.76496895E+03	34	2
23	2.00000000E+00	2.47600000E+03	5.62926556E+03	16	1
24	1.14103727E+00	3.54200000E+03	8.05284641E+03	48	4
25	5.70518637E-01	3.73200000E+03	8.48481630E+03	48	3
26	5.70518637E-01	4.02200000E+03	9.14414006E+03	48	2
27	9.80761584E-01	9.66300000E+03	2.19691249E+04	30	1
28	8.12208713E-01	1.26620000E+04	2.87874424E+04	34	1
29	5.70518637E-01	2.67150000E+04	6.07373650E+04	48	1

*** Compton scattering (Impulse Approximation).

Number of shells = 21

	Fi	Ui (ev)	Ji(0)	KZ	KS
1	7.17569765E+00	0.00000000E+00	8.26544638E-01	0	30
2	1.05686098E+01	1.43332590E+01	3.51009939E-01	0	30
3	2.15149993E+01	1.35714577E+02	1.70415317E-01	0	30
4	1.71155591E+00	4.08000000E+02	6.05000000E-02	48	9
5	1.14103727E+00	4.15000000E+02	6.00000000E-02	48	8
6	1.14103727E+00	6.21000000E+02	8.88000000E-02	48	7
7	5.70518637E-01	6.55000000E+02	8.64000000E-02	48	6
8	5.70518637E-01	7.75000000E+02	1.45000000E-01	48	5
9	1.96152317E+00	1.02400000E+03	5.49000000E-02	30	4
10	9.80761584E-01	1.04700000E+03	5.49000000E-02	30	3
11	9.80761584E-01	1.19800000E+03	1.08000000E-01	30	2
12	1.62441743E+00	1.43900000E+03	4.75000000E-02	34	4
13	8.12208713E-01	1.47900000E+03	4.75000000E-02	34	3
14	8.12208713E-01	1.65600000E+03	9.39000000E-02	34	2
15	2.00000000E+00	2.47600000E+03	5.53000000E-02	16	1
16	1.14103727E+00	3.54200000E+03	3.19000000E-02	48	4
17	5.70518637E-01	3.73200000E+03	3.07000000E-02	48	3
18	5.70518637E-01	4.02200000E+03	6.15000000E-02	48	2
19	9.80761584E-01	9.66300000E+03	2.90000000E-02	30	1
20	8.12208713E-01	1.26620000E+04	2.55000000E-02	34	1
21	5.70518637E-01	2.67150000E+04	1.71000000E-02	48	1

*** RELAX: Z = 48, no. of shells = 15, no. of transitions = 509

i	Shell	f	Ui (ev)
1	1s1/2 K	2	2.67150000E+04

```

2 2s1/2 L1 2 4.02200000E+03
3 2p1/2 L2 2 3.73200000E+03
4 2p3/2 L3 4 3.54200000E+03
5 3s1/2 M1 2 7.75000000E+02
6 3p1/2 M2 2 6.55000000E+02
7 3p3/2 M3 4 6.21000000E+02
8 3d3/2 M4 4 4.15000000E+02
9 3d5/2 M5 6 4.08000000E+02
10 4s1/2 N1 2 1.12000000E+02
11 4p1/2 N2 2 7.80000000E+01
12 4p3/2 N3 4 7.10000000E+01
13 4d3/2 N4 4 1.40000000E+01
14 4d5/2 N5 6 1.30000000E+01
17 5s1/2 O1 2 8.99000000E+00

```

	S0	S1	S2	Probability	Energy (eV)
K	L2			2.43038000E-01	2.29840000E+04
K	L3			4.56837000E-01	2.31740000E+04
K	M2			4.03067000E-02	2.60613000E+04
K	M3			7.82974000E-02	2.60954000E+04
K	M4			2.88988000E-04	2.63012000E+04
K	M5			4.02237000E-04	2.63078000E+04
K	N2			8.20524000E-03	2.66441000E+04
K	N3			1.59199000E-02	2.66441000E+04
K	N4			3.60657000E-05	2.67012000E+04
K	N5			4.96946000E-05	2.67025000E+04
K	L1	L1		1.17163000E-02	1.86998000E+04
K	L1	L2		1.35877000E-02	1.89630000E+04
K	L1	L3		1.84885000E-02	1.91585000E+04
K	L1	M1		4.01440000E-03	2.19385000E+04
K	L1	M2		2.46821000E-03	2.20461000E+04
K	L1	M3		3.36905000E-03	2.20813000E+04
K	L1	M4		2.08296000E-04	2.22738000E+04
K	L1	M5		2.40796000E-04	2.22810000E+04
K	L1	N1		7.86285000E-04	2.25805000E+04
K	L1	N2		4.39859000E-04	2.26157000E+04
K	L1	N3		5.93497000E-04	2.26217000E+04
K	L1	N4		2.69607000E-05	2.26762000E+04
K	L1	N5		3.06533000E-05	2.26769000E+04
K	L2	L2		1.89140000E-03	1.92262000E+04
K	L2	L3		4.10623000E-02	1.94217000E+04
K	L2	M1		1.92787000E-03	2.22017000E+04
K	L2	M2		6.19718000E-04	2.23093000E+04
K	L2	M3		6.25946000E-03	2.23445000E+04
K	L2	M4		2.59990000E-04	2.25370000E+04
K	L2	M5		8.96323000E-04	2.25442000E+04
K	L2	N1		3.64156000E-04	2.28437000E+04
K	L2	N2		1.08577000E-04	2.28789000E+04
K	L2	N3		1.06988000E-03	2.28849000E+04
K	L2	N4		3.32390000E-05	2.29394000E+04
K	L2	N5		1.12638000E-04	2.29401000E+04
K	L3	L3		2.11080000E-02	1.96172000E+04
K	L3	M1		2.59664000E-03	2.23972000E+04
K	L3	M2		6.15352000E-03	2.25048000E+04
K	L3	M3		6.59576000E-03	2.25400000E+04
K	L3	M4		1.08028000E-03	2.27325000E+04
K	L3	M5		1.01011000E-03	2.27397000E+04
K	L3	N1		4.89717000E-04	2.30392000E+04
K	L3	N2		1.06218000E-03	2.30744000E+04
K	L3	N3		1.13342000E-03	2.30804000E+04
K	L3	N4		1.37379000E-04	2.31349000E+04
K	L3	N5		1.27416000E-04	2.31356000E+04
K	M1	M1		3.38662000E-04	2.51773000E+04
K	M1	M2		3.53449000E-04	2.52848000E+04
K	M1	M3		4.76794000E-04	2.53200000E+04
K	M1	M4		2.76985000E-05	2.55126000E+04
K	M1	M5		3.10234000E-05	2.55198000E+04
K	M1	N1		1.32221000E-04	2.58193000E+04
K	M1	N2		6.31531000E-05	2.58544000E+04
K	M1	N3		8.42054000E-05	2.58604000E+04
K	M1	N4		3.69332000E-06	2.59149000E+04
K	M1	N5		4.06260000E-06	2.59157000E+04
K	M2	M2		4.87532000E-05	2.53924000E+04
K	M2	M3		9.52152000E-04	2.54276000E+04
K	M2	M4		3.06553000E-05	2.56201000E+04
K	M2	M5		1.06004000E-04	2.56273000E+04
K	M2	N1		6.68511000E-05	2.59268000E+04
K	M2	N2		1.69908000E-05	2.59620000E+04
K	M2	N3		1.63246000E-04	2.59680000E+04
K	M2	N4		4.06280000E-06	2.60225000E+04

K	M2	N5	1.32959000E-05	2.60232000E+04
K	M3	M3	5.16701000E-04	2.54627000E+04
K	M3	M4	1.34074000E-04	2.56553000E+04
K	M3	M5	1.22252000E-04	2.56625000E+04
K	M3	N1	9.01170000E-05	2.59620000E+04
K	M3	N2	1.64716000E-04	2.59971000E+04
K	M3	N3	1.77635000E-04	2.60032000E+04
K	M3	N4	1.69905000E-05	2.60577000E+04
K	M3	N5	1.55118000E-05	2.60584000E+04
K	M4	M5	1.55110000E-05	2.58551000E+04
K	M4	N1	5.17040000E-06	2.61546000E+04
K	M4	N2	5.17040000E-06	2.61897000E+04
K	M4	N3	2.21589000E-05	2.61958000E+04
K	M4	N5	1.84662000E-06	2.62510000E+04
K	M5	M5	3.83010000E-06	2.58623000E+04
K	M5	N1	6.12810000E-06	2.61618000E+04
K	M5	N2	1.80005000E-05	2.61969000E+04
K	M5	N3	2.06819000E-05	2.62030000E+04
K	M5	N4	1.91505000E-06	2.62574000E+04
K	M5	N5	7.66000000E-07	2.62582000E+04
K	N1	N1	1.35667000E-05	2.64613000E+04
K	N1	N2	1.24038000E-05	2.64964000E+04
K	N1	N3	1.66674000E-05	2.65025000E+04
K	N1	N4	7.75224000E-07	2.65569000E+04
K	N1	N5	7.75224000E-07	2.65577000E+04
K	N2	N2	1.47728000E-06	2.65316000E+04
K	N2	N3	2.80679000E-05	2.65376000E+04
K	N2	N4	7.38638000E-07	2.65921000E+04
K	N2	N5	2.21592000E-06	2.65928000E+04
K	N3	N3	1.63497000E-05	2.65436000E+04
K	N3	N4	3.19044000E-06	2.65981000E+04
K	N3	N5	2.79149000E-06	2.65988000E+04
K	N4	N5	4.05707000E-07	2.66533000E+04
L1	L2		1.87570000E-05	2.63200000E+02
L1	L3		1.64670000E-04	4.58700000E+02
L1	M2		6.45791000E-03	3.36723000E+03
L1	M3		1.06670000E-02	3.40148000E+03
L1	M4		7.47191000E-05	3.60760000E+03
L1	M5		1.11450000E-04	3.61449000E+03
L1	N2		1.19010000E-03	3.95138000E+03
L1	N3		1.98980000E-03	3.94900000E+03
L1	N4		6.51711000E-06	4.00660000E+03
L1	N5		9.75711000E-06	4.00800000E+03
L1	L2	N1	3.84431000E-02	1.49840000E+02
L1	L2	N2	2.64697000E-02	1.84980000E+02
L1	L2	N3	3.50907000E-02	1.91010000E+02
L1	L2	N4	7.48961000E-03	2.45490000E+02
L1	L2	N5	1.22871000E-02	2.46230000E+02
L1	L3	N1	5.44658000E-02	3.45340000E+02
L1	L3	N2	2.38780000E-02	3.80480000E+02
L1	L3	N3	4.64661000E-02	3.86510000E+02
L1	L3	N4	3.18858000E-02	4.40990000E+02
L1	L3	N5	4.14022000E-02	4.41730000E+02
L1	M1	M1	9.65185000E-03	2.48336000E+03
L1	M1	M2	1.90665000E-02	2.59094000E+03
L1	M1	M3	3.58278000E-02	2.62610000E+03
L1	M1	M4	2.84744000E-02	2.81867000E+03
L1	M1	M5	4.07401000E-02	2.82587000E+03
L1	M1	N1	3.24824000E-03	3.12537000E+03
L1	M1	N2	3.33128000E-03	3.16051000E+03
L1	M1	N3	6.18383000E-03	3.16654000E+03
L1	M1	N4	3.19738000E-03	3.22102000E+03
L1	M1	N5	4.52127000E-03	3.22176000E+03
L1	M2	M2	1.27059000E-04	2.69852000E+03
L1	M2	M3	8.03613000E-04	2.73368000E+03
L1	M2	M4	7.19757000E-04	2.92625000E+03
L1	M2	M5	1.02098000E-02	2.93345000E+03
L1	M2	N1	2.60661000E-03	3.23295000E+03

...
...
...

Figure A.5 Part of material data of CdSe/ZnS (*CdSe_ZnS.in*).

Appendix B

7 February, 2005

This file contains composition data and physical parameters for 280 materials, taken from the database of the ESTAR program of Berger (NISTIR 4999, 1992). The first 99 entries are the elements Z=1-99, ordered by atomic number Z. Materials 100 to 280 are compounds and mixtures, in alphabetical order. The data for each material are:

Identification no.	NAME			
No. of elements	Z/A	I(eV)	Density (g/cm**3)	
Element(Z)	Fraction by weight		Stoichiometric index	
Element(Z)	Fraction by weight		Stoichiometric index	
...	*****			
1	HYDROGEN (1)			1
1	9.92162E-01	1.92000E+01	8.37480E-05	
1	1.00000E+00	1.00000E+00		
2	HELIUM (2)			2
1	4.99675E-01	4.18000E+01	1.66322E-04	
2	1.00000E+00	1.00000E+00		
3	LITHIUM (3)			3
1	4.32214E-01	4.00000E+01	5.34000E-01	
3	1.00000E+00	1.00000E+00		
4	BERYLLIUM (4)			4
1	4.43844E-01	6.37000E+01	1.84800E+00	
4	1.00000E+00	1.00000E+00		
5	BORON (5)			5
1	4.62535E-01	7.60000E+01	2.37000E+00	
5	1.00000E+00	1.00000E+00		
6	AMORPHOUS CARBON (6)			6
1	4.99542E-01	8.10000E+01	2.00000E+00	
6	1.00000E+00	1.00000E+00		
7	NITROGEN (7)			7
1	4.99761E-01	8.20000E+01	1.16528E-03	
7	1.00000E+00	1.00000E+00		
8	OXYGEN (8)			8
1	5.00019E-01	9.50000E+01	1.33151E-03	
8	1.00000E+00	1.00000E+00		
9	FLUORINE (9)			9
1	4.73724E-01	1.15000E+02	1.58029E-03	
9	1.00000E+00	1.00000E+00		
10	NEON (10)			10
1	4.95565E-01	1.37000E+02	8.38505E-04	
10	1.00000E+00	1.00000E+00		
11	SODIUM (11)			11
1	4.78474E-01	1.49000E+02	9.71000E-01	
11	1.00000E+00	1.00000E+00		
12	MAGNESIUM (12)			12
1	4.93726E-01	1.56000E+02	1.74000E+00	
12	1.00000E+00	1.00000E+00		
13	ALUMINUM (13)			13
1	4.81811E-01	1.66000E+02	2.69890E+00	
13	1.00000E+00	1.00000E+00		
14	SILICON (14)			14

	1	4.98478E-01	1.73000E+02	2.33000E+00	
	14	1.00000E+00	1.00000E+00		
15		PHOSPHORUS (15)			15
	1	4.84281E-01	1.73000E+02	2.20000E+00	
	15	1.00000E+00	1.00000E+00		
16		SULFUR (16)			16
	1	4.99064E-01	1.80000E+02	2.00000E+00	
	16	1.00000E+00	1.00000E+00		
17		CHLORINE (17)			17
	1	4.79508E-01	1.74000E+02	2.99473E-03	
	17	1.00000E+00	1.00000E+00		
18		ARGON (18)			18
	1	4.50586E-01	1.88000E+02	1.66201E-03	
	18	1.00000E+00	1.00000E+00		
19		POTASSIUM (19)			19
	1	4.85955E-01	1.90000E+02	8.62000E-01	
	19	1.00000E+00	1.00000E+00		
20		CALCIUM (20)			20
	1	4.99002E-01	1.91000E+02	1.55000E+00	
	20	1.00000E+00	1.00000E+00		
21		SCANDIUM (21)			21
	1	4.67124E-01	2.16000E+02	2.98900E+00	
	21	1.00000E+00	1.00000E+00		
22		TITANIUM (22)			22
	1	4.59482E-01	2.33000E+02	4.54000E+00	
	22	1.00000E+00	1.00000E+00		
23		VANADIUM (23)			23
	1	4.51498E-01	2.45000E+02	6.11000E+00	
	23	1.00000E+00	1.00000E+00		
24		CHROMIUM (24)			24
	1	4.61574E-01	2.57000E+02	7.18000E+00	
	24	1.00000E+00	1.00000E+00		
25		MANGANESE (25)			25
	1	4.55058E-01	2.72000E+02	7.44000E+00	
	25	1.00000E+00	1.00000E+00		
26		IRON (26)			26
	1	4.65558E-01	2.86000E+02	7.87400E+00	
	26	1.00000E+00	1.00000E+00		
27		COBALT (27)			27
	1	4.58146E-01	2.97000E+02	8.90000E+00	
	27	1.00000E+00	1.00000E+00		
28		NICKEL (28)			28
	1	4.77083E-01	3.11000E+02	8.90200E+00	
	28	1.00000E+00	1.00000E+00		
29		COPPER (29)			29
	1	4.56362E-01	3.22000E+02	8.96000E+00	
	29	1.00000E+00	1.00000E+00		
30		ZINC (30)			30
	1	4.58856E-01	3.30000E+02	7.13300E+00	
	30	1.00000E+00	1.00000E+00		
31		GALLIUM (31)			31
	1	4.44636E-01	3.34000E+02	5.90400E+00	
	31	1.00000E+00	1.00000E+00		
32		GERMANIUM (32)			32
	1	4.40832E-01	3.50000E+02	5.32300E+00	
	32	1.00000E+00	1.00000E+00		
33		ARSENIC (33)			33
	1	4.40460E-01	3.47000E+02	5.73000E+00	
	33	1.00000E+00	1.00000E+00		
34		SELENIUM (34)			34
	1	4.30598E-01	3.48000E+02	4.50000E+00	
	34	1.00000E+00	1.00000E+00		
35		BROMINE (35)			35
	1	4.38026E-01	3.43000E+02	7.07218E-03	
	35	1.00000E+00	1.00000E+00		
36		KRYPTON (36)			36
	1	4.29594E-01	3.52000E+02	3.47832E-03	
	36	1.00000E+00	1.00000E+00		
37		RUBIDIUM (37)			37

	1	4.32912E-01	3.63000E+02	1.53200E+00	
	37	1.00000E+00	1.00000E+00		
38	STRONTIUM (38)				38
	1	4.33691E-01	3.66000E+02	2.54000E+00	
	38	1.00000E+00	1.00000E+00		
39	YTTRIUM (39)				39
	1	4.38666E-01	3.79000E+02	4.46900E+00	
	39	1.00000E+00	1.00000E+00		
40	ZIRCONIUM (40)				40
	1	4.38500E-01	3.93000E+02	6.50600E+00	
	40	1.00000E+00	1.00000E+00		
41	NIOBIUM (41)				41
	1	4.41304E-01	4.17000E+02	8.57000E+00	
	41	1.00000E+00	1.00000E+00		
42	MOLYBDENUM (42)				42
	1	4.37774E-01	4.24000E+02	1.02200E+01	
	42	1.00000E+00	1.00000E+00		
43	TECHNETIUM (43)				43
	1	4.39192E-01	4.28000E+02	1.15000E+01	
	43	1.00000E+00	1.00000E+00		
44	RUTHENIUM (44)				44
	1	4.35342E-01	4.41000E+02	1.24100E+01	
	44	1.00000E+00	1.00000E+00		
45	RHODIUM (45)				45
	1	4.37294E-01	4.49000E+02	1.24100E+01	
	45	1.00000E+00	1.00000E+00		
46	PALLADIUM (46)				46
	1	4.32250E-01	4.70000E+02	1.20200E+01	
	46	1.00000E+00	1.00000E+00		
47	SILVER (47)				47
	1	4.35718E-01	4.70000E+02	1.05000E+01	
	47	1.00000E+00	1.00000E+00		
48	CADMIUM (48)				48
	1	4.27008E-01	4.69000E+02	8.65000E+00	
	48	1.00000E+00	1.00000E+00		
49	INDIUM (49)				49
	1	4.26755E-01	4.88000E+02	7.31000E+00	
	49	1.00000E+00	1.00000E+00		
50	TIN (50)				50
	1	4.21265E-01	4.88000E+02	7.31000E+00	
	50	1.00000E+00	1.00000E+00		
51	ANTIMONY (51)				51
	1	4.18891E-01	4.87000E+02	6.69100E+00	
	51	1.00000E+00	1.00000E+00		
52	TELLURIUM (52)				52
	1	4.07524E-01	4.85000E+02	6.24000E+00	
	52	1.00000E+00	1.00000E+00		
53	IODINE (53)				53
	1	4.17637E-01	4.91000E+02	4.93000E+00	
	53	1.00000E+00	1.00000E+00		
54	XENON (54)				54
	1	4.11303E-01	4.82000E+02	5.48536E-03	
	54	1.00000E+00	1.00000E+00		
55	CESIUM (55)				55
	1	4.13828E-01	4.88000E+02	1.87300E+00	
	55	1.00000E+00	1.00000E+00		
56	BARIUM (56)				56
	1	4.07777E-01	4.91000E+02	3.50000E+00	
	56	1.00000E+00	1.00000E+00		
57	LANTHANUM (57)				57
	1	4.10351E-01	5.01000E+02	6.15400E+00	
	57	1.00000E+00	1.00000E+00		
58	CERIUM (58)				58
	1	4.13931E-01	5.23000E+02	6.65700E+00	
	58	1.00000E+00	1.00000E+00		
59	PRASEODYMIUM (59)				59
	1	4.18714E-01	5.35000E+02	6.71000E+00	
	59	1.00000E+00	1.00000E+00		
60	NEODYMIUM (60)				60

	1	4.15973E-01	5.46000E+02	6.90000E+00	
	60	1.00000E+00	1.00000E+00		
61		PROMETHIUM (61)			61
	1	4.20942E-01	5.60000E+02	7.22000E+00	
	61	1.00000E+00	1.00000E+00		
62		SAMARIUM (62)			62
	1	4.12344E-01	5.74000E+02	7.46000E+00	
	62	1.00000E+00	1.00000E+00		
63		EUROPIUM (63)			63
	1	4.14583E-01	5.80000E+02	5.24300E+00	
	63	1.00000E+00	1.00000E+00		
64		GADOLINIUM (64)			64
	1	4.06995E-01	5.91000E+02	7.90040E+00	
	64	1.00000E+00	1.00000E+00		
65		TERBIUM (65)			65
	1	4.08997E-01	6.14000E+02	8.22900E+00	
	65	1.00000E+00	1.00000E+00		
66		DYSPROSIUM (66)			66
	1	4.06154E-01	6.28000E+02	8.55000E+00	
	66	1.00000E+00	1.00000E+00		
67		HOLMIUM (67)			67
	1	4.06232E-01	6.50000E+02	8.79500E+00	
	67	1.00000E+00	1.00000E+00		
68		ERBIUM (68)			68
	1	4.06553E-01	6.58000E+02	9.06600E+00	
	68	1.00000E+00	1.00000E+00		
69		THULIUM (69)			69
	1	4.08443E-01	6.74000E+02	9.32100E+00	
	69	1.00000E+00	1.00000E+00		
70		YTTERBIUM (70)			70
	1	4.04531E-01	6.84000E+02	6.73000E+00	
	70	1.00000E+00	1.00000E+00		
71		LUTETIUM (71)			71
	1	4.05791E-01	6.94000E+02	9.84000E+00	
	71	1.00000E+00	1.00000E+00		
72		HAFNIUM (72)			72
	1	4.03384E-01	7.05000E+02	1.33100E+01	
	72	1.00000E+00	1.00000E+00		
73		TANTALUM (73)			73
	1	4.03431E-01	7.18000E+02	1.66540E+01	
	73	1.00000E+00	1.00000E+00		
74		TUNGSTEN (74)			74
	1	4.02502E-01	7.27000E+02	1.93000E+01	
	74	1.00000E+00	1.00000E+00		
75		RHENIUM (75)			75
	1	4.02778E-01	7.36000E+02	2.10200E+01	
	75	1.00000E+00	1.00000E+00		
76		OSMIUM (76)			76
	1	3.99579E-01	7.46000E+02	2.25700E+01	
	76	1.00000E+00	1.00000E+00		
77		IRIDIUM (77)			77
	1	4.00583E-01	7.57000E+02	2.24200E+01	
	77	1.00000E+00	1.00000E+00		
78		PLATINUM (78)			78
	1	3.99836E-01	7.90000E+02	2.14500E+01	
	78	1.00000E+00	1.00000E+00		
79		GOLD (79)			79
	1	4.01083E-01	7.90000E+02	1.93200E+01	
	79	1.00000E+00	1.00000E+00		
80		MERCURY (80)			80
	1	3.98823E-01	8.00000E+02	1.35460E+01	
	80	1.00000E+00	1.00000E+00		
81		THALLIUM (81)			81
	1	3.96315E-01	8.10000E+02	1.17200E+01	
	81	1.00000E+00	1.00000E+00		
82		LEAD (82)			82
	1	3.95753E-01	8.23000E+02	1.13500E+01	
	82	1.00000E+00	1.00000E+00		
83		BISMUTH (83)			83

	1	3.97166E-01	8.23000E+02	9.74700E+00	
	83	1.00000E+00	1.00000E+00		
84	POLONIUM (84)				84
	1	4.01948E-01	8.30000E+02	9.32000E+00	
	84	1.00000E+00	1.00000E+00		
85	ASTATINE (85)				85
	1	4.04787E-01	8.25000E+02	9.32000E+00	
	85	1.00000E+00	1.00000E+00		
86	RADON (86)				86
	1	3.87356E-01	7.94000E+02	9.06618E-03	
	86	1.00000E+00	1.00000E+00		
87	FRANCIUM (87)				87
	1	3.90100E-01	8.27000E+02	1.00000E+00	
	87	1.00000E+00	1.00000E+00		
88	RADIUM (88)				88
	1	3.89337E-01	8.26000E+02	5.00000E+00	
	88	1.00000E+00	1.00000E+00		
89	ACTINIUM (89)				89
	1	3.92022E-01	8.41000E+02	1.00700E+01	
	89	1.00000E+00	1.00000E+00		
90	THORIUM (90)				90
	1	3.87867E-01	8.47000E+02	1.17200E+01	
	90	1.00000E+00	1.00000E+00		
91	PROTACTINIUM (91)				91
	1	3.93878E-01	8.78000E+02	1.53700E+01	
	91	1.00000E+00	1.00000E+00		
92	URANIUM (92)				92
	1	3.86508E-01	8.90000E+02	1.89500E+01	
	92	1.00000E+00	1.00000E+00		
93	NEPTUNIUM (93)				93
	1	3.92325E-01	9.02000E+02	2.02500E+01	
	93	1.00000E+00	1.00000E+00		
94	PLUTONIUM (94)				94
	1	3.93220E-01	9.21000E+02	1.98400E+01	
	94	1.00000E+00	1.00000E+00		
95	AMERICIUM (95)				95
	1	3.90848E-01	9.34000E+02	1.36700E+01	
	95	1.00000E+00	1.00000E+00		
96	CURIUM (96)				96
	1	3.88554E-01	9.39000E+02	1.35100E+01	
	96	1.00000E+00	1.00000E+00		
97	BERKELIUM (97)				97
	1	3.92601E-01	9.52000E+02	1.40000E+01	
	97	1.00000E+00	1.00000E+00		
98	CALIFORNIUM (98)				98
	1	3.90314E-01	9.66000E+02	1.40000E+01	
	98	1.00000E+00	1.00000E+00		
99	EINSTEINIUM (99)				99
	1	3.92826E-01	9.80000E+02	1.40000E+01	
	99	1.00000E+00	1.00000E+00		
100	ACETONE (100)				100
	3	5.50966E-01	6.42000E+01	7.89900E-01	
	1	1.04122E-01	6.00000E+00		
	6	6.20405E-01	3.00000E+00		
	8	2.75473E-01	1.00000E+00		
101	ACETYLENE (101)				101
	2	5.37680E-01	5.82000E+01	1.09670E-03	
	1	7.74180E-02	1.00000E+00		
	6	9.22582E-01	1.00000E+00		
102	ADENINE (102)				102
	3	5.18027E-01	7.14000E+01	1.35000E+00	
	1	3.72940E-02	1.00000E+00		
	6	4.44430E-01	1.00000E+00		
	7	5.18275E-01	1.00000E+00		
103	ADIPOSE TISSUE (ICRP) (103)				103
	13	5.58468E-01	6.32000E+01	9.20000E-01	
	1	1.19477E-01	6.34657E-01		
	6	6.37240E-01	2.84051E-01		
	7	7.97000E-03	3.04645E-03		
	8	2.32333E-01	7.77462E-02		

	11	5.00000E-04	1.16441E-04	
	12	2.00000E-05	4.40562E-06	
	15	1.60000E-04	2.76566E-05	
	16	7.30000E-04	1.21908E-04	
	17	1.19000E-03	1.79707E-04	
	19	3.20000E-04	4.38192E-05	
	20	2.00000E-05	2.67162E-06	
	26	2.00000E-05	1.91735E-06	
	30	2.00000E-05	1.63779E-06	
104	AIR, DRY (NEAR SEA LEVEL) (104)			104
	4	4.99190E-01	8.57000E+01	1.20479E-03
	6	1.24000E-04	1.50187E-04	
	7	7.55267E-01	7.84430E-01	
	8	2.31781E-01	2.10748E-01	
	18	1.28270E-02	4.67111E-03	
105	ALANINE (105)			105
	4	5.38758E-01	7.19000E+01	1.42000E+00
	1	7.91900E-02	7.00000E+00	
	6	4.04439E-01	3.00000E+00	
	7	1.57213E-01	1.00000E+00	
	8	3.59159E-01	2.00000E+00	
106	ALUMINUM OXIDE (106)			106
	2	4.90382E-01	1.45200E+02	3.97000E+00
	8	4.70749E-01	3.00000E+00	
	13	5.29251E-01	2.00000E+00	
107	AMBER (107)			107
	3	5.51775E-01	6.32000E+01	1.10000E+00
	1	1.05930E-01	1.60000E+01	
	6	7.88973E-01	1.00000E+01	
	8	1.05096E-01	1.00000E+00	
108	AMMONIA (108)			108
	2	5.87185E-01	5.37000E+01	8.26019E-04
	1	1.77547E-01	3.00000E+00	
	7	8.22453E-01	1.00000E+00	
109	ANILINE (109)			109
	3	5.36895E-01	6.62000E+01	1.02350E+00
	1	7.57590E-02	7.00000E+00	
	6	7.73838E-01	6.00000E+00	
	7	1.50403E-01	1.00000E+00	
110	ANTHRACENE (110)			110
	2	5.27400E-01	6.95000E+01	1.28300E+00
	1	5.65500E-02	1.00000E+01	
	6	9.43450E-01	1.40000E+01	
111	B-100 BONE-EQUIVALENT PLASTIC (111)			111
	6	5.27397E-01	8.59000E+01	1.45000E+00
	1	6.54710E-02	4.23184E+01	
	6	5.36945E-01	2.91238E+01	
	7	2.15000E-02	1.00000E+00	
	8	3.20850E-02	1.30646E+00	
	9	1.67411E-01	5.74069E+00	
	20	1.76589E-01	2.87034E+00	
112	BAKELITE (112)			112
	3	5.27919E-01	7.24000E+01	1.25000E+00
	1	5.74410E-02	5.42852E+00	
	6	7.74591E-01	6.14285E+00	
	8	1.67968E-01	1.00000E+00	
113	BARIUM FLUORIDE (113)			113
	2	4.22069E-01	3.75900E+02	4.89000E+00
	9	2.16720E-01	2.00000E+00	
	56	7.83280E-01	1.00000E+00	
114	BARIUM SULFATE (114)			114
	3	4.45611E-01	2.85700E+02	4.50000E+00
	8	2.74212E-01	4.00000E+00	
	16	1.37368E-01	1.00000E+00	
	56	5.88420E-01	1.00000E+00	
115	BENZENE (115)			115
	2	5.37680E-01	6.34000E+01	8.78650E-01
	1	7.74180E-02	6.00000E+00	
	6	9.22582E-01	6.00000E+00	
116	BERYLLIUM OXIDE (116)			116

	2	4.79778E-01	9.32000E+01	3.01000E+00	
	4	3.60320E-01	1.00000E+00		
	8	6.39680E-01	1.00000E+00		
117	BISMUTH GERMANIUM OXIDE (117)				117
	3	4.20652E-01	5.34100E+02	7.13000E+00	
	8	1.54126E-01	1.20000E+01		
	32	1.74820E-01	3.00000E+00		
	83	6.71054E-01	4.00000E+00		
118	BLOOD (ICRP) (118)				118
	14	5.49953E-01	7.52000E+01	1.06000E+00	
	1	1.01866E-01	6.34614E-01		
	6	1.00020E-01	5.22884E-02		
	7	2.96400E-02	1.32874E-02		
	8	7.59414E-01	2.98039E-01		
	11	1.85000E-03	5.05283E-04		
	12	4.00000E-05	1.03339E-05		
	14	3.00000E-05	6.70713E-06		
	15	3.50000E-04	7.09532E-05		
	16	1.85000E-03	3.62331E-04		
	17	2.78000E-03	4.92367E-04		
	19	1.63000E-03	2.61775E-04		
	20	6.00000E-05	9.39985E-06		
	26	4.60000E-04	5.17197E-05		
	30	1.00000E-05	9.60401E-07		
119	BONE, COMPACT (ICRU) (119)				119
	8	5.30103E-01	9.19000E+01	1.85000E+00	
	1	6.39840E-02	5.27900E-01		
	6	2.78000E-01	1.92470E-01		
	7	2.70000E-02	1.60297E-02		
	8	4.10016E-01	2.13105E-01		
	12	2.00000E-03	6.84277E-04		
	15	7.00000E-02	1.87932E-02		
	16	2.00000E-03	5.18757E-04		
	20	1.47000E-01	3.04991E-02		
120	BONE, CORTICAL (ICRP) (120)				120
	9	5.21299E-01	1.06400E+02	1.85000E+00	
	1	4.72340E-02	4.75402E-01		
	6	1.44330E-01	1.21899E-01		
	7	4.19900E-02	3.04112E-02		
	8	4.46096E-01	2.82845E-01		
	12	2.20000E-03	9.18228E-04		
	15	1.04970E-01	3.43791E-02		
	16	3.15000E-03	9.96713E-04		
	20	2.09930E-01	5.31337E-02		
	30	1.00000E-04	1.55160E-05		
121	BORON CARBIDE (121)				121
	2	4.70580E-01	8.47000E+01	2.52000E+00	
	5	7.82610E-01	4.00000E+00		
	6	2.17390E-01	1.00000E+00		
122	BORON OXIDE (122)				122
	2	4.88378E-01	9.96000E+01	1.81200E+00	
	5	3.10551E-01	2.00000E+00		
	8	6.89449E-01	3.00000E+00		
123	BRAIN (ICRP) (123)				123
	13	5.54228E-01	7.33000E+01	1.03000E+00	
	1	1.10667E-01	6.54722E-01		
	6	1.25420E-01	6.22650E-02		
	7	1.32800E-02	5.65352E-03		
	8	7.37723E-01	2.74945E-01		
	11	1.84000E-03	4.77243E-04		
	12	1.50000E-04	3.68004E-05		
	15	3.54000E-03	6.81500E-04		
	16	1.77000E-03	3.29205E-04		
	17	2.36000E-03	3.96931E-04		
	19	3.10000E-03	4.72782E-04		
	20	9.00000E-05	1.33897E-05		
	26	5.00000E-05	5.33859E-06		
	30	1.00000E-05	9.12035E-07		

124	BUTANE (124)			124
	2	5.84966E-01	4.83000E+01	2.49343E-03
	1	1.73408E-01	5.00000E+00	
	6	8.26592E-01	2.00000E+00	
125	N-BUTYL ALCOHOL (125)			125
	3	5.66630E-01	5.99000E+01	8.09800E-01
	1	1.35978E-01	1.00000E+01	
	6	6.48171E-01	4.00000E+00	
	8	2.15851E-01	1.00000E+00	
126	C-552 AIR-EQUIVALENT PLASTIC (126)			126
	5	4.99687E-01	8.68000E+01	1.76000E+00
	1	2.46800E-02	2.68610E-01	
	6	5.01610E-01	4.58122E-01	
	8	4.52700E-03	3.10386E-03	
	9	4.65209E-01	2.68612E-01	
	14	3.97300E-03	1.55178E-03	
127	CADMIUM TELLURIDE (127)			127
	2	4.16649E-01	5.39300E+02	6.20000E+00
	48	4.68355E-01	1.00000E+00	
	52	5.31645E-01	1.00000E+00	
128	CADMIUM TUNGSTATE (128)			128
	3	4.27472E-01	4.68300E+02	7.90000E+00
	8	1.77644E-01	4.00000E+00	
	48	3.12027E-01	1.00000E+00	
	74	5.10329E-01	1.00000E+00	
129	CALCIUM CARBONATE (129)			129
	3	4.99555E-01	1.36400E+02	2.80000E+00
	6	1.20003E-01	1.00000E+00	
	8	4.79554E-01	3.00000E+00	
	20	4.00443E-01	1.00000E+00	
130	CALCIUM FLUORIDE (130)			130
	2	4.86700E-01	1.66000E+02	3.18000E+00
	9	4.86659E-01	2.00000E+00	
	20	5.13341E-01	1.00000E+00	
131	CALCIUM OXIDE (131)			131
	2	4.99292E-01	1.76100E+02	3.30000E+00
	8	2.85299E-01	1.00000E+00	
	20	7.14701E-01	1.00000E+00	
132	CALCIUM SULFATE (132)			132
	3	4.99495E-01	1.52300E+02	2.96000E+00
	8	4.70095E-01	4.00000E+00	
	16	2.35497E-01	1.00000E+00	
	20	2.94408E-01	1.00000E+00	
133	CALCIUM TUNGSTATE (133)			133
	3	4.37610E-01	3.95000E+02	6.06200E+00
	8	2.22270E-01	4.00000E+00	
	20	1.39202E-01	1.00000E+00	
	74	6.38529E-01	1.00000E+00	
134	CARBON DIOXIDE (134)			134
	2	4.99889E-01	8.50000E+01	1.84212E-03
	6	2.72916E-01	1.00000E+00	
	8	7.27084E-01	2.00000E+00	
135	CARBON TETRACHLORIDE (135)			135
	2	4.81072E-01	1.66300E+02	1.59400E+00
	6	7.80830E-02	1.00000E+00	
	17	9.21917E-01	4.00000E+00	
136	CELLULOSE ACETATE, CELLOPHANE (136)			136
	3	5.30400E-01	7.76000E+01	1.42000E+00
	1	6.21620E-02	1.00000E+01	
	6	4.44462E-01	6.00000E+00	
	8	4.93376E-01	5.00000E+00	
137	CELLULOSE ACETATE BUTYRATE (137)			137
	3	5.32794E-01	7.46000E+01	1.20000E+00
	1	6.71250E-02	6.60000E+01	
	6	5.45403E-01	4.50000E+01	
	8	3.87472E-01	2.40000E+01	
138	CELLULOSE NITRATE (138)			138
	4	5.14237E-01	8.70000E+01	1.49000E+00
	1	2.92160E-02	3.34784E+00	

	6	2.71296E-01	2.60870E+00	
	7	1.21276E-01	1.00000E+00	
	8	5.78212E-01	4.17392E+00	
139		CERIC SULFATE DOSIMETER SOLUTION (139)		139
	5	5.52785E-01	7.67000E+01	1.03000E+00
	1	1.07596E-01	6.59096E-01	
	7	8.00000E-04	3.52634E-04	
	8	8.74976E-01	3.37647E-01	
	16	1.46270E-02	2.81683E-03	
	58	2.00100E-03	8.81692E-05	
140		CESIUM FLUORIDE (140)		140
	2	4.21319E-01	4.40700E+02	4.11500E+00
	9	1.25069E-01	1.00000E+00	
	55	8.74931E-01	1.00000E+00	
141		CESIUM IODIDE (141)		141
	2	4.15689E-01	5.53100E+02	4.51000E+00
	53	4.88451E-01	1.00000E+00	
	55	5.11549E-01	1.00000E+00	
142		CHLOROBENZENE (142)		142
	3	5.15287E-01	8.91000E+01	1.10580E+00
	1	4.47720E-02	5.00000E+00	
	6	6.40254E-01	6.00000E+00	
	17	3.14974E-01	1.00000E+00	
143		CHLOROFORM (143)		143
	3	4.85852E-01	1.56000E+02	1.48320E+00
	1	8.44300E-03	1.00000E+00	
	6	1.00613E-01	1.00000E+00	
	17	8.90944E-01	3.00000E+00	
144		CONCRETE, PORTLAND (144)		144
	10	5.02737E-01	1.35200E+02	2.30000E+00
	1	1.00000E-02	1.68764E-01	
	6	1.00000E-03	1.41618E-03	
	8	5.29107E-01	5.62520E-01	
	11	1.60000E-02	1.18382E-02	
	12	2.00000E-03	1.39969E-03	
	13	3.38720E-02	2.13537E-02	
	14	3.37021E-01	2.04114E-01	
	19	1.30000E-02	5.65567E-03	
	20	4.40000E-02	1.86734E-02	
	26	1.40000E-02	4.26409E-03	
145		CYCLOHEXANE (145)		145
	2	5.70337E-01	5.64000E+01	7.79000E-01
	1	1.43711E-01	2.00000E+00	
	6	8.56289E-01	1.00000E+00	
146		1,2-DICHLOROBENZENE (146)		146
	3	5.03389E-01	1.06500E+02	1.30480E+00
	1	2.74250E-02	2.00000E+00	
	6	4.90233E-01	3.00000E+00	
	17	4.82342E-01	1.00000E+00	
147		DICHLORODIETHYL ETHER (147)		147
	4	5.17437E-01	1.03300E+02	1.21990E+00
	1	5.63810E-02	8.00000E+00	
	6	3.35942E-01	4.00000E+00	
	8	1.11874E-01	1.00000E+00	
	17	4.95802E-01	2.00000E+00	
148		1,2-DICHLOROETHANE (148)		148
	3	5.05257E-01	1.11900E+02	1.23510E+00
	1	4.07400E-02	2.00000E+00	
	6	2.42746E-01	1.00000E+00	
	17	7.16515E-01	1.00000E+00	
149		DIETHYL ETHER (149)		149
	3	5.66630E-01	6.00000E+01	7.13780E-01
	1	1.35978E-01	1.00000E+01	
	6	6.48171E-01	4.00000E+00	
	8	2.15851E-01	1.00000E+00	
150		N,N-DIMETHYL FORMAMIDE (150)		150
	4	5.47238E-01	6.66000E+01	9.48700E-01
	1	9.65230E-02	7.00000E+00	

	6	4.92965E-01	3.00000E+00	
	7	1.91625E-01	1.00000E+00	
	8	2.18887E-01	1.00000E+00	
151	DIMETHYL SULFOXIDE (151)			151
	4	5.37574E-01	9.86000E+01	1.10140E+00
	1	7.74030E-02	6.00000E+00	
	6	3.07467E-01	2.00000E+00	
	8	2.04782E-01	1.00000E+00	
	16	4.10348E-01	1.00000E+00	
152	ETHANE (152)			152
	2	5.98615E-01	4.54000E+01	1.25324E-03
	1	2.01115E-01	3.00000E+00	
	6	7.98885E-01	1.00000E+00	
153	ETHYL ALCOHOL (153)			153
	3	5.64373E-01	6.29000E+01	7.89300E-01
	1	1.31269E-01	6.00000E+00	
	6	5.21438E-01	2.00000E+00	
	8	3.47294E-01	1.00000E+00	
154	ETHYL CELLULOSE (154)			154
	3	5.44046E-01	6.93000E+01	1.13000E+00
	1	9.00270E-02	2.20000E+01	
	6	5.85182E-01	1.20000E+01	
	8	3.24791E-01	5.00000E+00	
155	ETHYLENE (155)			155
	2	5.70337E-01	5.07000E+01	1.17497E-03
	1	1.43711E-01	2.00000E+00	
	6	8.56289E-01	1.00000E+00	
156	EYE LENS (ICRP) (156)			156
	4	5.48767E-01	7.33000E+01	1.10000E+00
	1	9.92690E-02	2.58970E+01	
	6	1.93710E-01	4.24059E+00	
	7	5.32700E-02	1.00000E+00	
	8	6.53751E-01	1.07439E+01	
157	FERRIC OXIDE (157)			157
	2	4.75916E-01	2.27300E+02	5.20000E+00
	8	3.00567E-01	3.00000E+00	
	26	6.99433E-01	2.00000E+00	
158	FERROBORIDE (158)			158
	2	4.65068E-01	2.61000E+02	7.15000E+00
	5	1.62174E-01	1.00000E+00	
	26	8.37826E-01	1.00000E+00	
159	FERROUS OXIDE (159)			159
	2	4.73232E-01	2.48600E+02	5.70000E+00
	8	2.22689E-01	1.00000E+00	
	26	7.77311E-01	1.00000E+00	
160	FERROUS SULFATE DOSIMETER SOLUTION (160)			160
	7	5.53282E-01	7.64000E+01	1.02400E+00
	1	1.08259E-01	6.60026E-01	
	7	2.70000E-05	1.18452E-05	
	8	8.78636E-01	3.37458E-01	
	11	2.20000E-05	5.88035E-06	
	16	1.29680E-02	2.48556E-03	
	17	3.40000E-05	5.89306E-06	
	26	5.40000E-05	5.94168E-06	
161	FREON-12 (161)			161
	3	4.79680E-01	1.43000E+02	1.12000E+00
	6	9.93350E-02	1.00000E+00	
	9	3.14247E-01	2.00000E+00	
	17	5.86418E-01	2.00000E+00	
162	FREON-12B2 (162)			162
	3	4.48012E-01	2.84900E+02	1.80000E+00
	6	5.72450E-02	1.00000E+00	
	9	1.81096E-01	2.00000E+00	
	35	7.61659E-01	2.00000E+00	
163	FREON-13 (163)			163
	3	4.78656E-01	1.26600E+02	9.50000E-01
	6	1.14983E-01	1.00000E+00	
	9	5.45622E-01	3.00000E+00	

	17	3.39396E-01	1.00000E+00		
164	FREON-13B1 (164)				164
	3	4.56651E-01	2.10500E+02	1.50000E+00	
	6	8.06590E-02	1.00000E+00		
	9	3.82749E-01	3.00000E+00		
	35	5.36592E-01	1.00000E+00		
165	FREON-13I1 (165)				165
	3	4.38976E-01	2.93500E+02	1.80000E+00	
	6	6.13090E-02	1.00000E+00		
	9	2.90924E-01	3.00000E+00		
	53	6.47767E-01	1.00000E+00		
166	GADOLINIUM OXYSULFIDE (166)				166
	3	4.22655E-01	4.93300E+02	7.44000E+00	
	8	8.45280E-02	2.00000E+00		
	16	8.46900E-02	1.00000E+00		
	64	8.30782E-01	2.00000E+00		
167	GALLIUM ARSENIDE (167)				167
	2	4.42473E-01	3.84900E+02	5.31000E+00	
	31	4.82019E-01	1.00000E+00		
	33	5.17981E-01	1.00000E+00		
168	GEL IN PHOTOGRAPHIC EMULSION (168)				168
	5	5.39734E-01	7.48000E+01	1.29140E+00	
	1	8.11800E-02	5.46965E-01		
	6	4.16060E-01	2.35236E-01		
	7	1.11240E-01	5.39328E-02		
	8	3.80640E-01	1.61562E-01		
	16	1.08800E-02	2.30459E-03		
169	PYREX GLASS (169)				169
	6	4.97070E-01	1.34000E+02	2.23000E+00	
	5	4.00640E-02	7.04548E-02		
	8	5.39562E-01	6.41090E-01		
	11	2.81910E-02	2.33108E-02		
	13	1.16440E-02	8.20384E-03		
	14	3.77220E-01	2.55325E-01		
	19	3.32100E-03	1.61470E-03		
170	GLASS, LEAD (170)				170
	5	4.21007E-01	5.26400E+02	6.22000E+00	
	8	1.56453E-01	5.92957E-01		
	14	8.08660E-02	1.74593E-01		
	22	8.09200E-03	1.02481E-02		
	33	2.65100E-03	2.14558E-03		
	82	7.51938E-01	2.20057E-01		
171	GLASS, PLATE (171)				171
	4	4.97314E-01	1.45400E+02	2.40000E+00	
	8	4.59800E-01	1.07443E+01		
	11	9.64410E-02	1.56834E+00		
	14	3.36553E-01	4.48006E+00		
	20	1.07205E-01	1.00000E+00		
172	GLUCOSE (172)				172
	3	5.34888E-01	7.72000E+01	1.54000E+00	
	1	7.12040E-02	1.40000E+01		
	6	3.63652E-01	6.00000E+00		
	8	5.65144E-01	7.00000E+00		
173	GLUTAMINE (173)				173
	4	5.33714E-01	7.33000E+01	1.46000E+00	
	1	6.89650E-02	1.00000E+01		
	6	4.10926E-01	5.00000E+00		
	7	1.91681E-01	2.00000E+00		
	8	3.28427E-01	3.00000E+00		
174	GLYCEROL (174)				174
	3	5.42921E-01	7.26000E+01	1.26130E+00	
	1	8.75540E-02	8.00000E+00		
	6	3.91262E-01	3.00000E+00		
	8	5.21185E-01	3.00000E+00		
175	GRAPHITE (175)				175
	1	4.99542E-01	7.80000E+01	1.70000E+00	
	6	1.00000E+00	1.00000E+00		
176	GUANINE (176)				176
	4	5.16121E-01	7.50000E+01	1.58000E+00	
	1	3.33460E-02	5.00000E+00		

6	3.97380E-01	5.00000E+00	
7	4.63407E-01	5.00000E+00	
8	1.05867E-01	1.00000E+00	
177	GYPSUM, PLASTER OF PARIS (177)		177
4	5.11128E-01	1.29700E+02	2.32000E+00
1	2.34160E-02	4.00000E+00	
8	5.57572E-01	6.00000E+00	
16	1.86215E-01	1.00000E+00	
20	2.32797E-01	1.00000E+00	
178	N-HEPTANE (178)		178
2	5.78823E-01	5.44000E+01	6.83760E-01
1	1.60937E-01	1.60000E+01	
6	8.39063E-01	7.00000E+00	
179	N-HEXANE (179)		179
2	5.80204E-01	5.40000E+01	6.60300E-01
1	1.63741E-01	7.00000E+00	
6	8.36259E-01	3.00000E+00	
180	KAPTON POLYIMIDE FILM (180)		180
4	5.12644E-01	7.96000E+01	1.42000E+00
1	2.63620E-02	1.00000E+01	
6	6.91133E-01	2.20000E+01	
7	7.32700E-02	2.00000E+00	
8	2.09235E-01	5.00000E+00	
181	LANTHANUM OXYBROMIDE (181)		181
3	4.25878E-01	4.39700E+02	6.28000E+00
8	6.81380E-02	1.00000E+00	
35	3.40294E-01	1.00000E+00	
57	5.91568E-01	1.00000E+00	
182	LANTHANUM OXYSULFIDE (182)		182
3	4.27063E-01	4.21200E+02	5.86000E+00
8	9.36000E-02	2.00000E+00	
16	9.37780E-02	1.00000E+00	
57	8.12622E-01	2.00000E+00	
183	LEAD OXIDE (183)		183
2	4.03227E-01	7.66700E+02	9.53000E+00
8	7.16820E-02	1.00000E+00	
82	9.28318E-01	1.00000E+00	
184	LITHIUM AMIDE (184)		184
3	5.22569E-01	5.55000E+01	1.17800E+00
1	8.77830E-02	2.00000E+00	
3	3.02262E-01	1.00000E+00	
7	6.09955E-01	1.00000E+00	
185	LITHIUM CARBONATE (185)		185
3	4.87203E-01	8.79000E+01	2.11000E+00
3	1.87871E-01	2.00000E+00	
6	1.62550E-01	1.00000E+00	
8	6.49579E-01	3.00000E+00	
186	LITHIUM FLUORIDE (186)		186
2	4.62617E-01	9.40000E+01	2.63500E+00
3	2.67585E-01	1.00000E+00	
9	7.32415E-01	1.00000E+00	
187	LITHIUM HYDRIDE (187)		187
2	5.03214E-01	3.65000E+01	8.20000E-01
1	1.26797E-01	1.00000E+00	
3	8.73203E-01	1.00000E+00	
188	LITHIUM IODIDE (188)		188
2	4.18393E-01	4.85100E+02	3.49400E+00
3	5.18580E-02	1.00000E+00	
53	9.48142E-01	1.00000E+00	
189	LITHIUM OXIDE (189)		189
2	4.68519E-01	7.36000E+01	2.01300E+00
3	4.64570E-01	2.00000E+00	
8	5.35430E-01	1.00000E+00	
190	LITHIUM TETRABORATE (190)		190
3	4.84869E-01	9.46000E+01	2.44000E+00
3	8.20850E-02	2.00000E+00	
5	2.55680E-01	4.00000E+00	
8	6.62235E-01	7.00000E+00	

191	LUNG (ICRP) (191)		191
	13	5.49652E-01 7.53000E+01 0.30000E+00	
	1	1.01278E-01 6.33146E-01	
	6	1.02310E-01 5.36716E-02	
	7	2.86500E-02 1.28883E-02	
	8	7.57072E-01 2.98153E-01	
	11	1.84000E-03 5.04301E-04	
	12	7.30000E-04 1.89249E-04	
	15	8.00000E-04 1.62743E-04	
	16	2.25000E-03 4.42206E-04	
	17	2.66000E-03 4.72753E-04	
	19	1.94000E-03 3.12644E-04	
	20	9.00000E-05 1.41488E-05	
	26	3.70000E-04 4.17454E-05	
	30	1.00000E-05 9.63743E-07	
192	M3 WAX (192)		192
	5	5.55116E-01 6.79000E+01 1.05000E+00	
	1	1.14318E-01 6.32218E-01	
	6	6.55823E-01 3.04353E-01	
	8	9.21830E-02 3.21157E-02	
	12	1.34792E-01 3.09128E-02	
	20	2.88300E-03 4.00947E-04	
193	MAGNESIUM CARBONATE (193)		193
	3	4.98137E-01 1.18000E+02 2.95800E+00	
	6	1.42455E-01 1.00000E+00	
	8	5.69278E-01 3.00000E+00	
	12	2.88267E-01 1.00000E+00	
194	MAGNESIUM FLUORIDE (194)		194
	2	4.81527E-01 1.34300E+02 3.00000E+00	
	9	6.09883E-01 2.00000E+00	
	12	3.90117E-01 1.00000E+00	
195	MAGNESIUM OXIDE (195)		195
	2	4.96224E-01 1.43800E+02 3.58000E+00	
	8	3.96964E-01 1.00000E+00	
	12	6.03036E-01 1.00000E+00	
196	MAGNESIUM TETRABORATE (196)		196
	3	4.90140E-01 1.08300E+02 2.53000E+00	
	5	2.40837E-01 4.00000E+00	
	8	6.23790E-01 7.00000E+00	
	12	1.35373E-01 1.00000E+00	
197	MERCURIC IODIDE (197)		197
	2	4.09332E-01 6.84500E+02 6.36000E+00	
	53	5.58560E-01 2.00000E+00	
	80	4.41440E-01 1.00000E+00	
198	METHANE (198)		198
	2	6.23340E-01 4.17000E+01 6.67151E-04	
	1	2.51306E-01 4.00000E+00	
	6	7.48694E-01 1.00000E+00	
199	METHANOL (199)		199
	3	5.61763E-01 6.76000E+01 7.91400E-01	
	1	1.25822E-01 4.00000E+00	
	6	3.74852E-01 1.00000E+00	
	8	4.99326E-01 1.00000E+00	
200	MIXED WAX (200)		200
	5	5.64789E-01 6.09000E+01 9.90000E-01	
	1	1.34040E-01 6.58894E-01	
	6	7.77960E-01 3.20905E-01	
	8	3.50200E-02 1.08445E-02	
	12	3.85940E-02 7.86726E-03	
	22	1.43860E-02 1.48862E-03	
201	MS20 TISSUE SUBSTITUTE (201)		201
	6	5.38856E-01 7.51000E+01 1.00000E+00	
	1	8.11920E-02 5.46373E-01	
	6	5.83442E-01 3.29467E-01	
	7	1.77980E-02 8.61844E-03	
	8	1.86381E-01 7.90117E-02	
	12	1.30287E-01 3.63579E-02	
	17	9.00000E-04 1.72180E-04	
202	MUSCLE, SKELETAL (ICRP) (202)		202
	13	5.49378E-01 7.53000E+01 1.04000E+00	

	1	1.00637E-01	6.30942E-01	
	6	1.07830E-01	5.67296E-02	
	7	2.76800E-02	1.24876E-02	
	8	7.54773E-01	2.98100E-01	
	11	7.50000E-04	2.06147E-04	
	12	1.90000E-04	4.93978E-05	
	15	1.80000E-03	3.67221E-04	
	16	2.41000E-03	4.75010E-04	
	17	7.90000E-04	1.40807E-04	
	19	3.02000E-03	4.88088E-04	
	20	3.00000E-05	4.72980E-06	
	26	4.00000E-05	4.52595E-06	
	30	5.00000E-05	4.83253E-06	
203	MUSCLE, STRIATED (ICRU) (203)			203
	9	5.50051E-01	7.47000E+01 1.04000E+00	
	1	1.01997E-01	6.33111E-01	
	6	1.23000E-01	6.40672E-02	
	7	3.50000E-02	1.56330E-02	
	8	7.29003E-01	2.85060E-01	
	11	8.00000E-04	2.17704E-04	
	12	2.00000E-04	5.14807E-05	
	15	2.00000E-03	4.03967E-04	
	16	5.00000E-03	9.75700E-04	
	19	3.00000E-03	4.80036E-04	
204	MUSCLE-EQUIVALENT LIQUID, WITH SUCROSE (204)			204
	4	5.48281E-01	7.43000E+01 1.11000E+00	
	1	9.82340E-02	3.85081E+01	
	6	1.56214E-01	5.13864E+00	
	7	3.54510E-02	1.00000E+00	
	8	7.10100E-01	1.75357E+01	
205	MUSCLE-EQUIVALENT LIQUID, WITHOUT SUCROSE (205)			205
	4	5.50136E-01	7.42000E+01 1.07000E+00	
	1	1.01969E-01	3.99722E+01	
	6	1.20058E-01	3.94929E+00	
	7	3.54510E-02	1.00000E+00	
	8	7.42522E-01	1.83364E+01	
206	NAPHTHALENE (206)			206
	2	5.30532E-01	6.84000E+01 1.14500E+00	
	1	6.29090E-02	4.00000E+00	
	6	9.37091E-01	5.00000E+00	
207	NITROBENZENE (207)			207
	4	5.19856E-01	7.58000E+01 1.19867E+00	
	1	4.09350E-02	5.00000E+00	
	6	5.85374E-01	6.00000E+00	
	7	1.13773E-01	1.00000E+00	
	8	2.59918E-01	2.00000E+00	
208	NITROUS OXIDE (208)			208
	2	4.99855E-01	8.49000E+01 1.83094E-03	
	7	6.36483E-01	2.00000E+00	
	8	3.63517E-01	1.00000E+00	
209	NYLON, DU PONT ELVAMIDE 8062 (209)			209
	4	5.50625E-01	6.43000E+01 1.08000E+00	
	1	1.03509E-01	1.44516E+01	
	6	6.48415E-01	7.59678E+00	
	7	9.95360E-02	1.00000E+00	
	8	1.48539E-01	1.30645E+00	
210	NYLON, TYPE 6 AND TYPE 6/6 (210)			210
	4	5.47901E-01	6.39000E+01 1.14000E+00	
	1	9.79760E-02	1.10000E+01	
	6	6.36856E-01	6.00000E+00	
	7	1.23779E-01	1.00000E+00	
	8	1.41389E-01	1.00000E+00	
211	NYLON, TYPE 6/10 (211)			211
	4	5.52359E-01	6.32000E+01 1.14000E+00	
	1	1.07062E-01	1.50000E+01	
	6	6.80449E-01	8.00000E+00	
	7	9.91890E-02	1.00000E+00	
	8	1.13300E-01	1.00000E+00	
212	NYLON, TYPE 11 (RILSAN) (212)			212
	4	5.56486E-01	6.16000E+01 1.42500E+00	

	1	1.15476E-01	2.10000E+01		
	6	7.20819E-01	1.10000E+01		
	7	7.64170E-02	1.00000E+00		
	8	8.72890E-02	1.00000E+00		
213		OCTANE, LIQUID (213)			213
	2	5.77780E-01	5.47000E+01	7.02600E-01	
	1	1.58821E-01	9.00000E+00		
	6	8.41179E-01	4.00000E+00		
214		PARAFFIN WAX (214)			214
	2	5.72748E-01	5.59000E+01	9.30000E-01	
	1	1.48605E-01	2.08000E+00		
	6	8.51395E-01	1.00000E+00		
215		N-PENTANE (215)			215
	2	5.82122E-01	5.36000E+01	6.26200E-01	
	1	1.67635E-01	1.20000E+01		
	6	8.32365E-01	5.00000E+00		
216		PHOTOGRAPHIC EMULSION (216)			216
	8	4.54533E-01	3.31000E+02	3.81500E+00	
	1	1.41000E-02	4.07093E-01		
	6	7.22610E-02	1.75072E-01		
	7	1.93200E-02	4.01387E-02		
	8	6.61010E-02	1.20226E-01		
	16	1.89000E-03	1.71550E-03		
	35	3.49103E-01	1.27139E-01		
	47	4.74105E-01	1.27901E-01		
	53	3.12000E-03	7.15434E-04		
217		PLASTIC SCINTILLATOR (VINYLTOLUENE BASED) (217)			217
	2	5.41415E-01	6.47000E+01	1.03200E+00	
	1	8.50000E-02	1.10703E+00		
	6	9.15000E-01	1.00000E+00		
218		PLUTONIUM DIOXIDE (218)			218
	2	4.05828E-01	7.46500E+02	1.14600E+01	
	8	1.18055E-01	2.00000E+00		
	94	8.81945E-01	1.00000E+00		
219		POLYACRYLONITRILE (219)			219
	3	5.27671E-01	6.96000E+01	1.17000E+00	
	1	5.69830E-02	3.00000E+00		
	6	6.79056E-01	3.00000E+00		
	7	2.63962E-01	1.00000E+00		
220		POLYCARBONATE (MAKROLON, LEXAN) (220)			220
	3	5.26968E-01	7.31000E+01	1.20000E+00	
	1	5.54910E-02	1.40000E+01		
	6	7.55751E-01	1.60000E+01		
	8	1.88758E-01	3.00000E+00		
221		POLYCHLOROSTYRENE (221)			221
	3	5.25176E-01	8.17000E+01	1.30000E+00	
	1	6.18690E-02	1.80000E+01		
	6	6.96325E-01	1.70000E+01		
	17	2.41806E-01	2.00000E+00		
222		POLYETHYLENE (222)			222
	2	5.70337E-01	5.74000E+01	9.40000E-01	
	1	1.43711E-01	2.00000E+00		
	6	8.56289E-01	1.00000E+00		
223		POLYETHYLENE TEREPHTHALATE (MYLAR) (223)			223
	3	5.20371E-01	7.87000E+01	1.40000E+00	
	1	4.19590E-02	4.00000E+00		
	6	6.25017E-01	5.00000E+00		
	8	3.33025E-01	2.00000E+00		
224		POLYMETHYL METHACRALATE (LUCITE, PERSPEX, PLEXIGLASS) (224)			224
	3	5.39369E-01	7.40000E+01	1.19000E+00	
	1	8.05380E-02	8.00000E+00		
	6	5.99848E-01	5.00000E+00		
	8	3.19614E-01	2.00000E+00		
225		POLYOXYMETHYLENE (225)			225
	3	5.32868E-01	7.74000E+01	1.42500E+00	
	1	6.71350E-02	2.00000E+00		
	6	4.00017E-01	1.00000E+00		
	8	5.32848E-01	1.00000E+00		
226		POLYPROPYLENE (226)			226

	2	5.70337E-01	5.65000E+01	9.00000E-01	
	1	1.43711E-01	2.00000E+00		
	6	8.56289E-01	1.00000E+00		
227		POLYSTYRENE (227)			227
	2	5.37680E-01	6.87000E+01	1.06000E+00	
	1	7.74180E-02	1.00000E+00		
	6	9.22582E-01	1.00000E+00		
228		POLYTETRAFLUOROETHYLENE (TEFLON) (228)			228
	2	4.79925E-01	9.91000E+01	2.20000E+00	
	6	2.40183E-01	1.00000E+00		
	9	7.59817E-01	2.00000E+00		
229		POLYTRIFLUOROCHLOROETHYLENE (229)			229
	3	4.80810E-01	1.20700E+02	2.10000E+00	
	6	2.06250E-01	2.00000E+00		
	9	4.89354E-01	3.00000E+00		
	17	3.04395E-01	1.00000E+00		
230		POLYVINYL ACETATE (230)			230
	3	5.34323E-01	7.37000E+01	1.19000E+00	
	1	7.02450E-02	3.00000E+00		
	6	5.58066E-01	2.00000E+00		
	8	3.71689E-01	1.00000E+00		
231		POLYVINYL ALCOHOL (231)			231
	3	5.44798E-01	6.97000E+01	1.30000E+00	
	1	9.15170E-02	4.00000E+00		
	6	5.45298E-01	2.00000E+00		
	8	3.63185E-01	1.00000E+00		
232		POLYVINYL BUTYRAL (232)			232
	3	5.45366E-01	6.72000E+01	1.12000E+00	
	1	9.28020E-02	1.30000E+01		
	6	6.80561E-01	8.00000E+00		
	8	2.26637E-01	2.00000E+00		
233		POLYVINYL CHLORIDE (233)			233
	3	5.12010E-01	1.08200E+02	1.30000E+00	
	1	4.83800E-02	3.00000E+00		
	6	3.84360E-01	2.00000E+00		
	17	5.67260E-01	1.00000E+00		
234		POLYVINYLIDENE CHLORIDE, SARAN (234)			234
	3	4.95132E-01	1.34300E+02	1.70000E+00	
	1	2.07930E-02	1.00000E+00		
	6	2.47793E-01	1.00000E+00		
	17	7.31413E-01	1.00000E+00		
235		POLYVINYLIDENE FLUORIDE (235)			235
	3	4.99730E-01	8.88000E+01	1.76000E+00	
	1	3.14800E-02	1.00000E+00		
	6	3.75141E-01	1.00000E+00		
	9	5.93379E-01	1.00000E+00		
236		POLYVINYL PYRROLIDONE (236)			236
	4	5.39844E-01	6.77000E+01	1.25000E+00	
	1	8.16160E-02	9.00000E+00		
	6	6.48407E-01	6.00000E+00		
	7	1.26024E-01	1.00000E+00		
	8	1.43953E-01	1.00000E+00		
237		POTASSIUM IODIDE (237)			237
	2	4.33728E-01	4.31900E+02	3.13000E+00	
	19	2.35528E-01	1.00000E+00		
	53	7.64472E-01	1.00000E+00		
238		POTASSIUM OXIDE (238)			238
	2	4.88344E-01	1.89900E+02	2.32000E+00	
	8	1.69852E-01	1.00000E+00		
	19	8.30148E-01	2.00000E+00		
239		PROPANE (239)			239
	2	5.89620E-01	4.71000E+01	1.87939E-03	
	1	1.82855E-01	8.00000E+00		
	6	8.17145E-01	3.00000E+00		
240		PROPANE, LIQUID (240)			240
	2	5.89620E-01	5.20000E+01	4.30000E-01	
	1	1.82855E-01	8.00000E+00		
	6	8.17145E-01	3.00000E+00		
241		N-PROPYL ALCOHOL (241)			241
	3	5.65765E-01	6.11000E+01	8.03500E-01	

	1	1.34173E-01	8.00000E+00	
	6	5.99595E-01	3.00000E+00	
	8	2.66232E-01	1.00000E+00	
242		PYRIDINE (242)		242
	3	5.30966E-01	6.62000E+01	9.81900E-01
	1	6.37100E-02	5.00000E+00	
	6	7.59217E-01	5.00000E+00	
	7	1.77073E-01	1.00000E+00	
243		RUBBER, BUTYL (243)		243
	2	5.70337E-01	5.65000E+01	9.20000E-01
	1	1.43711E-01	2.00000E+00	
	6	8.56289E-01	1.00000E+00	
244		RUBBER, NATURAL (244)		244
	2	5.57854E-01	5.98000E+01	9.20000E-01
	1	1.18371E-01	8.00000E+00	
	6	8.81629E-01	5.00000E+00	
245		RUBBER, NEOPRENE (245)		245
	3	5.19560E-01	9.30000E+01	1.23000E+00
	1	5.69200E-02	5.00000E+00	
	6	5.42646E-01	4.00000E+00	
	17	4.00434E-01	1.00000E+00	
246		SILICON DIOXIDE (246)		246
	2	4.99299E-01	1.39200E+02	2.32000E+00
	8	5.32565E-01	2.00000E+00	
	14	4.67435E-01	1.00000E+00	
247		SILVER BROMIDE (247)		247
	2	4.36700E-01	4.86600E+02	6.47300E+00
	35	4.25537E-01	1.00000E+00	
	47	5.74463E-01	1.00000E+00	
248		SILVER CHLORIDE (248)		248
	2	4.46550E-01	3.98400E+02	5.56000E+00
	17	2.47368E-01	1.00000E+00	
	47	7.52632E-01	1.00000E+00	
249		SILVER HALIDES IN PHOTOGRAPHIC EMULSION (249)		249
	3	4.36633E-01	4.87100E+02	6.47000E+00
	35	4.22895E-01	4.97514E-01	
	47	5.73748E-01	5.00000E-01	
	53	3.35700E-03	2.48665E-03	
250		SILVER IODIDE (250)		250
	2	4.25944E-01	5.43500E+02	6.01000E+00
	47	4.59458E-01	1.00000E+00	
	53	5.40542E-01	1.00000E+00	
251		SKIN (ICRP) (251)		251
	13	5.49326E-01	7.27000E+01	1.10000E+00
	1	1.00588E-01	6.19977E-01	
	6	2.28250E-01	1.18053E-01	
	7	4.64200E-02	2.05881E-02	
	8	6.19002E-01	2.40345E-01	
	11	7.00000E-05	1.89152E-05	
	12	6.00000E-05	1.53357E-05	
	15	3.30000E-04	6.61861E-05	
	16	1.59000E-03	3.08092E-04	
	17	2.67000E-03	4.67848E-04	
	19	8.50000E-04	1.35054E-04	
	20	1.50000E-04	2.32493E-05	
	26	1.00000E-05	1.11236E-06	
	30	1.00000E-05	9.50171E-07	
252		SODIUM CARBONATE (252)		252
	3	4.90618E-01	1.25000E+02	2.53200E+00
	6	1.13323E-01	1.00000E+00	
	8	4.52861E-01	3.00000E+00	
	11	4.33815E-01	2.00000E+00	
253		SODIUM IODIDE (253)		253
	2	4.26968E-01	4.52000E+02	3.66700E+00
	11	1.53373E-01	1.00000E+00	
	53	8.46627E-01	1.00000E+00	
254		SODIUM MONOXIDE (254)		254
	2	4.84036E-01	1.48800E+02	2.27000E+00

	8	2.58143E-01	1.00000E+00		
	11	7.41857E-01	2.00000E+00		
255	SODIUM NITRATE (255)				255
	3	4.94149E-01	1.14600E+02	2.26100E+00	
	7	1.64795E-01	1.00000E+00		
	8	5.64720E-01	3.00000E+00		
	11	2.70485E-01	1.00000E+00		
256	STILBENE (256)				256
	2	5.32597E-01	6.77000E+01	9.70700E-01	
	1	6.71010E-02	6.00000E+00		
	6	9.32899E-01	7.00000E+00		
257	SUCROSE (257)				257
	3	5.31699E-01	7.75000E+01	1.58050E+00	
	1	6.47790E-02	2.20000E+01		
	6	4.21070E-01	1.20000E+01		
	8	5.14151E-01	1.10000E+01		
258	TERPHENYL (258)				258
	2	5.21485E-01	7.17000E+01	1.23400E+00	
	1	4.45430E-02	5.00000E+00		
	6	9.55457E-01	9.00000E+00		
259	TESTES (ICRP) (259)				259
	13	5.51083E-01	7.50000E+01	1.04000E+00	
	1	1.04166E-01	6.41370E-01		
	6	9.22700E-02	4.76740E-02		
	7	1.99400E-02	8.83465E-03		
	8	7.73884E-01	3.00173E-01		
	11	2.26000E-03	6.10062E-04		
	12	1.10000E-04	2.80865E-05		
	15	1.25000E-03	2.50447E-04		
	16	1.46000E-03	2.82611E-04		
	17	2.44000E-03	4.27107E-04		
	19	2.08000E-03	3.30146E-04		
	20	1.00000E-04	1.54836E-05		
	26	2.00000E-05	2.22244E-06		
	30	2.00000E-05	1.89839E-06		
260	TETRACHLOROETHYLENE (260)				260
	2	4.82410E-01	1.59200E+02	1.62500E+00	
	6	1.44856E-01	1.00000E+00		
	17	8.55144E-01	2.00000E+00		
261	THALLIUM CHLORIDE (261)				261
	2	4.08613E-01	6.90300E+02	7.00400E+00	
	17	1.47822E-01	1.00000E+00		
	81	8.52178E-01	1.00000E+00		
262	TISSUE, SOFT (ICRP) (262)				262
	13	5.51210E-01	7.23000E+01	1.00000E+00	
	1	1.04472E-01	6.30465E-01		
	6	2.32190E-01	1.17582E-01		
	7	2.48800E-02	1.08042E-02		
	8	6.30238E-01	2.39596E-01		
	11	1.13000E-03	2.98966E-04		
	12	1.30000E-04	3.25332E-05		
	15	1.33000E-03	2.61178E-04		
	16	1.99000E-03	3.77544E-04		
	17	1.34000E-03	2.29895E-04		
	19	1.99000E-03	3.09581E-04		
	20	2.30000E-04	3.49043E-05		
	26	5.00000E-05	5.44564E-06		
	30	3.00000E-05	2.79097E-06		
263	TISSUE, SOFT (ICRU FOUR-COMPONENT) (263)				263
	4	5.49750E-01	7.49000E+01	1.00000E+00	
	1	1.01172E-01	5.40761E+01		
	6	1.11000E-01	4.97859E+00		
	7	2.60000E-02	1.00000E+00		
	8	7.61828E-01	2.56517E+01		
264	TISSUE-EQUIVALENT GAS (METHANE BASED) (264)				264
	4	5.49926E-01	6.12000E+01	1.06409E-03	
	1	1.01869E-01	3.22000E+02		
	6	4.56179E-01	1.21000E+02		
	7	3.51720E-02	8.00000E+00		
	8	4.06780E-01	8.10000E+01		

265	TISSUE-EQUIVALENT GAS (PROPANE BASED) (265)	265
	4 5.50268E-01 5.95000E+01 1.82628E-03	
	1 1.02672E-01 2.20000E+03	
	6 5.68940E-01 1.02300E+03	
	7 3.50220E-02 5.40000E+01	
	8 2.93366E-01 3.96000E+02	
266	TISSUE-EQUIVALENT PLASTIC (A-150) (266)	266
	6 5.49031E-01 6.51000E+01 1.12700E+00	
	1 1.01327E-01 5.83655E-01	
	6 7.75501E-01 3.74845E-01	
	7 3.50570E-02 1.45307E-02	
	8 5.23160E-02 1.89836E-02	
	9 1.74220E-02 5.32389E-03	
	20 1.83780E-02 2.66207E-03	
267	TITANIUM DIOXIDE (267)	267
	2 4.75721E-01 1.79500E+02 4.26000E+00	
	8 4.00592E-01 2.00000E+00	
	22 5.99408E-01 1.00000E+00	
268	TOLUENE (268)	268
	2 5.42651E-01 6.25000E+01 8.66900E-01	
	1 8.75100E-02 8.00000E+00	
	6 9.12490E-01 7.00000E+00	
269	TRICHLOROETHYLENE (269)	269
	3 4.87103E-01 1.48100E+02 1.46000E+00	
	1 7.67100E-03 1.00000E+00	
	6 1.82831E-01 2.00000E+00	
	17 8.09498E-01 3.00000E+00	
270	TRIETHYL PHOSPHATE (270)	270
	4 5.38001E-01 8.12000E+01 1.07000E+00	
	1 8.29980E-02 1.50000E+01	
	6 3.95628E-01 6.00000E+00	
	8 3.51334E-01 4.00000E+00	
	15 1.70040E-01 1.00000E+00	
271	TUNGSTEN HEXAFLUORIDE (271)	271
	2 4.29760E-01 3.54400E+02 2.40000E+00	
	9 3.82723E-01 6.00000E+00	
	74 6.17277E-01 1.00000E+00	
272	URANIUM DICARBIDE (272)	272
	2 3.96870E-01 7.52000E+02 1.12800E+01	
	6 9.16690E-02 2.00000E+00	
	92 9.08331E-01 1.00000E+00	
273	URANIUM MONOCARBIDE (273)	273
	2 3.91938E-01 8.62000E+02 1.36300E+01	
	6 4.80360E-02 1.00000E+00	
	92 9.51964E-01 1.00000E+00	
274	URANIUM OXIDE (274)	274
	2 3.99959E-01 7.20600E+02 1.09600E+01	
	8 1.18502E-01 2.00000E+00	
	92 8.81498E-01 1.00000E+00	
275	UREA (275)	275
	4 5.32841E-01 7.28000E+01 1.32300E+00	
	1 6.71310E-02 4.00000E+00	
	6 1.99999E-01 1.00000E+00	
	7 4.66459E-01 2.00000E+00	
	8 2.66411E-01 1.00000E+00	
276	VALINE (276)	276
	4 5.46320E-01 6.77000E+01 1.23000E+00	
	1 9.46410E-02 1.10000E+01	
	6 5.12645E-01 5.00000E+00	
	7 1.19565E-01 1.00000E+00	
	8 2.73150E-01 2.00000E+00	
277	VITON FLUOROELASTOMER (277)	277
	3 4.85849E-01 9.86000E+01 1.80000E+00	
	1 9.41700E-03 2.00000E+00	
	6 2.80555E-01 5.00000E+00	
	9 7.10028E-01 8.00000E+00	
278	WATER, LIQUID (278)	278
	2 5.55087E-01 7.50000E+01 1.00000E+00	
	1 1.11894E-01 2.00000E+00	
	8 8.88106E-01 1.00000E+00	

279	WATER VAPOR (279)			279
	2	5.55087E-01	7.16000E+01	7.56182E-04
	1	1.11894E-01	2.00000E+00	
	8	8.88106E-01	1.00000E+00	
280	XYLENE (280)			280
	2	5.46309E-01	6.18000E+01	8.70000E-01
	1	9.49350E-02	5.00000E+00	
	6	9.05065E-01	4.00000E+00	